

THE UNIVERSITY OF HULL

Intrinsic Conducting Polymer Current Limiting Device

being a Thesis submitted for the Degree of

Doctor of Philosophy

in the University of Hull

by

Noor H Jabarullah, MSc (Electronic Engineering)

November 2013

Abstract

This thesis investigates the development of novel intrinsic conducting polymer current limiting devices (CLDs), which are small self-resettable components used to protect circuitry in portable electronic appliances during situations of overcurrent. There are many existing solutions that enable the interruption and limitation of current surges in devices. A simple and common device is the use of a hybrid system of small metallic/semiconducting particles embedded in a thermally responsive polymeric material. During an overcurrent situation the positive temperature coefficient resistance (PTCR) of the polymeric material expands due to joule heating, which causes the percolating current pathways in the device to break which in turn causes the device to become temporarily non conducting. Although commonly used in the electronics industry today there are some limitations in the conductive fillers such as fretting and degradation that cause unwanted shifts in the percolation threshold, which can result in faulty operation. There is also increasing demand for faster operating devices as well as cheaper and more convenient methods of fabrication. One possibility that has emerged is the use of intrinsic conducting polymers as current limiting materials. There are several benefits of this for commercialization, such as cheap starting materials, simple chemical or electrochemical solution-based methods for device fabrication and potentially very fast device operation if the mechanism is electronic rather than mechanical in nature. Although preliminary measurements in these materials have shown evidence of switching to a non-conducting state at high currents, which is resettable upon cooling, the mechanism that causes the switching has not been established and no studies on this effect have been reported in the literature.

This motivates further work into developing current limiting devices based on these materials. The intention of this research is (1) to develop current limiting devices based on the intrinsic conducting polymer polyaniline (PANI), (2) to improve the electronic properties of the device, ideally we desire to have low resistance at low current level (normal operating conditions) and saturated or limited conductivity at high current level (overcurrent/short-circuit conditions), (3) elucidate the switching mechanism of the devices and (4) investigate the devices stability and resetability characteristics in different environmental conditions.

The results of this thesis show that the presence of moisture in the conducting polymer plays an important role in the current limiting performance. Our results indicate that the electronic switching of the devices is a result of a partial de-doping/re-doping effect caused by water diffusing into and out of the polymer film during joule heating/ cooling of the devices. We speculate that the polymer/metal interface region plays an important role in this and as such significant improvement in the electrical properties were made using self-assembled monolayer (SAM) modified electrodes

Studies were also performed to understand the temperature dependent electrical resistivity of the polymer material, shown to be variable range hopping in three dimensions, and as well, investigations were made to understand device performance in different environmental conditions (varying from vacuum to 100% relative humidity). Stability and degradation testing was performed in order to find the best operational and stable conditions for the current limiting devices. Results showed that devices were very stable in low to medium voltage values. In an effort to understand the effect of dopant type on the moisture content in the polymer film, thermal analyses (thermogravimetric and differential scanning calorimetry) of samples with different dopants were

investigated. Polyaniline doped with methanesulfonic acid was found to be among the samples with the highest moisture content.

CONTENTS

Abstract	1
CONTENTS	5
List of Figures	7
List of Tables	18
Acknowledgement	19
Chapter 1 INTRODUCTION	20
Background	23
Introduction to Conducting Polymer	26
1.1 Conducting Polymers	27
1.2 Polyaniline	40
1.3 Motivation of Study	47
1.4 Thesis Outline	51
Chapter 2 DEVICE FABRICATION	53
2.1 Device Schematic	53
2.2 Polymerisation of Polyaniline Methanesulfonic Acid (MSA)	54
2.3 Self-Assembled Monolayer (SAM) Modified Devices	55
Chapter 3 DEVICE AND MATERIALS CHARACTERIZATION	60
3.1 Cyclic Voltammetry	60
3.2 Contact Angle Measurements	65

3.2.1 Polymerisation of PANI-MSA on Gold Containing Self-Assembled Monolayer of 1-Dodecanethiol (DDT).	70
3.3 Electrical Measurements	73
3.4 Temperature Dependent Measurements	74
3.5 Contact Resistance Measurements	78
3.5 Differential Scanning Calorimetry (DSC)	80
3.6 Thermo-gravimetric Analysis (TGA)	82
3.7 Morphological Studies	84
Chapter 4 RESULTS & DISCUSSION	85
4.1 Current limiting device, switching mechanism properties and morphology	85
4.2 Surface modified electrode using self-assembled monolayer a novel approach for current-limiting device.	103
4.3 Stability, reproducibility and effect of different dopants on moisture contents in polyaniline.	146
Chapter 5 CONCLUSIONS	172
Chapter 6 FUTURE WORK	175
Chapter 7 Appendices	177
Appendix 1	177
Appendix 2	190
Chapter 8 REFERENCES	201

List of Figures

Figure 1.1: The example of I-V curves, A-showing just normal Ohmic and linear resistive behaviour, B – true saturating behaviour and can handle high power dissipation after switching, C – similar to B with a slight foldback, D – full foldback but all voltage dropped across device.....	21
Figure 1.2: Number of research publications in conducting polymers (N) during the last 18 years. Before 1991 the total was 8174. Data taken and reproduced from Inzelt [15].	27
Figure 1.3: Structures of some examples of conjugated polymers reproduced from [6].	29
Figure 1.4: Energy band structure of conductors (overlapping bands), semiconductors (< 1 eV) and insulators (> 3-5 eV).	30
Figure 1.5: Example of insulator which is in the form of a saturated backbone structure of polyethylene.	31
Figure 1.6: Unsaturated conjugated polymer of polyacetylene as example of semiconducting polymer.....	32
Figure 1.7: Example of transport of a polaron in a lightly doped film; (a) intra-chain transfer and (b) inter-chain transfer.....	33
Figure 1.8: Charge transport in highly doped grains with a low concentration of conjugated polymers chains in between the metallic islands. The lines represent the polymers lines. Inside the islands, charges are delocalized and migrate easily, while charges need to hop between the islands (dash square marks) passing over the low conducting phases [20]......	34
Figure 1.9: Formation of polaron and bipolaron shown in forms of band diagrams and chemical structure.	35

Figure 1.10: Showing the mechanism of hopping conduction. The localized electron can hop from site i with energy E_i to site j with energy E_j separated by the distance R.....	37
Figure 1.11: Redox forms of polyaniline.....	42
Figure 1.12: Structure of Leucoemeraldine as determine by Epstein et al. [40].....	42
Figure 1.13: Structure of Pernigraniline as determined by Epstein et al. [40].....	43
Figure 1.14: Structure of emeraldine base as determined by Epstein et al. [40].....	43
PANI can thus be illustrated as having four benzene ring repeat units as shown in Fig 1.15 below: Figure 1.15: Structure of Polyaniline repeat unit as determined by Epstein et al. [40].....	44
Figure 1.16: Doped and Undoped forms of polyaniline.....	45
Figure 1.17: Principle operation of the Polymeric Positive Temperature Coefficient device.	48
Figure 1.18: Example of operating curve for PPTC device.	49
Figure 2.1: Illustration of the specification for the substrate used on alumina substrate.....	53
Figure 2.2: The standard electrochemical set-up employed in the experiment.....	54
Figure 2.3: A typical self-assembling surfactant molecule consisting of three parts: surface group, alkyl or derivatized alkyl group, and surface-active head group [48].....	55
Figure 2.4: Illustration of self-assembly of DDT on gold substrate [48].....	56
Figure 2.5: Schematic of the self-assembly set-up in the laboratory [46].	58
Figure 2.6: Schematic representation of the self-assembly process.....	59
Figure 3.1: Typical excitation signal for cyclic voltammetry, a triangular potential switching potential at $E_{initial}$ and E_{final} versus reference electrode.....	60

Figure 3.2: Typical example of a cyclic voltammogram for a reversible redox process [59]..	62
Figure 3.3: Cyclic voltammogram of PANI-MSA with potential vs Ag/AgCl reference electrode.	62
Figure 3.4: Basic principle of potentiostat [70].	63
Figure 3.5: The three- phase contact angle θ is the angle measured between the liquid and the solid by drawing a tangent to the drop profile at the contact line. ..	65
Figure 3.6: Hydrophobic and hydrophilic surfaces criteria.....	66
Figure 3.7: Advancing and receding contact angles by tilting base method. The inclined plate method; a- is the advancing angle, r- correspond the receding angle and t-is the tilting angle.	67
Figure 3.8: Contact angle changes when increasing droplet volume and contracting it, where advancing angle must always be larger than receding angle.	68
Figure 3.9: Apparatus set-up used to measure drop shape to obtain contact angles.	69
Figure 3.10: Example of advancing and receding measurement for SAM on gold device. Noise in the data could be due to dust, vibrations or draught interference measurement.....	71
Figure 3.11: Sample 15- Drop images during advancing	71
Figure 3.12: Sample 14 - Drop images during receding	72
Figure 3.13: The simplified schematic representation of the electrical measurement set-up	73
Figure 3.14: Morphology of polymer chains on a surface showing separate regions of well-aligned chains representing the heterogeneous disorder in highly conducting chains; from Percec <i>et al.</i>[75]	74

Figure 3.15: Temperature dependent measurement experimental setup	76
Figure 3.16: Illustration of simple contact resistance geometry of the device.....	78
Figure 3.17: Example of extrapolation method using different length of known resistors.	79
Figure 3.18: Schematic principle of TGA measurement.	82
Figure 4.1: I-V characteristics for PANI-MSA current limiting device from 0 V up to maximum value given in the legend	85
Figure 4.2 : I-V characteristics for PANI-MSA current limiting device from 0 V up to the maximum values given in the legend.	86
Figure 4.3: Reproducibility of I-V characteristics for PANI-MSA current limiting device performed after resettability of resistance, from 1 V to 5 V	87
Figure 4.4: Reproducibility of I-V characteristics for PANI-MSA current limiting device performed after the resistance recovered, from 6 V to 10 V	88
Figure 4.5: Current-voltage characteristics in vacuum from 1 V to 5 V.	89
Figure 4.6: Current-voltage characteristics in vacuum from 6 V to 10 V	90
Figure 4.7: The infra-red camera images up to maximum applied bias of 10 V illustrate the hot spot during IV sweep which relates to the increase in temperature on the device.	91
Figure 4.9: Temperature dependence from 77K to 300K	96
Figure 4.10: The temperature dependence of dc conductivity of PANI-MSA showing a fit to 3D VRH model.	98
Figure 4.11: Comparison of temperature dependence for different dopants. Data points extracted and re-plotted from the literature [102-105].	99
Figure 4.12: SEM image at 1000 times magnification showed the typical polymer morphology for electrochemical polymerisation of PANI-MSA on Au	100

Figure 4.13:SEM image at 5000 times magnification showed the typical polymer morphology for electrochemical polymerisation of PANI-MSA on Au	101
Figure 4.14:SEM image at 10000 times magnification showed the typical polymer morphology for electrochemical polymerisation of PANI-MSA on Au	101
Figure 4.15:SEM image at 20000 times magnification showed the typical polymer morphology for electrochemical polymerisation of PANI-MSA on Au.	102
Figure 4.16: I-V characteristics of Sample 16 (24 H 1mM).Top graph (a) for voltage sweeps up to 5 V while the second graph (b) is for voltage sweeps up to 10 V.....	105
Figure 4.17: I-V characteristics of Sample 17(24H 5mM). Top graph (a) for voltage sweeps up to 5 V while the second graph (b) is for voltage sweeps up to 10 V.....	107
Figure 4.18: I-V characteristics of Sample 18 (24H 10mM). Top graph (a) for voltage sweeps up to 5 V while the second graph (b) is for voltage sweeps up to 10 V.....	108
Figure 4.19: I-V characteristics of Sample 19 (48H 1mM). Top graph (a) for voltage sweeps up to 5 V while the second graph (b) is for voltage sweeps up to 10 V.....	110
Figure 4.20: I-V characteristics of Sample 20 (48H 5mM). Top graph (a) for voltage sweeps up to 5 V while the second graph (b) is for voltage sweeps up to 10 V.....	111
Figure 4.21: I-V characteristics of Sample 21(48H 10mM). Top graph (a) for voltage sweeps up to 5 V while the second graph (b) is for voltage sweeps up to 10 V.....	113

Figure 4.22: I-V characteristics of Sample 22 (72H 1mM). Top graph (a) for voltage sweeps up to 5 V while the second graph (b) is for voltage sweeps up to 10 V.....	115
Figure 4.23: I-V characteristics of Sample 23 (72H 5mM). Top graph (a) for voltage sweeps up to 5 V while the second graph (b) is for voltage sweeps up to 10 V.....	116
Figure 4.24: I-V characteristics of Sample 24 (72H 10mM). Top graph (a) for voltage sweeps up to 5 V while the second graph (b) is for voltage sweeps up to 10 V.....	117
Figure 4.25: SAM concentration and immersion time with regards to the percentage resistance changes from linear form to non linear behaviour.....	118
Figure 4.26: I-V sweeps for PANI with 24 H SAM device in 100% high humidity condition from 1 V to 5 V.	121
Figure 4.27: I-V sweeps for PANI with 48 H SAM device in 100% humidity condition from 1 V to 5 V.	122
Figure 4.28: I-V sweeps for PANI with 72 H SAM device in 100% humidity condition from 1 V to 5 V.	122
Figure 4.29: Polyaniline growth structure on a hydrophobic surface [115]......	124
Figure 4.30: Polyaniline growth structure on a hydrophilic surface [115]......	124
Figure 4.31: The change in current values compared for different samples in 100% humidity level for different voltage sweep from 1 V to 5 V.	126
Figure 4.32: I-V measurement for samples without SAM in 4 different humidity levels.	127
Figure 4.33 : I-V measurement for samples with 72 H SAM in 4 different humidity levels	128

Figure 4.34: I-V sweeps for samples in different humidity at maximum potential 10 V (a) without SAM and (b) I-V measurement on SAM samples.	129
Figure 4.35: Contact resistance of the device with SAM before and after I-V sweeps.	133
Figure 4.36: Contact resistance of the device without SAM before and after I-V sweeps.	134
Figure 4.37: Schematic of contact resistance with different power dissipation level across the contact area on device with SAM and without SAM	135
Figure 4.38: Scanning electron micrograph of polyaniline deposited potentiostatically at +85mV (vs Ag/Ag Cl) from 0.5 M polyaniline in 1.0 M methanesulfonic acid. The top left of the micrograph showed the polyaniline deposited on non-modified gold electrode with x1000 magnification followed by the x5000 on the top right. The bottom left and bottom right images represent the magnification at x10000 and x20000 respectively.	137
Figure 4.39: Scanning electron micrograph of polyaniline deposited potentiostatically at +85mV (vs Ag/Ag Cl) from 0.5 M polyaniline in 1.0 M methanesulfonic acid. The top left of the micrograph showed the polyaniline deposited on SAM modified gold electrode with x1000 magnification followed by the x5000 on the top right. The bottom left and bottom right images represent the magnification at x10000 and x20000 respectively.	138
Figure 4.40 : Morphology SEM studies with various polymerization times for the current limiting device with SAM from (a) 25 seconds to (e) 100 seconds.	140
Figure 4.41 : Profile for polymer film on (a) device without SAM and (b) device with SAM on gold substrate.	141

Figure 4.42: Potentiostatic deposition of polyaniline film (a) on non modified gold substrate (b) on SAM modified gold substrate and showing slower onset of growth for the SAM device.....	143
Figure 4.43: Illustrations of polyaniline growth and its formation on (A) gold with SAM and (B) gold without SAM indicating the growth and uniformity difference between the two methods used.	145
Figure 4.44: I-V sweeps for the 1 st hour to the 24 th hour with 2.5 V maximum voltage.....	147
Figure 4.45: I-V sweeps for the 7 th hour to the 12 th hour with 2.5 V maximum voltage.....	147
Figure 4.46: I-V sweeps for the 13 th hour to the 18 th hour with 2.5 V maximum voltage.....	148
Figure 4.47: I-V sweeps from 19 th to 24 th hour with 2.5 V maximum voltage.....	148
Figure 4.48: I-V sweeps for the 1 st hour to the 6 th hour with 5 V maximum voltage	
Figure 4.49: I-V sweeps for the 7 th hour to the 12 th hour with 5 V maximum voltage.....	150
Figure 4.50: I-V sweeps for the 13 th hour to the 18 th hour with 5 V maximum voltage	
Figure 4.51: I-V sweeps for the 19 th hour to the 24 th hour with 5 V maximum voltage	151
Figure 4.52: I-V sweeps for the 1 st hour to the 6 th hour with 9 V maximum voltage	
Figure 4.53: I-V sweeps for the 7 th hour to the 12 th hour with 9 V maximum voltage.....	153
Figure 4.54: I-V sweeps for the 13 th hour to the 18 th hour with 9 V maximum voltage.....	154

Figure 4.55: I-V sweeps for the 19th hour to the 24th hour with 9 V maximum voltage.....	154
Figure 4.56: Comparison of stability of the device with different maximum voltage level by means of slope resistance change from the first sweep to the final measurement of the 24 hours duration.	156
Figure 4.57: Thermograms of PANI-MSA recorded from 100 to 600 °C (a) showed the TGA in air and N₂, (b) showed TGA after annealed at 100°C for 30 minutes	159
Figure 4.58: DSC thermogram of PANI-MSA in air and N₂.	160
Figure 4.59: Thermogravimetric analysis for different dopant of polyaniline showing weight loss when polymer sample is heated.....	162
Figure 4.60: Derivatives for the thermogravimetric analysis for different dopant of polyaniline showing the percentage of weight loss at each step.....	163
Figure 4.61: Differential scanning calorimetry for different protonated polyaniline showing thermal transition of the polymer samples.	167
Figure 4.62: SEM images for the polyaniline doped with different dopants (A) methanesulfonic acid (B) Sulphuric acid (C) Hydrochloric acid (D) Dodecylbenzenesulfonic acid (E) Perchloric acid and (F) <i>p</i>-tolouenesulfonic acid.	169
Figure 4.63: I-V sweep for PANI-SA without SAM.....	170
Figure 4.64: I-V sweeps for PANI-SA with SAM.....	171
Figure 7.1: Advancing and receding angles for Sample 7	177
Figure 7.2: Sample 7 Drop images during advancing.....	178
Figure 7.3: Sample 7 drop images during receding	178
Figure 7.4: Advancing and receding angles for Sample 8	179
Figure 7.5: Sample 8- Drop images during advancing	179
Figure 7.6: Sample 8 drop images during receding	180

Figure 7.7: Advancing and receding angles for Sample 9	180
Figure 7.8: Sample 9- Drop images during advancing	181
Figure 7.9: Sample 9- Drop images during receding	181
Figure 7.10: Advancing and receding angles for Sample 10	182
Figure 7.11: Sample 10- Drop images during advancing	182
Figure 7.12: Sample 10- Drop images during receding	183
Figure 7.13: Advancing and receding angles for Sample 10	183
Figure 7.14: Sample 11- Drop images during advancing	184
Figure 7.15: Sample 11- Drop images during receding	184
Figure 7.16: Advancing and receding angles for Sample 12	185
Figure 7.17; Sample 12- Drop images during advancing	185
Figure 7.18: Sample 12- Drop images during receding	186
Figure 7.19: Advancing and receding angles for Sample 13	186
Figure 7.20: Sample 13- Drop images during advancing	187
Figure 7.21: Sample 13- Drop images during receding	187
Figure 7.22: Advancing and receding angles for Sample 14	187
Figure 7.23 Sample 13- Drop images during advancing.....	188
Figure 7.24: Sample 14 - Drop images during receding	188
Figure 7.25: Advancing and receding angles for Sample 15	189
Figure 7.26: Sample 15- Drop images during advancing	189
Figure 7.27: Sample 14 - Drop images during receding	190
Figure 7.28: The I-V sweep with 10 V of potential applied for sample with 24H SAM of 1mM DDT with total 10 consecutive runs with 10 minute interval between each run.....	191

Figure 7.29: The I-V sweep with 10 V of potential applied for sample with 24H SAM of 5mM DDT with total 10 consecutive runs with 10 minute interval between each run.....	192
Figure 7.30: The I-V sweep with 10 V of potential applied for sample with 24H SAM of 10mM DDT with total 10 consecutive runs with 10 minute interval between each run.....	193
Figure 7.31: The I-V sweep with 10 V of potential applied for sample with 48H SAM of 1mM DDT with total 10 consecutive runs with 10 minute interval between each run.....	194
Figure 7.32: The I-V sweep with 10 V of potential applied for sample with 48H SAM of 5mM DDT with total 10 consecutive runs with 10 minute interval between each run.....	195
Figure 7.33: The I-V sweep with 10 V of potential applied for sample with 48H SAM of 10mM DDT with total 10 consecutive runs with 10 minute interval between each run.....	197
Figure 7.34: The I-V sweep with 10 V of potential applied for sample with 72H SAM of 1mM DDT with total 10 consecutive runs with 10 minute interval between each run.....	198
Figure 7.35: The I-V sweep with 10 V of potential applied for sample with 72H SAM of 5mM DDT with total 10 consecutive runs with 10 minute interval between each run.....	199
Figure 7.36: The I-V sweep with 10 V of potential applied for sample with 72H SAM of 10mM DDT with total 10 consecutive runs with 10 minute interval between each run.....	200

List of Tables

Table 1-1: Various compositions of polyaniline	46
Table 4-1: Resistance value for all SAM samples in air, vacuum and after air admittance in the vacuum chamber	119
Table 4-2: Drop Shape Analysis to confirm the existence of a Self Assembled Monolayer (SAM) after having been dipped in electrolyte.....	131
Table 4-3: The moisture contents for different protonated polyaniline extracted from the TGA plot at around 100°C.	166

Acknowledgement

This thesis was only made possible thanks to the help, support and guidance from many people along the way.

I would like to express my sincere gratitude to my supervisor Dr Neil T Kemp for the continuous support of my PhD study and research, for his patience, motivation and immense knowledge. I would also like to thank Prof Mary O'Neill, my second supervisor for her insightful advice and support. Thanks to Dr Jay Wadhawan for his suggestions and advice for the chemistry sides. I also like to thank Mr Luis Navarro and his team in TE Connectivity, California for sharing information and feedback during the early stage of my research. I would like to thank Dr Li Chen from University of Leeds for his time and technical support during my work in their EPSRC clean room facility. I also extend gratitude to Prof Dimitris Tsoukalas from National Technical University of Athens, Greece for his help with the humidity measurements. I am particularly grateful to Mr Gordon Sowersby for the excellent technical support, advice and help during my study. Thanks to, Dr Rob Farley, Mr Garry Robinson, Mr John Metheringham, Mr Ian Dobson and Ms Ronnie Hewer for their help and advice. I am also grateful to Ms Sheila Dryden, for her time, advice and moral support in helping me cope with the situation during my difficult times in the University. I am also thankful to all my colleagues and the staff in the University of Hull for helping me directly and indirectly during my studies.

I would like to express my gratitude to University of Hull and TE Connectivity for the funding provided. Finally, I would like to thank my loving husband and my whole family for their unconditional support throughout my studies.

Chapter 1 INTRODUCTION

This research explored the development of polymeric devices for self-resetting over-current protection of microelectronic circuits based on the electrically conducting polymer polyaniline (PANI). This emerging application of PANI is motivated by several factors that appear to be attractive to the lucrative worldwide usage for current limiting devices (CLDs). Compared with the industry standard CLDs (polymeric positive temperature coefficient device, PPTC) and combined circuits presently employed, such as bipolar transistors in a reactive circuit [1], PANI-based CLDs may offer some important advantages in terms of performance, inherent simplicity, size and cost.

Interest in PANI as a CLD material stems from the general current-voltage (I-V) response that has been observed in some conducting polymer devices. In some configurations and polymers the much sought after I-V function that has a peak in the response curve for current limitation as well as a dissipating current response when the voltage is increased has been observed but there is no clear understanding to why this occurs and this will be discussed in the I-V measurement for the devices. The aim of a CLD device is to reduce current to acceptable limits during a current surge. Examples and ideal I-V properties of such a device are shown in Fig. 1.1. Other device technologies such as superlattice heterostructures have emerged with similar I-V characteristics [2], but they are intrinsically more complex and presumably more difficult to manufacture than those speculated for PANI based CLD.

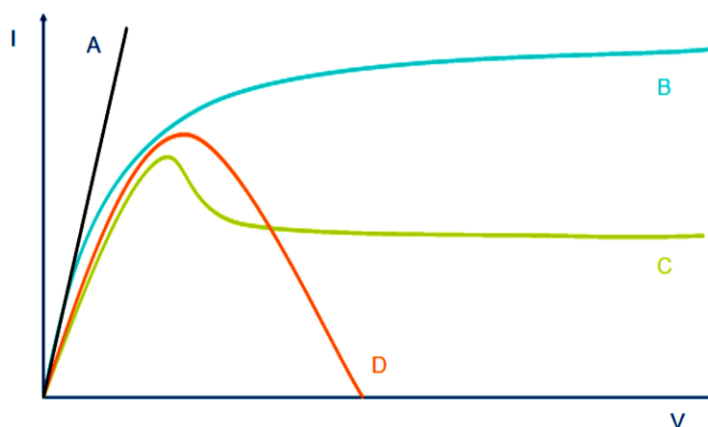


Figure 1.1: The example of I-V curves, A-showing just normal Ohmic and linear resistive behaviour, B – true saturating behaviour and can handle high power dissipation after switching, C – similar to B with a slight foldback, D – full foldback but all voltage dropped across device.

On the other hand the linkage between the process variables associated with synthesizing, doping and depositing PANI on a substrate and realizing the desired peak function in the device I-V response has been convincing. To further the study of the viability of PANI based CLDs, a series of experimental measurements have been carried out to gain a clearer understanding for the device performance in different environmental conditions and how the switching of the device can be affected by these different conditions. This research also investigates the temperature-dependent charge-transfer (conduction) mechanism in gap junction CLDs containing PANI doped with methane sulfonic acid.

The preliminary investigations indicated that the contact interface may be of high importance in the conducting polymers CLD. Using this we developed a new approach for making the conducting polymers CLD devices using self-assembled monolayer (SAM) of thiols to modify the substrate of CLDs. Thiols with different concentrations on gold have been compared and analysed to understand the best combination with the polyaniline film into producing the optimised device performance on current limitation

behaviour. The studies showed significant improvement on the current limiting behaviour and some hypotheses on the results have been discussed.

CLDs stability and reproducibility were also investigated in order to get a good grasp of the device limitation. Different types of dopants ranging from organics, inorganics and aromatics have also been investigated with a view to understanding why CLDs fabricated using polyaniline doped with methane sulfonic acid showed good switching properties.

Background

Polymers, for a long time, were only thought to be insulating, and not so long ago any electrical conduction that has relation with polymers which is mostly due to loosely bound ions was thought to be an undesirable phenomenon. The ionic conductivity of polymer electrolytes and polyelectrolyte has been widely applied and used in the field of electrochemistry over the past few decades mainly in batteries and solid-state developments related to electrochemical devices and sensors. Discovery of electronically conducting polymers has resulted in a paradigm change in researchers' thought and opened up a new era in physics and chemistry [3].

The 1970s is where the thought changed, when a new class of polymer showing high electronic conductivity in the partially oxidized state was discovered by three collaborating scientists. This major breakthrough by Alan J. Heeger, Alan G. MacDiarmid and Hideki Shirakawa received the Nobel Prize in Chemistry in 2000 "*for the discovery and development of electrically conductive polymers*" [4]. There were also other pioneers to this discovery in the history of science, including some theoretical calculations and predictions made by quantum chemists and physicists, as well as different conducting polymers that had already been made. This can be explained when Henry Letheby prepared polyaniline by anodic oxidation of aniline, which showed conductivity and electrochromic behaviour [5]. Nevertheless, the preparation of polyacetylene by Shirakawa and his research team reported large increase in its conductivity after doping by the group directed by MacDiarmid and Heeger [6].

Electrochemistry has played an important role in the preparation and characterisation of these novel materials. Electrochemical techniques are especially well suited to the controlled synthesis of these compounds and for the tuning of a well-defined oxidation state. The centre of research activity in electrochemistry is the preparation, characterization and application of electronically, electrochemically active conducting polymers. Some main reasons for the intense research that has been of interest to most researchers are the intellectual curiosity on the behaviour of the system, to be exact the mechanism of charge transfer and the processes that happens during redox reaction of the conducting polymers. The other reason is the promising technology of these compounds that has applications in various fields such as corrosion protection, electrochromic displays, energy storage, bioelectrochemistry, photoelectrochemistry, electrocatalysis, electroanalysis, sensors, electronic devices, microsystems technologies, microwave screening and many more.

After more than three decades of research in this field, the basic nature of charge propagation can be now generally understood as the transport of electrons via hopping between the neighbouring redox sites in redox polymers, and by the movement of delocalized electrons through conjugated systems in the case of intrinsically conducting polymers for example polyaniline or polypyrrole. The charge has also been carried by the movement of electroinactive ions during electrolysis in most of the cases, or in short, these materials made up of mixed conductors. These systems are known to be diversely capable and complex for instance the chemical changes such as dimerization cross-linking, ion pair formation etc., and their polymeric properties such as changes in the morphology, chain/segmental motion, slow relaxation, where all these relations adding with the discovery of new system brings in new problems to be solved, and

plenty more research are needed to achieve a more detailed understanding of all the procedures and steps related to the static and dynamic properties of various interacting molecules specific to the polymer network. Despite all the complicated and utilizable properties of the conducting polymers, the most essential feature is the variability of their conductivity which allows the polymeric materials to be switched between insulating and conducting forms or vice versa.

In this work, the topics that are discussed are of great interest in this field, emphasizing the application of the conducting polymer to electronic devices specifically towards intrinsic current limiting devices with fast switching. Some of the most important literature, fundamental topics regarding this group of material are outlined. Some chapters are devoted to the most important techniques used as method and characterization of these systems. A detailed outline of the thesis is given in section 1.4.

Introduction to Conducting Polymer

The discovery of intrinsically conducting polymers in 1960 has led to them becoming an attractive subject of research because of their interesting properties and numerous application possibilities. It was expected that intrinsic conducting polymers would find their potential applications in multidisciplinary areas such as electrical, electronics, thermoelectric, electrochemical, electromagnetic, electroluminescence, electro-rheological, chemical, membrane, and sensors [7-10]. Many of the potential uses for the intrinsically conducting polymers have yet to be explored because of a number of obstacles such as stability and processibility. Among the available intrinsic conducting polymers, polyaniline (PANI) is found to be the most promising because of its low cost monomer, better stability compared to other intrinsic conducting polymers, tuneable properties and ease of synthesis [11-13]. Hence many researchers have carried out extensive studies on the synthesis, characterization and application of PANI for the past three decades. A narrow review conducted by Inzelt has shown that the amount of research in conducting polymers has kept increasing over the past 18 years [14]. The statistical results have been reproduced and presented in Fig.1.2. The highest numbers of research are found to be for polyaniline which consists 42% of the research conducted, followed by polythiophene and polypyrrole. All other polymers play a minor role in comparison with the polymers mentioned with the thousands of research conducted in this fascinating field.

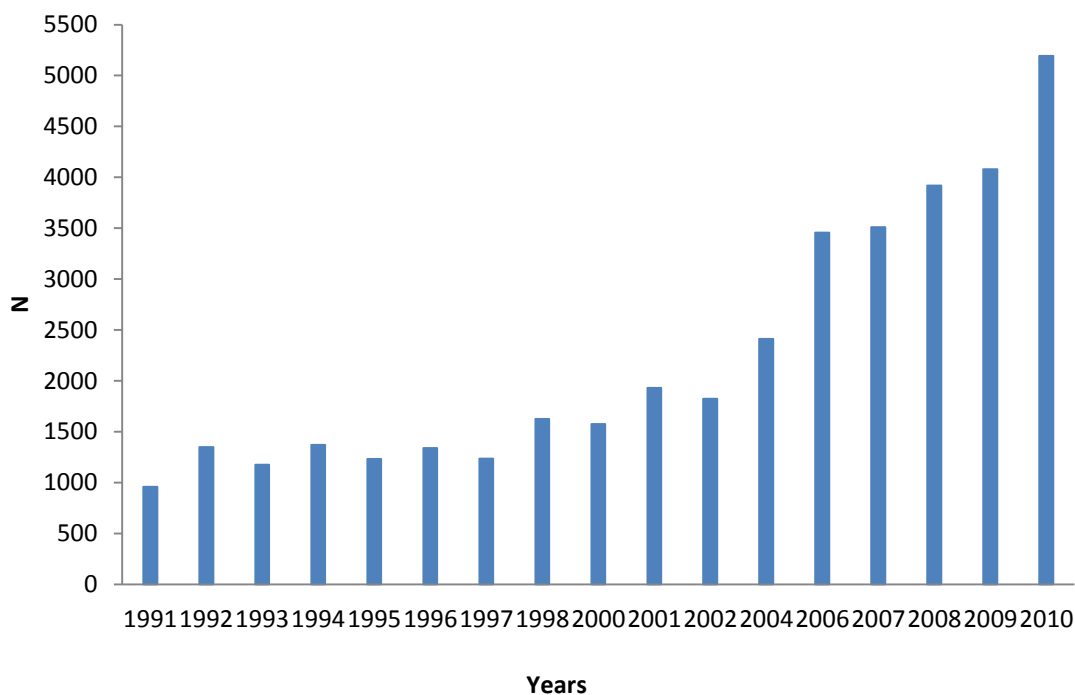


Figure 1.2: Number of research publications in conducting polymers (N) during the last 18 years. Before 1991 the total was 8174. Data taken and reproduced from Inzelt [15].

1.1 Conducting Polymers

In the late 19th century, synthetic polymers were introduced but were not fully developed for commercial or industrial purpose until the 1940-1950's. These polymers are easy to fabricate, cheap, robust and their plasticity nature attracted many potential uses. They were mainly used as insulators in electrical appliances as they possessed high electrical resistance.

The phrase 'electrical conduction' is usually synonymous with metals or alloys. Polymers with inherent properties of semiconductors and metals are a relatively recent development which is commonly known as organic synthetic metals [16]; that combines the conductive properties of inorganics with the added benefits from the light weight of the polymeric materials, are easy to handle and relatively cheap to produce [17].

Intrinsically conducting polymers (ICP's) conduct because the electrons are delocalised in the conjugated structure. This in turn brings insolubility and infusibility to the polymers, resulting in poor processibility. Various methods have been expanded to address these concerns including block copolymerisation [18], incorporating the flexible centres in the main chain to increase plasticity, side chain replacement by adding different side groups to the polymer backbone, implementation of precursor polymers and formation of polymer blends [19]. Conducting polymers can be categorised into two major groups based on their electronic transport. The first category is known as *polymer electrolytes* or *polymer ionics* that shows ionic conduction which can be demonstrated by a typical example of polyethylene oxide where the lithium ion is mobile. The second group are materials that are electronically conductive which is commonly known as *intrinsically conducting polymers (ICP)* or *conjugated polymers*. ICPs principal structure is the conjugation of carbon p_z orbitals or in other terms an alternation of single and double bonds in a carbon-carbon chain. Figure 1.3 shows some of the common examples of conjugated polymers [6].

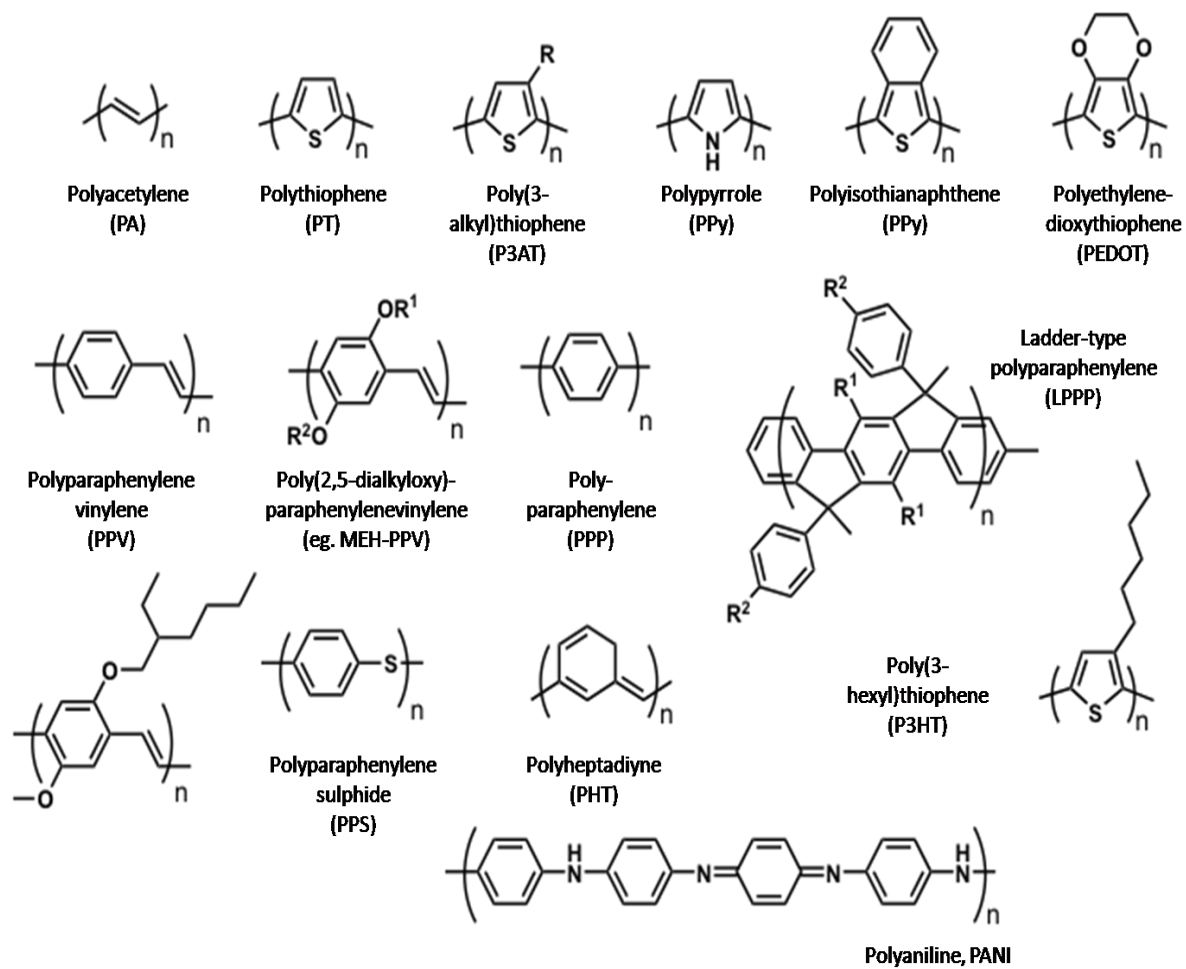


Figure 1.3: Structures of some examples of conjugated polymers reproduced from [6].

The principal feature of conducting polymers is a π - π^* band structure. The overlap of bonding orbitals produces the valence band. Non-bonding states from the conduction band for instance extended overlap of π -bands forms the valence band and the π^* -bands forms the conduction band. The bands are separated by a bandgap. The energy of the bandgap determines the conductivity of materials as shown in Figure 1.4

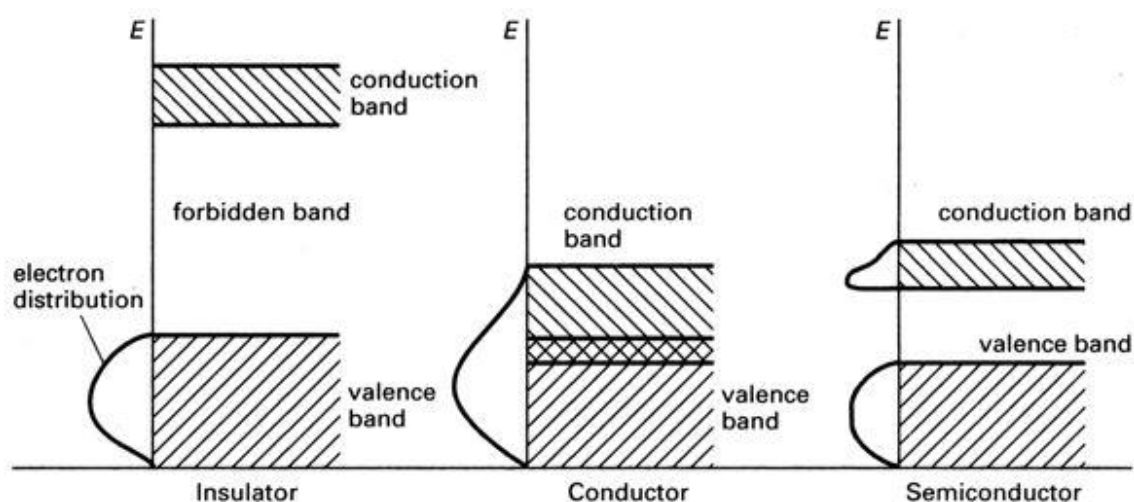


Figure 1.4: Energy band structure of conductors (overlapping bands), semiconductors (< 1 eV) and insulators (> 3-5 eV).

In the general concept of polymers, the molecular orbitals responsible for C-C interaction are of composed sp^3 sigma hybridized orbitals. In this type of hybridisation, all four electrons of the valence band for the carbon are used up in sigma bonds; therefore it is suited for extensive orbital overlap. This fact serves to localise the electrons between the bonding carbons, and results in the inability of the electrons to contribute to the conduction process. In terms of simple band theory, this type of bonding generates a large energy gap between the valence band and the conduction band giving the polymer the characteristics of a good insulator as shown in the example in Figure 1.5.

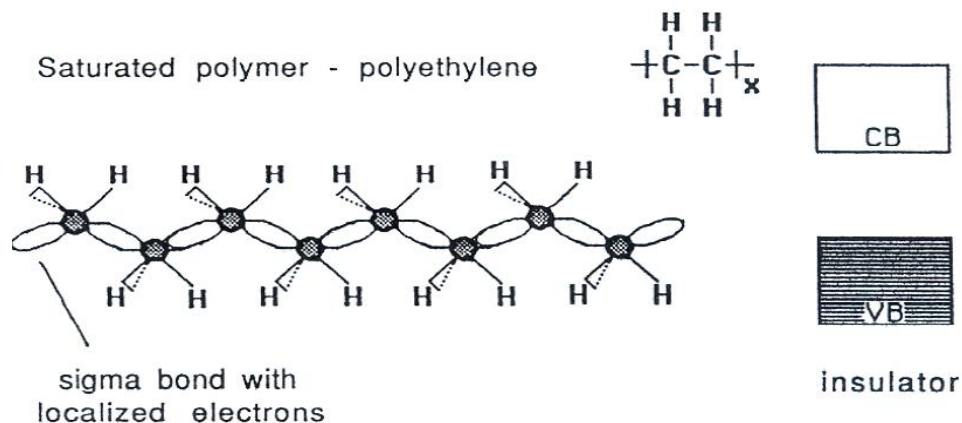


Figure 1.5: Example of insulator which is in the form of a saturated backbone structure of polyethylene.

The creation of an electrically conductive polymer therefore requires a continuous system of atomic orbitals that can allow the formation of delocalised electronic states. This type of molecular array can be found in polymers that contain conjugated unsaturated bonds along their backbone. In this system chemical bonding leads to one unpaired electron per carbon atom. The carbon orbitals with π -bonding for the sp^2p_z configuration where p_z orbital is oriented perpendicular to the backbone of polymer. The polymer configuration is also capable of overlapping with neighbouring polymer backbone which helps in electron delocalization along the polymer backbone as shown in Figure 1.6. Charge mobility along the polymer chain backbone was enhanced by the electron delocalization [6]. Intrinsically conducting polymers (ICPs) have a relatively small energy gap between highest occupied energy band and lowest unoccupied energy band allowing excited electrons to reach the energy level of the conduction bands.

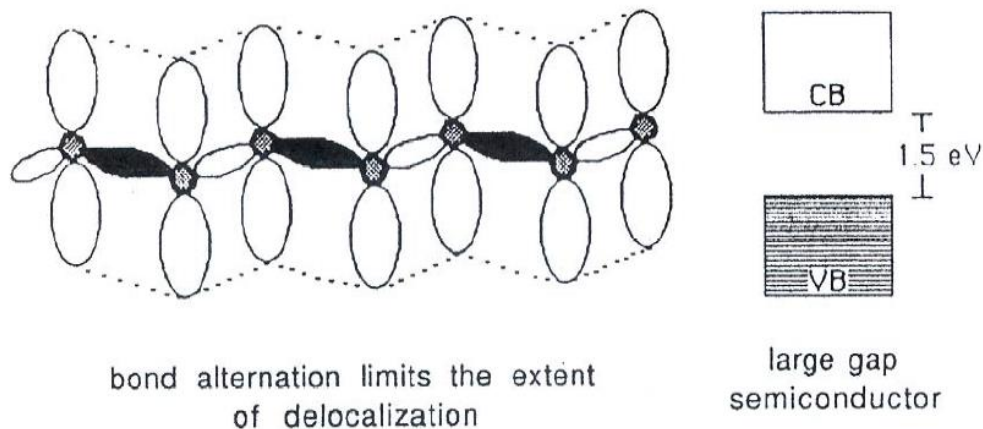


Figure 1.6: Unsaturated conjugated polymer of polyacetylene as example of semiconducting polymer.

In the solid state, polymer films are usually disordered with chains forming random coils. The π -system of the conjugated polymers makes the polymer straight and rigid but chemical defects or torsion can break of the conjugation along the chain. The charge is transported through rearrangement of the bonds known as *intra-chain transport* (see (a) in Figure 1.7) which is not as fast as in organic crystalline semiconductors. However, this bonds rearrangement is limited by movement of nuclei that are very slow compared to the electron rearrangement. Another mechanism of charge transport is hopping of charges between chain and around defects in the bulk and this is known as *inter-chain hopping* as demonstrated in the example in Figure 1.7 (b).

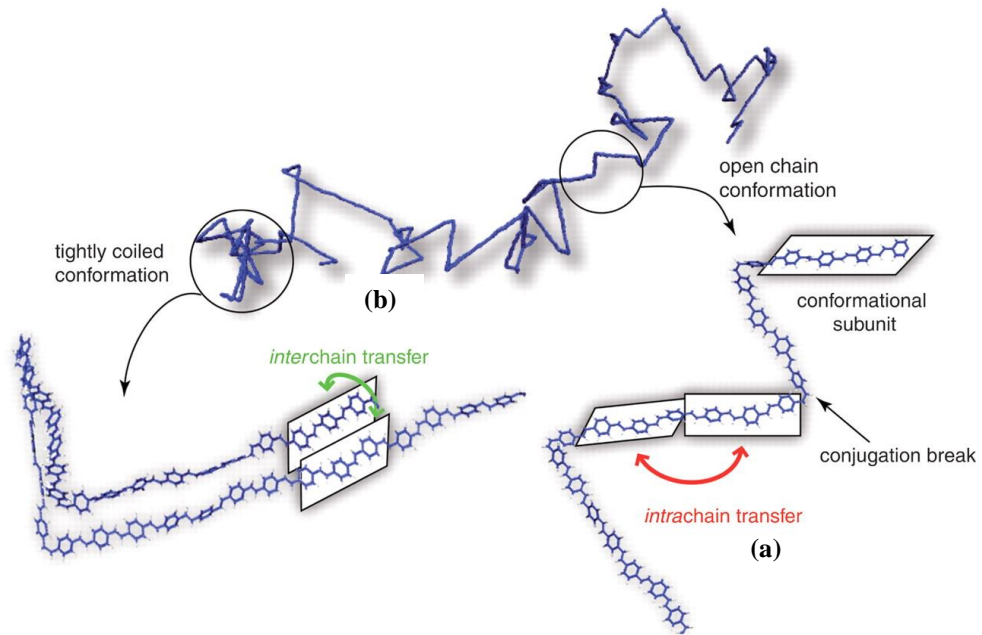


Figure 1.7: Example of transport of a polaron in a lightly doped film; (a) intra-chain transfer and (b) inter-chain transfer

A polaron is formed when a charge carrier deforms the surrounding lattice or polymer backbone and carries this deformation along with it under the influence of an external electric field. The polaron may be large or small; this depends on spatial extent of the polaron and when the spatial extension of the polaron is of the order of lattice constant, a small polaron is formed. When the polaron extends beyond the lattice constant a large polaron is formed. In heavily doped polymer films, the polarons interact from bands inside the band gap promoting transport of the charge carriers in the bulk. Highly conductive regions and poorly conducting regions are created due to inhomogeneity in doping level and morphology. According to Prigodin *et. al.*, [20] the doped conducting polymer systems can also be treated as metallic islands coupled into a network with twisted and tangled polymer chains as the schematic structure in Figure 1.8 shows. Even though the electronic conductivity is high in the metallic islands, the transport is limited as the regions outside the islands have poor conductivity [20].

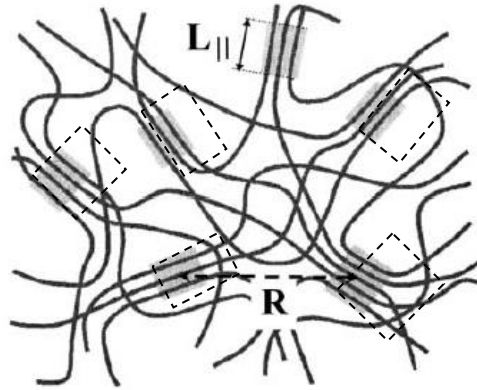


Figure 1.8: Charge transport in highly doped grains with a low concentration of conjugated polymers chains in between the metallic islands. The lines represent the polymers lines. Inside the islands, charges are delocalized and migrate easily, while charges need to hop between the islands (dash square marks) passing over the low conducting phases [20].

Principle of conduction

The method of conduction using band theory was initially applied to most conducting polymers. It was found that the polymer could more efficiently lower its energy to bond alteration via doping, hence making it similar to a higher energy gap semiconductor [21]. The importance of understanding the charge stored along the polymer chain and its effect is very useful in order to completely comprehend the conductivity of the polymer.

Polymers usually store charge in two ways. In an oxidation process, it could either localize the charge over a small section of the chain or lose an electron from one of the bonds [22]. The energy of the polymer can be reduced by the localization of charge that creates local distortion and an efficient change in geometry [23]. The generation of the local geometry increases its electron affinity, hence increasing the ability to accommodate newly formed charges. Reductive processes will also have similar

occurrence. The ability to reduce or oxidize is the main criteria as it is not lowering the stability of the polymer. The combination of a charge site and a free radical is known as a polaron [24]. Upon further oxidation the free radical of the polaron is removed, creating a new spinless effect called a bipolaron as shown in Fig.1.9.

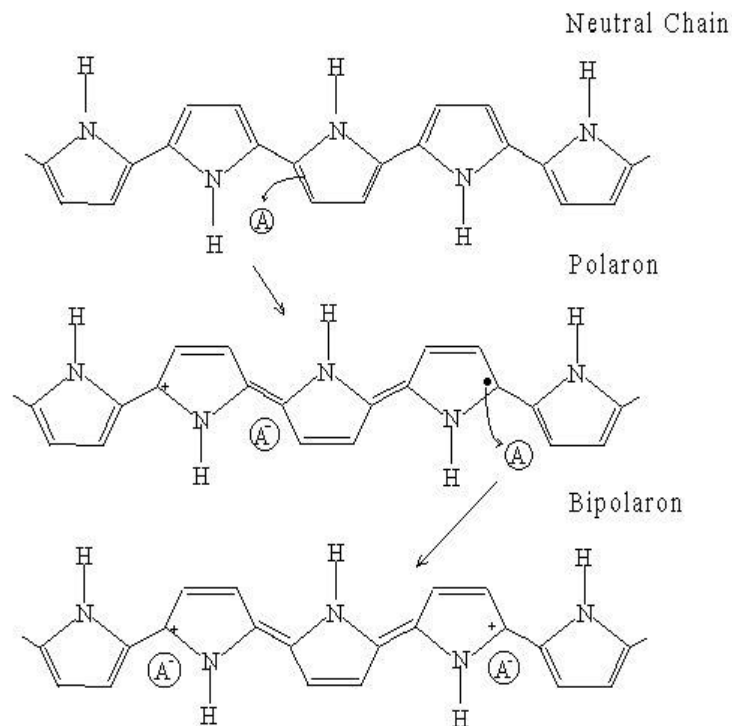
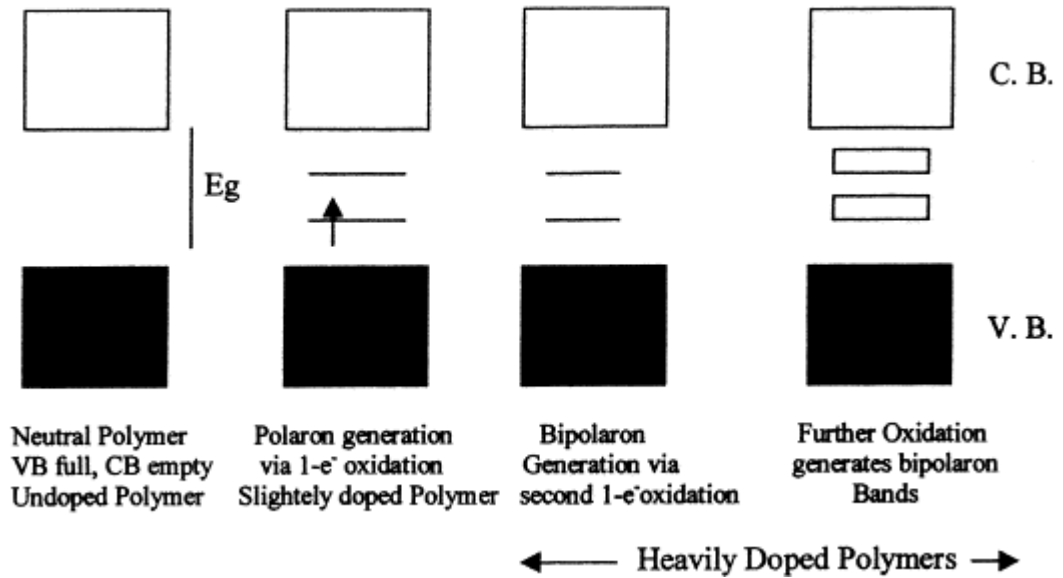


Figure 1.9: Formation of polaron and bipolaron shown in forms of band diagrams and chemical structure.

Heavily doped polymers conceived the conduction band close into producing partially filled bands that causes by the merging of the upper and the lower bipolaron bands therefore giving the polymer a metal-like conductivity. Charge transfer between the conducting domains can occur by thermally activated hopping or tunnelling [25-27].

Variable range hopping

One of the most important results in the study of disordered insulators is Mott's formula for the DC conductivity due to variable range hopping. Mott's variable range hopping theory, proposed in 1968, described the low temperature behaviour of the resistivity for strongly disordered systems where states are localized at 0K with finite electronic states at E_F . Considering an insulator at low temperatures, and imagining the electrons are all single particles in localized states. Consider there are two states located at distance R apart. The state on the left is at energy R_i and the state on the right is energy R_j . Suppose $R = R_j - R_i > 0$. An electron can hop from left to right by the absorption of a phonon with energy, E . Through a sequence of such hops it can conduct electricity [28]. It is thought that electrons will only hop to the nearest neighbouring states since the probability varies exponentially smaller with distance. However, a state which is further away might be closer in energy, and therefore exponentially easier to reach in temperature. The competition between these two different effects leads to variable range hopping [29].

When an electron that is in its localized electronic localized state, ψ hops to another one distance R away, where the electron wavefunction decays exponentially at a large distances (r) in a symmetrical potential:

$$\psi(r) \approx \exp\left(-\frac{r}{a}\right) \quad (1.1)$$

where a is its characteristic radius to measure localisation extent. The hopping probability between the two localized states centred at R_i and R_j depends on the probability for one electron to tunnel to the unoccupied state that depends on the overlapping of the wave functions of the two states and only happens if the overlap of the wave functions is finite. The overlapping integral of the two states is

$$\int \psi^*(r - R_i)\psi(r - R_j)dr \approx \exp(-R/a) \quad (1.2)$$

Where R_i, R_j are the locations of the states and $R = R_j - R_i$

Since the probability, P of a transition from R_i to R_j is proportional to the square of the overlap integral, we have the relation below:

$$P \propto \exp\left(-\frac{2R}{a}\right) \quad (1.3)$$

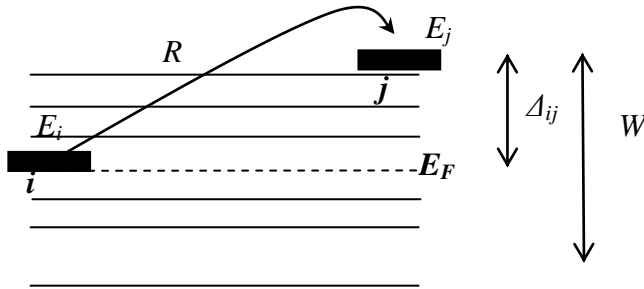


Figure 1.10: Showing the mechanism of hopping conduction. The localized electron can hop from site i with energy E_i to site j with energy E_j separated by the distance R .

Even when R is large enough to make the overlap integral very small, hopping from site i to j will still occur if the energy difference W is compensated for by absorption or emission of a phonon. Thus the probability for hopping is modulated with the rate of excitation of a phonon and the probability of finding a phonon with energy [30].

$$P = v_{ph} \exp(-|\Delta_{ij}|/k_B T) \exp(-2R/a) \quad (1.4)$$

Where $\Delta_{ij} = E_i - E_j$ and v_{ph} is the characteristic frequency of phonons

Assuming only a single site j is available within the distance R from the site i , provided that their energy difference is within Δ_{ij} . This implies that the number of electrons in the energy range W across E_F must be unity in a spherical volume with the radius R which leads to:

$$\frac{4\pi}{3} R^3 N(E_F) \Delta_{ij} \approx 1 \quad (1.5)$$

Where $N(E_F)$ is the density of state per unit volume at E_F . Substituting Eq. (1.5) into Eq. (1.4) for W yields:

$$P = v_{ph} \exp\left(\frac{3}{4\pi R^3 N(E_F) k_B T} - \frac{2R}{a}\right)$$

(1.6)

Maximizing and rearranging Eq. (1.6), we find

$$R = \left[\frac{9a}{8\pi N(E_F) k_B T} \right]^{-1/4} \quad (1.7)$$

Since the electrical conductivity increases in proportion to the transition probability, the temperature dependence on the conductivity $\sigma(T)$ can be expressed as:

$$\sigma(T) = \sigma_0 e^{-\left(\frac{T_0}{T}\right)^{1/4}} \quad (1.8)$$

where T_0 is the Mott's characteristic temperature and σ_0 the conductivity at room temperature. The key insight of Mott is that the conductance should be determined by optimizing the competition between the overlapping term $\exp(-2R/a)$, which favours short hops and the energy activation $(-\Delta_{ij}/k_B T)$, which favours long hops [30].

1.2 Polyaniline

Polyaniline was initially described as *aniline black*, in 1835 based on its formation after the outcome of the oxidation process [31]. Later on, uncertain analysis of the products acquired by the chemical oxidation of the aromatic amine was continued by Fritsche [32]. After over three decades of studies and research, in 1856, Perkin performed the oxidation of aniline using potassium dichromate as the oxidizing agent [33]. This resulted in the formation of a black precipitate which was probably a mixture of aniline black and polyaniline [32, 34].

Further to that, Perkin extracted a purple dye called mauveine. It was the first commercially synthesized dyestuff. A partially conductive substance was synthesized via the anodic oxidation of aniline in aqueous sulphuric acid by Letheby in 1862 at the college of the London Hospital. Later on, in 1896 pure aniline was subjected to further oxidation to obtain psuedomauveine, which implies that in the course of the oxidation of aniline a soluble protonated phenazinium structure would be formed. In the early twentieth century, organic chemists started to investigate the nature of ‘aniline black’ and its intermediate products [35]. Wilstatter (1907 and 1909) considered aniline black to be an eight-nuclei chain compound with an indamine structure. Providing an alternative view, Green and Woodhead proposed a linear octameric structure of the quinine-imines type in the para-position, for the product obtained by the chemical oxidation of aniline [36]. It was fairly recently (in the 1980’s) that interest in synthetic materials such as polyaniline picked up and its structure was identified [37].

Polyaniline is the most important industrial organic conducting polymer found today due to its ease of synthesis and processing, low cost and environmental stability. It also has two very attractive properties: intrinsic redox state and reversible doping/ dedoping of acid/base [38]. This material therefore has potential applications in the future such as microwave absorbing systems, super capacitors and batteries [39]. There has been a great deal of uncertainty and differing thoughts about the structure of PANI since the emerging interest in this material. The MacDiarmid's investigations in the 1980s resulted in the formulation of a proposed structure for polyaniline together with a modification of its classification based on the older beliefs.

Given that the nitrogen atoms in the polyaniline structures inhibit primary sites in the chain backbone, PANI exhibits much more complex properties and structure than most conductive polymers. These atoms play a key role in controlling the properties of the system since there are no continuous carbon-carbon chains. Polyaniline thus can take various forms, such as the reduced or oxidised form as illustrated in Fig 1.11 or salt form and therefore have different colours.



Figure 1.11: Redox forms of polyaniline.

Polyaniline can be considered to be a family of any of the following three polymers (depending on the oxidation state).

1) Leucoemeraldine

This is the reduced form and is also known as poly (paraphenyleneamine) and has the simplest backbone as illustrated in the figure below (Fig 1.12). The colour of this polymer ranges from white to light brown and is an insulator due to its unconjugated backbone. The polymer is unstable with respect to oxidation in air.

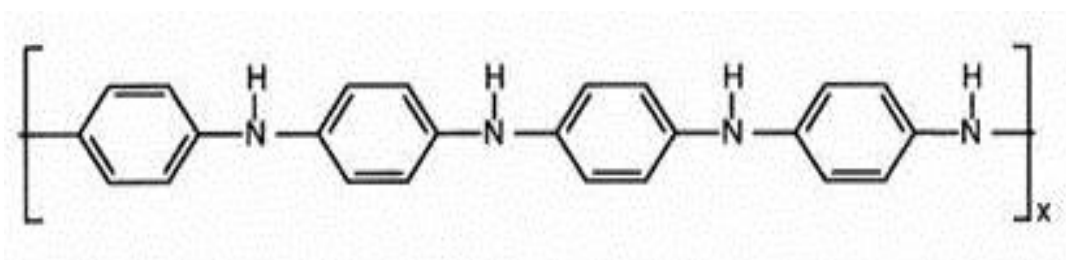


Figure 1.12: Structure of Leucoemeraldine as determine by Epstein et al. [40]

2) Pernigraniline

This is the fully oxidised form and is known as poly (paraphenyleneimine) where all the nitrogens are present in the quinonediimine form. This is illustrated in figure 1.13 below. It is difficult to synthesize in aqueous media due to the susceptibility of the quinoid sites in its structure to hydrolysis. The system is fully conjugated and thus is optically most interesting as it is strongly coloured. It is a weak semiconductor due to

the difficulty of delocalisation of any charge on the nitrogen atoms amongst other resonance structures.

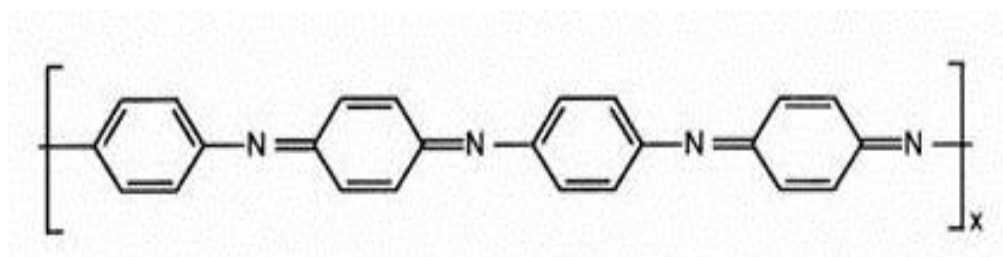


Figure 1.13: Structure of Pernigraniline as determined by Epstein et al. [40]

3) Emeraldine base

This polymer is also known as poly (paraphenylenamineimine) and refers to a 50% oxidised polymer as illustrated in the figure below (Fig. 1.14). The ring can have either a benzoid or quinoid structure as the nitrogen atom bridging the neighbouring phenyl rings can exist either as the oxidised or imines (-N=) form or as the reduced or amine (-NH-) form.

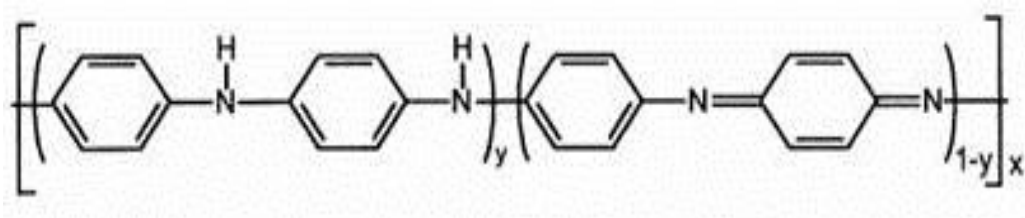


Figure 1.14: Structure of emeraldine base as determined by Epstein et al. [40]

PANI can thus be illustrated as having four benzene ring repeat units as shown in Fig 1.15

below:

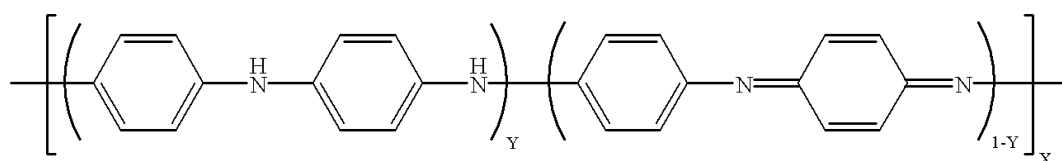


Figure 1.15: Structure of Polyaniline repeat unit as determined by Epstein et al. [40]

The electronic properties of polyaniline are governed by two distinct parameters: the oxidation level as described above and the protonation level. Thus it can be converted from an insulating state to a highly conductive one via necessary oxidation and protonation procedures [11]. Although the three oxidation states mentioned above result in polymers that are insulators, the emeraldine base when treated with acid of $\text{pH} < 3$ produces a salt form. This increases the electrical conductivity of the material by a factor in the region of 10^{11} [41]. The extent of protonation can be varied by controlling the pH of the acid used. Lower pH values cause higher levels of protonation. Maximum doping levels occur when half of the nitrogen sites on the chain are protonated [42].

There are two reasons why the transition to conductive behaviour that occurs with acid doping is extremely interesting. Firstly, the process of protonation does not alter the number of electrons on the chain. Secondly, the emeraldine base form of the polymer is not strictly conjugated i.e. alternation of the single and double bonding does not extend along the entire length of polymer repeat unit, as it does in the pernigraniline structure.

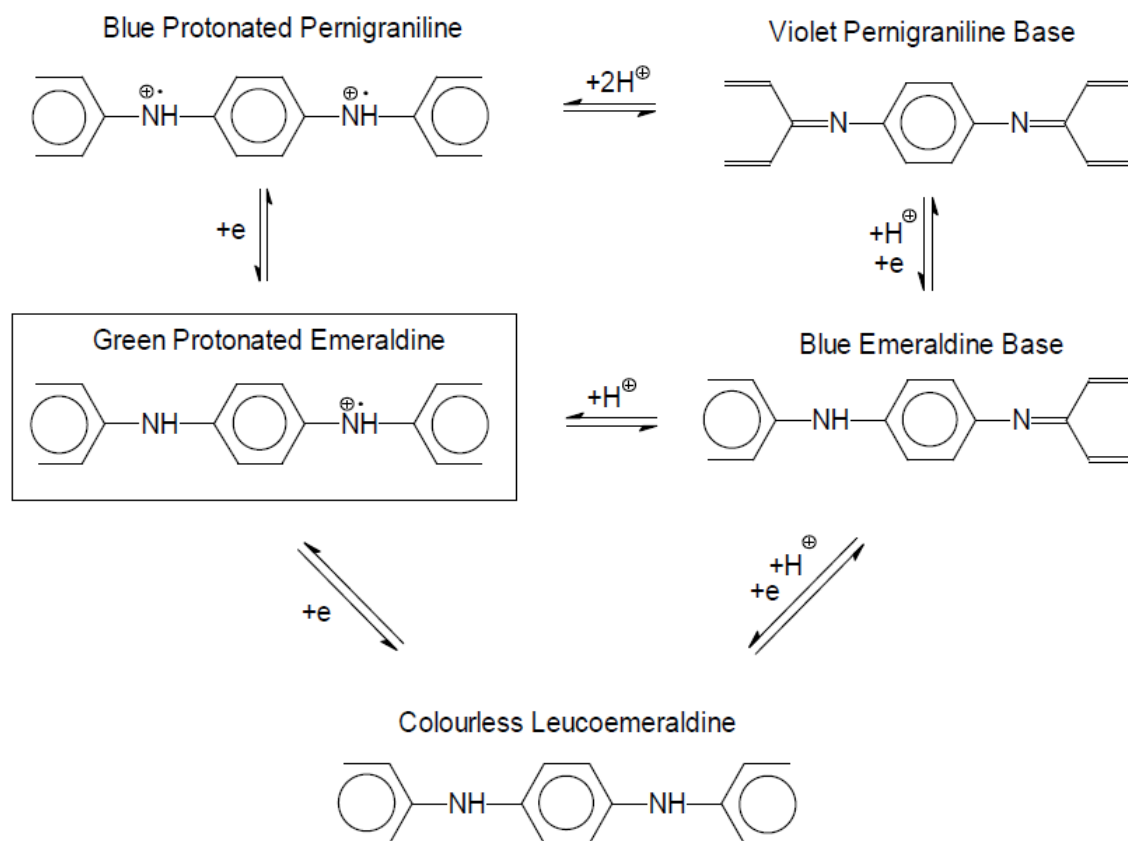


Figure 1.16: Doped and Undoped forms of polyaniline.

It is possible to completely or partly protonate the five forms of polyaniline with a protonic acid to produce the corresponding salt. In this process, either one or both nitrogen atoms in a repeat unit may be protonated, depending on the pH of the medium to which the polymer has been exposed. Different compounds can be formed according to differing oxidation and protonation levels (Fig. 1.16). Table 1.1 shows a list of their approximate compositions along with both names and colours.

Table 1-1: Various compositions of polyaniline

x	Name	Base form	Protonated form
1	Leucoemeraldine	Colourless	Pale Yellow
0.75	Protoemeraldine	Violet	Light Green
0.5	Emeraldine	Dark Blue	Green
0.25	Nigraniline	Blue-black	Blue
0	Pernigraniline	Violet	Purple

The possibility of the combination of charge and the delocalisation amongst the possible resonance forms of the structure causes the emeraldine salt to be a good electric conductor. There is strong visible absorption due to the conjugation. Treating protonated polyaniline with aqueous alkali results in de-protonation and the insulating emeraldine base form is recreated.

1.3 Motivation of Study

As electronic devices become denser and more complicated, research is increasingly finding a need to distribute circuit protection devices among all steps in a system. Earlier implementations would involve a single fuse/circuit breaker that would protect an entire system, but in today's systems, for example computerised machines, PCB currents are relatively small and subsystem protection might not re-act fast enough to prevent serious damage to an individual item in a system [43]. This inadequacy in the system provides motivation to produce a device with faster and better response time.

Conventional fuses maybe the designer's first choice, as they come in many different styles, sizes, melting times as well as fit nearly all application system [44]. However, these fuses protect mainly the primary side of power supply, the load and source. Semiconductor components also require protection on the load side of power supply but they require faster and smaller fuses that can be easily mounted are reliable and resettable with fast response time. Organic and polymeric materials have significant advantages over inorganic material as they are more flexible, have scalable dimensions, excellent mechanical strengths and amenability to processing onto many types of substrates [45]. Many of these promising materials exhibit useful charge transport mechanisms and their resistive switching behaviour can be utilised to produce a current limiting device with tuneable parameters.

Currently a product called Polymeric Positive Temperature Coefficient (PPTC) is available in the market which is a resettable over current protection device made of a polymer filled with a conductive material (carbon black).

In normal operation the device has a resistance that is much lower than the circuit in use where at this stage the conductive particles in the device form a low-resistance network in the polymer. However, if the temperature rises above the device's switching temperature, either from high current through the part or from an increase in the ambient temperature, the crystalline parts in the polymer melt and become amorphous (see Figure 1.17). The increase in volume during melting of the crystalline phase separates the conductive particles resulting in a large non-linear increase in the device's resistance. In response to an overcurrent condition, the device increases in resistance, and trips therefore reducing the current in the circuit to a minimum value that can be safely carried by any of the circuit elements. The tripping of the device happened when the PPTC device is heated internally due to power dissipated (I^2R) within the device. Upon cooling the device will recover to its original condition (low resistance), which is also sometimes referred to as a 'resettable fuse'.

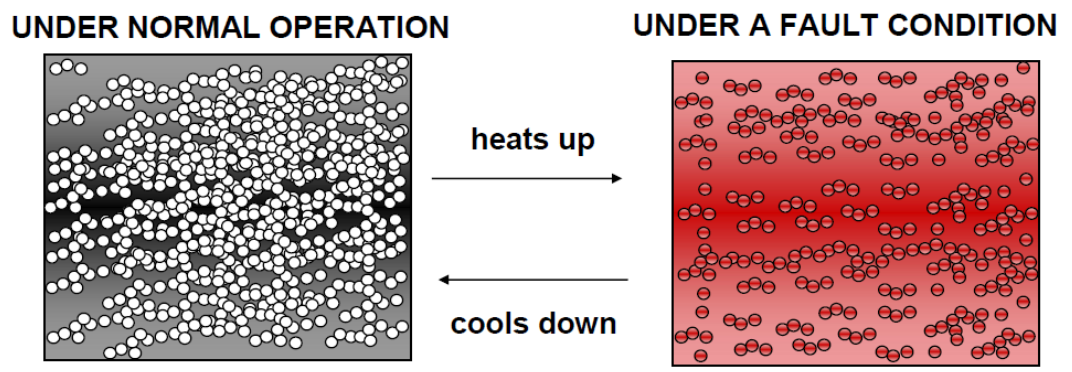


Figure 1.17: Principle operation of the Polymeric Positive Temperature Coefficient device.

The principle of operation of this device is based on an overall energy balance. Under normal operating conditions, the heat generated by the device and the heat lost by the device to the environment are balanced at a relatively low temperature as shown in point 1 in Figure 1.18. If the current passing through the device is increased while the ambient temperature is kept constant, the temperature of the device increases. Further increases in either current, ambient temperature or both cases will cause the device to reach temperature where the resistance rapidly increases as illustrated in point 3 (see Figure 1.18). Any further increase in current or ambient temperature will cause the device to generate heat at a rate greater than the rate at which heat can be dissipated thus causing the device to heat up rapidly. At this stage a very large resistance occurs for a very small change in temperature which is between points 3 and 4 in Figure 1.18. This is the normal operating region for a device in the tripped state. The large change in resistance causes a corresponding decrease in the current flowing in the circuit. This relation holds until the device resistance reaches the upper knees of the curve (point 4 of Figure 1.18).

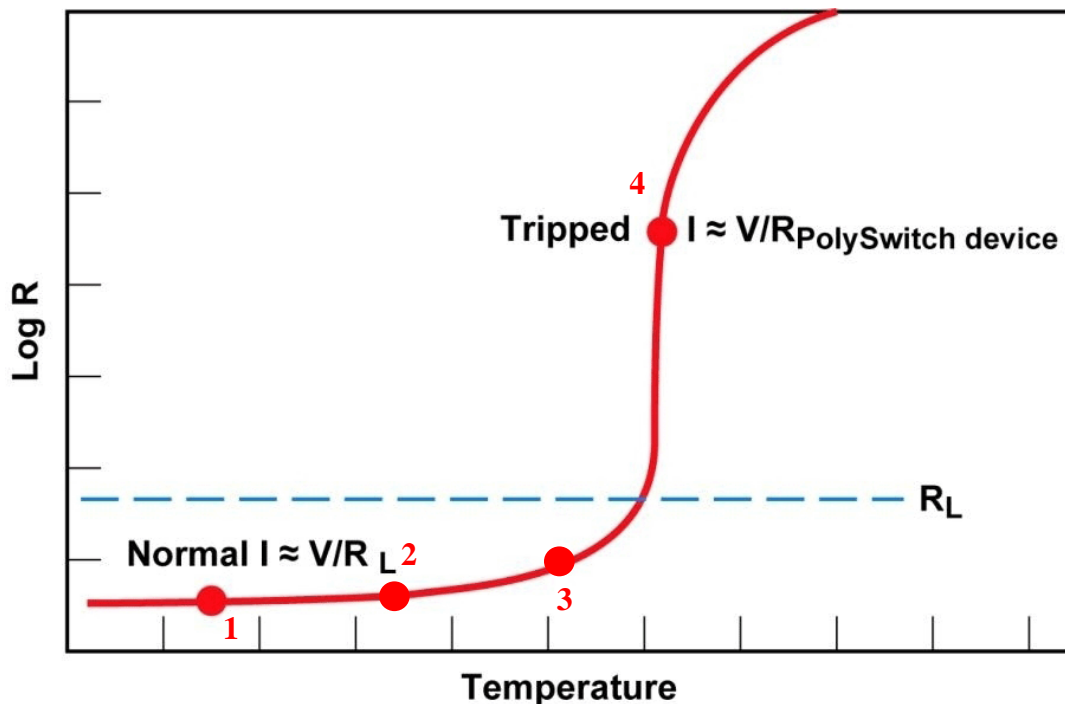


Figure 1.18: Example of operating curve for PPTC device.

As long as the applied voltage remains at this level, the device will remain in the tripped state (which means the device will remain latched in its protective state). Once the power or applied voltage is removed the device will reset. Limitations of this device include that it is not suitable for low power systems because they require very fast switching while this particular device only allows switching due to severe over-current in seconds. Lower power applications mostly require less response time to overcurrent protection. The existing material used also heats up quickly which shows a high possibility to damage or degradation in the short term.

This research aims at developing current limiting devices based on intrinsic conducting polymers to protect overcurrent in electronic applications. Studies performed used intrinsic conducting polymer as the active material due to them being easy to obtain and cheap which is suitable for commercial production. The objective is to investigate device performance and switching behaviour when using organic material in the current limiter.

1.4 Thesis Outline

The overall purpose of this thesis is to produce novel intrinsic current limiting device and understand the behaviour of the devices fabricated. Chapter 2 provides the background to the areas we will investigate in the subsequent chapters, including the generic methods of fabrication and electrode modification for the devices. Chapter 3 details the actual experimental methods and equipment used for the experimental results presented in Chapter 4.

Chapter 4 is divided into three subsections which cover different aspects of characterization of the samples. In section 4.1 we investigate the current-voltage behaviour of the current limiting device polymerised on gold substrates in different environments. The electronic transport mechanism is identified by performing temperature dependent measurements. We also explored the morphology that is responsible for the current limiting behaviour of the device.

The effect of self-assembled monolayer effect on current limiting is investigated in section 4.2. The drop shape analysis method was employed to characterise good monolayer formation. Here we use the contact resistance measurement technique to investigate if the contact near the polymer has any influence on the overall performance of the current limiting device. Devices current-voltage measurements in different humidity levels have also been covered in this section. Samples with different dopants are fabricated and characterised in section 4.3, using five other different dopants for polyaniline with our standard methanesulfonic acid dopant as reference sample. We will investigate how the molecular structure of the dopant influences the moisture contents of the samples and if this affects the efficiency and other performance parameters related to current limiting device performance. The weight loss due to annealing is

investigated for the six different dopants and performed using a thermogravimetric analysis and a differential scanning calorimetry. We also consider the stability of the current limiting device with repeated electrical measurements. We investigate the morphology of all six devices using a scanning electron microscope. Finally, in Chapter 5 we summarise and conclude the findings from the experimental work carried out in Chapter 4. Potential improvements are highlighted along with how these can be realised through future work in Chapter 6.

Chapter 2 DEVICE FABRICATION

2.1 Device Schematic

Polyaniline was deposited on gold electrode deposited on ceramic substrate (Tyco Electronics) employing MSA (Aldrich, 99.5%) as electrolyte medium. Figure 2.1 illustrates the schematic of the substrate used in all the procedures of the research.

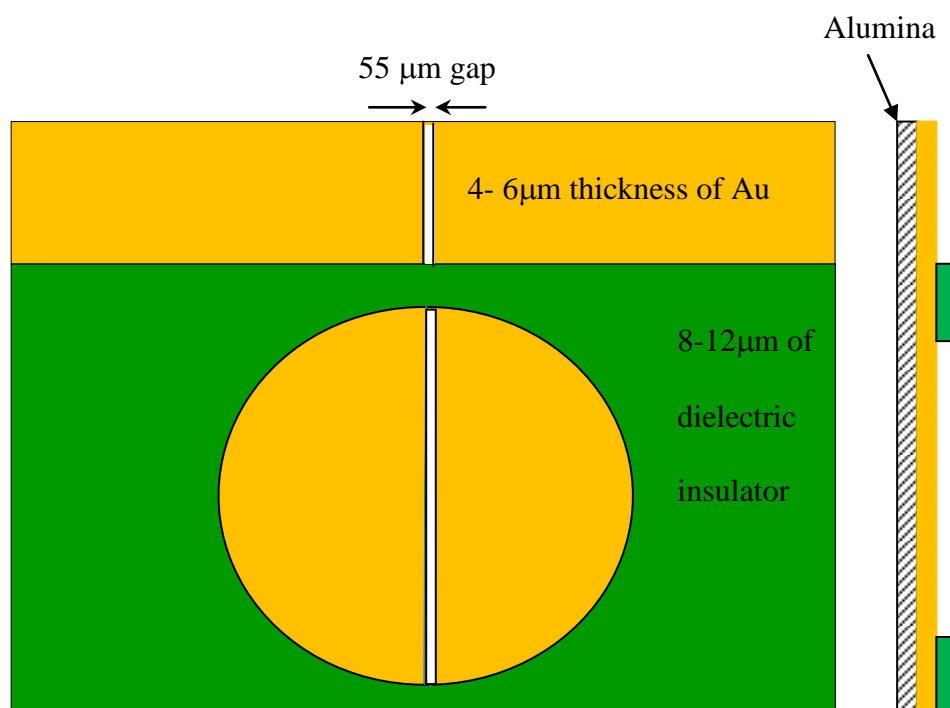


Figure 2.1: Illustration of the specification for the substrate used on alumina substrate.

A standard three-electrode setup (see Figure 2.2) with platinum (Pt) wire and Ag/AgCl as counter electrode (CE) and reference electrodes (RE), respectively, were used together with the gold as the working electrode (WE). The Pt wire thickness was 0.5 mm and the distance between the electrodes were approximately 15 mm.

2.2 Polymerisation of Polyaniline Methanesulfonic Acid (MSA)

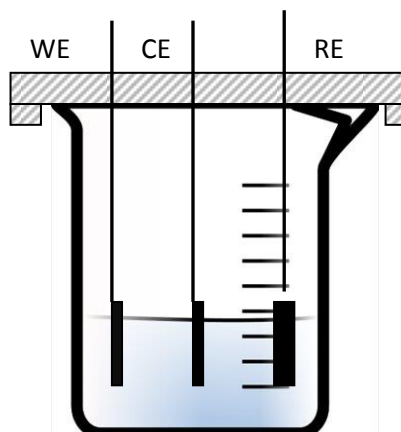


Figure 2.2: The standard electrochemical set-up employed in the experiment

The electrolyte solution of 200 mL (2.0 M MSA, 0.5 M aniline in deionised water) was introduced into a beaker with a plastic screw lid for electropolymerization. Using an electrochemical analyser (BiStat 3200) electropolymerization was performed potentiostatically at 0.85V vs.Ag/AgCl. A green colour PANI-MSA film was deposited by performing electrolysis for approximately 55 seconds. The film was washed in deionised water and kept in an air tight container for future use. The resistance of the device was measured after the device was rinsed in deionised water. Samples are then characterised by means of I-V curve. Results will be discussed in the following chapter.

2.3 Self-Assembled Monolayer (SAM) Modified Devices

Self-Assembly Monolayers (SAM's) are highly ordered molecular assemblies formed by chemisorptions and self-organisation of long chain molecules on the surface of noble metals. Over the years the mechanism has been extensively studied and explained [46]. A simple way of creating surfaces that have virtually any desired chemistry is by aplacing gold substrate into a millimolar solution of alkanethiol solution in ethanol. It is found that a typical alkanethiol monolayer forms a $(\sqrt{3} \times \sqrt{3}) R 30^\circ$ structure on gold with the thiol chains tilted approximately 30° from the surface normal. The structure of the monolayer usually depends on the chemistry of the chain. An alkanethiol contains 3 important parts, a sulphur terminal to attach to the metal surface, a spacer chain and a functional head group as shown in Figure 2.3 [47]. The head group can be designed to provide any desired surface chemistry , binding capacity or property.

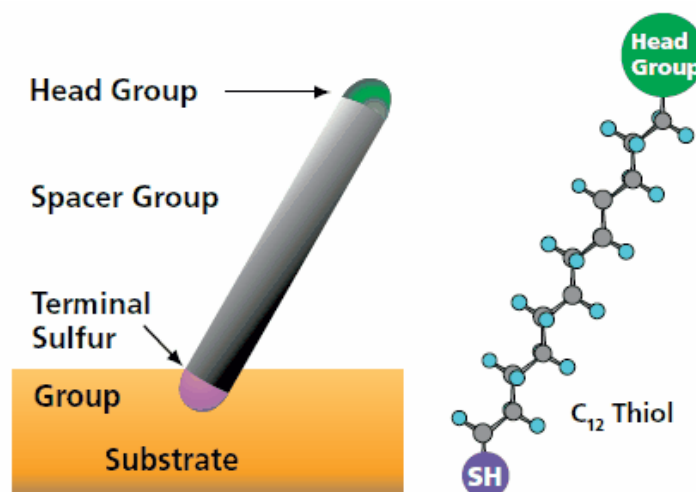


Figure 2.3: A typical self-assembling surfactant molecule consisting of three parts: surface group, alkyl or derivatized alkyl group, and surface-active head group [48].

Self assembling monolayer formation is a single-layer of molecules on a substrate in which the molecules exhibit a high degree of orientation, ordering, and packing as

illustrated in Figure 2.4. It is generally believed that formation of the SAMs on gold substrate involves two steps, first being the chemical interaction (chemisorptions) between the head group (-SH) and the gold substrate, and secondly aliphatic chain reorganization [49].

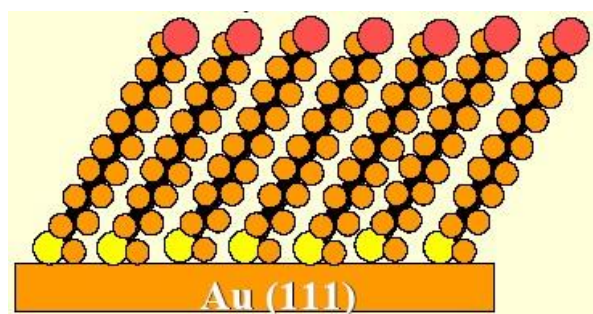


Figure 2.4: Illustration of self-assembly of DDT on gold substrate [48].

SAM on gold have been extensively studied for their interfacial characterisation for example adhesion, corrosion, tribology and wettability [50]. Gold is chosen as the substrate as it is widely studied in the literature, easy to obtain, straightforward to prepare, easy to pattern, and gold is an inert material which is not easily oxidised and does not react with most chemicals. The most common procedure for preparing SAM on gold is immersion of a freshly clean substrate into a dilute ethanolic solution of thiols at room temperature. Dense coverage of adsorbates can be obtained very quickly from mM of solutions in minutes; however a slow reorganization process requires time on the order of hours to maximize the density of molecules and at the same time reducing defects in SAM. There are a few factors that can be considered for this experiment to ensure the good structure of SAM result. Solvent is one of the factors that needs to be looked at and the most commonly used in preparing SAMs is ethanol as it solvates in many types of alkanethiols with different chain lengths, is cheap to obtain, has low

toxicity and is easily available in high purity [51]. Some studies also suggest that SAM formed from solutions of thiols in other solvents are less organised than SAM with ethanol [52]. Pure ethanol is used to ensure successful assembly. The oxygen during the formation of SAM must also be minimized as it will create defects. It is necessary to reduce the head space above the solution and backfill the space with an inert gas, such as argon to improve the reproducibility of the materials properties of SAM [53]. Any container size used can only be filled halfway to reduce head space above solution. Cleanliness is another important factor to think about during the SAM preparation. Samples, containers and all equipment used to handle the procedure will need careful cleaning, preferably with ethanol. Containers that can be easily sealed are a good option and each substrate used to be placed in a separate container to avoid overlapping. Concentration and immersion time are also essential factors, where are inversely related to each other. Solutions with low thiol concentration required longer immersion time [54]. Varying assembly times have been discussed in the literature, but if a well assembled monolayer is desired the recommended time is between 24 to 48 hours [55]. In general, longer assembly times tend to result in better packed monolayers [56].

An organosulfur compound, 1-dodecanthiol (DDT), $C_{12}H_{26}S$ is the material chosen for this experiment. DDT has been chosen not only because it has straight chain alkanethiols with relatively simple head groups but also medium length carbon chains that improves its solubility in ethanol and stability in the SAM procedure. It has been reported for straight chain alkanethiols that a chain length more than 10 carbons is required to form an ordered monolayer [52].

The self-assembled monolayers are formed simply by immersing the gold substrate into a solution of surface active material (see Figure 2.5). DDT self-assembled monolayers

are prepared by immersing the substrates in 1mM DDT ethanolic solutions for 24 to 48 hours

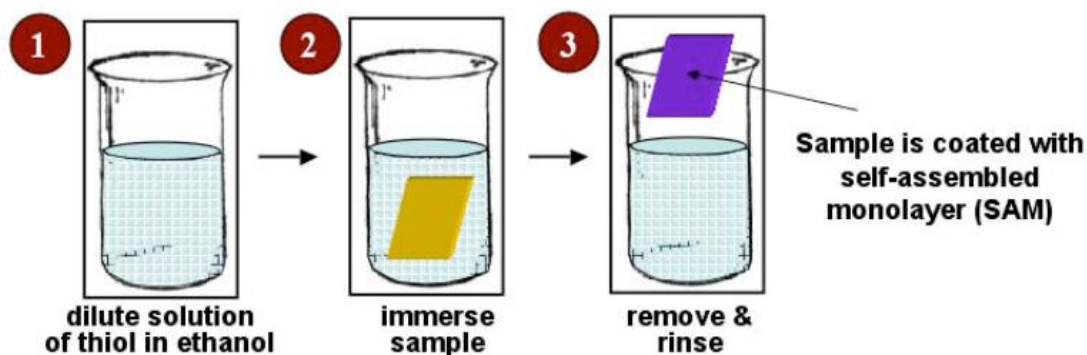


Figure 2.5: Schematic of the self-assembly set-up in the laboratory [46].

Over time, as the layer continues to form, van der Waals forces between the hydrocarbon chains help pack the molecules into a well-ordered, crystalline layer. During this ordering phase, contaminants are displaced, solvents are expelled from the monolayer, and defects are reduced so that the layers become more ordered and well packed. The mechanics of the formation of SAM from its initial stage to complete formation is illustrated in Figure 2.6. Initially alkanethiols come down onto the gold surface. As more alkanethiols come to the surface, the layer begins to organize and pack into an ordered monolayer. This self-assembly process occurs over minutes to hours.

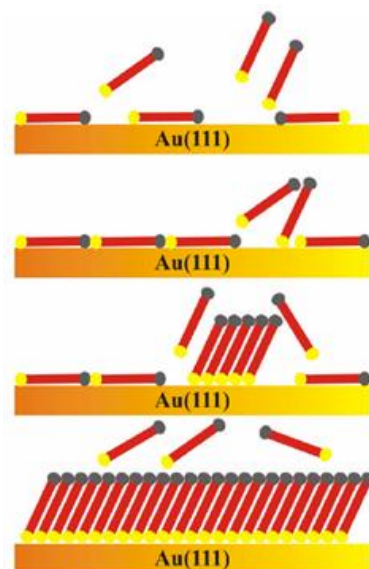


Figure 2.6: Schematic representation of the self-assembly process.

After the formation of SAMs, the gold substrates were rinsed with a copious amount of ethanol to remove the weakly absorbed species and this was followed with de-ionized water, and finally dried using a stream of argon gas. This procedure was repeated for different solution concentrations and immersion.

Chapter 3 DEVICE AND MATERIALS

CHARACTERIZATION

3.1 Cyclic Voltammetry

Cyclic voltammetry is the most popular technique that has been used for getting both qualitative and quantitative information on the electrochemical reactions. The usefulness of cyclic voltammetry is due to its ability to rapidly provide significant information on the thermodynamics of the redox processes, on the kinetics of heterogeneous electron-transfer reactions and on adsorption or chemical reaction processes [57]. The first experiment performed in electrochemical activity is usually cyclic voltammetry as it offers fast location of redox potentials of the electroactive species, and potential switching information on the effect of media upon the redox process [58]. Cyclic voltammetry involves scanning linearly the voltage of the stationary working electrode using a triangular shaped potential waveform (see Figure 3.1)

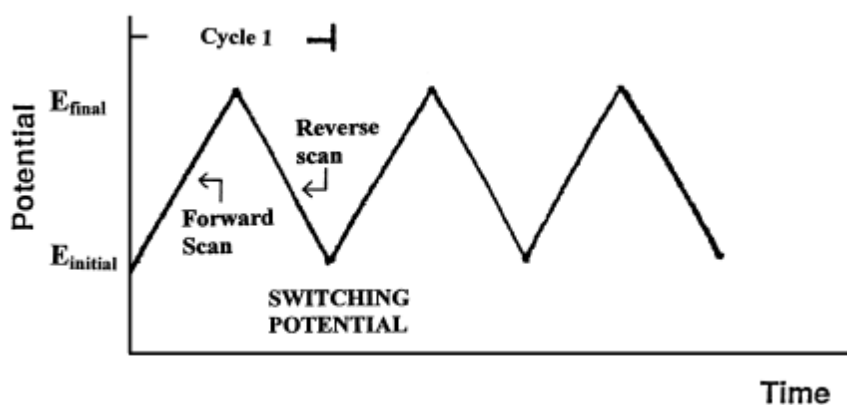


Figure 3.1: Typical excitation signal for cyclic voltammetry, a triangular potential switching potential at E_{initial} and E_{final} versus reference electrode

Single or multiple cycles can be performed depending on the information sought. The potentiostat measures the current resulting from the applied potential during the scan sweep. The result consists of current versus potential which is a complicated, time-dependent function of a large number of chemical and physical parameters or also termed a cyclic voltammogram [59]. The expected response of the reversible redox couple during a single potential cycle is illustrated in Figure 3.2. The oxidized form O is assumed to be present initially. Starting from a value where no reduction happens, a negative value potential scan should be chosen for the first half-cycle. As the applied potential reaches the initial potential for the redox process, a cathodic current starts to rise, until a peak is approached. After crossing the potential region in which the reduction process takes place, the direction of the sweep is reversed. R molecules which are generated from the forward half-cycle are reoxidized and back to O during the reverse scan. The formation of the diffusion layer near the electrode surface forms the characteristic peaks in the cyclic voltammogram [60]. Figure 3.2 shows four different concentration gradients for the reactant and results at varied times corresponding to (a) the initial voltage, (b) and (d) the coupling formal potential during forward and reverse scans respectively and (c) to the achievement of a zero reactant surface concentration.

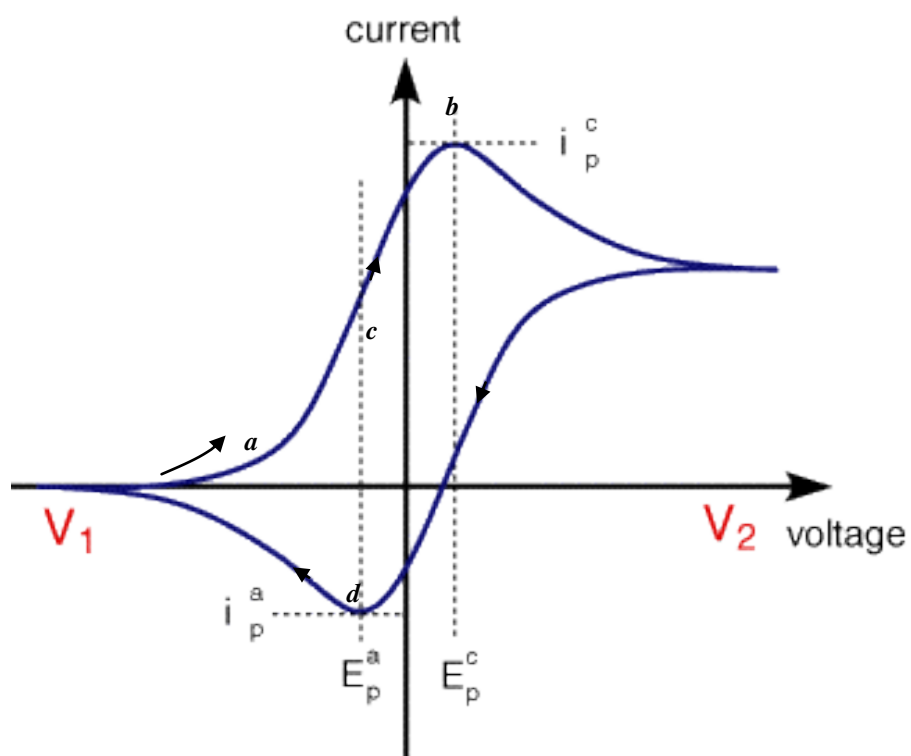


Figure 3.2: Typical example of a cyclic voltammogram for a reversible redox process [59].

3.1.1 Cyclic Voltammogram

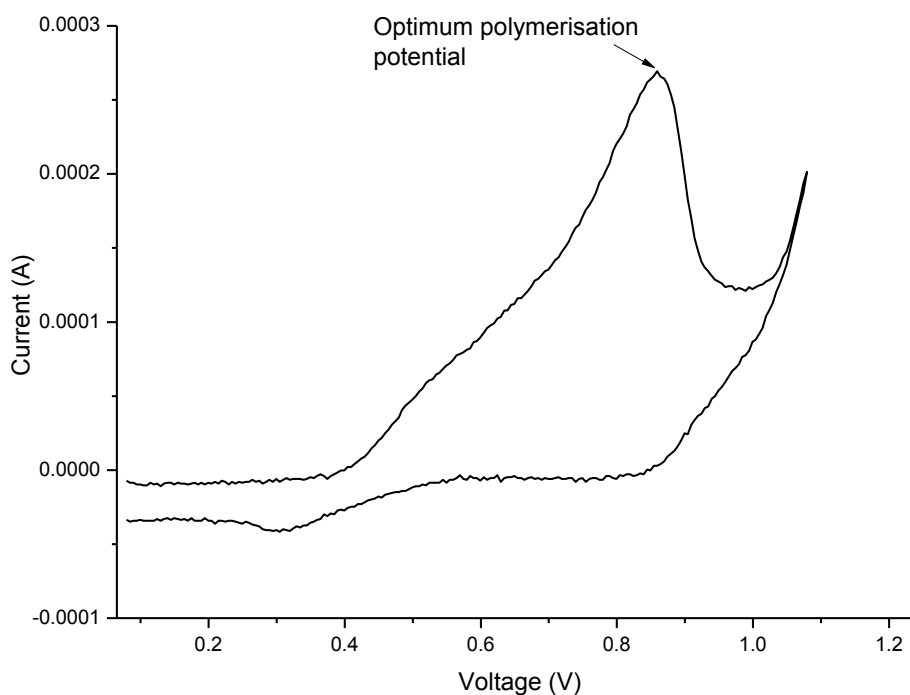


Figure 3.3: Cyclic voltammogram of PANI-MSA with potential vs Ag/AgCl reference electrode.

It is important to understand that from the cyclic voltammogram in Fig.3.3, oxidation of PANI took place during the ascending region of the peak. An increase in the linearity in PANI chains that promote the diffusion of electrons along the chain will then help to understand the conductivity of PANI [61]. The maximum value obtained from the peak is ~ 0.85 V and this value is then used in the chronoamperometry method for electrochemical polymerisation of polyaniline.

3.1.2 Potentiostatic method

The potentiostatic technique of electrochemical polymerization is characterized by pronounced changes in the current i.e. polymerization rate, and during polymerization the polymer obtained is in its doped form [62]. It was observed that the potentiostatic method could be useful in obtaining polyaniline films [63]. Many other researches have also used the potentiostatic technique to obtain polyaniline electrochemically [64-66]. The basic principle of the potentiostat in the experimental setup has been explained by Hickling when he first built the first three electrode potentiostat [67]. This potentiostat automatically controls the cell potential using the third electrode; the reference electrode. This principle remains the same today [68]. The basic potentiostat schematic is shown in Fig 3.4

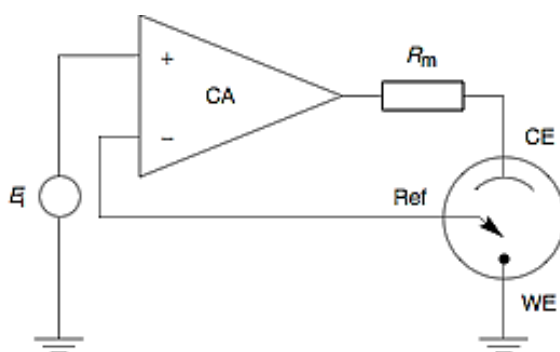


Figure 3.4: Basic principle of potentiostat [69].

A potentiostat measures the potential difference between the working electrode and the reference electrode, applies the current through the counter electrode and measures the current as IR drop over a resistor in series R_m . The control amplifier, CA is responsible for keeping the voltage between the working electrode and the reference electrode as close as possible to the input source E_i , which is also a feedback system. It adjusts its output automatically to control the cell's current so that the equality condition is satisfied.

3.2 Contact Angle Measurements

A contact angle can be measured by producing a drop of liquid on a solid. Contact angle is the angle formed between the solid/liquid (*sl*) interface as well as the liquid/vapor (*lv*) interface. The most common method for measurement involves looking at the profile of the drop and measuring two-dimensionally the angle formed between the solid and the drop profile with the vertex at the three-phase line as shown in Figure 3.5. The basic law determining the equilibrium shape of a liquid drop on a surface was formulated by Thomas Young in 1807. The interaction between the forces of cohesion, adhesion and surface energy measurement can be described by Young's equation:

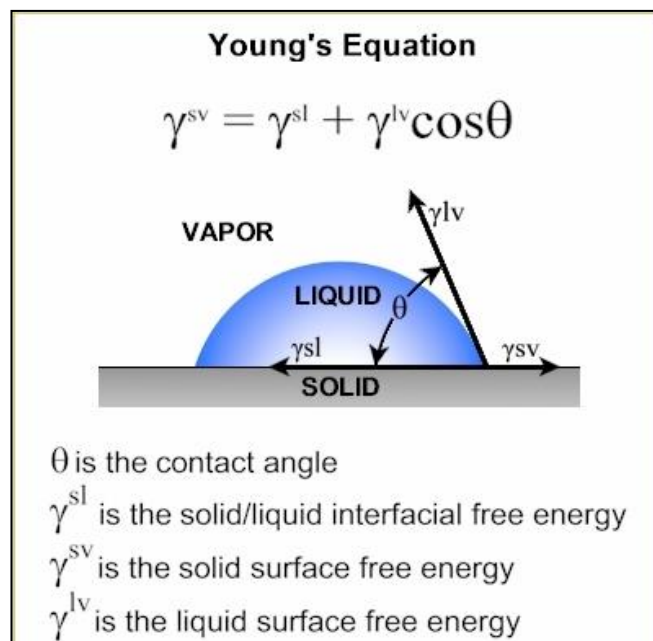
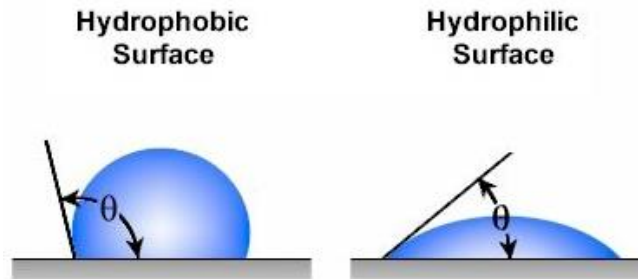


Figure 3.5: The three- phase contact angle θ is the angle measured between the liquid and the solid by drawing a tangent to the drop profile at the contact line.

Solid surfaces having contact angles with a water drop below 90° are considered hydrophilic, while those with contact angles above 90° are hydrophobic. Contact angles below 90° indicate good wetting, while contact angles above 90° indicate poor wetting.

Figure 3.6 illustrates and summarises the relationship between hydrophilic and hydrophobic surfaces to all the parameters that can be obtained from the drop shape analysis measurement.



Surface Criteria	Hydrophobic	Hydrophilic
Contact Angle	High	Low
Adhesiveness	Poor	Good
Wettability	Poor	Good
Solid surface free energy	Low	High

Figure 3.6: Hydrophobic and hydrophilic surfaces criteria.

3.2.1 Types of Contact Angle Measurements

Static contact angle is the most common type of measurement. A single reading on a static sessile drop shortly after its creation is captured when a thermodynamic equilibrium is reached between solid, liquid, and gas (all three phases). Static contact angle measurements provide valuable information about the properties of the surface. Any contact angle instrument can be used to capture the static contact angle.

Static contact angle is often used to measure cleanliness. Organic contaminants will prevent wetting and result in higher contact angles on hydrophilic surfaces. As a surface is cleaned and treated to remove contaminants the contact angle typically will decrease

as wetting improves and surface energy increases. This method is more likely to be suitable for measuring the results of semiconductor fabrication products after etching, passivation, ultrasonic agitation or other surface that has been treated to ensure that it is very clean, and also a very accurate qualitative measure towards the effect of resins, primers, and oxidation, annealing and polishing. In this case the surface that has been absorbed with other chemicals might not be the optimum surface to use this method.

Another commonly used method is the tilting plate method to measure the contact angle on both the right and left side of a sessile drop while the substrate is being inclined typically from 0° to 90° . Gravity causes the contact angle on the downhill side to increase while the contact angle on the uphill side decreases at the stage of where the substrate placed is inclined. These contact angles are referred to advancing and receding angles. The difference between advancing and receding contact angle is the contact angle hysteresis. The drop might roll off the solid as wetting occurs at the roll-off angle, so the last valid readings are measured and normally represent the advancing and receding contact angles. The solid can tilt all the way to 90° without the drop being released on some surfaces. The final left and right contact angles are used [70]. Figure 3.7 illustrates a sessile drop as the solid is inclined.

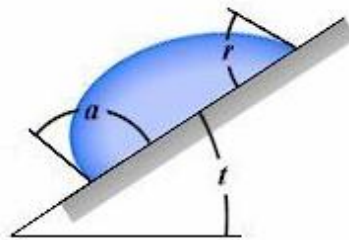


Figure 3.7: Advancing and receding contact angles by tilting base method. The inclined plate method; a- is the advancing angle, r- correspond the receding angle and t-is the tilting angle.

There are also other ways to measure advancing and receding contact angles especially suitable for surfaces with imperfections such as roughness and heterogeneity. This approach requires adding volume to the drop dynamically to the maximum volume permitted without displacement of the three-phase line. The resulting maximum possible contact angle is referred to as the advancing angle. Volume is then removed from the drop. When the maximum volume that can be removed without reducing the three-phase line is reached, the resulting contact angle is measured. This angle is the receding angle. The average of the difference between the advancing and receding angles is called the hysteresis and it characterizes surface topology. It can help quantify contamination, surface chemical heterogeneity, and the effect of surface treatments, surfactants and other solutes [71]. Figure 3.8 shows the sessile drop method used to measure the advancing and receding contact angles [72].

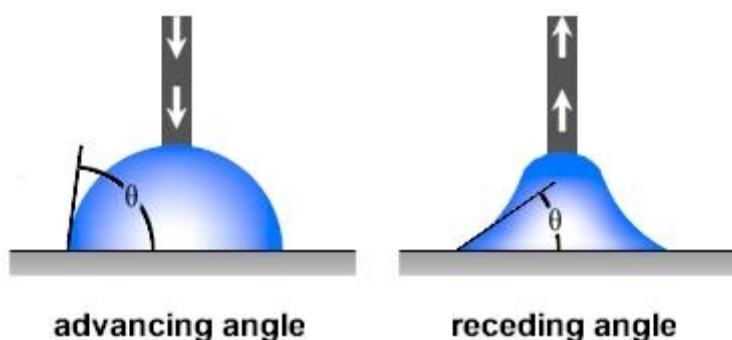


Figure 3.8: Contact angle changes when increasing droplet volume and contracting it, where advancing angle must always be larger than receding angle.

Contact angle measurement for the samples was performed to understand the characteristics of the surface of the SAM surface on gold. Drop shape analysis is a convenient way to measure the advancing and receding contact angles, thereby determining surface energy [53]. Figure 3.9 is the apparatus used to measure the contact

angle measurement using the Krüss Drop Shape Analysis (DSA10) equipped with a CCD camera. The liquid used for this method is deionised water.

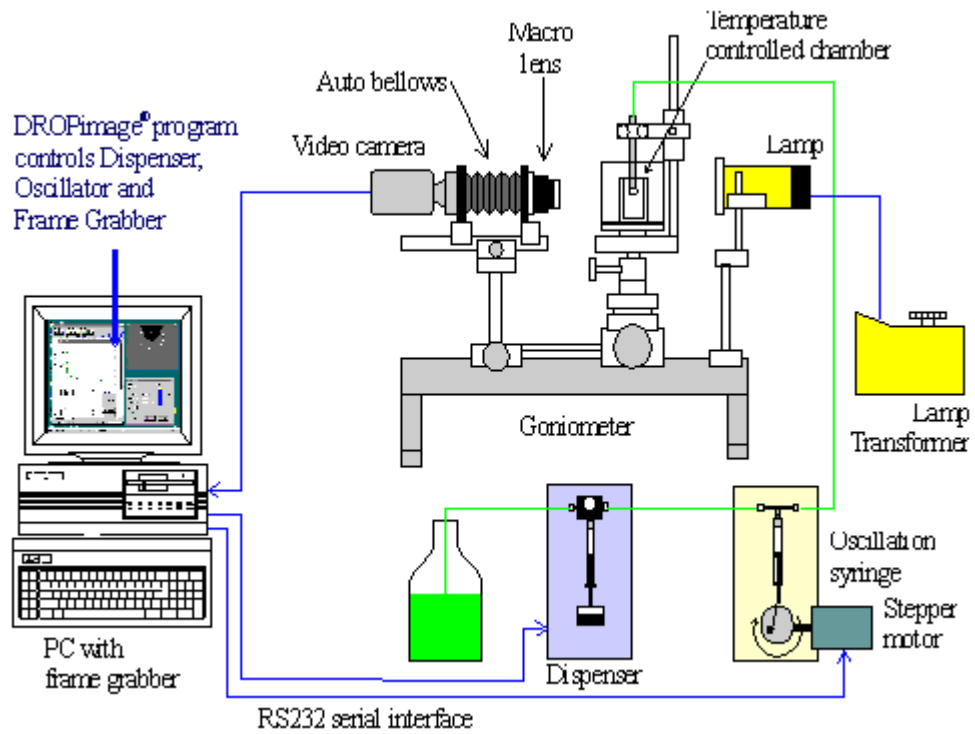


Figure 3.9: Apparatus set-up used to measure drop shape to obtain contact angles.

3.2.1 Polymerisation of PANI-MSA on Gold Containing Self-Assembled Monolayer of 1-Dodecanethiol (DDT).

3.2.1.1 Contact Angle Measurements

Gold substrates were immersed into the DDT ethanolic solution with three different concentrations, 1mM, 5mM and 10mM for 24 hours and repeated for immersion times of 48 and 72 hours. Nine samples were generated from this experiment and characterized using drop shape analysis to understand the surface properties. Sessile drop experiments were performed by Kruss DSA10 to determine the advancing and receding contact angles. Temperature and relative humidity were maintained at $21\pm 0.5^{\circ}\text{C}$ and mainly independent of the central air conditioning unit in the laboratory.

Below are the individual descriptions for each sample that have been produced:

- *Sample 7:* SAM in 1mM DDT ethanolic solution for 24 hours
- *Sample 8:* SAM in 5mM DDT ethanolic solution for 24 hours
- *Sample 9:* SAM in 10mM DDT ethanolic solution for 24 hours
- *Sample 10:* SAM in 1mM DDT ethanolic solution for 48 hours
- *Sample 11:* SAM in 5mM DDT ethanolic solution for 48 hours
- *Sample 12:* SAM in 10mM DDT ethanolic solution for 48 hours
- *Sample 13:* SAM in 1mM DDT ethanolic solution for 72 hours
- *Sample 14:* SAM in 5mM DDT ethanolic solution for 72hours
- *Sample 15:* SAM in 10mM DDT ethanolic solution for 72 hours

Results are presented as advancing and receding measurement in graphical forms in Fig. 3.10 and it can be observed that the 1-dodecanethiol on gold by means of SAM has produced a hydrophobic surface.

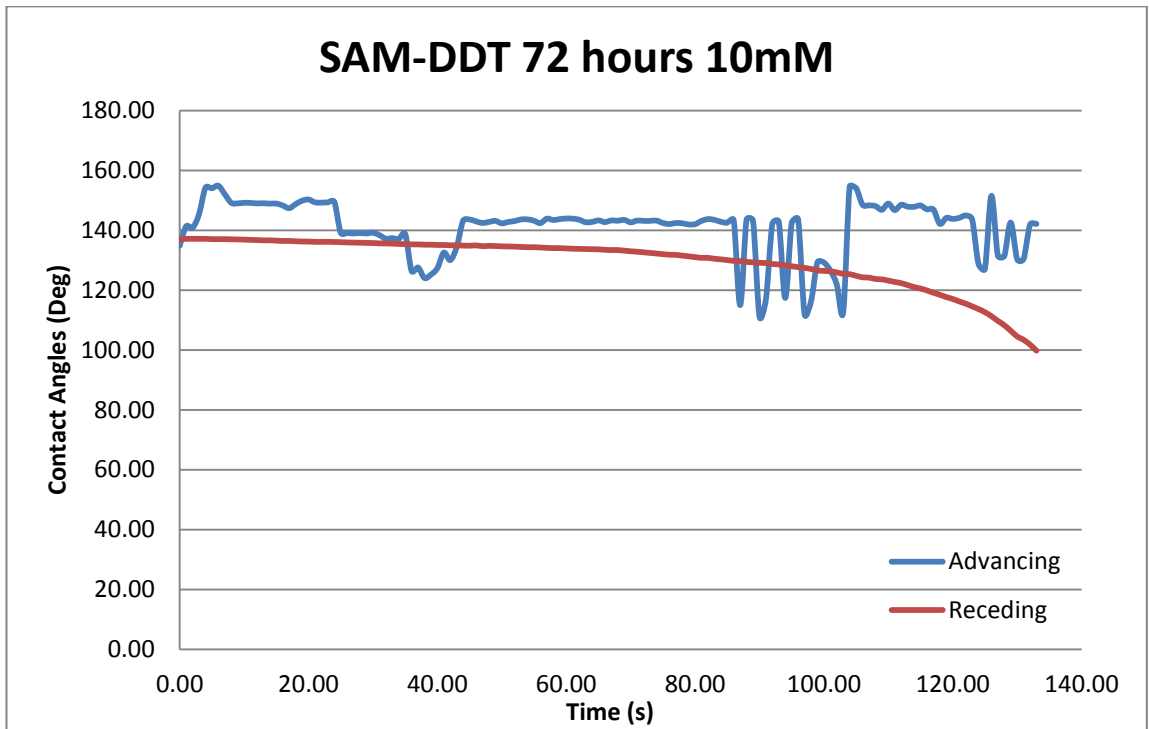
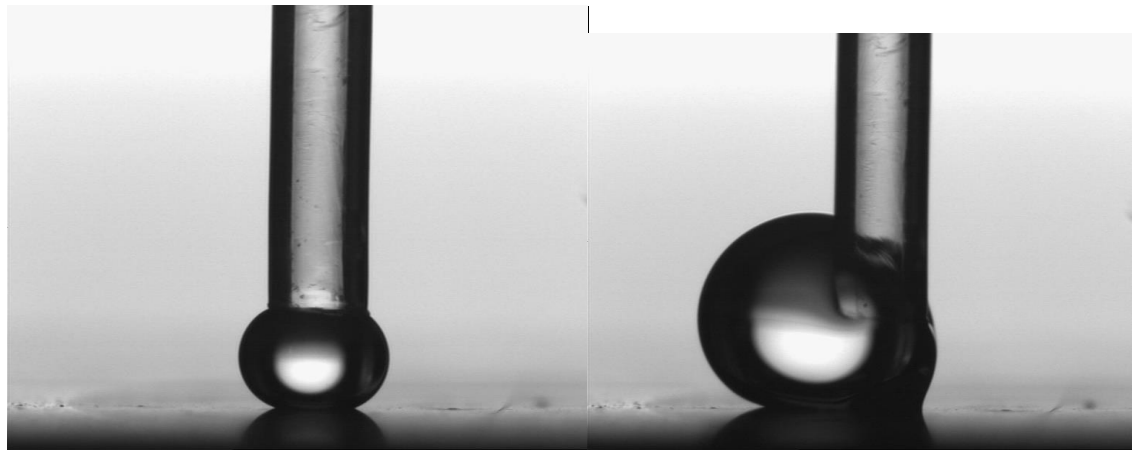


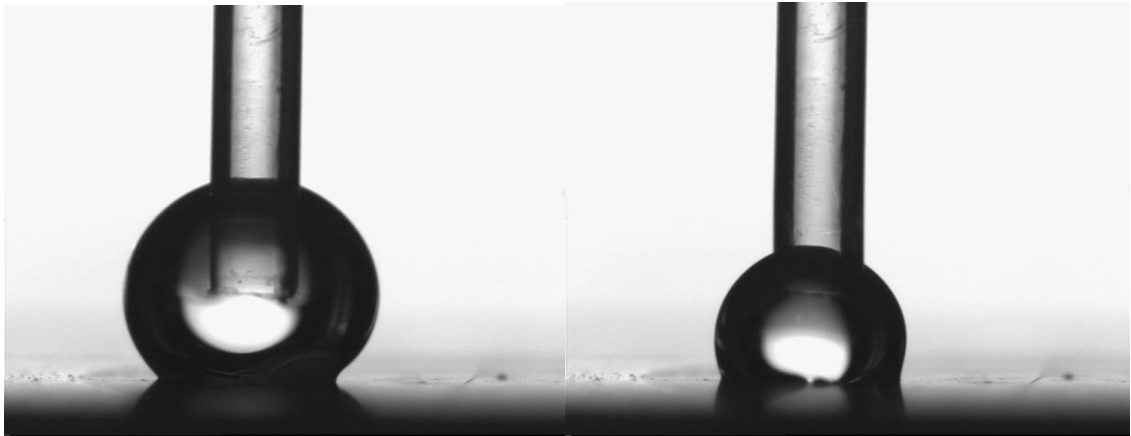
Figure 3.10: Example of advancing and receding measurement for SAM on gold device. Noise in the data could be due to dust, vibrations or draught interference measurement.



134.8 ± 0.52°

154.1 ± 0.11

Figure 3.11: Sample 15- Drop images during advancing



$137.1 \pm 0.45^\circ$

$112.6 \pm 0.16^\circ$

Figure 3.12: Sample 14 - Drop images during receding

The surface contact angle images showed a range from $\sim 97.9^\circ$ to 154.1° and other devices' details are presented in Appendix 1. However, there are some samples that show less hydrophobicity from the results. This could be due to some defects on parts of the surface. Given that the sample has only a small surface area that is covered with gold, any form of defect will affect almost the whole proportion of the contact angles. Defects could be due to oxidization, insufficient immersing time corresponding to the solution concentration, or surface contamination. The largest contact angles are known to have the best formation of self-assembled monolayer as this reflects on the average composition of SAM and this can impact on the hydrophobicity of the surface. Results shown all gold with SAM immersion procedure have a good contact angle showing hydrophobicity. The device with longest immersion time of 72H showing super-hydrophobic surface as exhibited in Fig. 3.11 and 3.12. These results were used to determine the best parameters in fabricating new current limiting devices with a self-assembled monolayer. However since all the surfaces are hydrophobic, devices are produced with all SAM conditions and the measurements can be used to differentiate which surface contact angles are the best for the current limiting devices.

3.3 Electrical Measurements

The current-voltage characteristic electrical properties of the devices were characterized using high speed two probe DC measurements. This characterization of the device is simply known as an I-V curve, corresponds directly to the standard symbols of current and voltage. In these measurements, ohmic behaviour, typically observed in metals and circuit resistors, is a linear response for which current versus voltage has a straight line and constant gradient. However, other factors such as temperature, and the material characteristics of the device can produce a non-linear curve. Figure 3.13 shows the concept that has been used to measure the I-V curve in the form of a simplified version of a schematic diagram. The results of the I-V measurement help to understand the effect of positive temperature coefficient of the device.

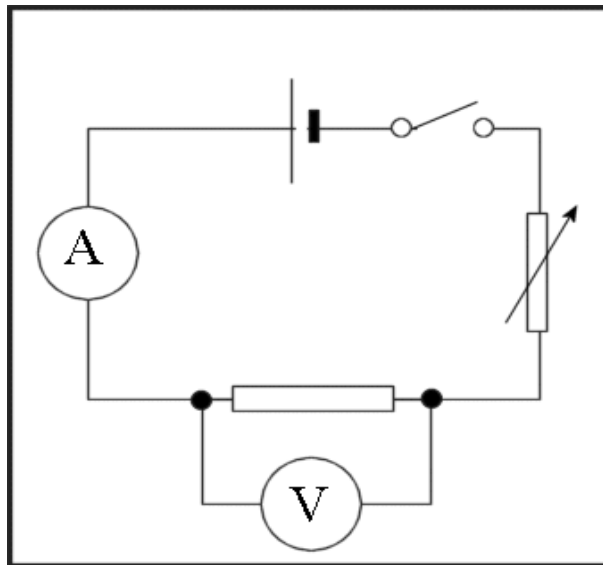


Figure 3.13: The simplified schematic representation of the electrical measurement set-up

3.4 Temperature Dependent Measurements

The conduction process in conducting polymers has some unusual features. Highly conducting samples exhibit electronic transport that shows a mixture of metallic and non-metallic character which is most easily explained in terms of the heterogeneous morphology [73] of the polymers as presented in Fig. 3.14.

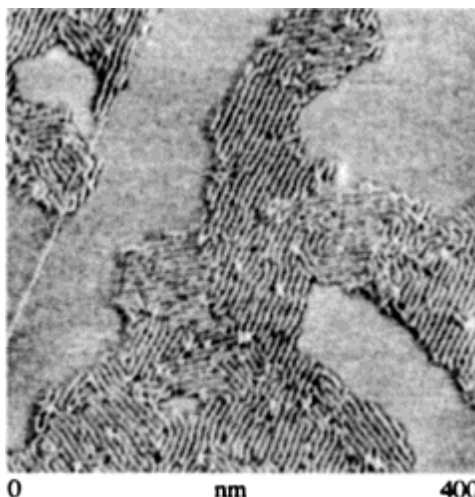


Figure 3.14: Morphology of polymer chains on a surface showing separate regions of well-aligned chains representing the heterogeneous disorder in highly conducting chains; from Percec *et al.*[74]

A key feature of the conductivity of most conducting polymers is their surprisingly large magnitude for materials with low carrier density and considerable disorder. Temperature coefficient of the highly conducting polymers shows non-metallic behaviour over a wide range of temperature and applies mostly to all types of conducting polymer. However the change to metallic behaviour at higher temperatures only happens for certain polymers [75]. Various researchers have proposed different mechanisms of electrical conduction in polyaniline. From the temperature dependent conductivity, the models proposed are quasi one-dimensional (1D) variable range hopping (VRH) [76, 77], 3D VRH [78-81], combination of 1D and 3D VRH [82], charging energy limiting tunnelling (CELT) for granular metals [83], and a

heterogeneous model where the temperature dependence of conductivity ranges from metallic to non-metallic.

There are certain variables that influenced the conductivity of polyaniline such as the type of dopants used and their concentration level, oxidation stage and molecular arrangements, percentage of crystallinity and inter-chain separation, as well as molecular weight. Thus, the temperature dependence of polymer films may differ according to these variable combinations and not always the same even though the same materials were used. Temperature dependent measurements were performed in order to understand the conduction mechanism that is responsible for the switching behaviour for the current limiting device using the chosen material and dopant.

Samples produced were measured at different temperatures ranging from 77 K to 300 K. A four probe method was used to measure the electrical conductivity of the polyaniline film on a gold substrate. A simple system was constructed which consisted of Oxford Instruments variable temperature liquid nitrogen cryostat, in conjunction with a temperature controller, model ITC4, also manufactured by Oxford Instruments,. A schematic diagram of the experimental setup is shown in Fig. 3.15.

A heat exchanger with heater and temperature sensor sits slightly above the sample. Following the insertion of the test device, the inner chamber is pumped down and flushed with nitrogen and this procedure is repeated several times to remove any water vapour which would otherwise condense at sub-zero temperature and may short out electrical contacts.

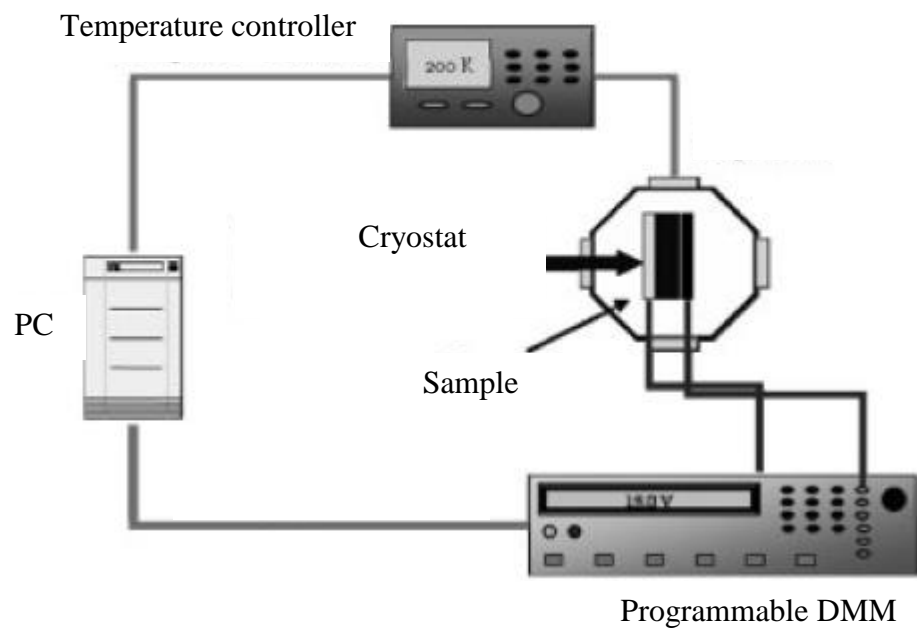
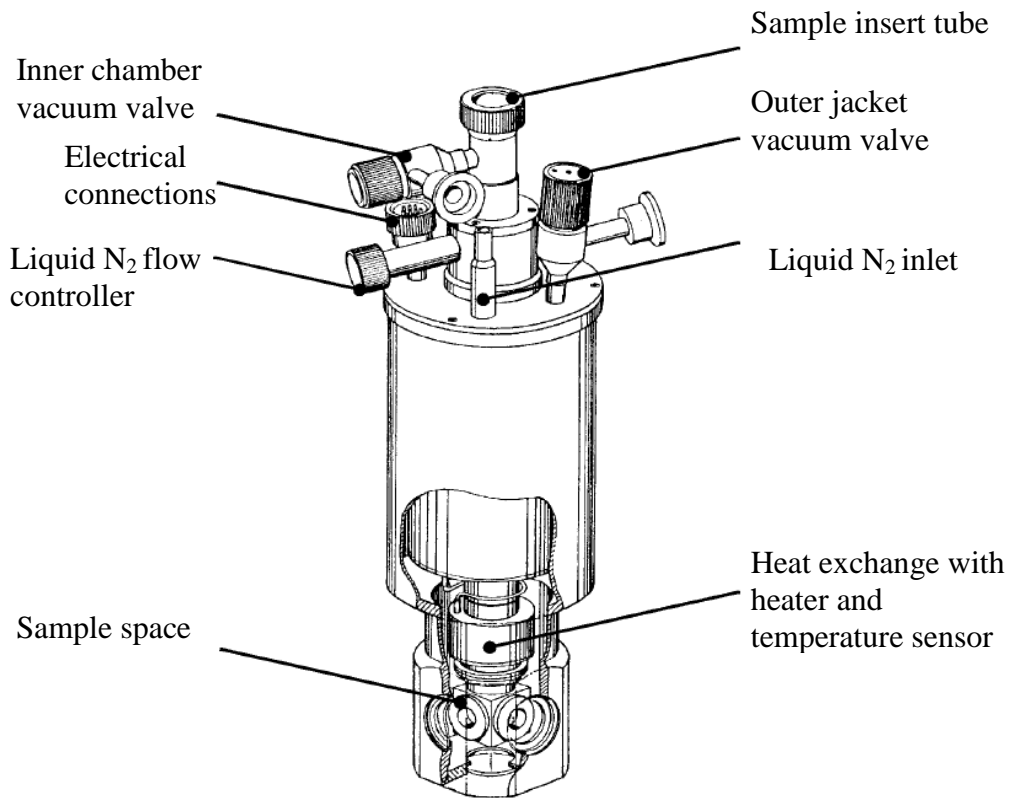


Figure 3.15: Temperature dependent measurement experimental setup

Temperature control is achieved by setting the target on the ITC4 temperature controller and adjusting the liquid nitrogen flow rate into the heat exchanger where it is opened progressively for lowering the temperature or closed for raising the temperature. The temperature monitoring thermocouple mounted on the insert rod is first calibrated against the temperature reading of the ITC4 controller display. This conductivity measurement was achieved by passing a 10 μ A current from a calibrated constant current source through the device and measuring the voltage drop across it with a programmable digital volt meter connected to a computer and readings were recorded every 2 minutes. Conductivity from the measurements was then determined by:

$$\sigma = \frac{1}{\rho} = \frac{l}{RA} \quad (2.1)$$

where A is the cross-sectional area, L is the length, R is the resistance, ρ is the resistivity and σ is the conductivity of the polymer film.

3.5 Contact Resistance Measurements

Contact resistance refers to the resistance associated with the metal/polymer barrier at the interface between the polymer film and the metal contact. In the current limiting device for example, current travelling laterally in the polymer film towards a gap must pass through this interface before travelling in the contact. Consider the schematic as a simple resistor in series as shown in Fig. 3.16:

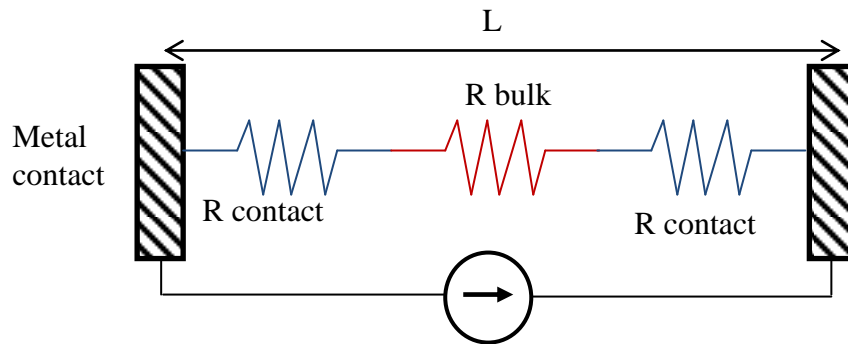


Figure 3.16: Illustration of simple contact resistance geometry of the device.

The magnitude of this contact resistance depends on the polymer material and dopant type, and the contact material but it depends most strongly on the doping concentration near the polymer surface. Low values of contact resistance are associated with heavy doping and vice-versa. A technique for measuring the contact resistance associated with the metal-semiconductor interface was first proposed by Shockley in 1964 [84]. The voltage drop across the metal-semiconductor device of constant area is plotted as a function of the length of the device. The contact resistance is then obtained by extrapolating the value to zero distance. This method was shown to be effective by Berger and Schuldt for thin conducting films [85, 86]. Fig 3.16 shows the two contacts are located at the end of the polymer and each has a contact area of A_c . The measured contact resistance consists of several components,

$$R_T = 2R_m + 2R_c + R_{polymer} \quad (2.2)$$

Where R_m is the resistance of due to the contact metal, R_c is associated with the metal/polymer interface and $R_{polymer}$ is the conducting polymer resistance. The resistance of a single contact would be $R_m + R_c$. However in most situations the resistance of inert material such as gold on the contact is very low, that $R_c \gg R_m$, and so R_m is negligible and usually ignored. R_s is the sheet resistance.

The polymer resistance is:

$$R_{polymer} = R_s \frac{L}{W} \quad (2.3)$$

$$R_T = \frac{R_s}{W} L + 2R_c \quad (2.4)$$

These results suggest a method for measuring the contact resistance. If resistors of several different lengths are constructed, keeping all the other detail the same, the total resistance of each resistor can be measured and plotted as shown in Fig. 3.17.

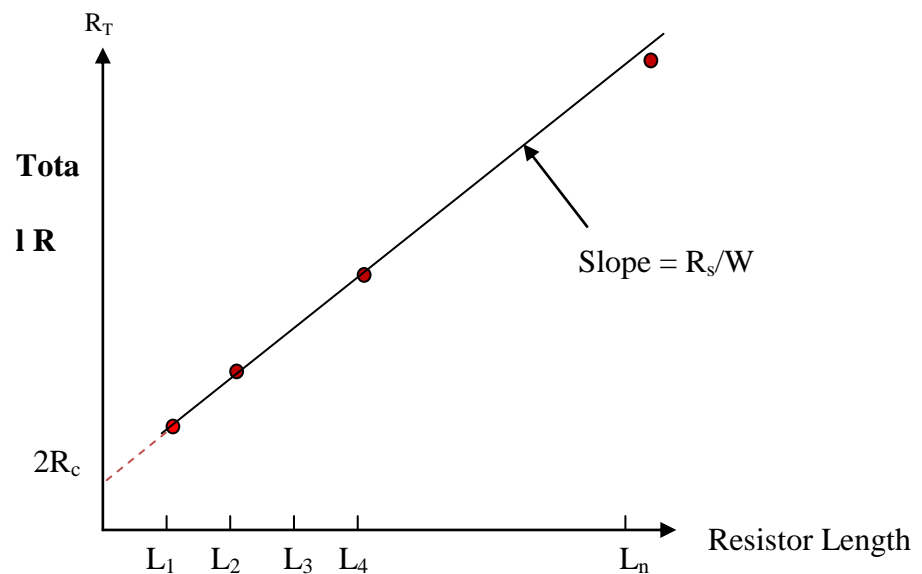


Figure 3.17: Example of extrapolation method using different length of known resistors.

In the limit of a zero-length resistor the residual resistance would be just twice the contact resistance. This can be found by extrapolating back to $L=0$.

3.5 Differential Scanning Calorimetry (DSC)

Conducting polymers may exhibit many mesophases between crystalline and amorphous, which may have either first or second order phase transitions. First order transitions involve a latent heat, where the system absorbs or releases a fixed amount of energy. The temperature of the system will remain constant as heat is added during the transition, during which the system is in a mixed-phase regime where some parts of the system have completed the transition and others have not. The melting of ice or the boiling of water are common examples of first order transitions. Second order phase transitions are also referred to as continuous phase transitions, where the old phase transforms into the new phase in a smooth, continuous manner. Ferromagnetic transitions, super conductor and the super fluid transitions are examples of second order phase transitions

Calorimetric experiments can be used to obtain the temperature dependency of the energy or enthalpy $H(T)$ for a material. This is often achieved by measuring the heat capacity, which is related to the rate of change in enthalpy as a function of temperature. However, for first order phase transitions a direct measurement of the enthalpy is needed as the latent heat information cannot be obtained from the measurement of the heat capacity. There are several techniques which can be used for this purpose such as differential scanning calorimetry (DSC), adiabatic calorimetry (both scanning and non-scanning), ac calorimetry, photo acoustic and photo pyroelectric methods. Here we focus on the DSC measurement technique which will be used to investigate materials within this research. Differential scanning calorimetry (DSC) is viewed as the standard technique for measuring transition temperatures and the enthalpy changes that occur at

these transitions. This technique is widely used to investigate phase transitions and thermal properties of conducting polymers [87, 88]. The principles of this measurement are quite straight forward. The sample is compared to a reference material over a pre-determined temperature range. Two small aluminium pans are used to contain the sample and reference materials, with just a few milligrams of the material under study required. A fixed rate of heating (or cooling) is chosen to be applied to the sample and reference pans over the predetermined temperature range. A servo system then ensures that the sample material tracks the temperature of the reference sample throughout the heating and cooling cycles selected. In order to keep the temperature of the sample and reference equal to each other during heating and cooling, the required heating power is varied. This differential power input is recorded throughout the heating/cooling cycle as a plot of the rate of change of enthalpy, dH/dT , against temperature. Hence it is possible to observe enthalpy change, including the latent heat for a first order phase transition.

Figure 3.9 illustrates a typical DSC pan set up.

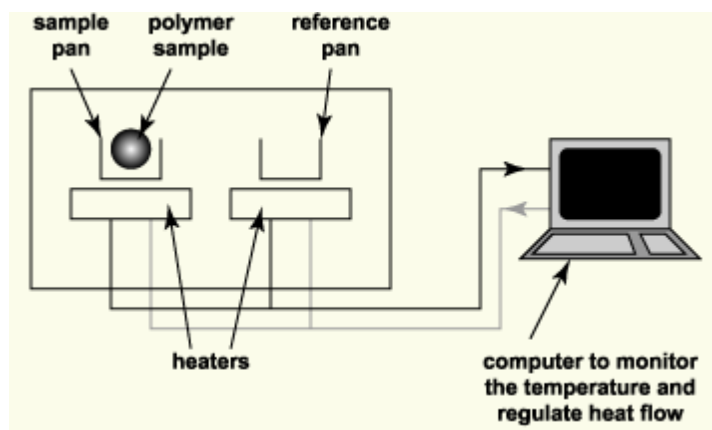


Figure 3.9 : Schematic for a typical DSC pan setup.

3.6 Thermo-gravimetric Analysis (TGA)

Thermogravimetric analysis (TGA) is one of the members of the family of thermal analysis techniques used to characterize a wide variety of materials [89]. TGA provides complimentary and supplementary characterization information to the most commonly used thermal technique, DSC. TGA measures the amount and rate of change in the mass of a sample as a function of temperature or time in a controlled atmosphere. The measurements are used primarily to determine the thermal and/or oxidative stabilities of materials as well as their compositional properties. The technique can analyse materials that exhibit either mass loss or gain due to decomposition, oxidation or loss of volatiles (such as moisture). It is especially useful for the study of polymeric materials, including thermoplastics, thermosets, elastomers, composites, films, fibers, coatings and paints . TGA measurements provide valuable information that can be used to select materials for applications, predict product performances and improve device fabrication techniques. The schematic principle of the TGA measurement is shown in figure 3.18.

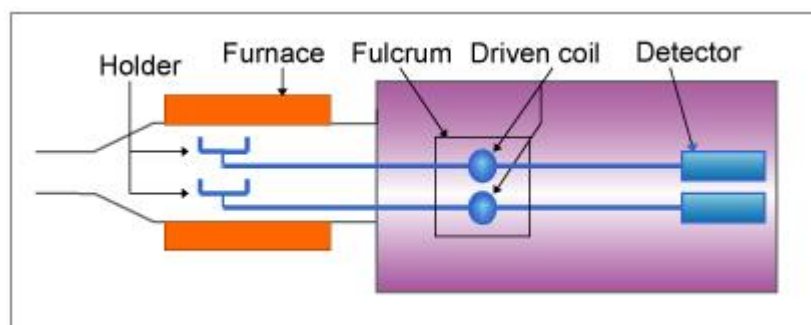


Figure 3.18: Schematic principle of TGA measurement.

The sample is heated under nitrogen or air with constant heating rate while the difference of the mass during this process is measured. The balance beams for the sample and the reference are located in the furnace. The masses of the sample and the reference are measured by the weight sensitive calibrated drive coils separately. The mass difference is sent as TG signal. By the differential mass measurement, the effects of the beam expansion, the convection flow, and buoyant force are cancelled. Thus the highly sensitive thermogravimetry measurement is achieved. The mass measurement of the sample and the reference by the independent drive coils enables the easy adjustment of the TG baseline drift electrically. A mass loss could be as a result of the material's thermal stability and purity as well as indicating the water content.

3.7 Morphological Studies

The samples have been studied to determine the micro and nano morphological patterns of the samples that have been produced corresponding to the combination of chemicals and methods chosen. The Scanning Electron Microscope (SEM) has been used for this purpose as the imaging technique can pick up most of the details needed to understand the structure of the samples.

The SEM is a microscope that uses electrons instead of light to form an image. The SEM has led to new areas of study in the medical and physical science communities since its development in the early 1950's which also allowed scientists to examine and understand a wider range of different specimens. The SEM has many advantages over traditional microscopes, for example large depth of field, which permits a larger range of topology to be in focus at a time. A much higher resolution can be supported by the SEM; therefore closely spaced samples can be magnified to much higher levels. The degree of magnification can be controlled easily as the SEM varies the scan length on the sample. At the top of the microscope there is an electron gun which produces an electron beam which then follows the vertical path down focused towards the sample. As soon as the beam hits the sample, x-rays and electrons ejected from the sample and are collected by the backscattered electron and secondary electron detectors. The signal is then amplified and converted into an image on the screen [90].

The samples used were placed on aluminium stubs, using epoxy glue. As if the sample charges in the chamber noise in the image is produced, the samples were all coated with a thin layer of gold using a Polaron gold sputter system. All SEM images obtained were taken on a Leica Cambridge Stereoscan 360 Scanning Electron Microscope (SEM), operated at 15kV accelerating voltage.

Chapter 4 RESULTS & DISCUSSION

4.1 Current limiting device, switching mechanism properties and morphology

Devices were fabricated and dried in air after washing repeatedly in a copious amount of deionised water. To examine the electronic characteristics of the devices current-voltage (I-V) sweeps were performed on the devices. Different ranges of voltages were applied to the device and current flowing out of the devices was measured. A short interval of one minute is introduced to ensure the device is not overheated between each sweep and this practise was applied to all other samples. I-V characteristics of polyaniline doped with methanesulphonic acid (MSA) are shown in Fig. 4.1 and 4.2.

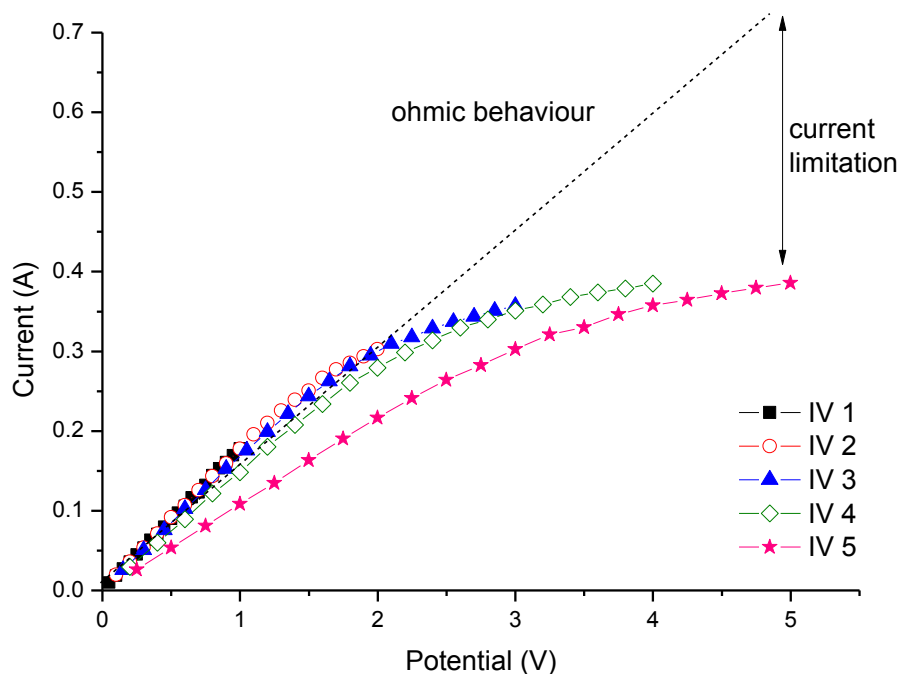


Figure 4.1: I-V characteristics for PANI-MSA current limiting device from 0 V up to maximum value given in the legend

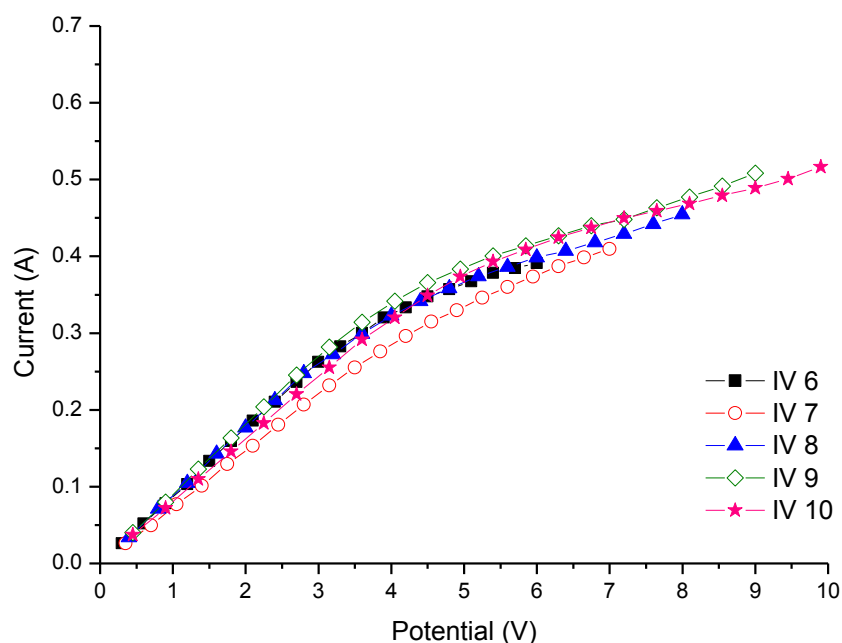


Figure 4.2 : I-V characteristics for PANI-MSA current limiting device from 0 V up to the maximum values given in the legend.

It is possible to construct a plausible explanation for the features of switching mechanism in the Polyaniline-MSA based on the resistance as when the voltage applied was increased, the current increased but not quite linearly and this describes the device characteristics as shown from the results. This device shows an increase in current as the applied voltage is increased. The initial resistance of the device is less than 1 Ω . This value was measured using a small current value and measuring the resistance value across the junction before any electrical measurements or connections were made. The device started showing non-linear behaviour after 3.5V in Fig 4.1. The sweeps are reversible up to 4 V of maximum potential, but was slightly irreversible at IV 5 sweep and stayed reversible after IV 6 sweep onwards in Fig. 4.2

This particular sample shows that the current is limited as the voltage is increased from 6 V to 10 V, but the concept of resistance increasing when the current reaches a certain value could be observed as the current only reached the maximum of 0.4 A, at

maximum applied bias. After that resistance stayed at the same level and limited the level of current passing through the polymer device.

To examine the reproducibility of the current limiting behaviour the device was re-tested after being removed from all electrical connections and left in air for 24 hours.

The results in Fig 4.3 show a reversible pattern and current is limited to 0.4 A.

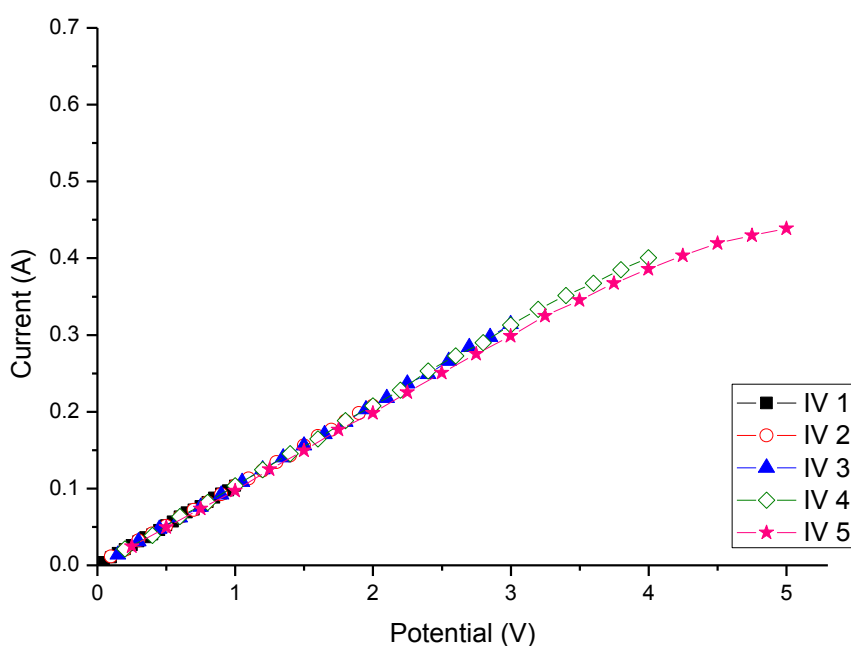


Figure 4.3: Reproducibility of I-V characteristics for PANI-MSA current limiting device performed after resettability of resistance, from 1 V to 5 V

Results for the electrical measurement in Fig. 4.4 showed the sweeps of IV 6 to IV 10 that represented a current limitation from 5 V onwards. However, the measurements at higher voltages did not show reversible I-V formation. This phenomenon could be due to the polymer film having been heated up from the repeated cycles of overcurrent and showed early signs of polymer degradation.

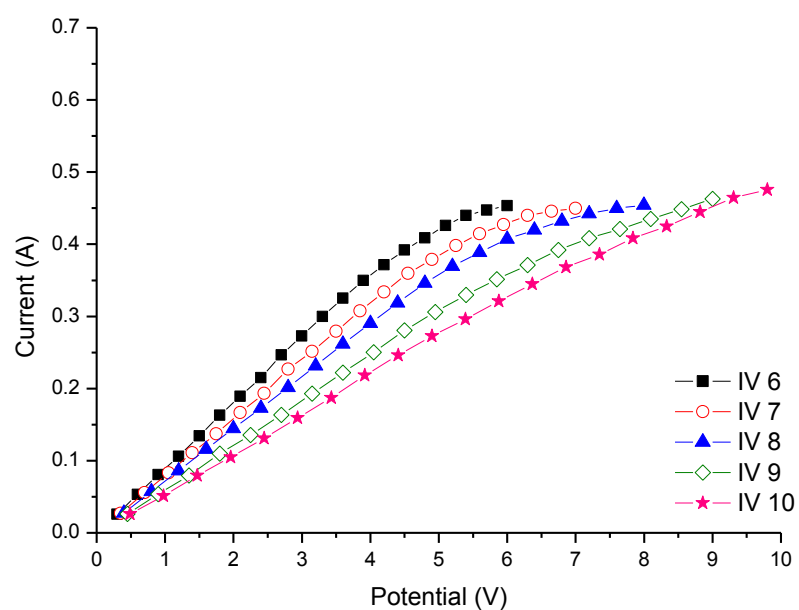


Figure 4.4: Reproducibility of I-V characteristics for PANI-MSA current limiting device performed after the resistance recovered, from 6 V to 10 V

To further understand the polymer switching behaviour another sample which has been freshly produced was tested under vacuum conditions. The chamber where the sample was placed was pumped out for 12 hours until a pressure of 3.5×10^{-6} mBar was reached. I-V sweeps of the device in vacuum are plotted in Fig 4.5 and 4.6

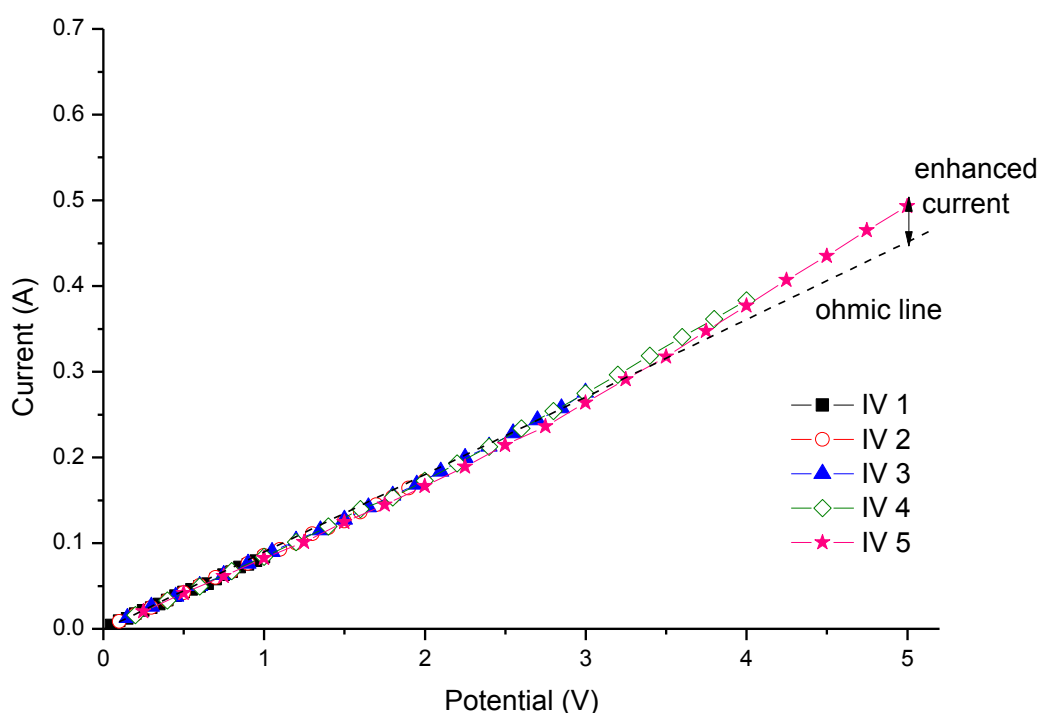


Figure 4.5: Current-voltage characteristics in vacuum from 1 V to 5 V.

Results shown for I-V sweeps in vacuum did not exhibit any current limitation. The initial resistance of the device is 1.3Ω before any electrical measurements and after pumping for 12 hours to the device resistance increased to 7.2Ω . Sweeps IV 1 to IV 5 in Fig 4.5 showed reversible pattern and almost linear behaviour. The slight increase in current at higher applied bias could be due to polymer heating up extensively.

Fig 4.6 showed from 0.6 A in IV 6 and gradual current decrease to 0.45 A in current limitation as the voltage increases could be direct relation to heating on the polymer film as pumping air out from the system leads to higher temperature and increased the device resistance. The IV sweeps did not show reversible sweeps indicating that the polymer film might change its properties during each sweep as the film is heated faster in vacuum due to the fact that air can also act as a cooling medium. The I-V pattern in Fig 4.6 is almost linear showing almost no current limitation could be also because of

moisture content in the polymer film having been removed during the pumping of the chamber prior to electrical measurements.

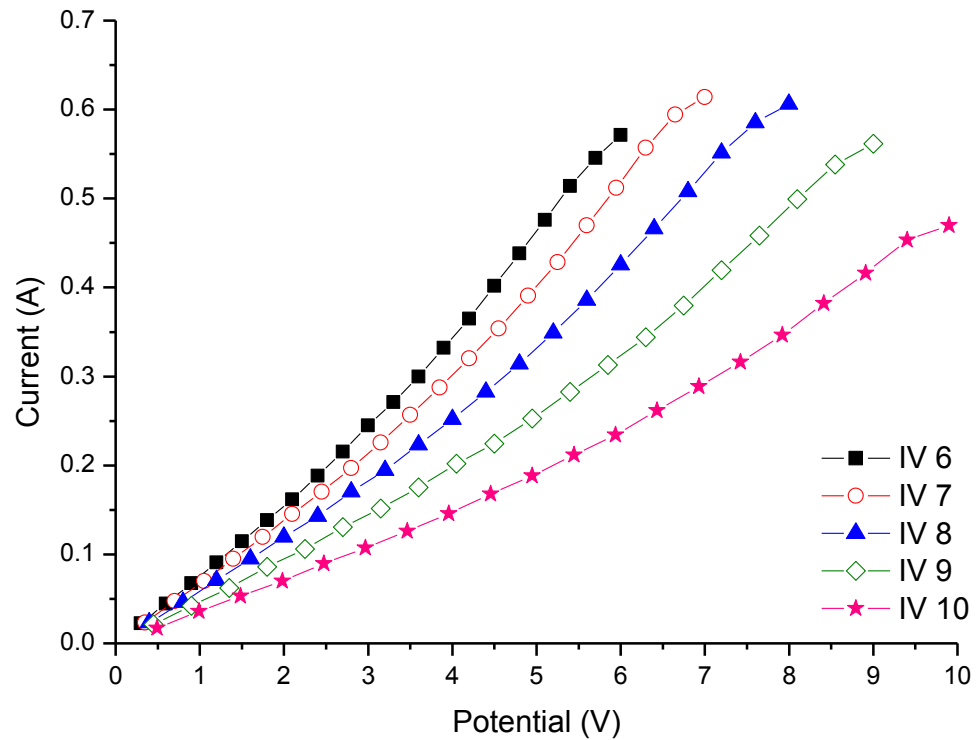


Figure 4.6: Current-voltage characteristics in vacuum from 6 V to 10 V

This effect is suspected to be related to the loss of moisture in the polymer composition caused by heating of the device. It is also apparent that the current decreases as the voltage is increased. Thus as the voltage increases, the rate of energy dissipation by joule heating increases and hence the resistance of the device must increase and at the same time acting as a current limiter. During high voltage load (over-current), the temperature of the polymer spot becomes close to the transition temperature and the current limitation is strongly increased due to drastic resistivity increase, which causes the formation of hot spots. This phenomenon can be explained by the infra-red image in Fig 4.7.

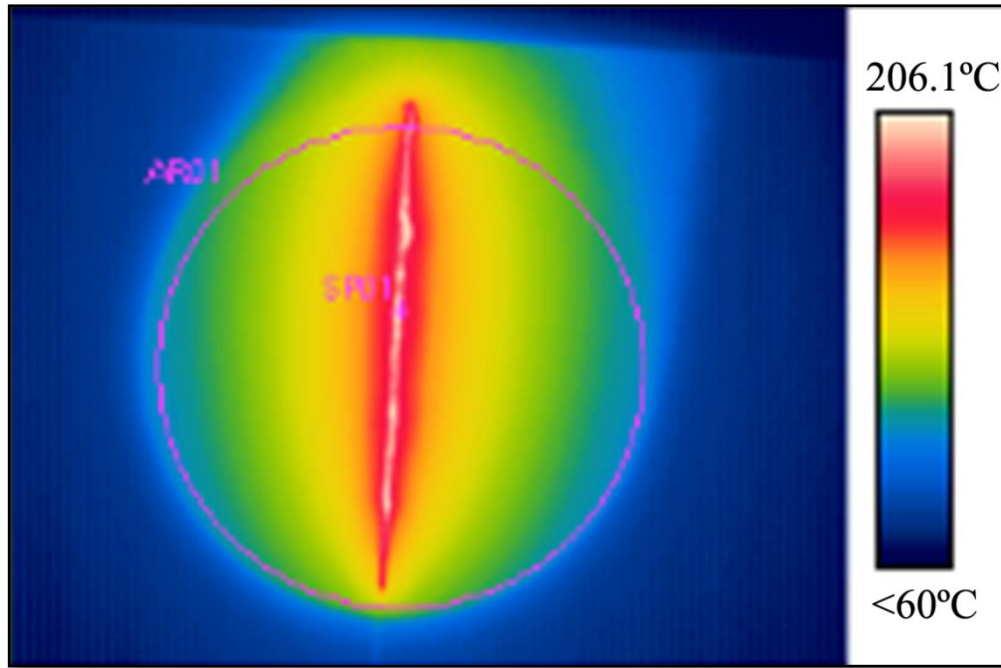


Figure 4.7: The infra-red camera images up to maximum applied bias of 10 V illustrate the hot spot during IV sweep which relates to the increase in temperature on the device.

This temperature data was obtained during thermal imaging while performing I-V sweeps at TE Connectivity Ltd. I-V sweep measurement is conducted with 5ms pulses at a 100ms period of repetition. This data shows that 5ms pulses can heat the material to $>200^{\circ}\text{C}$, and then the device cools rapidly during rest periods.

Preliminary hypothesis

The preliminary hypothesis at this stage based on the current - voltage measurement in air and in vacuum, and the temperature profile of the device using the infra-red camera measurement indicates that heating and water are playing important role in the current limiting device behaviour.

It is believed that pumping the samples under vacuum easily removes water molecules adsorbed by the N-sites in the metallic islands as water contributes to enhanced

conductivity by increasing the size of metallic islands [91]. Moisture presence leads to additional spin and charge delocalization, most probably by solvating the dopant anions and thereby reducing the electrostatic interaction between the positive charge and the anions [92]. According to Travers and Nechtschein the presence of water plays an essential role in the conduction process on polyaniline in term of electron hopping between localized states with the assistance of proton transfer [93, 94]. It has been shown in the results for electrical measurements performed in vacuum that the resistivity of the sample increases therefore decreasing all the currents corresponding to the voltage sweeps in vacuum. Upon placing the samples in vacuum chamber, it can be seen the increase of resistivity where pumping reflects an increase in the width of barrier between metallic islands and a decrease in conductivity [95].

It has been proposed that the presence of moisture plays an important role in the new term of conduction mechanism based on electron hopping between localized states, with the help of proton transfer [91-96]. This new conduction term is known as proton exchange-assisted conduction of electrons (PEACE).

In order to justify and confirm the relation of moisture loss with the device performance, another measurement has been performed on a freshly produced device where the initial resistance was measured. The resistance of the same device is measured in the vacuum condition and after letting the air in the system the resistance is re-measured to further understand any moisture loss effect on the device's resistance. Results obtained showed the initial resistance is 1.3 Ω and after pumping for 6 hours the resistance increased to 4.5 Ω , after letting air back in for a 10 minutes the resistance recovered to 1.6 Ω . The resistivity recovery is almost back to original resistance which

reflects water is replenished upon exposure to moisture nearly as rapidly as when is taken away from the vacuum [96].

We continued to investigate the mechanism of this effect by performing measurements in very high humidity level and the results are shown in Fig. 4.8. The polymer devices were exposed to water by placing it in an enclosure where the presence of water is maintained.

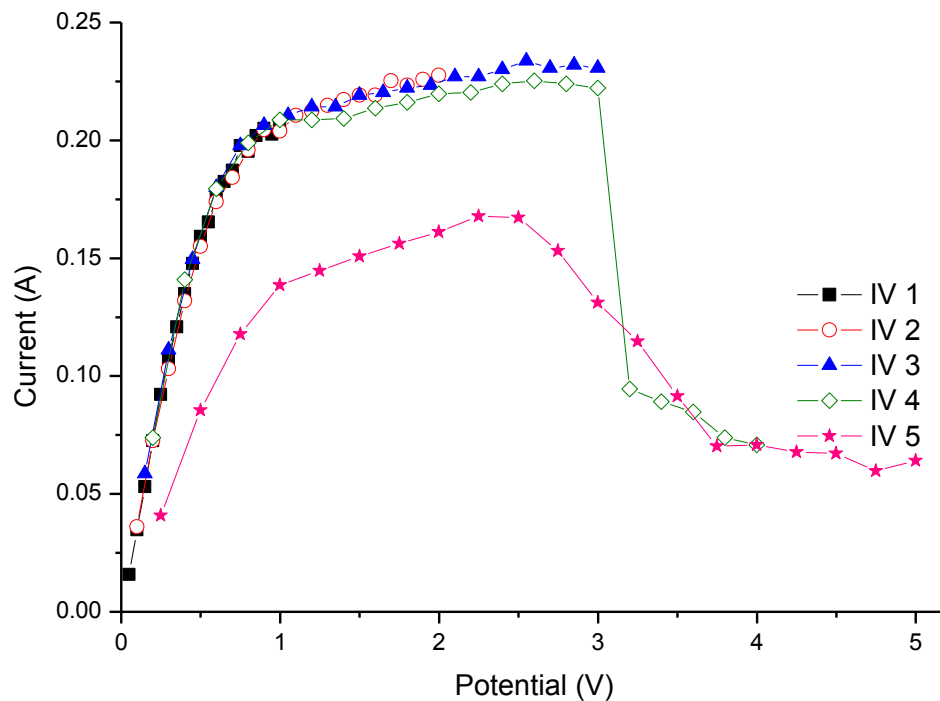


Figure 4.8: I-V characteristic for CLD performed in 100% humidity level, shows very significant current limitation.

Although the moisture level did not wet the surface of the polymer it was noted that the devices typically decreased in resistance after contact with the water. eg. a decrease from 0.7Ω to 0.6Ω , this indicates that some of the water was absorbed in to the polymer film.

Current-voltage sweeps were performed on the devices from 1 V to 5 V. The graph exhibits non-linear behaviour after 0.5 V, showing a plateau and the current started to drop across the current limiting device at 3 V. After 3.5 V the current showed a very sharp decrease, which was in direct relation to the high resistance of the device. This continuous presence of moisture content indicates better current limitation properties. Upon cooling down in between sweeps, the device returned to metallic state (low resistance). The device showed reproducibility of the current limitation (insulating state) during the IV 4 and IV 5 sweep with maximum 5 V of the applied voltage.

Temperature Dependent Resistivity Measurement

It is known that some forms of polyaniline show an opposite temperature dependence of the resistivity to that which is normally seen in most conducting polymers. Those polyaniline types showed a cross over to metallic behaviour near room temperature which related to the increasing resistivity with increasing temperature, opposite to that for thermally activated hopping. To eliminate this in our devices and to further understand the mechanism that is responsible for the switching properties of the current limiting device, temperature dependence measurements have been performed in a cryostat. The temperature was controlled by an Oxford Instrument ITC4 temperature controller. During the measurements the sample temperature was monitored carefully to avoid any self-heating in the sample. Conductivity measurements were made over the range of 77 K to 300 K. A current of 500 μA was passed through the device and the potential different between the electrodes were measured. The temperature was raised to 300K in steps of 5K with conductivity measurement made every 2 minutes. Results obtained are the average for five different samples and plotted in Figure 4.9.

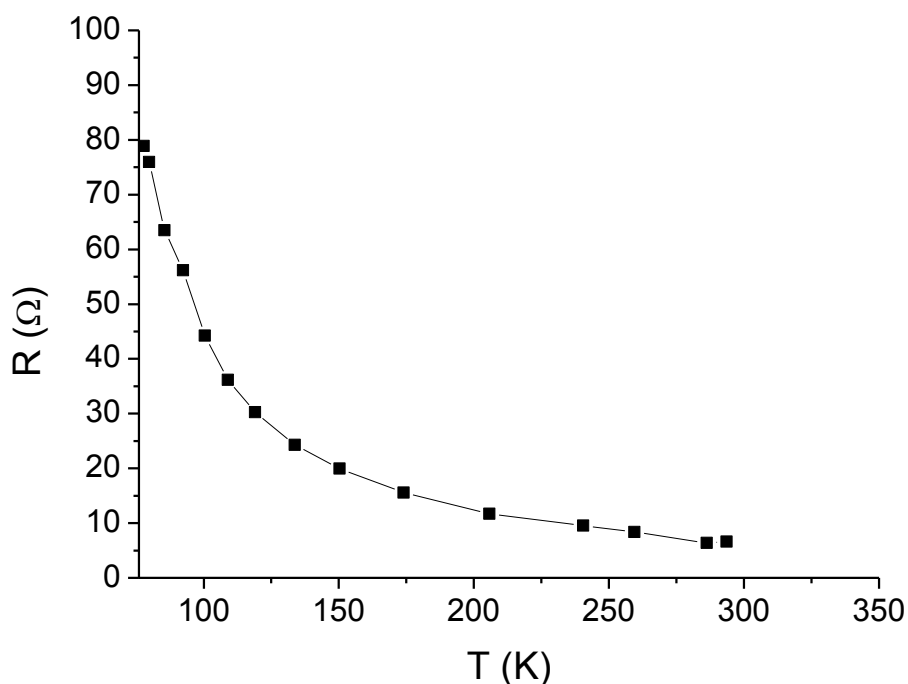


Figure 4.9: Temperature dependence from 77K to 300K

Results in Fig 4.9 showed that the resistance at low temperature is almost insulating and the resistance started to reduce exponentially as the temperature increased gradually up to room temperature. The conduction of polyaniline shows a maximum around room temperature which is in agreement with other studies [97-99]. However, the final resistance after temperature measurement are now higher from sample mentioned earlier because the measurements have been done in a dry environment.

The conduction mechanisms of electronically conducting polymers have attracted attention during the last 15 years. Rather soon, most of the experimental observations showed that the temperature dependence of the DC conductivity, σ , could be described by the following type of law. $\sigma = \sigma_0 \exp -(T/T_0)^\gamma$ with $1/4 \leq \gamma \leq 1/2$. Such a type of law

is characteristic of highly disordered system. The value of γ in particular, is related to the dimensionality of the transport process, d , as follows:

$$\gamma = \frac{1}{d+1} \quad (4.1)$$

In three dimensions, when the density of the localized states near the Fermi level does not depend on energy, γ is equal to 1/4. The bi-dimensional VRH is obtained for $d = 2$ ($\gamma = 1/3$) and the one-dimensional VRH is found for $d = 1$ ($\gamma = 1/2$).

A basis for understanding low temperature electrical carrier transport in disordered material has been given by Mott's seminal paper, predicting a $T^{-1/(d+1)}$ dependence of variable range hopping where d , is the hopping space dimensionality [25]. Conducting polymers are predominantly polycrystalline or amorphous in character and have a substantial amount of disorder.

As a result of hopping or tunnelling, conduction is generally observed and the dependence of Figure 4.10 can be represented by the 3D variable range hopping model in Eq. 4.2.

$$\sigma_{(t)} = \sigma_0 \exp \left[\left(\frac{T_0}{T} \right)^{1/4} \right] \quad (4.2)$$

where T_0 is the Mott's characteristic temperature and σ_0 is the conductivity at room temperature

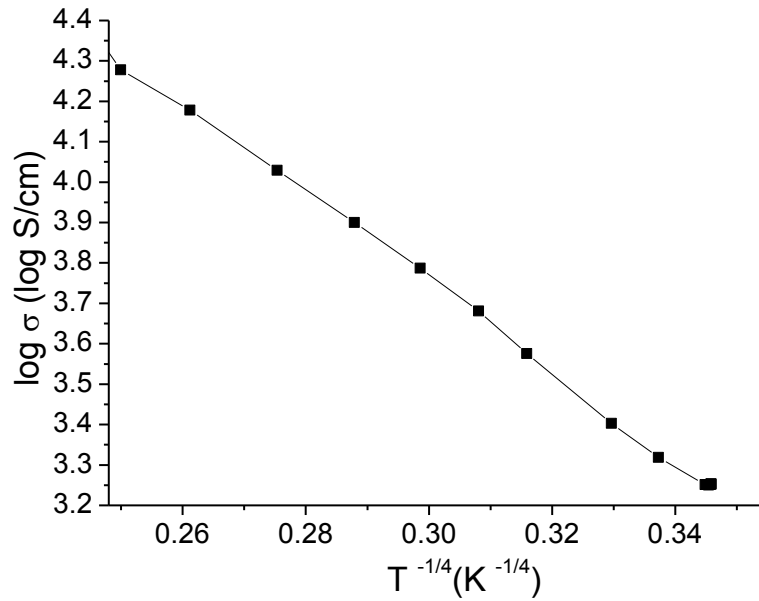


Figure 4.10: The temperature dependence of dc conductivity of PANI-MSA showing a fit to 3D VRH model.

In the variable range hopping model the hopping refers to tunnelling transitions from occupied to unoccupied localized states, the state energy difference being bridged by emission or absorption of one or several phonons. For PANI-MSA $\log \sigma$ versus $T^{-1/4}$ is observed to obey the characteristic of 3D VRH which is normally observed in fully doped polyaniline [76]. This mechanism could probably be due to a better interchain coupling upon doping with MSA that allow more sites available for hopping in three dimensions.

In the metallic region, the localization of carriers arises even for weak disorder because of quantum interference of static scattering. At higher temperatures, phonon scattering dominates impurity scattering. The results shown in Fig. 4.10 are in agreement with studies conducted by Sanjai *et al.* [100]. The results from other studies have also shown similar hopping transport but not all are the same dimensions. The results from these

studies have been extracted and plotted to fit the VRH model and most of the polyaniline showed transport in two dimensions as in Fig. 4.11.

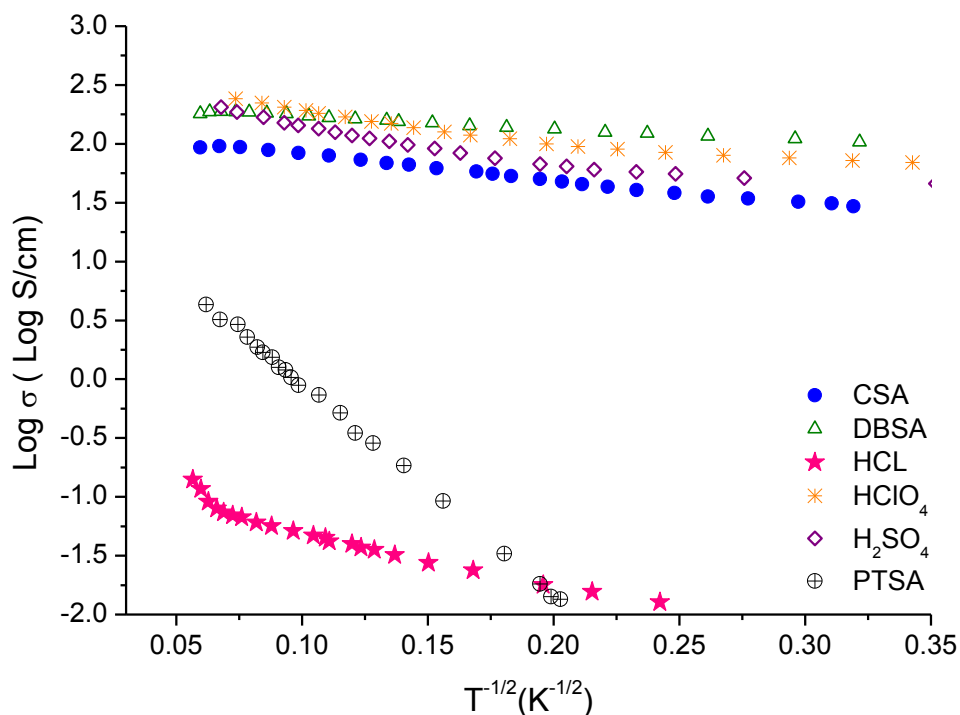


Figure 4.11: Comparison of temperature dependence for different dopants. Data points extracted and re-plotted from the literature [101-104].

The results deduced from literature showed good fit for the two dimensional model of the variable range hopping for six types of different dopants except for PANI-MSA as it is out of scale and not easily compared with the other dopants. This has suggested why the temperature results fit better with the three dimensional VRH model as presented in Fig. 4.10. Variantin in the dimensionality could be due to the altered delocalization levels for different dopants used [76, 105].

Device Morphology

Scanning electron microscopy (SEM) was used to characterize the morphology of the polymer and to see if the structure has an affect on the current limiting behaviour. The figure below presents the SEM images on the PANI CLDs for four different magnifications. The SEM images of the electrodes after polymer deposition shows nanofibres growth with a spaghetti type pattern on the Au electrodes. The highest magnification, at 20000 times image showed small nodules on the nanofibres growth. SEM images are presented in Fig. 4.12 to Fig.4.15.

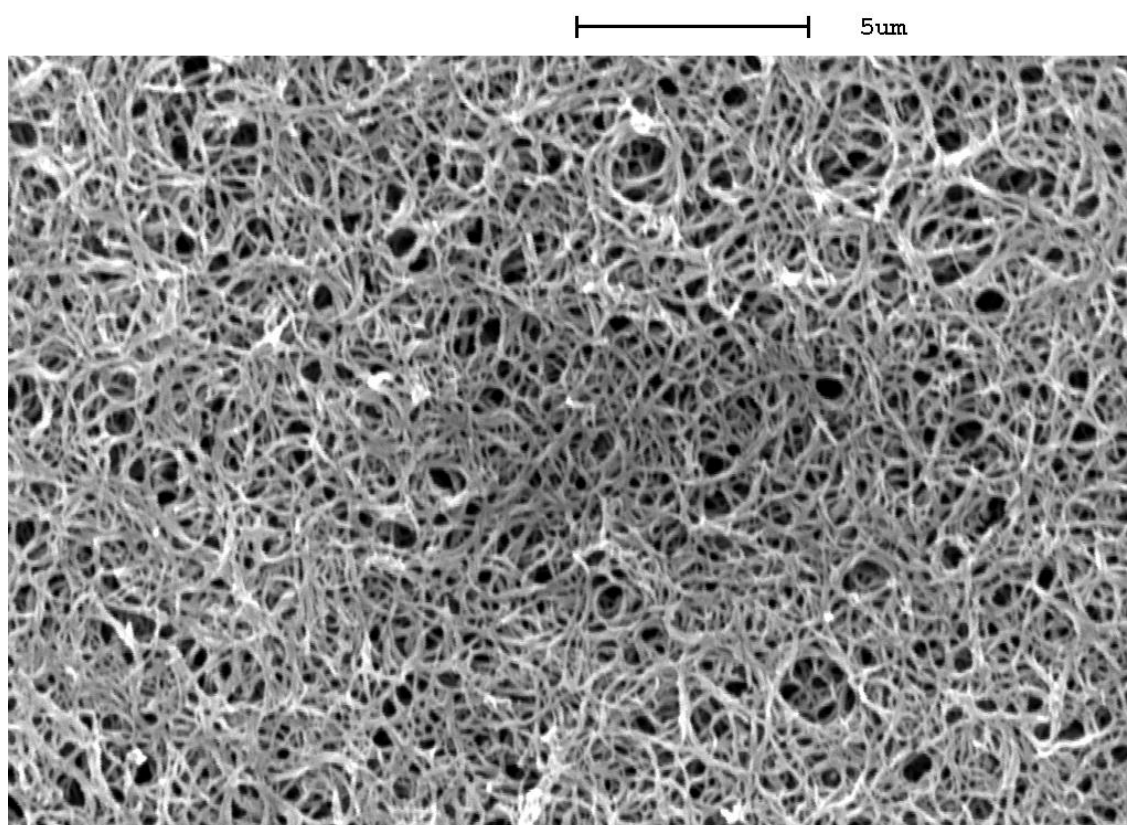


Figure 4.12:SEM image at 1000 times magnification showed the typical polymer morphology for electrochemical polymerisation of PANI-MSA on Au

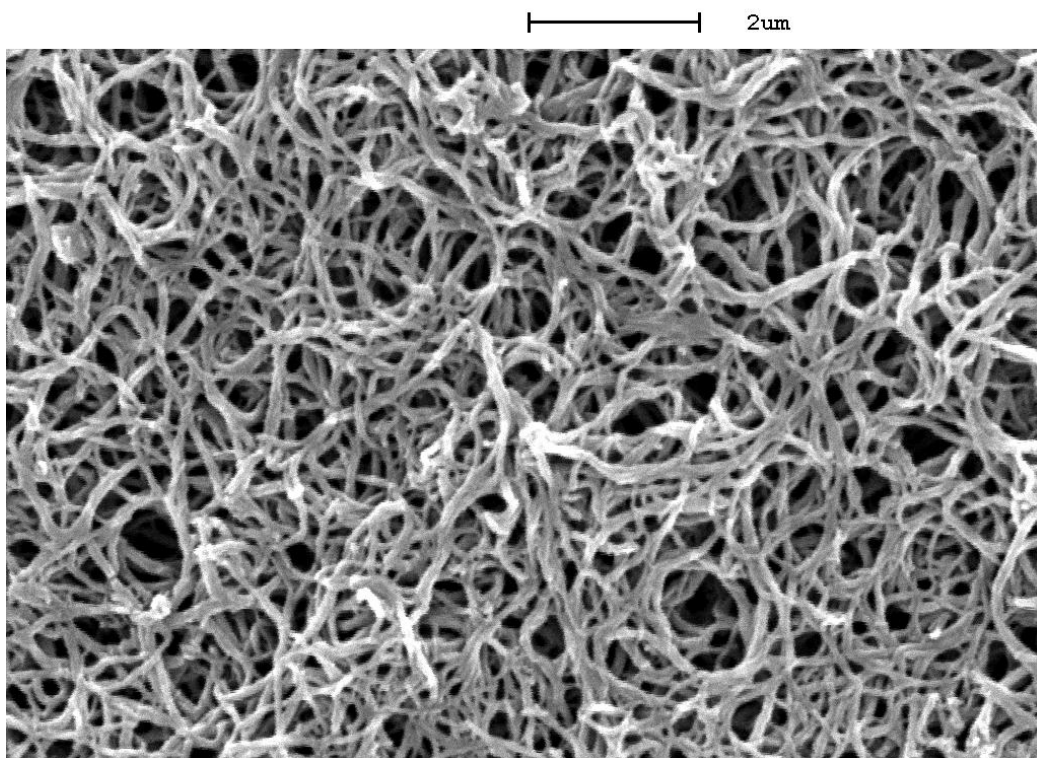


Figure 4.13:SEM image at 5000 times magnification showed the typical polymer morphology for electrochemical polymerisation of PANI-MSA on Au

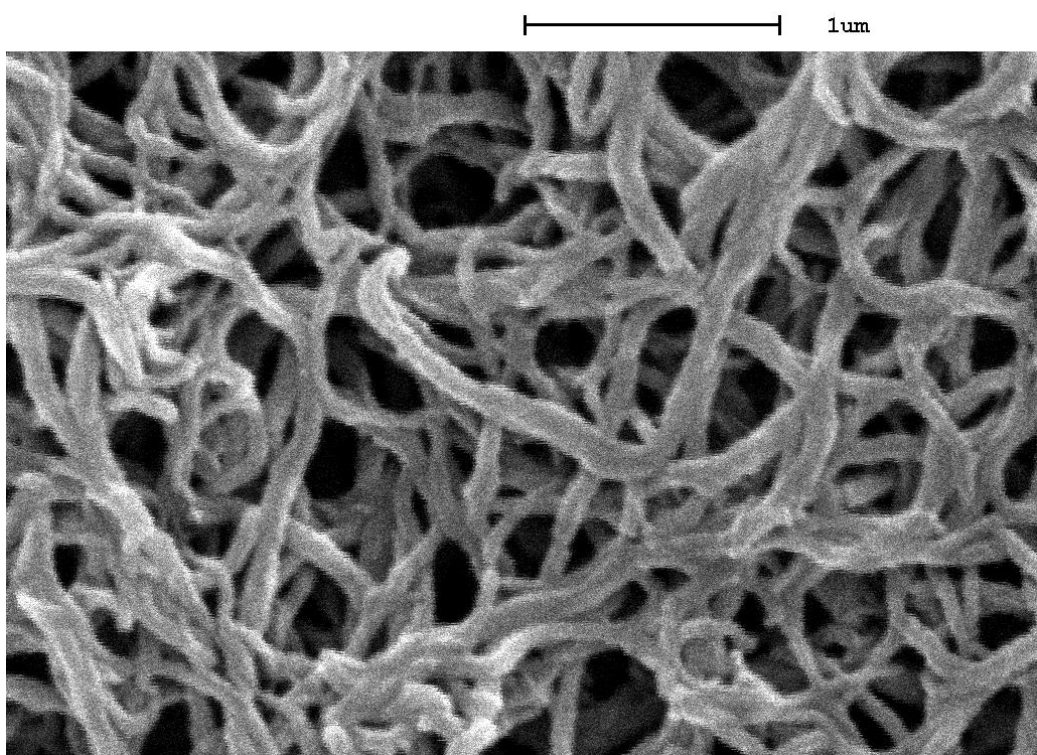


Figure 4.14:SEM image at 10000 times magnification showed the typical polymer morphology for electrochemical polymerisation of PANI-MSA on Au

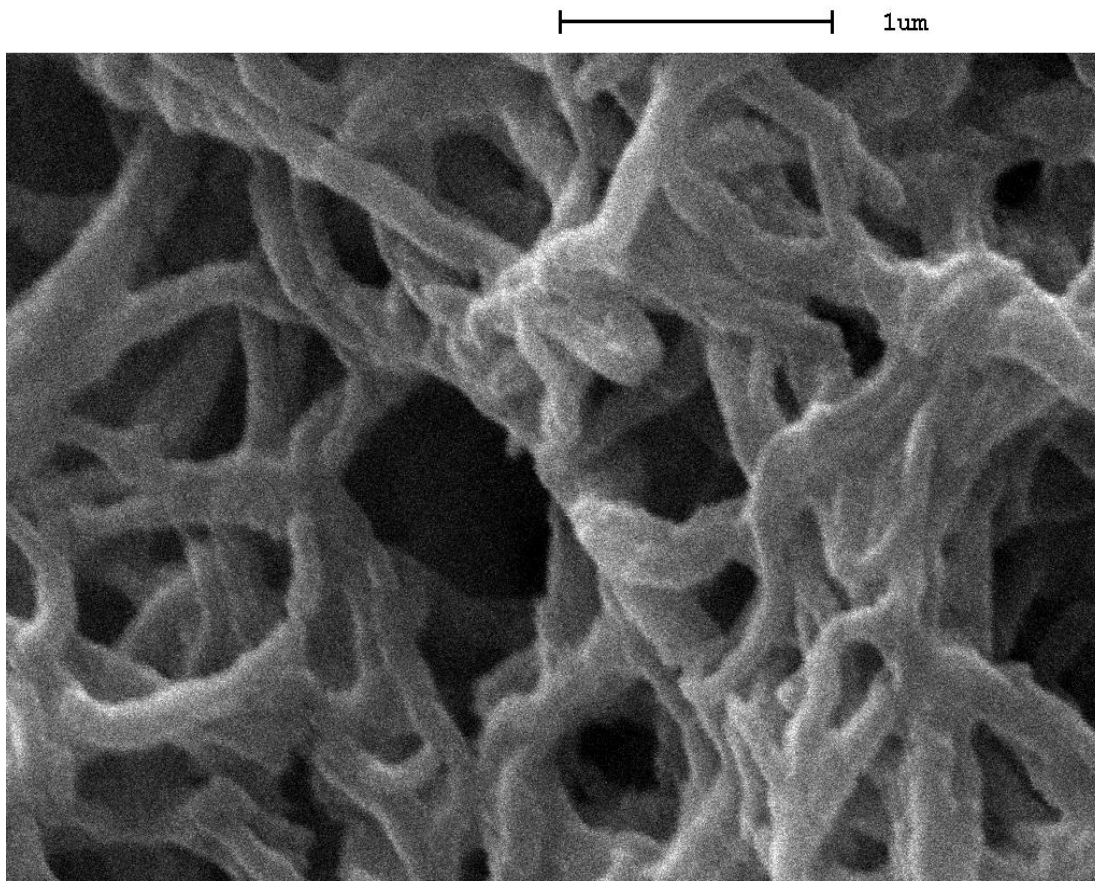


Figure 4.15:SEM image at 20000 times magnification showed the typical polymer morphology for electrochemical polymerisation of PANI-MSA on Au.

The SEM images revealed a highly fibrillar and porous morphology which is likely to explain the fast diffusion of water molecules out of the material during a high current surge. It also explains the quick recovery of the polymer as the porous structure permits water absorption back into the polymer film from the atmosphere.

4.2 Surface modified electrode using self-assembled monolayer a novel approach for current-limiting device.

Self- assembled monolayers (SAM) are rapidly entering surface engineering for modifying organic electronics where they are believed to be in charge of controlling the morphology and energetics of the interfaces. SAMs represents a chemical approach that allows the device to go beyond the present limits of organic electronics. Many SAM approaches have been studied but monolayers of alkanethiolates on gold are the most studied SAM. Previous studies suggested that it can be a useful tool to improve and tune the performance such as the morphology, energetics of surfaces and polymer interfaces depending on the type of monolayer [106]. This motivated us to implement this technique on the CLDs and observe the effects on the device performance.

After SAM processes and characterisations, the samples were then polymerised as previously described in the experimental section using the electrochemical deposition method. The samples' current-voltage sweep was performed to determine the characteristic of this Au-SAM-PANI device. Each sample produced with this technique has different control parameters and is described as below:

- *Sample 16:* SAM in 1mM DDT ethanolic solution (24H) followed by polymerisation of PANI-MSA for 85 seconds
- *Sample 17:* SAM in 5mM DDT ethanolic solution (24H) followed by polymerisation of PANI-MSA for 85 seconds
- *Sample 18:* SAM in 10mM DDT ethanolic solution (24H) followed by polymerisation of PANI-MSA for 85 seconds
- *Sample 19:* SAM in 1mM DDT ethanolic solution (48H) followed by polymerisation of PANI-MSA for 85 seconds

- *Sample 20*: SAM in 5mM DDT ethanolic solution (48H) followed by polymerisation of PANI-MSA for 85 seconds
- *Sample 21*: SAM in 10mM DDT ethanolic solution (48H) followed by polymerisation of PANI-MSA for 85 seconds
- *Sample 22*: SAM in 1mM DDT ethanolic solution (72H) followed by polymerisation of PANI-MSA for 85 seconds
- *Sample 23*: SAM in 5mM DDT ethanolic solution (72H) followed by polymerisation of PANI-MSA for 85 seconds
- *Sample 24*: SAM in 10mM DDT ethanolic solution (72H) followed by polymerisation of PANI-MSA for 85 seconds

Figure 4.16 shows a plot of sample 16, where the conditions of sample growth are as previously described, and shows increments in the current value when the voltage is increased. However, when the applied voltage reached 5 V and higher, the current showed non-ohmic values. From the initial resistance of the sample and internal resistance of the measurement system, it can be calculated that the resistance of the device increased but not linearly as the voltage increased. In between voltage sweeps, the resistance of the sample regained its initial low resistance and was then capable of switching to higher resistance again.

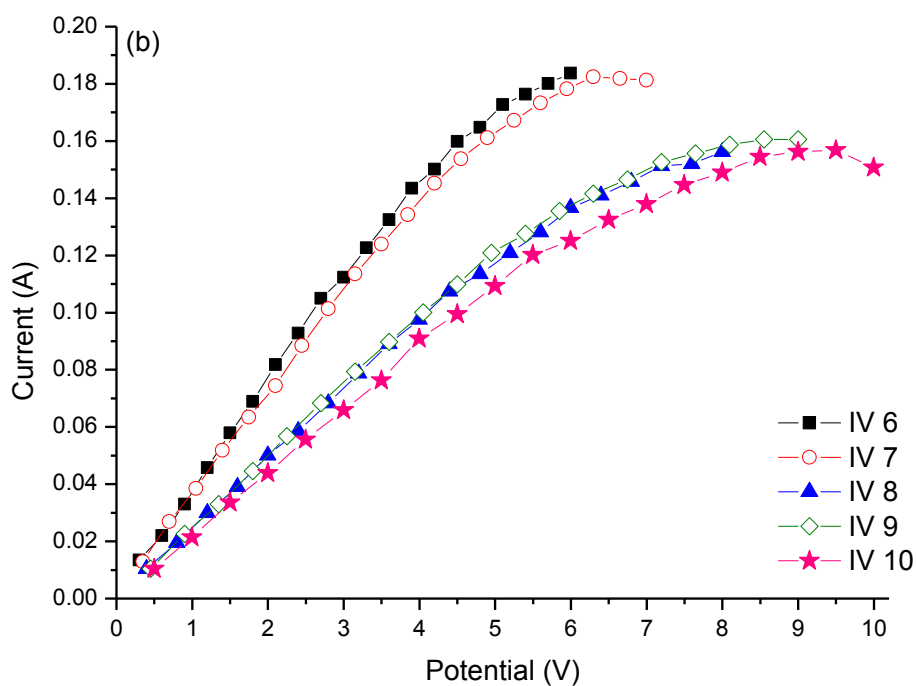
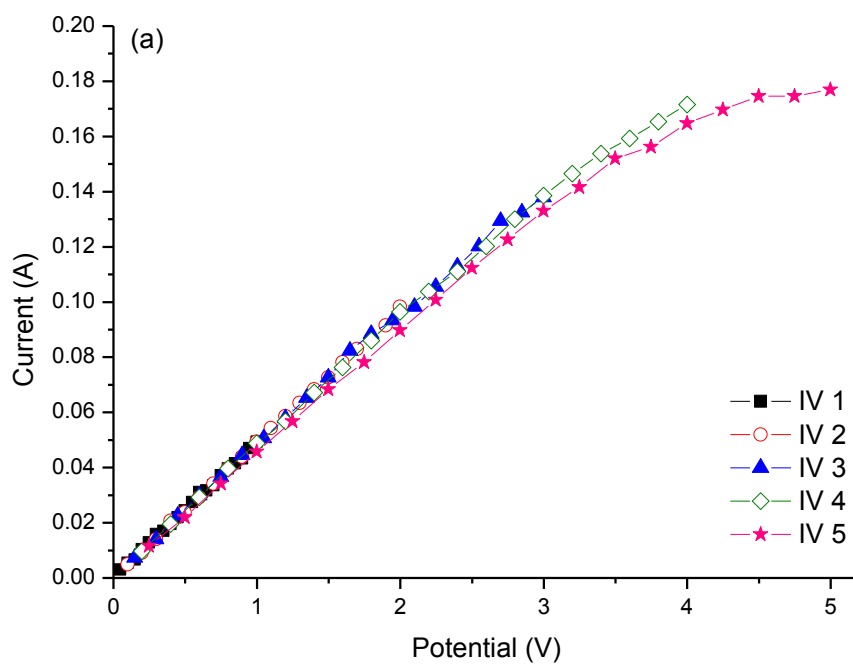


Figure 4.16: I-V characteristics of Sample 16 (24 H 1mM). Top graph (a) for voltage sweeps up to 5 V while the second graph (b) is for voltage sweeps up to 10 V.

Sample 17 in figure 4.17 I-V sweeps showed a similar pattern to sample 16 but indicated that current decreased before the sweep hits the maximum voltage applied to the device. At maximum applied voltages, the current showed slight current foldback, indicating current limitation. Conductivity of the sample can be recovered after waiting for a certain recovery time. The length of time depends on the current and voltage applied, as more moisture loss would require longer time.

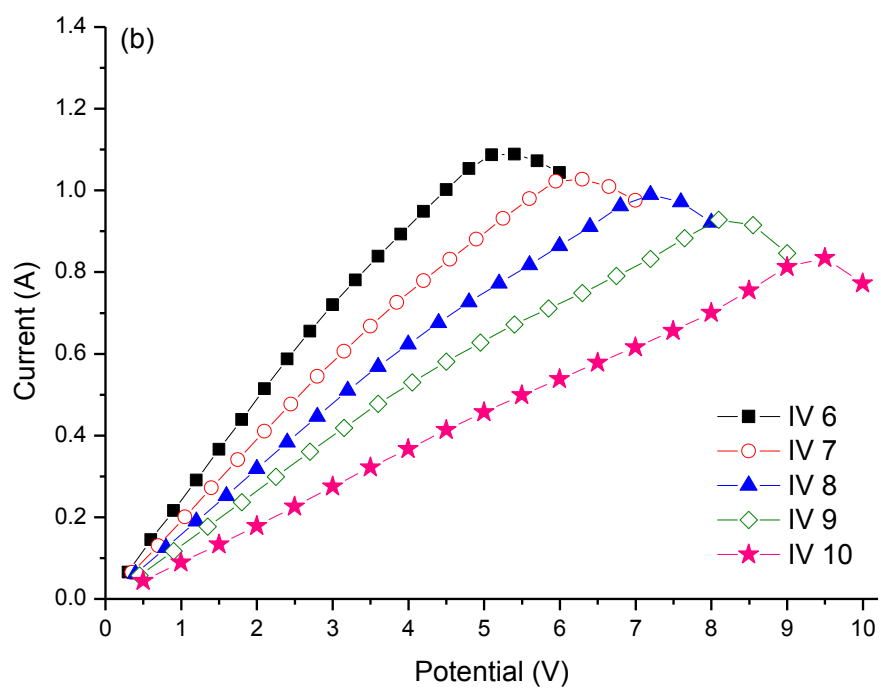
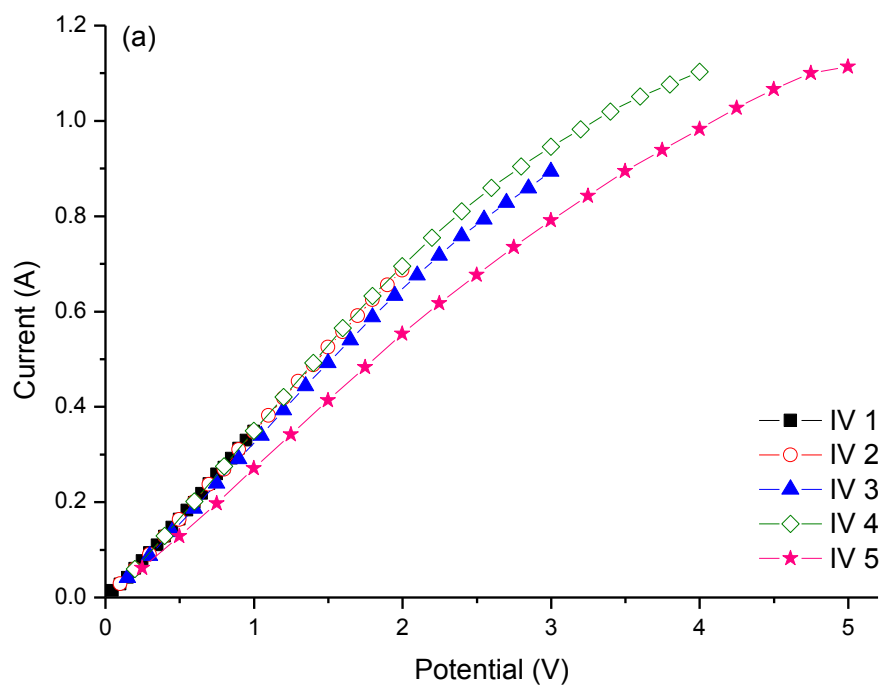


Figure 4.17: I-V characteristics of Sample 17(24H 5mM). Top graph (a) for voltage sweeps up to 5 V while the second graph (b) is for voltage sweeps up to 10 V.

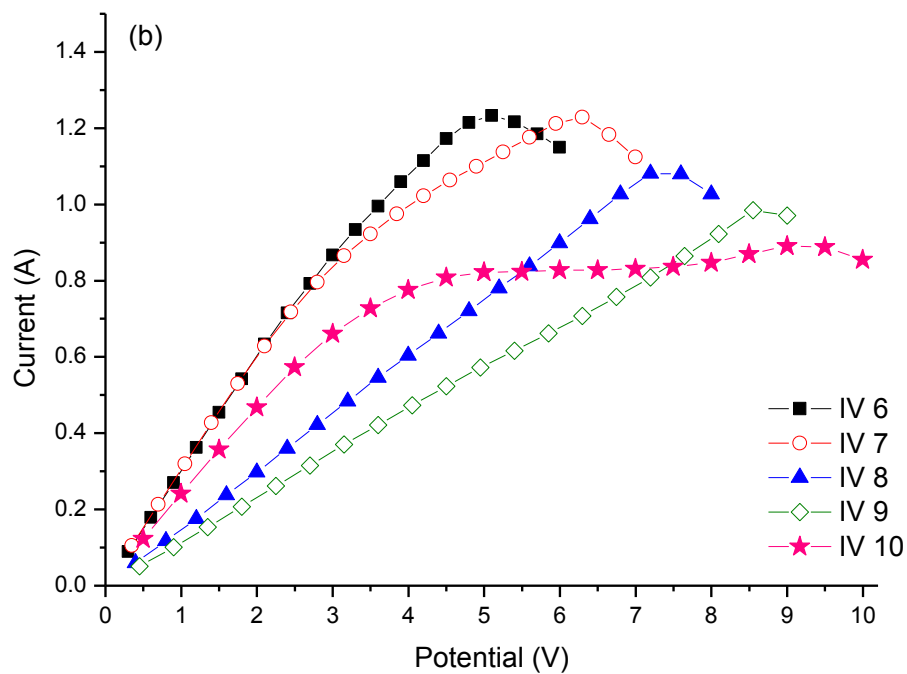
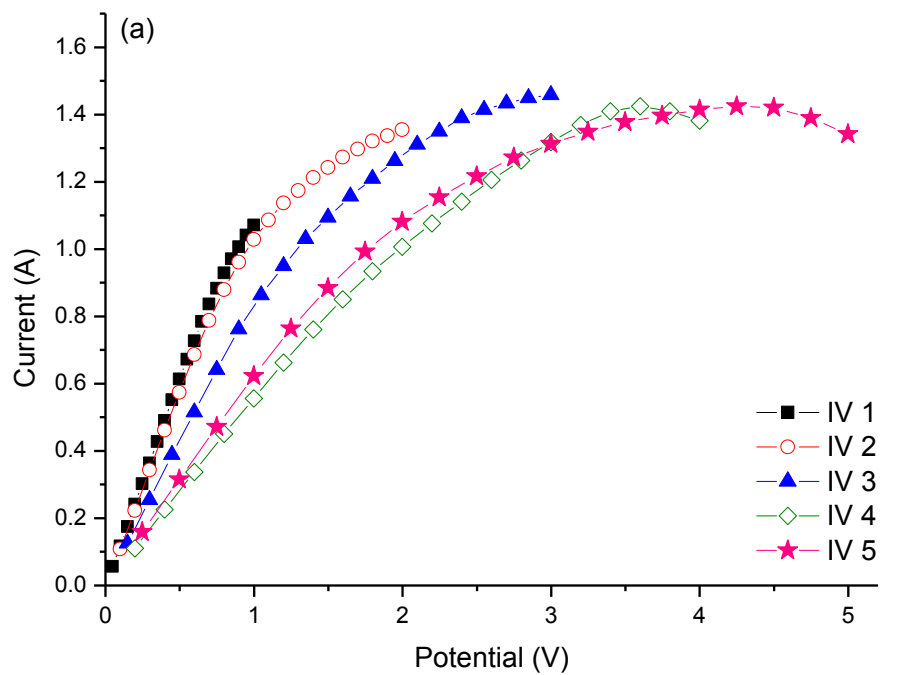


Figure 4.18: I-V characteristics of Sample 18 (24H 10mM). Top graph (a) for voltage sweeps up to 5 V while the second graph (b) is for voltage sweeps up to 10 V.

Sample 18 in Figure 4.18 showed current decreasing steadily for all the voltage sweeps applied from 1 V to 10 V. Current showed a slight fold-back response once the current reaches 1.2 A which showed good current limitation. Further voltage beyond 9 V showed that current was constant at 0.8 A.

Results for sample 19 presented in Fig. 4.19, where the electrodes have been immersed in the DDT ethanolic solution for 2 days before polymerisation, showed slight current limitation almost similar to device without SAM on gold. This could be due to the low concentration of the thiol solutions created defects or disordered monolayers does not give the full impact of SAM on the polymer film.

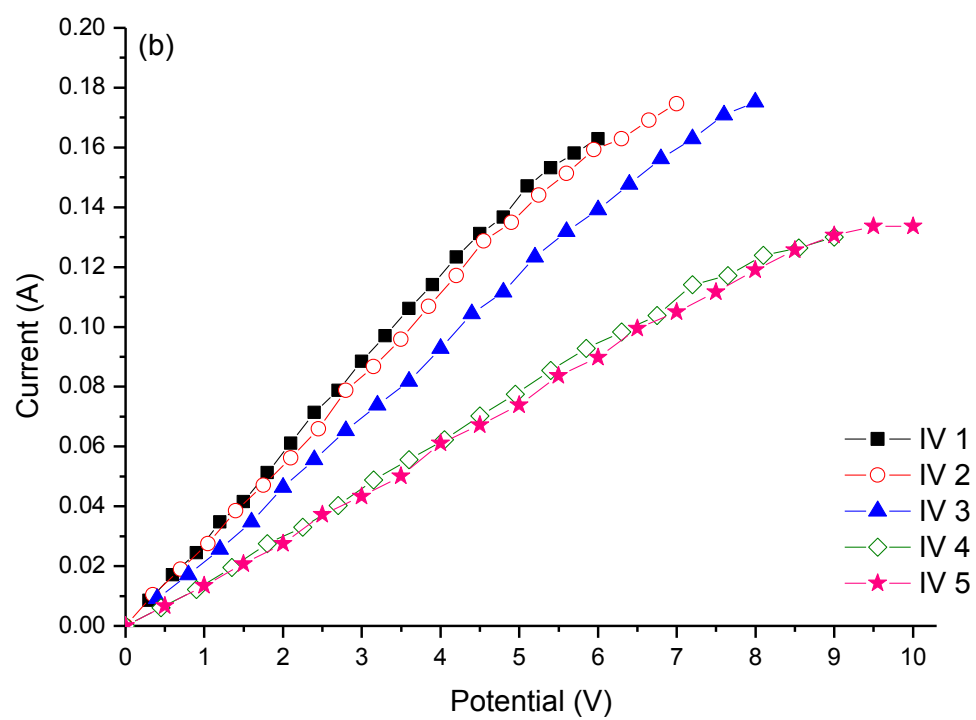
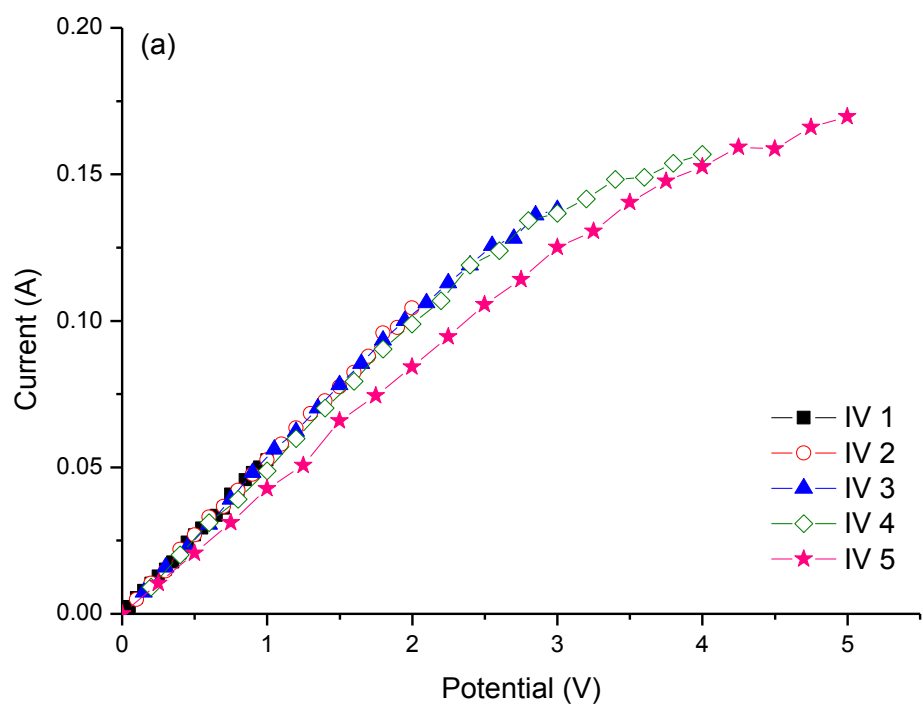


Figure 4.19: I-V characteristics of Sample 19 (48H 1mM). Top graph (a) for voltage sweeps up to 5 V while the second graph (b) is for voltage sweeps up to 10 V.

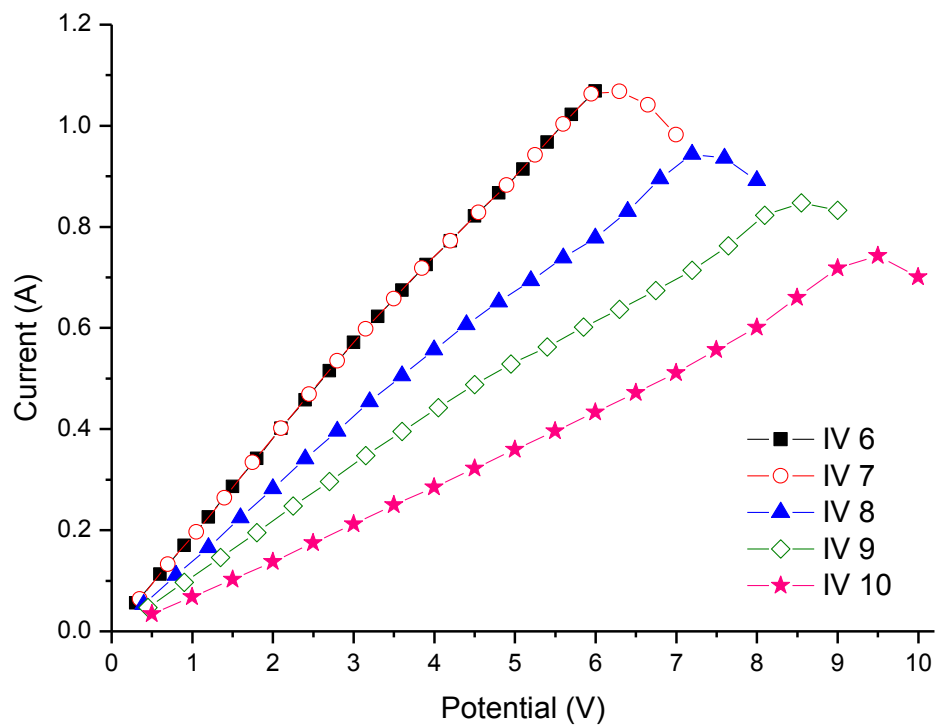
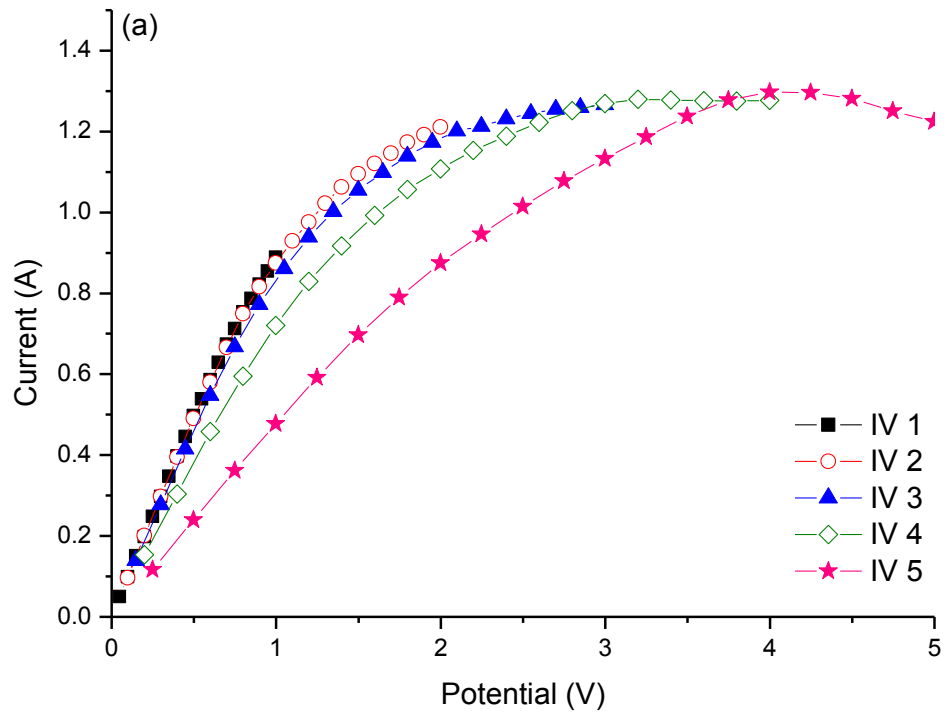


Figure 4.20: I-V characteristics of Sample 20 (48H 5mM). Top graph (a) for voltage sweeps up to 5 V while the second graph (b) is for voltage sweeps up to 10 V.

Sample 20, with 5mM of DDT concentration for self-assembly monolayer, showed consistent results as represented in Fig 4.20. As the voltage sweep across the device increased, the resistance increased too. The current showed decrease in value just before the maximum applied voltages were reached. Current showed peak function pattern for sweeps from 6 V and beyond. This could be to the DDT solution concentration having formed a better SAM to alter the behaviour of the device into a more improved current limiter.

Sample 21 results as plotted in Figure 4.21, showed constant current values as the voltage sweeps increased from 5 V gradually constant current can be observed all the way to applied voltage up to 10 V. Maximum current values allowed by the sample decreased steadily as the voltage sweep increased across each measurement and this is suspected to be due to higher applied bias leading to more moisture lost; therefore the device had higher resistivity, thus limiting the amount of current that are allowed to pass through the sample. I-V sweeps showed performance starting from 2 V the current started to be limited. Fig. 4.21(b) showed better current limitation from previous results and this is due to this device using higher concentration of the DDT which in theory limited the defects and increased chance for a more uniformed SAM.

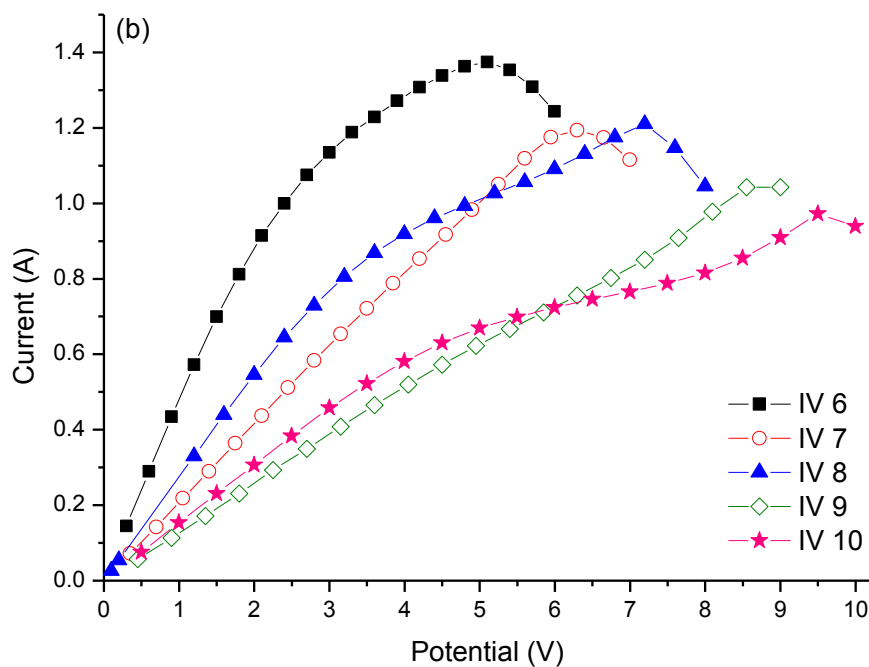
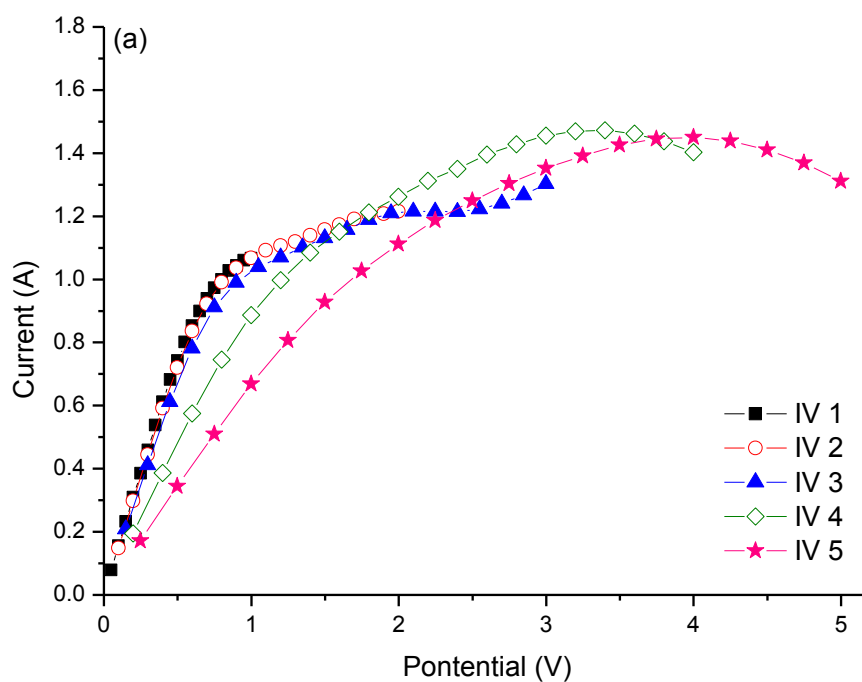


Figure 4.21: I-V characteristics of Sample 21(48H 10mM). Top graph (a) for voltage sweeps up to 5 V while the second graph (b) is for voltage sweeps up to 10 V.

Repeated measurements were performed for samples 22, 23 and 24 which has the longest immersion time for the SAM and results are presented in Fig. 4.22, 4.23 and 4.24 respectively. I-V sweeps have shown very significant improvements of current limitation especially in samples with the highest solution concentration and longest immersion time as exhibited in Fig. 4.24. All the SAM devices changes in the current-voltage measurement from linear to non-linear behaviour have been analysed as a function of resistance changes with regards to the SAM immersion time and concentration level. Results of the analysis have been plotted in Fig. 4.25 and showed that devices with highest concentration of the thiol solution and highest immersion time a have a substantial change of resistance percentage from ohmic to non-ohmic behaviour which is almost 80% of resistance increased. This indicated the CLD have a better current limiting performance. However device with other parameters also showed good percentage change with increasing of resistance around 30% to 50% from the calculated ohmic resistance value.

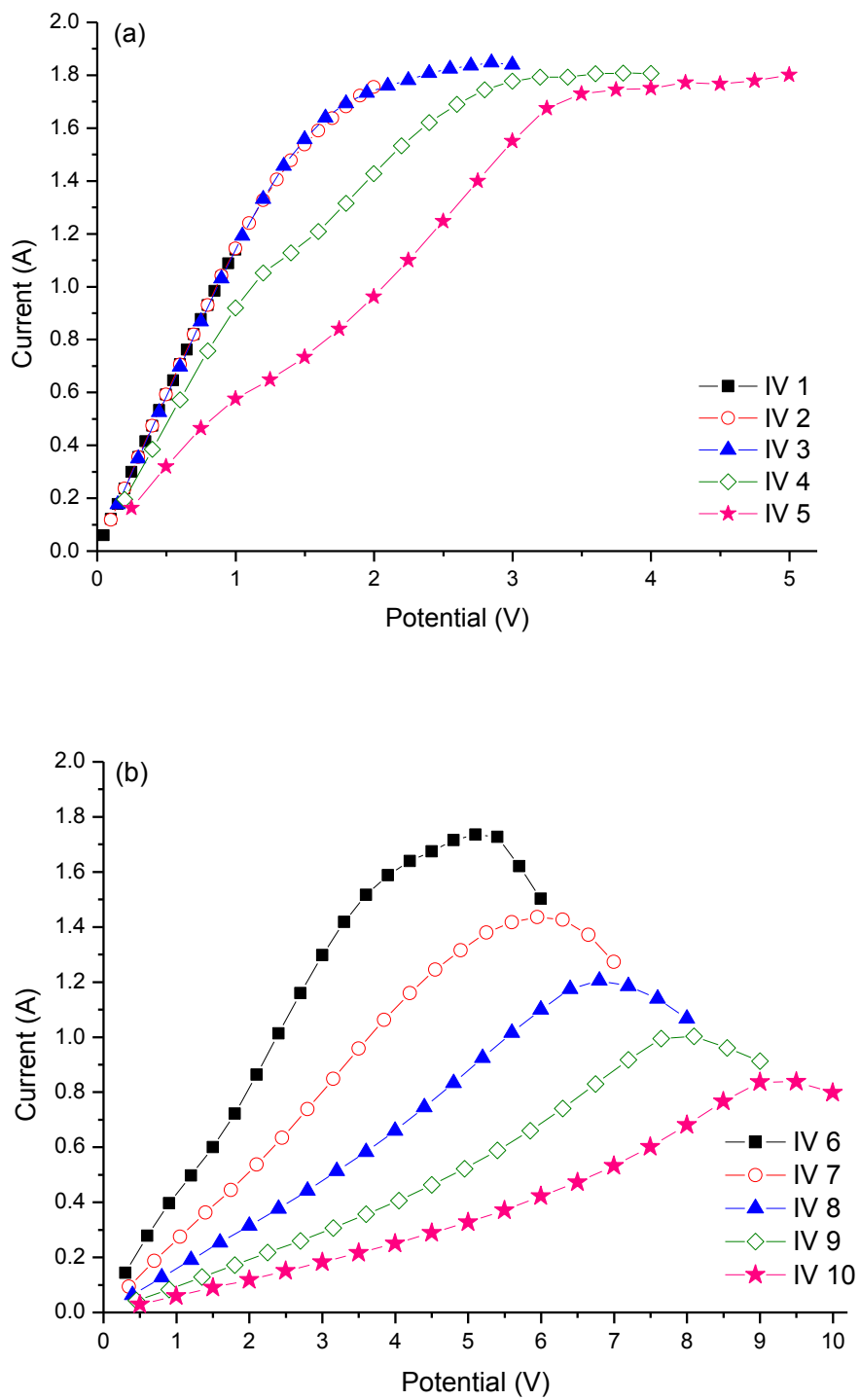


Figure 4.22: I-V characteristics of Sample 22 (72H 1mM). Top graph (a) for voltage sweeps up to 5 V while the second graph (b) is for voltage sweeps up to 10 V.

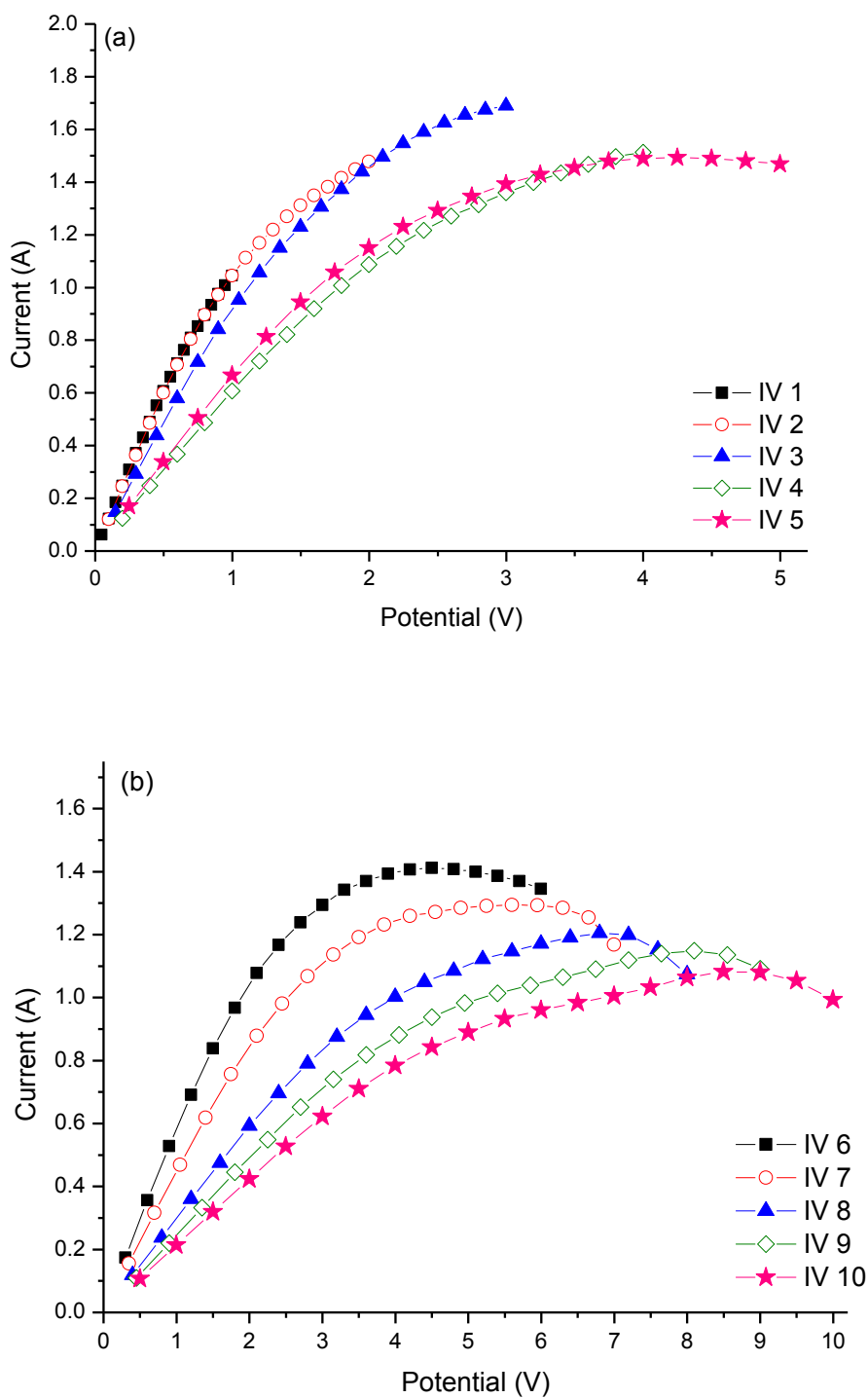


Figure 4.23: I-V characteristics of Sample 23 (72H 5mM). Top graph (a) for voltage sweeps up to 5 V while the second graph (b) is for voltage sweeps up to 10 V.

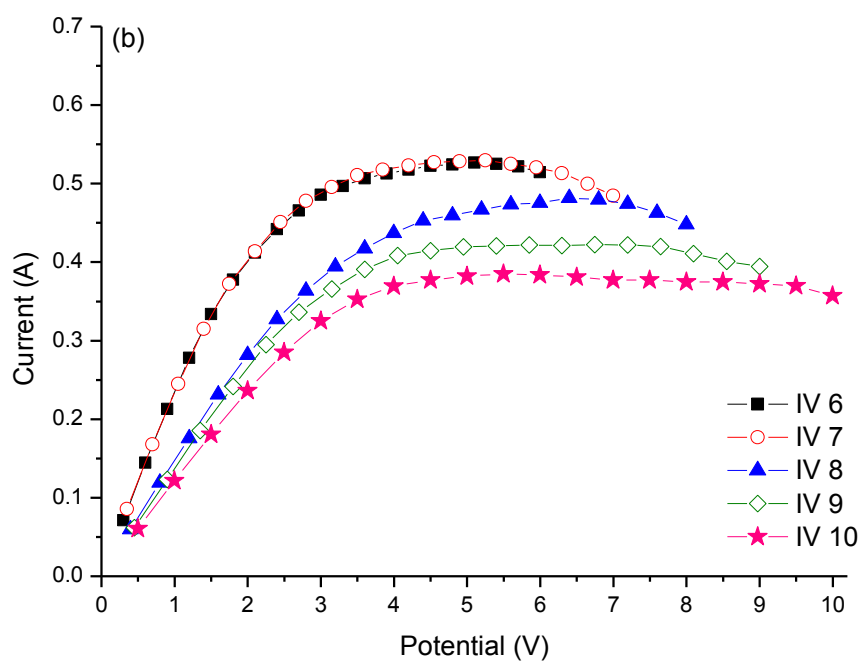
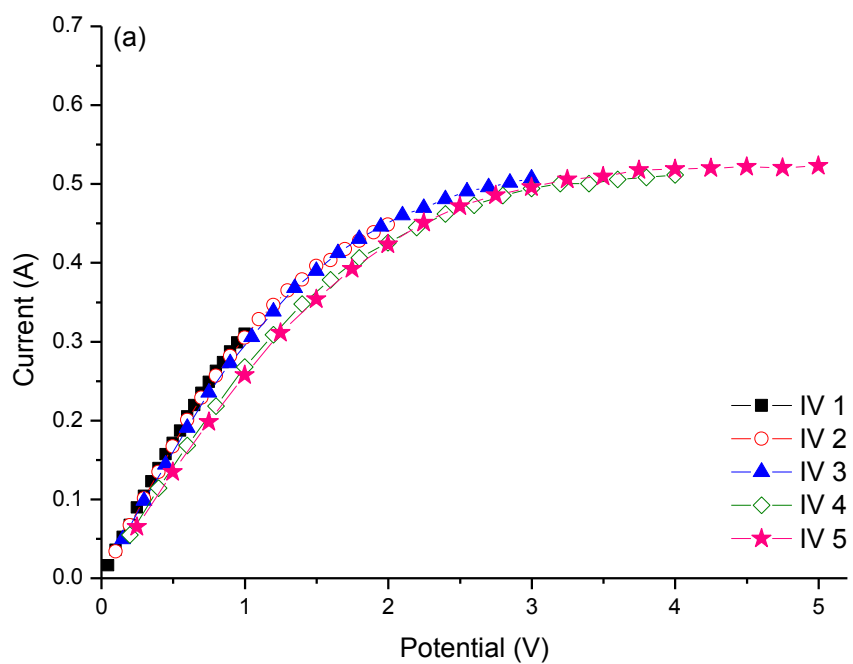


Figure 4.24: I-V characteristics of Sample 24 (72H 10mM). Top graph (a) for voltage sweeps up to 5 V while the second graph (b) is for voltage sweeps up to 10 V.

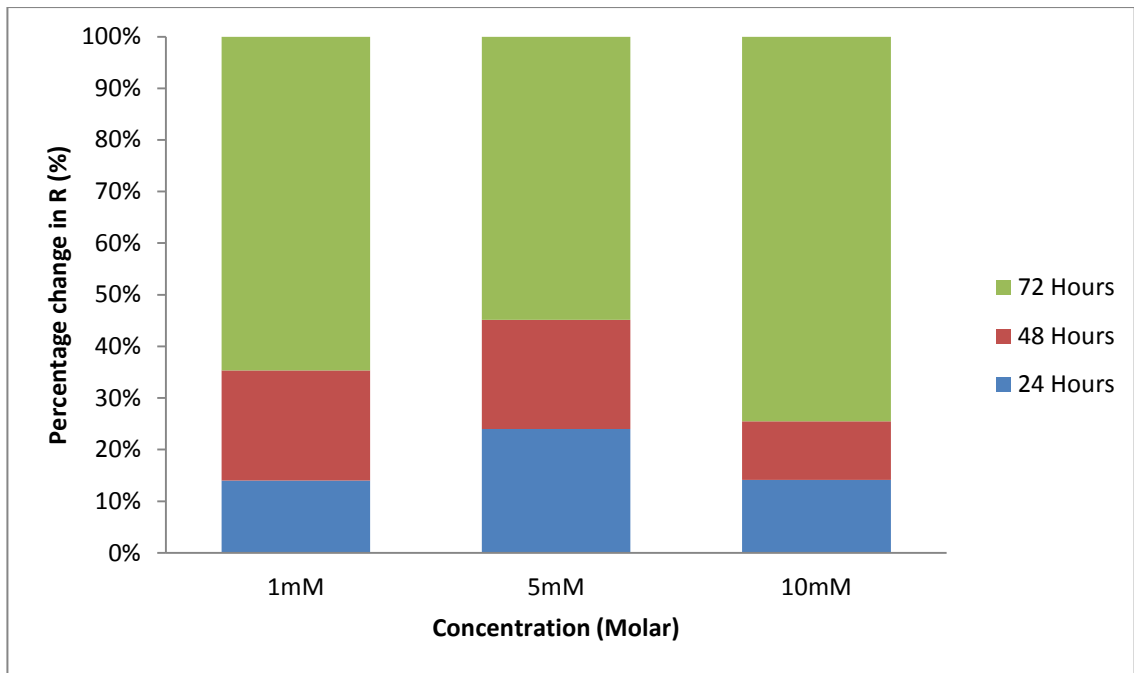


Figure 4.25: SAM concentration and immersion time with regards to the percentage resistance changes from linear form to non linear behaviour

In order to justify the relation of moisture loss with the device performance, another measurement was performed on freshly produced devices where the initial resistance are measured. The next step was to measure the same device resistance in a vacuum condition and after letting the air in the system resistance was re-measured to further understand any moisture loss effect on the device resistance. Results obtained are tabulated and shown in Table 4.1. This result matches with studies conducted by Pinto *et al.* where moisture recovery can be implied by the improvement in resistivity that is almost similar to the initial device resistance. The resistivity recovery is better than 85% which reflects water is replenished upon exposure to moisture nearly as rapidly as when is taken away from the vacuum [96].

Table 4-1: Resistance value for all SAM samples in air, vacuum and after air admittance in the vacuum chamber

SAM condition	Initial Resistance (Ω)	Resistance in vacuum (Ω)	Resistance in air (Ω)
24 Hours of Immersion in DDT			
Sample 25 (1 mM)	0.5	1.3	0.9
Sample 26 (5 mM)	0.9	2	1
Sample 27 (10 mM)	0.7	2.1	0.7
48 Hours of Immersion in DDT			
Sample 28 (1 mM)	0.5	1.7	0.6
Sample 29 (5 mM)	0.4	1.3	0.5
Sample 30 (10 mM)	0.7	2.9	0.8
72 hours of Immersion in DDT			
Sample 31 (1 mM)	0.7	2.9	0.7
Sample 32 (5 mM)	0.9	5.2	1.0
Sample 33 (10 mM)	0.9	5.7	1.0

Some studies suggested that protonated polyaniline conductivity can be enhanced by the presence of moisture [96, 107, 108]. According studies by Kahol et. al the degree of crystallinity in the polyaniline samples that are exposed to moisture is higher than a dry sample. The interplanar lattice spacing that leads to better interchain hopping hence increasing conductivity is caused by moisture presence. It has been argued that the presence of moisture has lowered the barriers between metallic islands, therefore increasing conductivity [95]. All the results show almost similar patterns as the applied

voltage sweep increased the resistance increased due to joule heating indicating that the conduction mechanism has been affected and is more likely to be of an activation or variable-range hopping type [109]. This can also lead to loss of moisture if the samples are heated by the increasing voltage across the polyaniline. The dependence of resistivity on joule heating is not influenced by gases such as oxygen or nitrogen as discussed by Pinto *et al.* [92]. The removal of moisture by joule heating has the effect of reducing the structural order between polymer chains in the crystalline regions (metallic regions) as well as chains bridging the metallic regions. The disorder is believed to reduce the localization length of the electronic wave function leading simultaneously to increased resistivity of the samples. The increase of charge localization especially on bridging chains, a delocalization to localization transition takes place and the system undergoes a metallic to non-metallic state upon joule heating [45].

Humidity studies on polyaniline film

The next step is to understand the effect of moisture combined with the characterised gold electrode by means of SAM of thiols on the current limiting behaviour. Three samples with different immersion times in the ethanolic solution have been tested in 100% humidity level. The ethanolic solutions were on 10mM as from previous results it was proven that the highest ethanolic concentrations had the most current limitation properties and showed better performance.

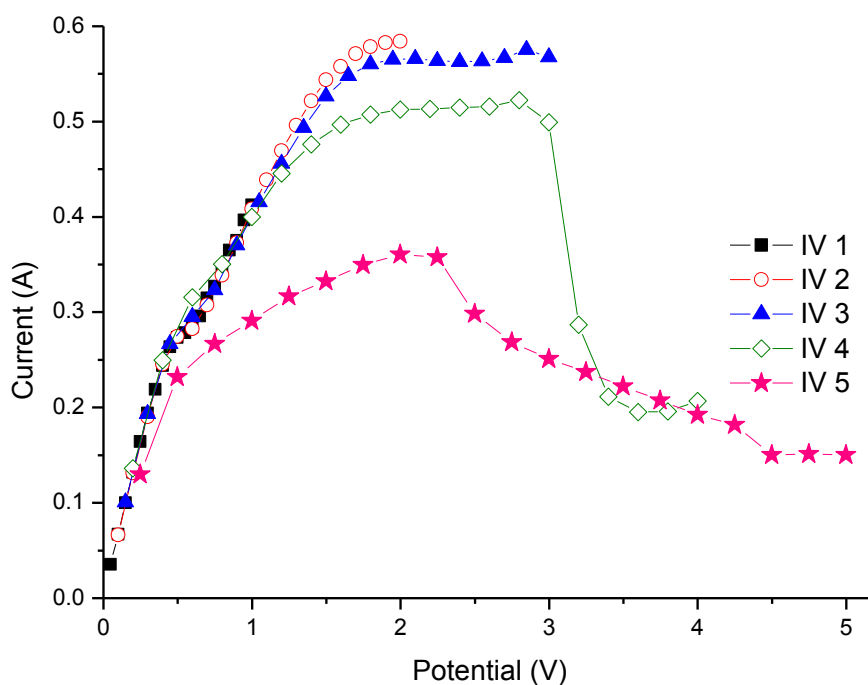


Figure 4.26: I-V sweeps for PANI with 24 H SAM device in 100% high humidity condition from 1 V to 5 V.

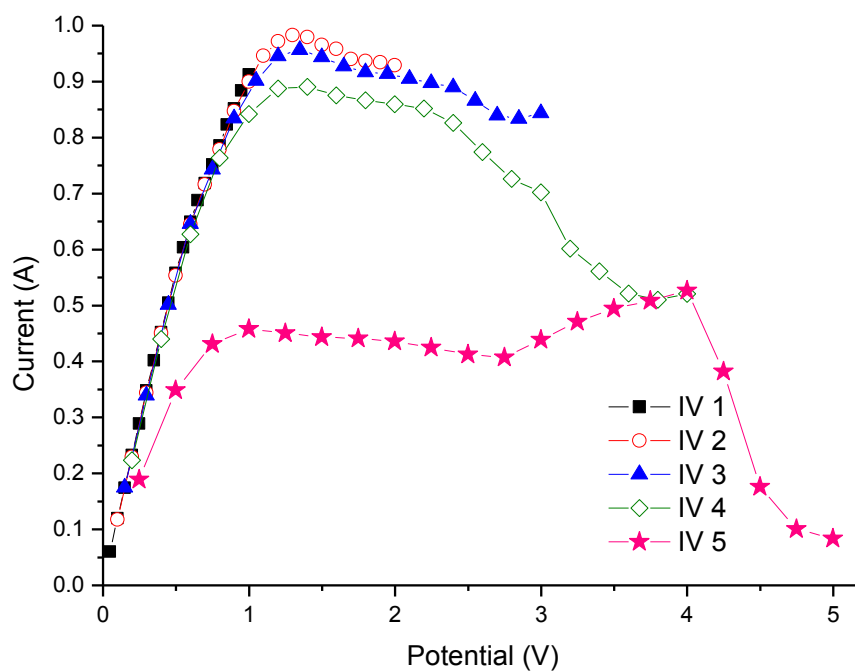


Figure 4.27: I-V sweeps for PANI with 48 H SAM device in 100% humidity condition from 1 V to 5 V.

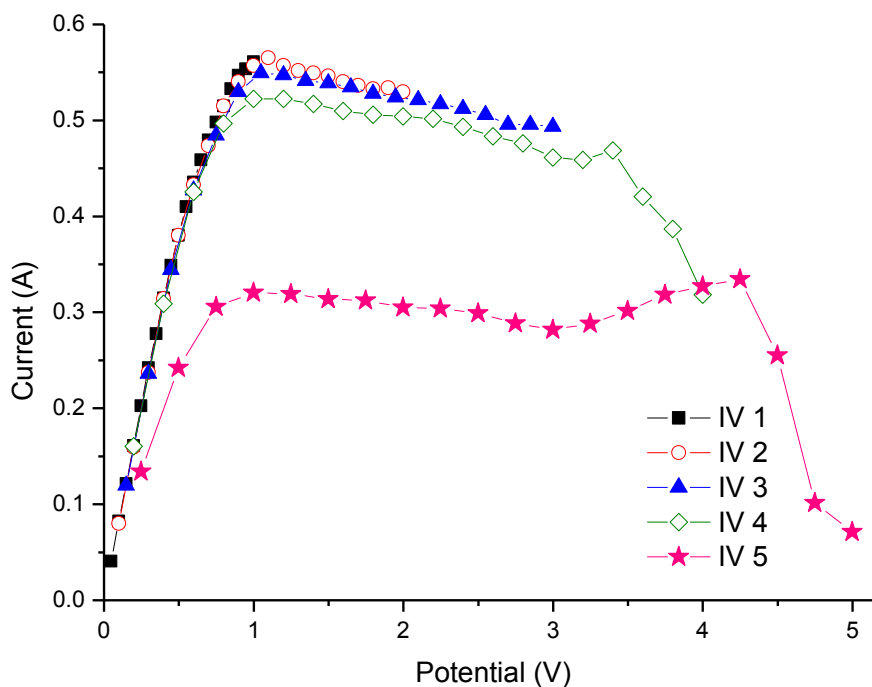


Figure 4.28: I-V sweeps for PANI with 72 H SAM device in 100% humidity condition from 1 V to 5 V.

From the results presented in Fig. 4.26 to Figure 4.28, the current is starting to show a negative coefficient from 0.5 V, which implies a more significant current limiting behaviour compared to results with no SAM and with SAM in a normal environment. It can be seen from the results that devices with SAM and presence of water showed better switching behaviour. Fig 4.25 I-V sweeps showed reversible results from IV 1 to IV 4, starting to exhibit irreversible patterns and more current limitation. Fig 4.27 with 48H immersion time showed similar pattern to the I-V sweep with reversible patterns in the first two sweeps and then irreversible sweeps with significant current limitation properties. Fig 4.28 showed that current values starting to reduce at 0.5 A, 0.3 A and 0.06 A for the sweep up to maximum 5 V (IV 5) of applied bias. This current limitation only occurs at maximum voltage applied 7 V onwards for devices without SAM performed in ambient humidity. Non-ohmic behaviour only occurs after 3 V on the device performed in normal environment humidity which showed that humidity level can change the response of the current limitation.

The SAM immersion time can be used to determine and tailor the maximum allowable fault current in the device application. This is due to the fact that longer immersion time will result in formation of denser and closely packed monolayers. This packed monolayer can prevent the rate of water to access the polymer surface, especially the polymer layer that is nearest to the SAM and gold surface. The device will heat up faster than less dense monolayer, therefore current limitation will occur at a lower applied voltage.

Devices with and without SAM showed significant differences in the current limitation range. The SAM devices exposed to 100% moisture level exhibits higher range of

current limitation from the range of 0.5 to 0.9 A. This reflects that devices with SAM have better conductivity which therefore, affects the current limiting behaviour. This is due to the initial growth of PANI on characterized gold being different from the growth of the PANI on bare gold. Gold with SAM creates a very hydrophobic surface. Normal gold with the roughness surface of less than 900 Å has a slightly hydrophilic surface. Polyaniline chains grow from the nucleates adsorbed on gold surfaces immersed in the thiol mixture. MacDiarmid proposed that the adsorption of aniline oligomers plays a fundamental role in the film formation [110]. The adsorption of nucleates on hydrophobic surface is more uniform [111-113]. Polyaniline chains growing from adsorbed nucleates are organised in parallel to produce a brush-like morphology as illustrated in Fig. 4.29.

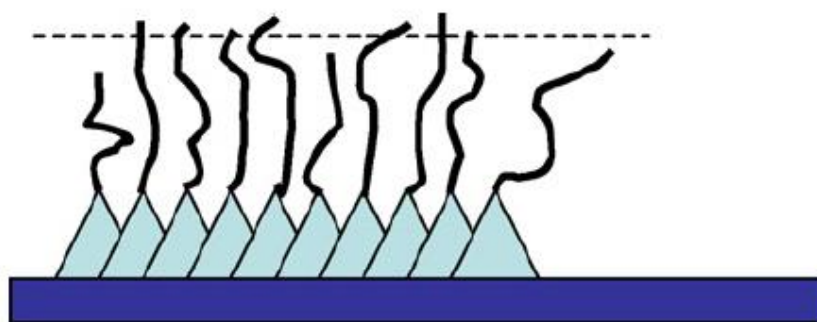


Figure 4.29: Polyaniline growth structure on a hydrophobic surface [114].

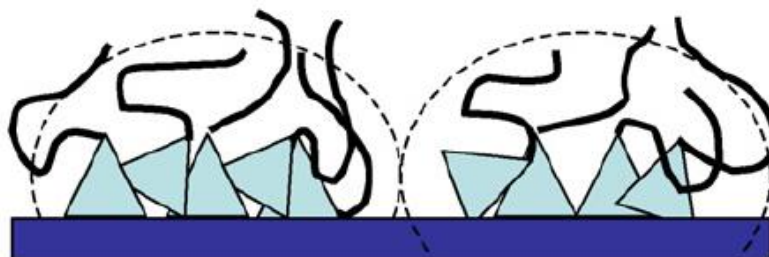


Figure 4.30: Polyaniline growth structure on a hydrophilic surface [114].

On hydrophilic surfaces, the aniline nucleates produce a 'droplet' like shape and PANI from them generates a granular structure where the organization of the chains is reduced as shown in Figure 4.30.

From the growth formation of the PANI on different surface characters, it is clear that water can be easily recovered after joule heating due to overcurrent due to the straight and uniform PANI structure. Unlike the PANI structure in Figure 6, the disorganised structure limits the amount of water absorbed and recovery process during the switching activity, therefore increasing the resistivity of the device due to increase of the barrier width between the metal islands.

Based on the I-V results with SAM and without SAM exposed to very high humidity, the current changes with regards from linear behaviour to non-linear has been plotted as the function of percentage of current declination with the potential changes to further understand the current limitation at different conditions. The result in Fig. 4.31 shows that the current reduced as the voltage increased in all devices with exposure to high moisture level. Device with 48 hours of SAM showed sharp decrease in current as voltage increases. This behaviour is similar on the 72 hour SAM and 24 hour SAM, where the current showed limitation as the voltage increased. Devices without SAM still have current limitation properties but with the least slope values.

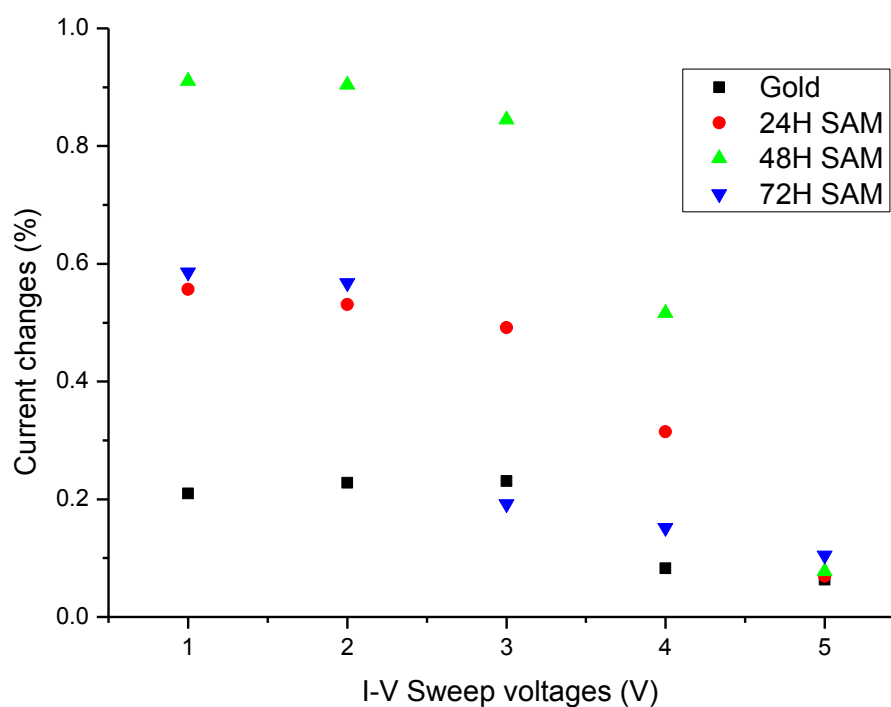


Figure 4.31: The change in current values compared for different samples in 100% humidity level for different voltage sweep from 1 V to 5 V.

Looking at the significant changes to the current limitation performance with the change in humidity level motivated further studies of the I-V characteristics in different humidity levels. Previous results that have been compiled showed that SAM devices and humidity changes have showed improvements in the switching properties of the devices. SAM samples that have shown best results have been selected and fabricated with the same concentration and immersion time. Samples with SAM and without SAM have been tested in different humidity levels at the facility in the National Technical University of Athens. Different humidity levels are compared with two different conditions which is non-SAM and SAM samples. SAM samples at this stage have been selected to be immersed in DDT for 72 H with concentration level of 10 mM. Results obtained are plotted in Fig 4.32 and 4.33.

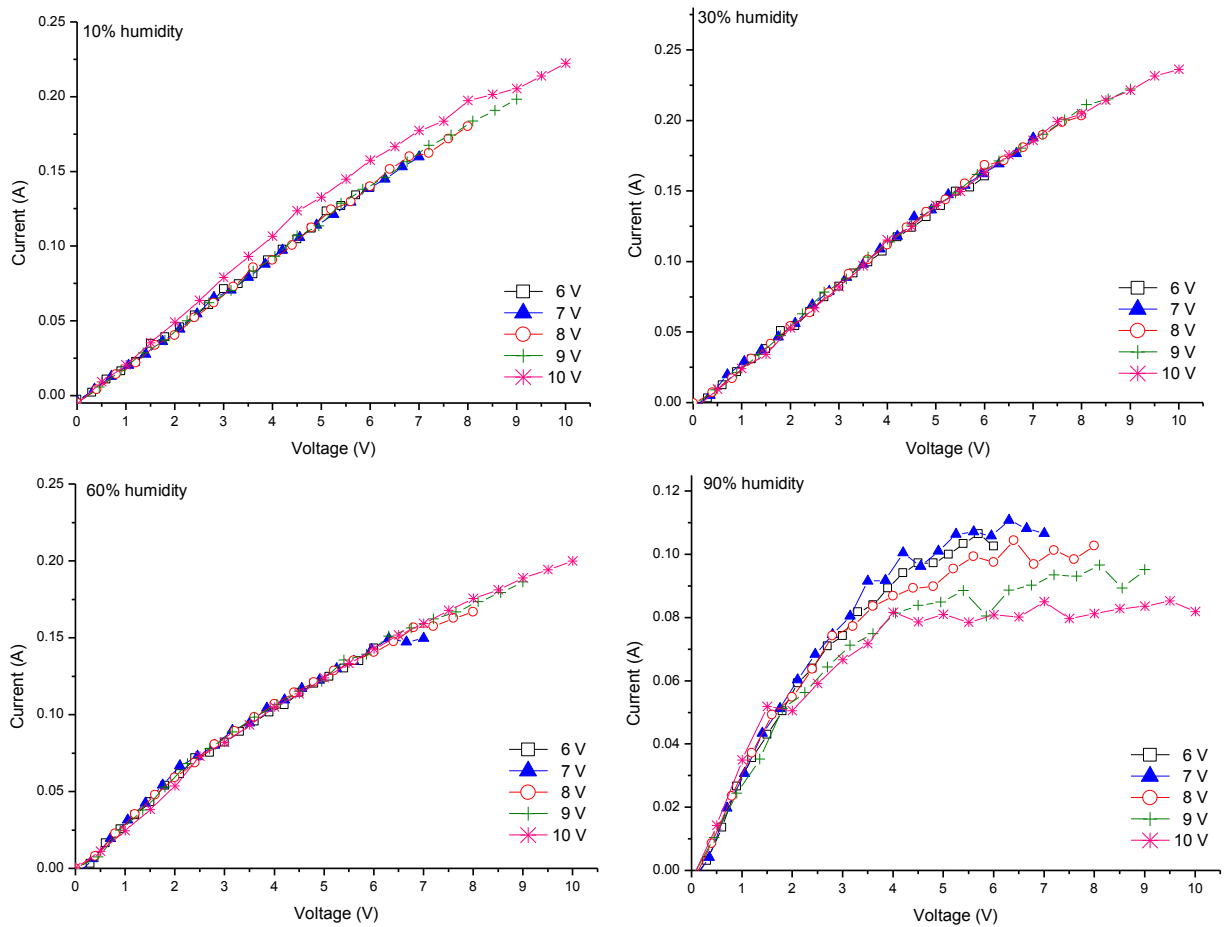


Figure 4.32: I-V measurement for samples without SAM in 4 different humidity levels.

The results presented in Figure 4.32 showed I-V sweeps in four different levels of humidity starting from 10% up to 90%. The results for 10% humidity showed almost linear behaviour and in agreement with the results in vacuum with almost no humidity. Voltage sweeps in 30% and 60% humidity level starting to show non-linear behaviour with current limitation starting to show at 7 V onwards. These I-V sweep forms are very similar to the electrical measurement performed in air and it is known that ambient relative humidity is around 40% to 50%. I-V sweep in 90% humidity started showing substantial current limitation and started at around 3 V of voltage sweep and the current output started to show a constant formation.

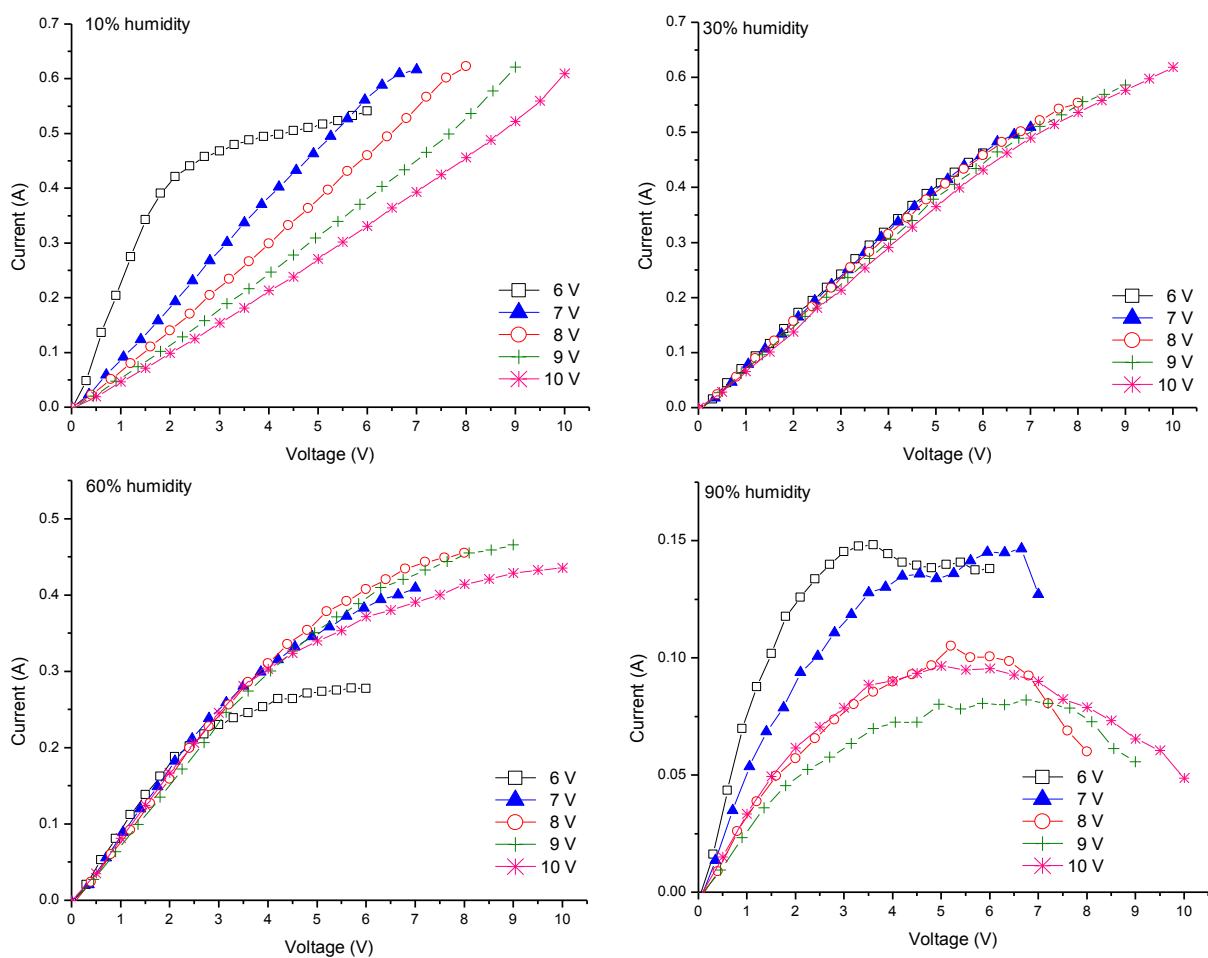


Figure 4.33 : I-V measurement for samples with 72 H SAM in 4 different humidity levels

Results presented in Figure 4.33 showed I-V sweeps for SAM samples in four different levels of humidity starting from 10% up to 90%. The first sweep showed in 10% humidity showed some current limitation due to the SAM modified electrodes and then once the moisture had been removed the I-V showed almost linear behaviour and showed an irreversible sweep pattern. Voltage sweeps at the 30% and 60% humidity level started to show non-linear behaviour with current limitation beginning at 3 V onwards. These results are in agreement with the 72 H SAM results presented earlier in this section performed in air.

I-V sweeps in 90% humidity started showing good current limitation behaviour with a foldback current that started at around 3 V of voltage sweep and the current output started to show current gradually increasing as voltage was increased up to the maximum voltage.

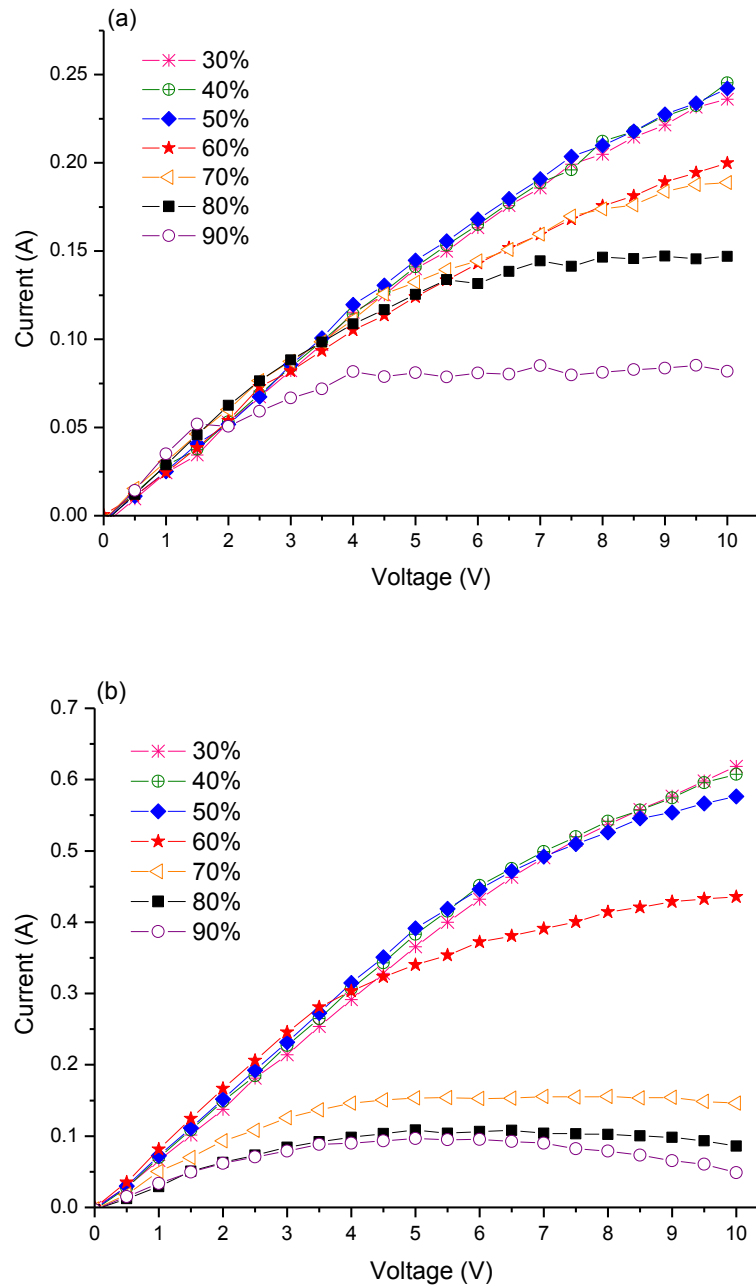
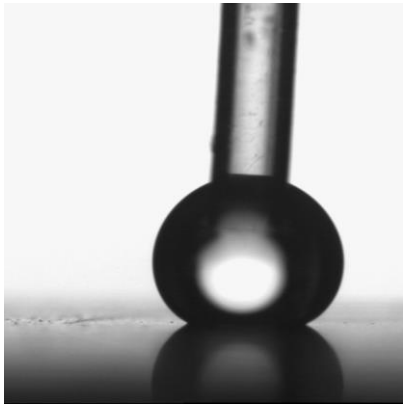
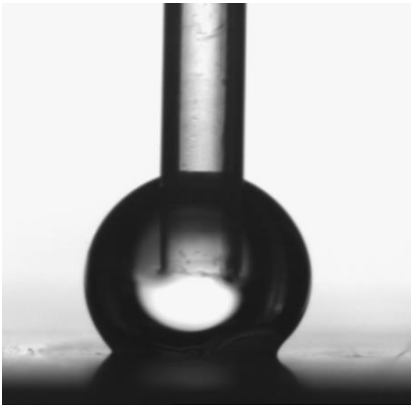
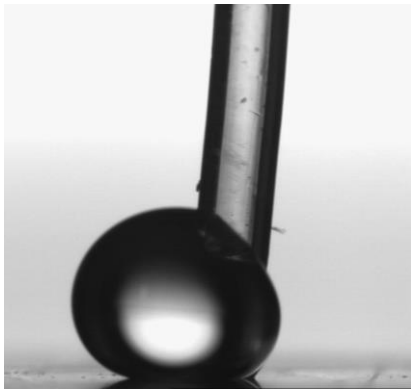
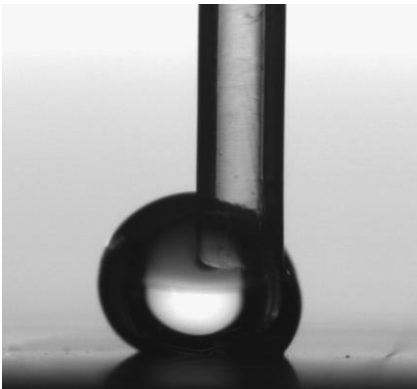
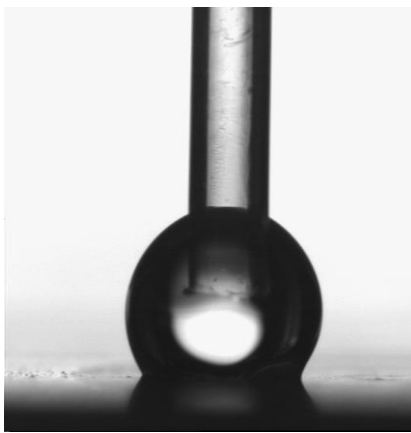
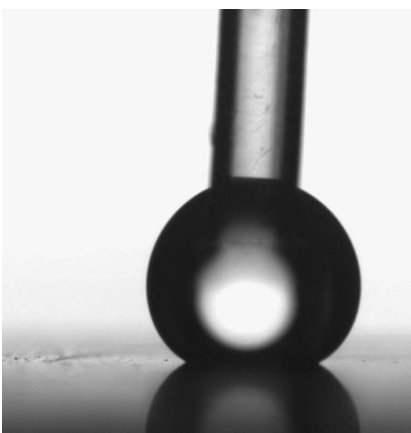


Figure 4.34: I-V sweeps for samples in different humidity at maximum potential 10 V (a) without SAM and (b) I-V measurement on SAM samples.

Fig. 4.34 showed results compiled at seven different humidity levels starting from 30% to 90% on SAM devices and non-SAM devices. This measurement is another way of combining humidity and SAM effect into understanding the current limiting device behaviour. Results in 4.33 (a) showed the I-V characteristics of the non-modified device that exhibited the CLD showed current limitation at 60% but and significantly improved better limiting behaviour at 90% humidity. Compared to the results in Fig 4.34 (b) the device started showing good current limitation at 60% humidity and continue to do so with reversible sweeps. Beyond 70% humidity the I-V sweep characteristic is irreversible, but showed a better and improved current limitation and this behaviour continues up to 90% humidity. This confirms that the PANI-MSA SAM device with good moisture content produces a very good current limiting device.

Another concern on the SAM surface is the durability in electrolyte solutions during polymerisation of the polyaniline. The SAM could be removed during this process due to the acidic electrolyte solution. To further validate this argument, Drop Shape Analysis (DSA) tests have been performed to verify the existance of the monolayers after the immersion of the gold-SAM substrates in the electrolytes during polymerisation. Three substrates have been immersed in DDT ethanolic solutions for 24 hours in order to get a decent formation of self-assembled monolayer. The drop shape analysis of each sample was taken using the Kruss DSA10. All substrates were found to be very hydrophobic. The three samples were then immersed in the electrolyte for a duration of 1 minute, 10 minutes and 1 hour respectively. The DSA of each of these samples with different immersion times in the electrolyte were repeated. All samples showed very hydrophobic surface areas. The summary of the DSA and contact angles are shown in Table 4.2.

Table 4-2: Drop Shape Analysis to confirm the existence of a Self Assembled Monolayer (SAM) after having been dipped in electrolyte.

Sample	DSA before immersion in electrolyte (contact angle)	DSA after Immersion in electrolyte (contact angle)	
10mM DDT for 24 hours	132.1 ⁰ 	134.8 ⁰ 	1 min
10mM DDT for 24 hours	138.6 ⁰ 	129.6 ⁰ 	10 mins
10mM DDT for 24 hours	147.4 ⁰ 	144.6 ⁰ 	60 mins

After confirming the existence of the SAMs after the polymerisation process, further test were made to understand the SAM device contact resistance compared to devices without SAM. Contact resistance has a significant impact on the electrical characteristics of the polymer film which helps to distinguish the resistance associated with the gold/polymer barrier at the interface between the polymer film and the gold substrate. The technique for measuring the contact resistance associated with metal-semiconductor (conducting polymer) interface was first proposed by Shockley in 1964 [84]. The method employed for the study is based on investigation of the dependence of the resistance on the distance between two electrodes and determination of the contact resistance by subsequent extrapolation of the dependence to zero distance as explained in detail in Chapter 3.5. This technique is known to be very informative as it also provides the information for homogeneity of the polymer film. However it requires a number of devices and experiments to get a single measurement of the contact resistance. The devices were fabricated using photolithography method to get a few devices with several different gap lengths using a symmetrical design. Results are shown in Fig. 4.35 and Fig. 4.36.

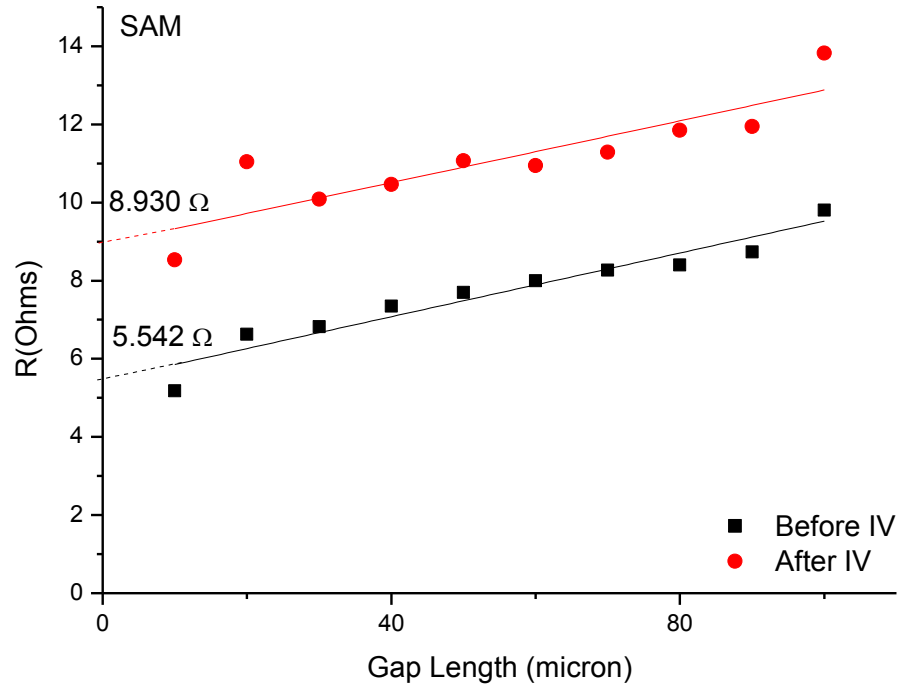


Figure 4.35: Contact resistance of the device with SAM before and after I-V sweeps.

Contact resistance shown in Fig. 4.35 are samples produced with SAM on gold electrodes. Samples have been produced along different channel lengths ranging from as small as $5\mu\text{m}$ to $100\mu\text{m}$. The resistance of the device for different length is then plotted so the contact resistance of the device can be extrapolated from the results [115]. I-V sweeps were then performed on the device and contact resistance was re-measured. The resistance increased but the slope of the plots remains constant showing good stability of the device's bulk resistance.

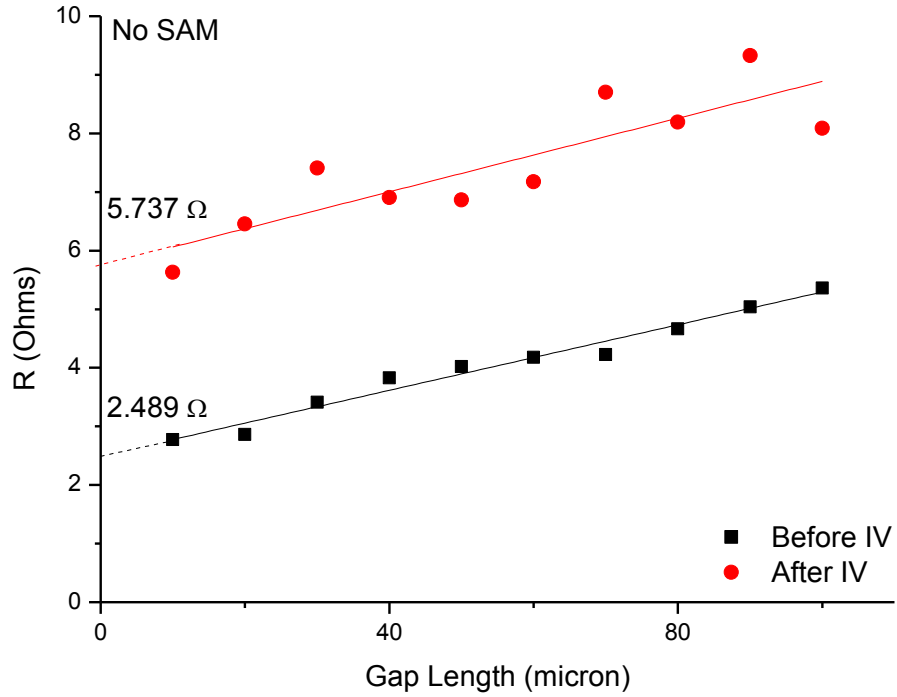


Figure 4.36: Contact resistance of the device without SAM before and after I-V sweeps.

Fig. 4.36 showed the contact resistance extrapolated using the plots obtained across a range of different channel lengths to compare with the SAM devices in Fig. 4.35. From the results it can be seen that the different gaps imply the transfer length where the current transfer from the gold to the polymer as proposed by study from Berger shown in Fig 3.41 [85].

Assuming the measurements yield values for contact resistance, R_c and transfer length, L_T and yield the following relations:

$$R(L) = \frac{R_{bulk}}{W} (L + 2L_T) \quad (4.3)$$

$$R(L = 0) = 2R_c = \frac{R_{bulk}}{W} 2L_T \quad (4.4)$$

where R_{bulk} is the resistance of the polymer.

Contact resistance of the device is found to be 2.771 Ω for SAM devices and 1.245 Ω for device without SAM which is not far from the current limiting device resistance value around the range of ~ 1.2 to 2.5 Ω . Fig.4.37 demonstrates the condition of contact resistance on device with contact resistance and without contact resistance.

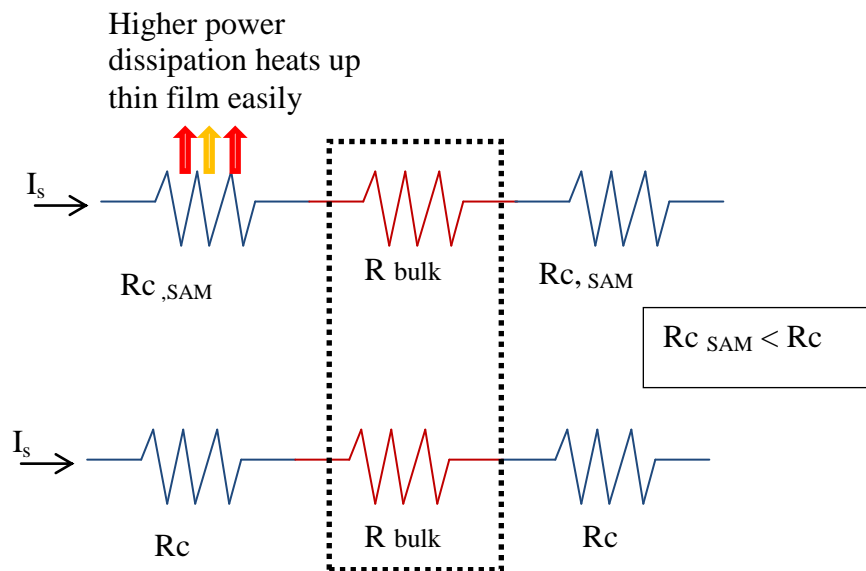


Figure 4.37: Schematic of contact resistance with different power dissipation level across the contact area on device with SAM and without SAM

The resistance of the bulk polymer are same for both devices but the resistance at the contact area differs from the device with SAM and without SAM. This is due to more energy being needed to surpass the monolayer for the current to reach the bulk polymer resulting in higher power dissipation across $R_{C,SAM}$ than the power dissipation across needed R_c . I-V properties at the devices therefore are dominated by the bulk polymer layer. Device with SAM have different properties due to higher power being dissipated across the contacts with thin film heats up the polymer quickly and releases the moisture contents, so the current in the SAM device as a whole is reduced. This showed a very substantial proof that the existing results obtained from the measurements

performed on the device have a small influence from the contact resistance value that is almost negligible.

Contact resistance for devices without SAM is hypothesized to be lower than the SAM device as proven in the results. This is due to the polymer film on the CLD gap junction having different morphologies. It is suggested that the devices with SAM have different thickness and morphology due to the retardation of polyaniline growth during electropolymerization [89]. The contact resistance of the device is not much different from that of the polymer itself.

Studying the structural growth of the polyaniline on modified and un-modified electrodes helps to further validate the argument of the polymer growth and this is support the different electrical switching behaviour of the device on SAM modified gold substrates. The SAM treated electrodes are known to have a hydrophobic surface and this is supported by the results presented in Table 4.2. The hydrophobicity of ordered monolayers of alkanethiols blocked the electrode to ionic redox species, the polarity and charge of the surface is of much greater importance in blocking the electrooxidation of aniline. A monolayer of dodecanethiol initially retards the rate of aniline oxidation and has been studied previously [116]. The SAM does not cause an increase in the rate of polymer deposition over the rate at on unmodified electrode once nucleation has occurred [106, 117]. Oxidative polymerization of aniline gives rise to a thick film of polyaniline on non-modified regions as shown in Fig. 4.38 and a thinner film of the polymer on the dodecanethiol-covered electrode in Fig. 4.39.

However increasing of the magnification of the micrograph showed that any differences in polymer morphology arising from the different surfaces are small. This is in agreement with the observation that rate of polyaniline deposition remains slow on modified electrodes and never accelerates beyond the rate for oxidation at unmodified electrodes [106].

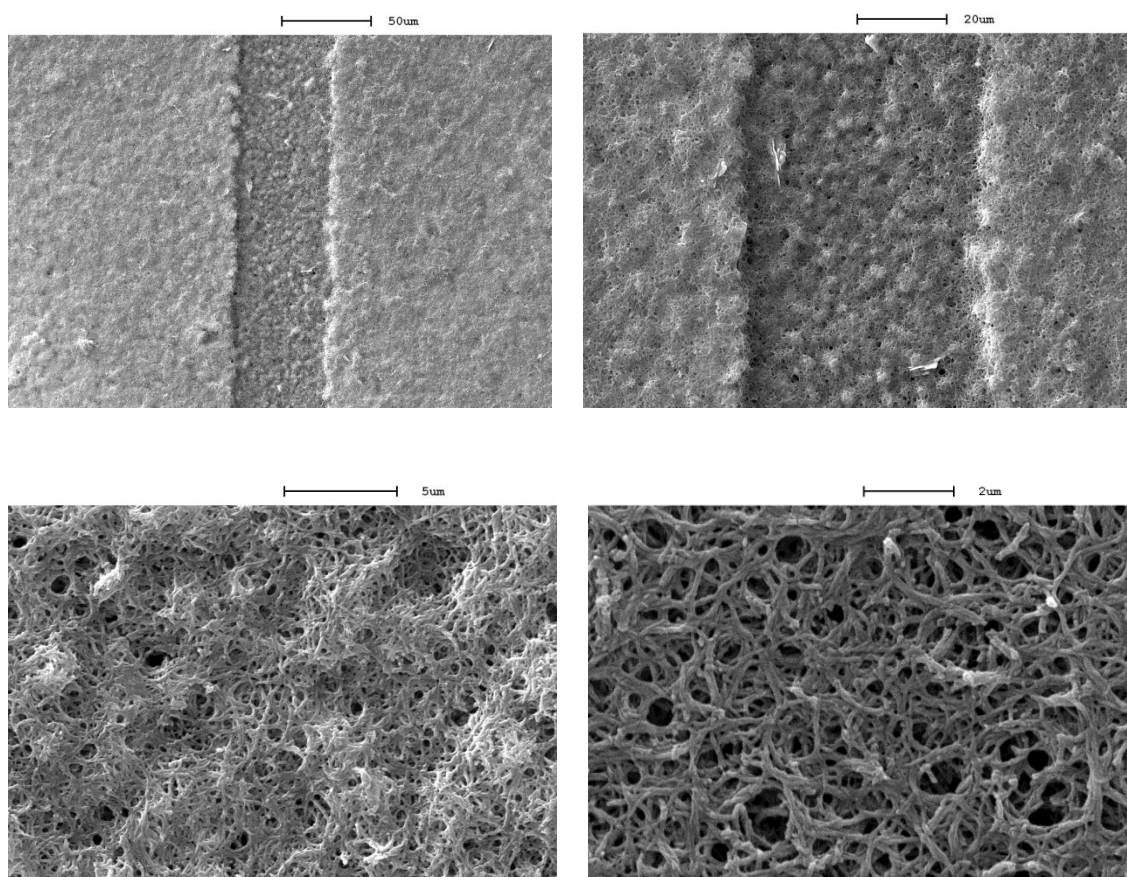


Figure 4.38: Scanning electron micrograph of polyaniline deposited potentiostatically at +85mV (vs Ag/Ag Cl) from 0.5 M polyaniline in 1.0 M methanesulfonic acid. The top left of the micrograph showed the polyaniline deposited on non-modified gold electrode with x1000 magnification followed by the x5000 on the top right. The bottom left and bottom right images represent the magnification at x10000 and x20000 respectively.

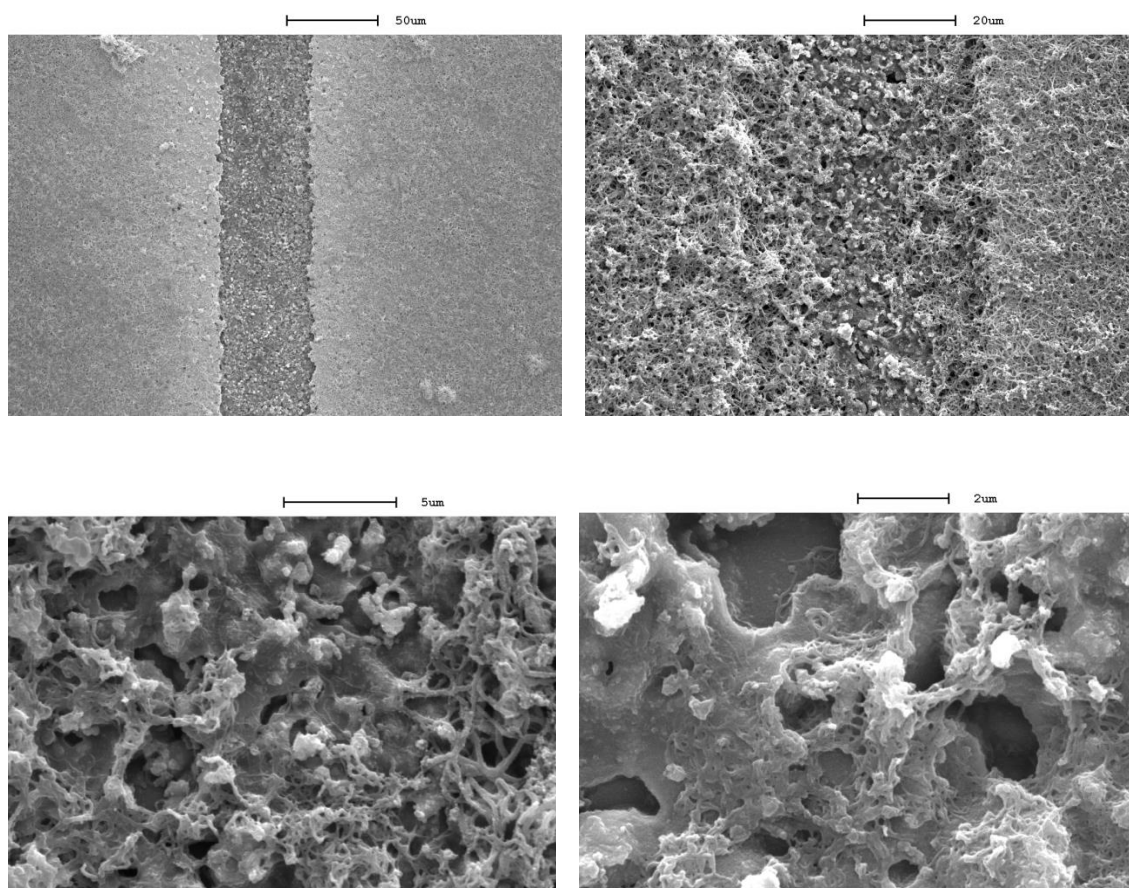
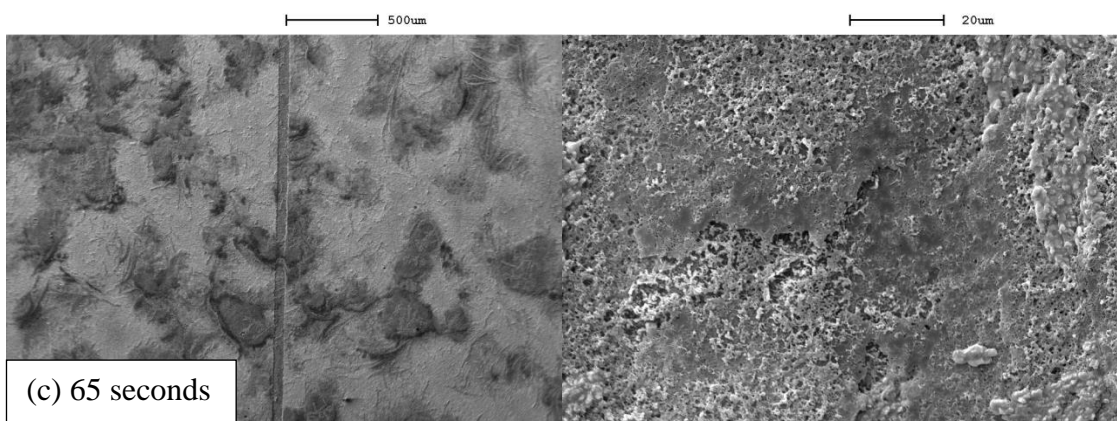
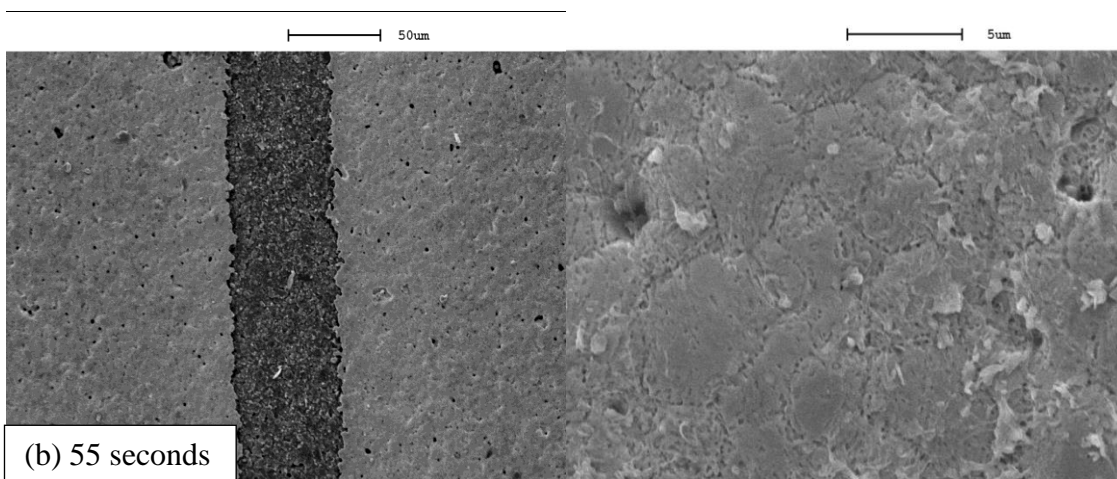
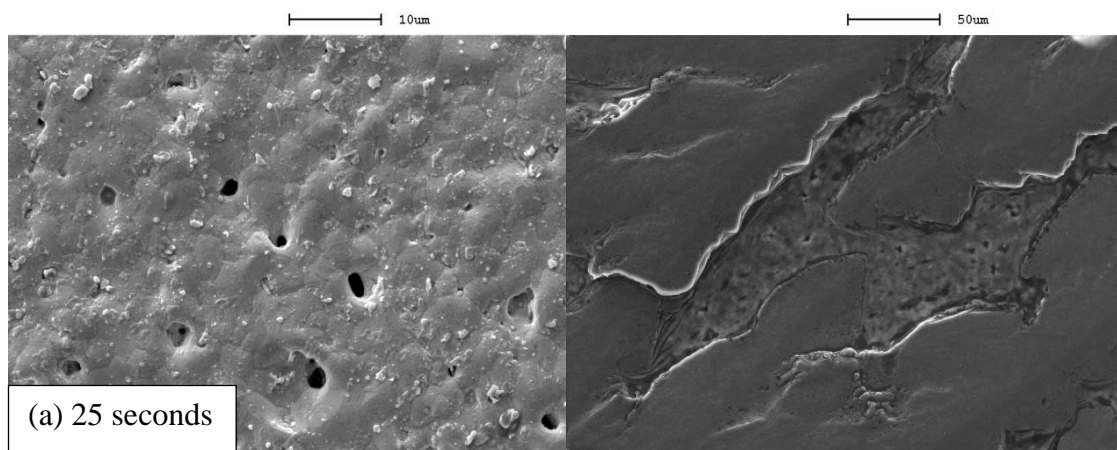


Figure 4.39: Scanning electron micrograph of polyaniline deposited potentiostatically at +85mV (vs Ag/Ag Cl) from 0.5 M polyaniline in 1.0 M methanesulfonic acid. The top left of the micrograph showed the polyaniline deposited on SAM modified gold electrode with x1000 magnification followed by the x5000 on the top right. The bottom left and bottom right images represent the magnification at x10000 and x20000 respectively.

The device with SAM had to be polymerized longer than the device without SAM in order to get the polyaniline to bridge the gap across the electrodes. It was observed that once the nucleation had been established on the SAM substrates during polymerization, the polymer structure replicates the same growth as the device with an unmodified substrate as shown in Fig. 4.40 (e). However the polymerization for the SAM device is always longer than the rapid growth of the unmodified substrate as presented in Fig. 4.40 as normally it took only 55 seconds for the polymer to bridge the gap on non-modified electrodes. SAM device took 85 seconds for the polymer to bridge the gap and 100 seconds to have the same morphology as the non-SAM device. The retardation of

polymerization has been ascribed to the blocking of defects in the monolayer and formation of a densely packed layer atop the SAM.



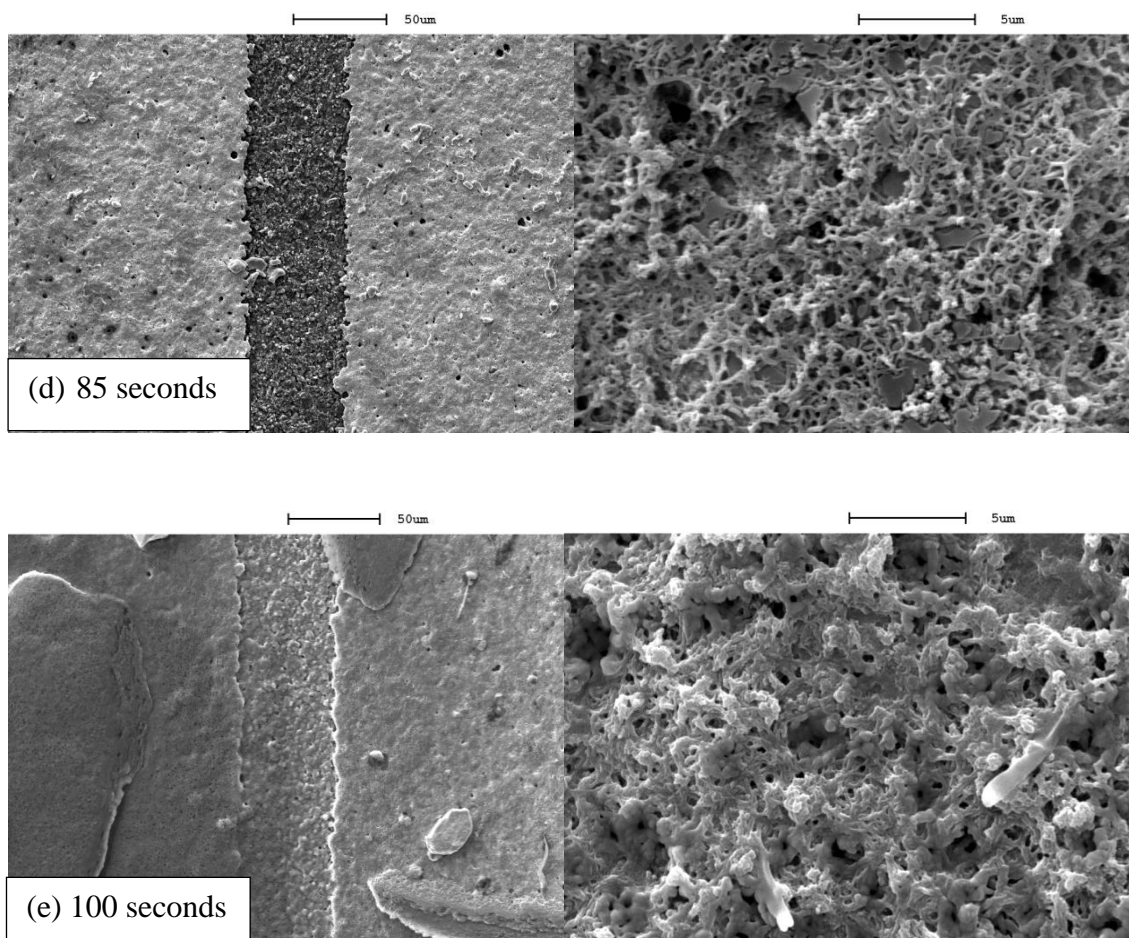


Figure 4.40 : Morphology SEM studies with various polymerization times for the current limiting device with SAM from (a) 25 seconds to (e) 100 seconds.

The profile measurement of the polymer film with the modified substrates without SAM and were measured using a Dektak profilometer. The results obtained in Fig. 4.40 showed the polymer film on the unmodified gold substrate has a significantly thicker polymer growth. The device in Fig 4.41 (a) has been polymerised potentiostatically for 55 seconds. Devices with SAM on the gold substrate showed evidence of the growth retardation as the average thickness of the polymer with SAM was less than double of the polymer without SAM. The devices with SAM have been polymerised electrochemically for 85 seconds to ensure the polymer film bridges the gap.

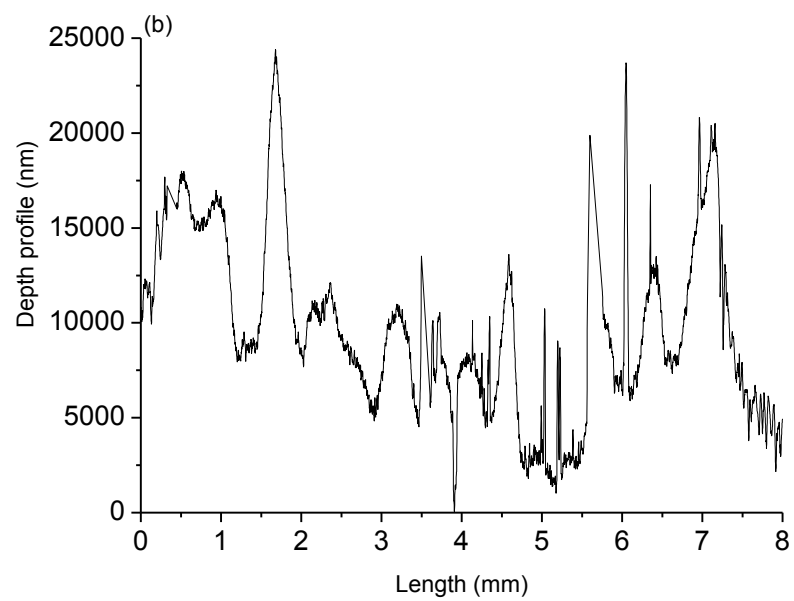
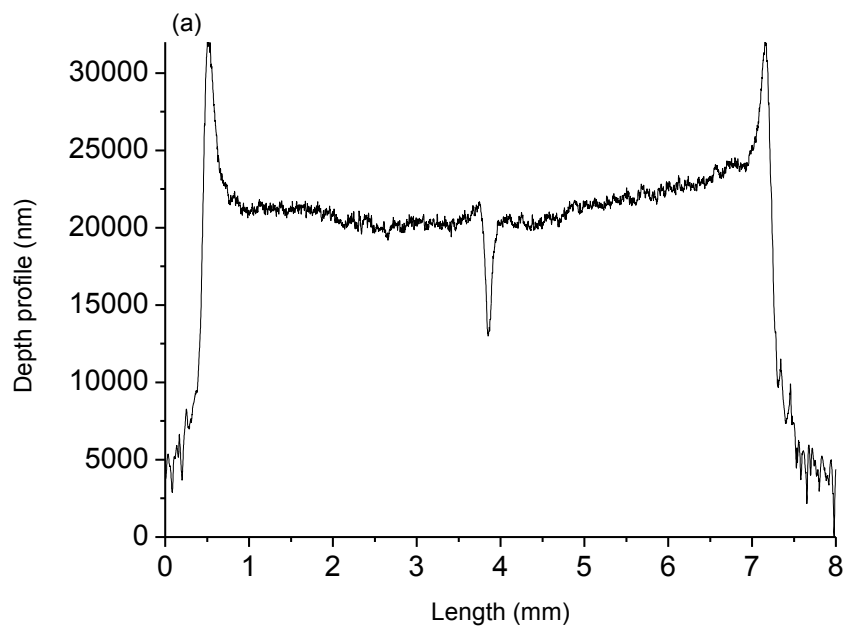


Figure 4.41 : Profile for polymer film on (a) device without SAM and (b) device with SAM on gold substrate.

The dip area where the 55 μm junction is present is also thinner for the samples with SAM suggests some retardation in the polymer growth. The profile shown in Fig. 4.41 (b) has a rougher surface and more sharp peaks due to the fact that the surface area of this device has larger porosity as presented in the SEM micrographs in Fig. 4.39. Hence, the profilometer tips would be able to detect on more structural details on the slow scan on the polymer film. The device without SAM have also high porosity (as shown in Fig 4.38) but the profilometer could not catch the small pinholes due to the tip size restriction.

The retardation growth can also be seen during the polymer growth on different substrates of the electrochemical polymerization as depicted in Fig. 4.42. The results showed characteristic current versus time response curves of potentiostatic deposition of polyaniline film at potential of +0.85 V for 55 seconds for non-modified electrode and the with same potential of 100 seconds for SAM modified electrodes. The continuous rise in current suggesting continuous growth of polyaniline as the deposition progresses for the polymer [118]. The nature of current as a function of time response curve in the potentiostatic deposition is due to the use of MSA as an electrolyte. The similar type of curve follows the same nature was reported for the H_2SO_4 method [119]. In this case the polymerization is due to 2.0 M MSA electrolyte used at 0.5 M aniline concentration of monomer solution. The electro-oxidation of aniline at constant potential produces green coloured polyaniline thin films.

Polymer growth on non modified SAM is very rapid and only took 55 seconds to completely bridged the gap between the two gold electrodes as shown in Fig 4.42 (a). Results in Fig 4.42 (b) showed growth initiation after 45 seconds as shown by the sharp

current increase and fully bridge the gap around 85 seconds of growth which confirms the growth retardation hypothesis.

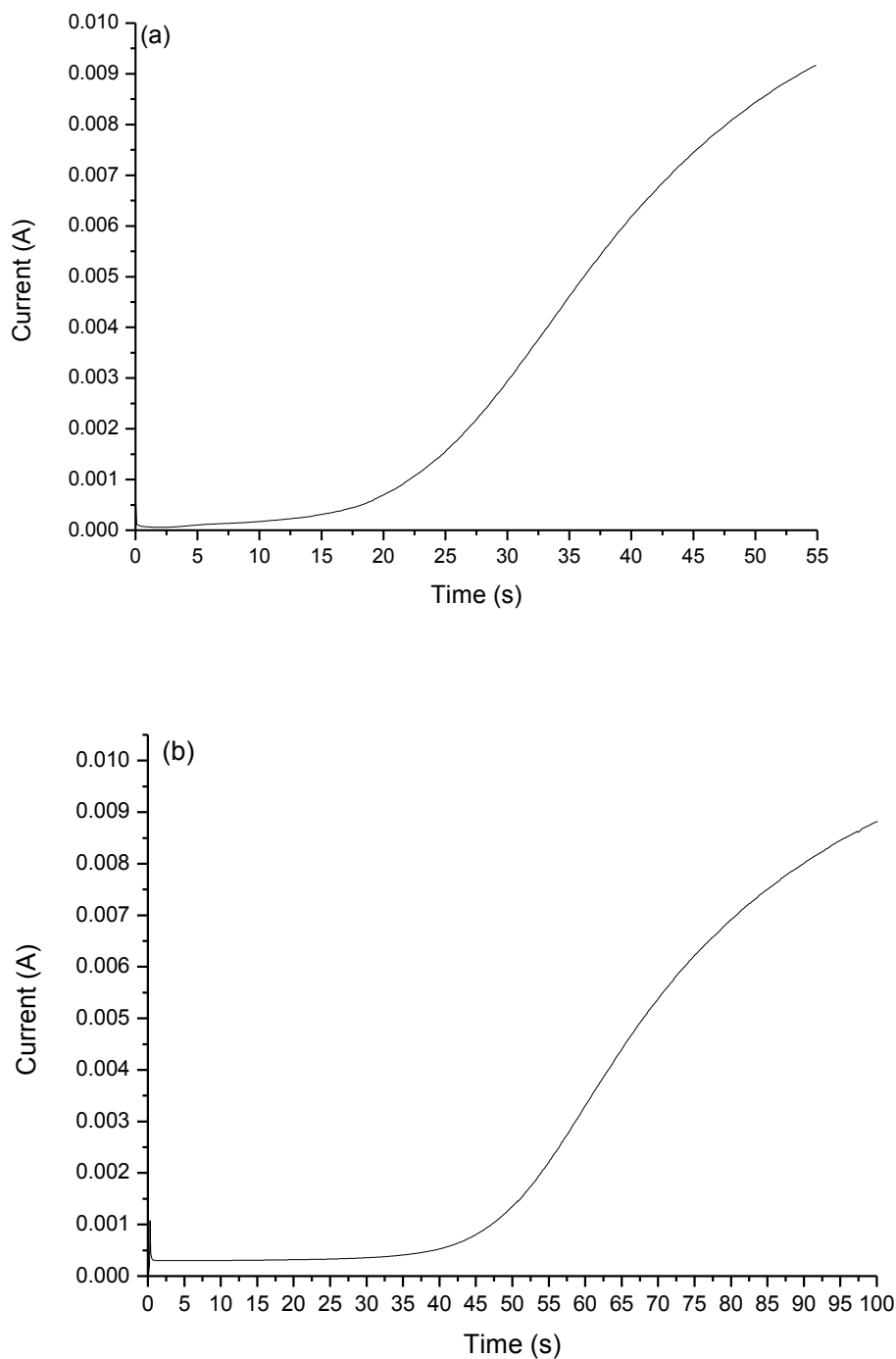


Figure 4.42: Potentiostatic deposition of polyaniline film (a) on non modified gold substrate (b) on SAM modified gold substrate and showing slower onset of growth for the SAM device.

Overall results of the electrical measurements have been presented for non-SAM and SAM devices. SAM devices clearly indicated better current limiting performance compared to the non-modified substrate. Contact resistances that have been compared with these two different conditions also showed definite differences where the SAM substrate indicated a higher contact resistance. Morphology of the SAM polymerization showed different structure from the non-modified gold and this is suspected to be the reason why these two devices showed different current limiting properties. Non-modified electrodes showed a spaghetti-like morphology with long fibrils and high porosity, while SAM devices have shown more compact polymer films with some porosity and agglomeration near the junction area. This could directly be due to the dodecanthiol monolayers acting as a barrier for the polymerization of aniline to form initially and needed more time to establish the polymer branches before proper film growth. We speculated that some pinholes in the SAM formation gave room for the initiation of the polymer to inaugurate growth on the electrodes. The hindered growth on the SAM surface also created more steps of hills and valleys as presented in Fig. 4.42 (b) on polymer films instead of a much more uniform layer as on the non-SAM surface. The uneven polymer surface is because of the initiation of growth for each polymer nucleation is not the thickness depending on the uniformity of SAM formation and the monomer orientation growth direction between the SAM on the gold substrate as illustrated in Fig. 4.43 for better understanding. This created a rougher surface which indirectly creates more surface area for charge interaction when an external voltage is applied to the current limiting device. Devices without SAM have a more uniform layer and thicker polymer films due to its rapid growth on the gold substrate which explains why the device has less current limiting effect.

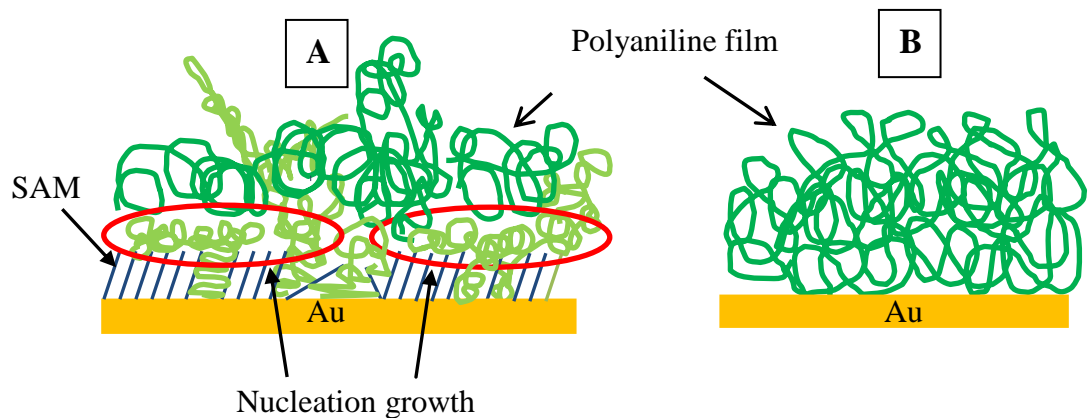


Figure 4.43: Illustrations of polyaniline growth and its formation on (A) gold with SAM and (B) gold without SAM indicating the growth and uniformity difference between the two methods used.

The devices with SAM can also be associated with less heating of the polymer film due to the monolayer formation as higher voltage across the device and have limited path before reaching to the polymer film. This not only creates better current limitation but helps the polymer film protect the moisture from being driven out too fast at higher voltage levels. This also explains why devices with SAM have higher initial resistance value. The device without SAM has a more direct path to the polymer film during electrical measurement but does then not greatly help to limit current due to the lower resistance value of the device.

4.3 Stability, reproducibility and effect of different dopants on moisture contents in polyaniline.

The results so far have shown evidence that SAM modified electrodes significantly improved the performance of the current limiting behaviour. With regard to that, we are interested in understanding the stability of the device after more than just a few runs of overcurrent event. Devices were tested for 24 hours of with 144 I-V sweeps across the device for 10 minutes delay giving the chance for the polymer to recover between each over current cycle. Maximum voltage applied are adjusted to be from low (2.5 V), medium (5 V) and high voltage (9 V) level to see the effect on the stability of the polymer on long term exposure of on different surge level.

Results were shown on the device for 24 hours of 144 runs with 10 minutes interval. Results were recorded and averaged every hour to see the effect on current limitation up to 24 hours. The first set of results with maximum of 2.5 V for 24 hours are shown in Fig 4.44 to Fig. 4.47. The data indicates there are no noticeable changes with repeated measurements at maximum 2.5 V.

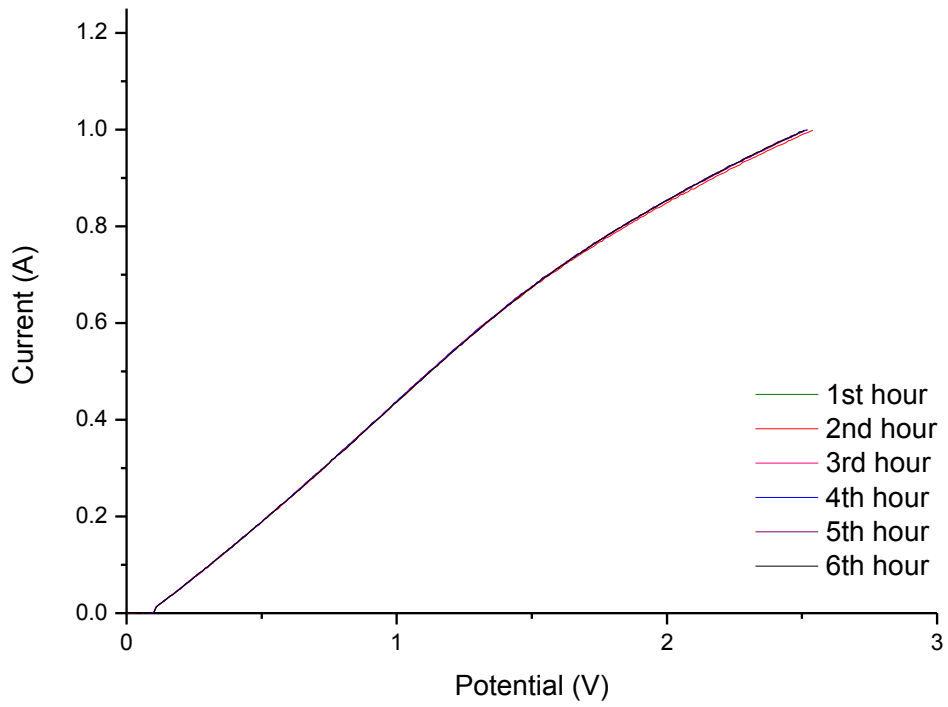


Figure 4.44: I-V sweeps for the 1st hour to the 24th hour with 2.5 V maximum voltage

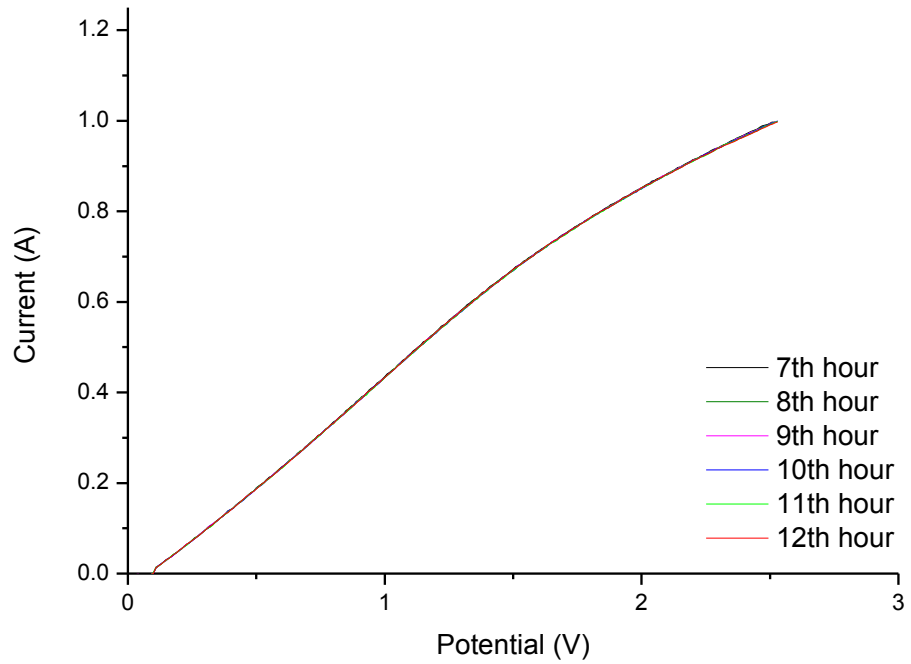


Figure 4.45: I-V sweeps for the 7th hour to the 12th hour with 2.5 V maximum voltage

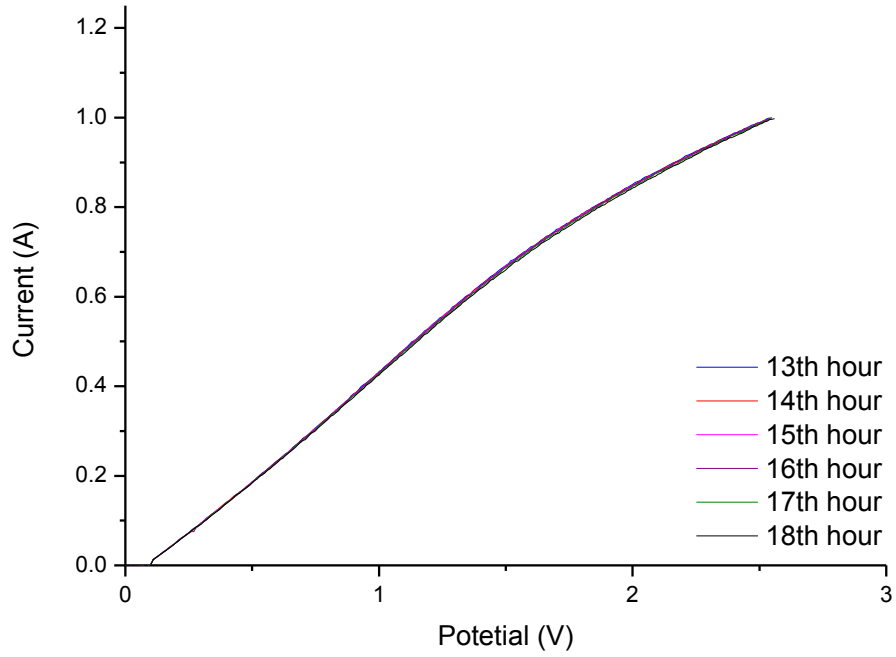


Figure 4.46: I-V sweeps for the 13th hour to the 18th hour with 2.5 V maximum voltage

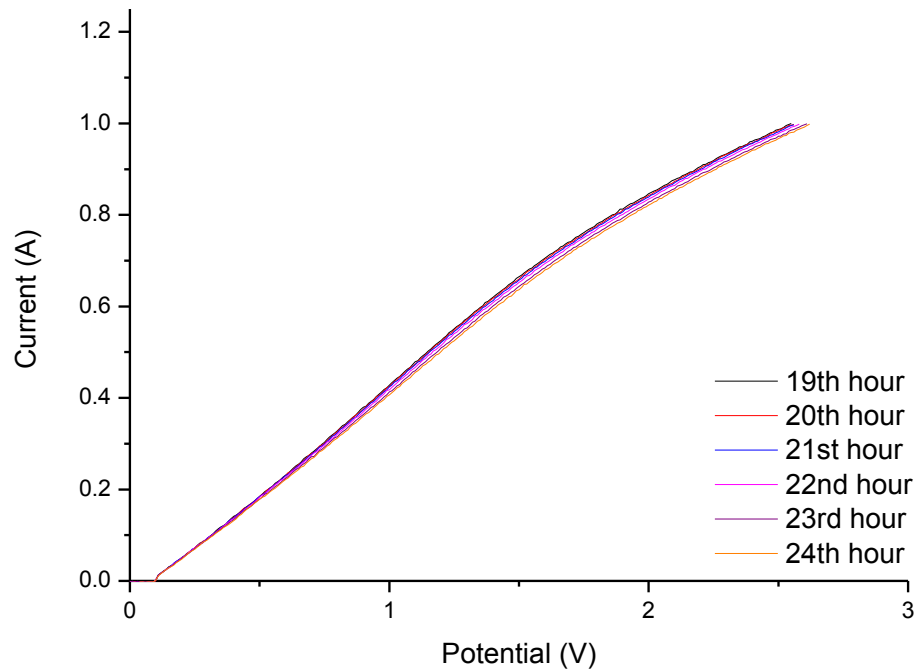


Figure 4.47: I-V sweeps from 19th to 24th hour with 2.5 V maximum voltage.

Results for a maximum applied voltage of 2.5 V for 24 hours of continuous running showed a good stability of the device across all the durations. This could be due to the level of voltage not causing heating which decreased the damage level on the polymer film. The initial resistance of the device before measurement was 2.2 Ω . After 24 hours of 144 of surge current, the device resistance value change to 2.7 Ω . The resistance change showed the continuous current-voltage sweep had some effect on the polymer film but not very significant and the device was still reversible.

Based on the results with 2.5 V maximum potential, it is interesting to know what happened to the device durability if voltage applied during the I-V sweeps were doubled and let it run continuously in 24 hours for 144 runs. Results obtained from the measurements are presented in Fig. 4.48 to Fig.4.51. Results shown have some offset voltage values and this only occurred for stability measurements and suspected due to issues from system setup and programming and need to be looked at in detail to understand the cause of the issue.

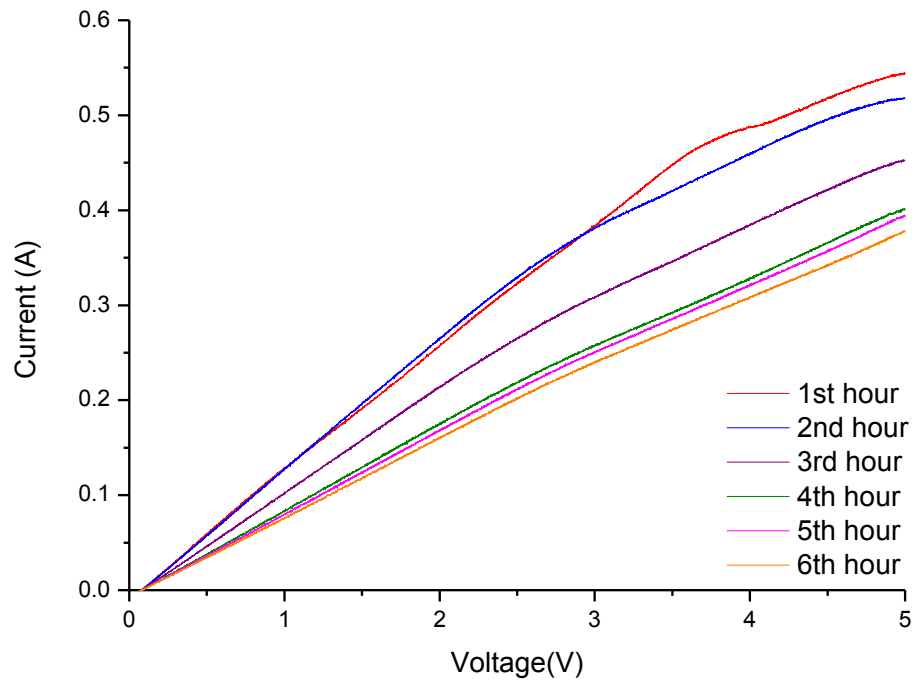


Figure 4.48: I-V sweeps for the 1st hour to the 6th hour with 5 V maximum voltage

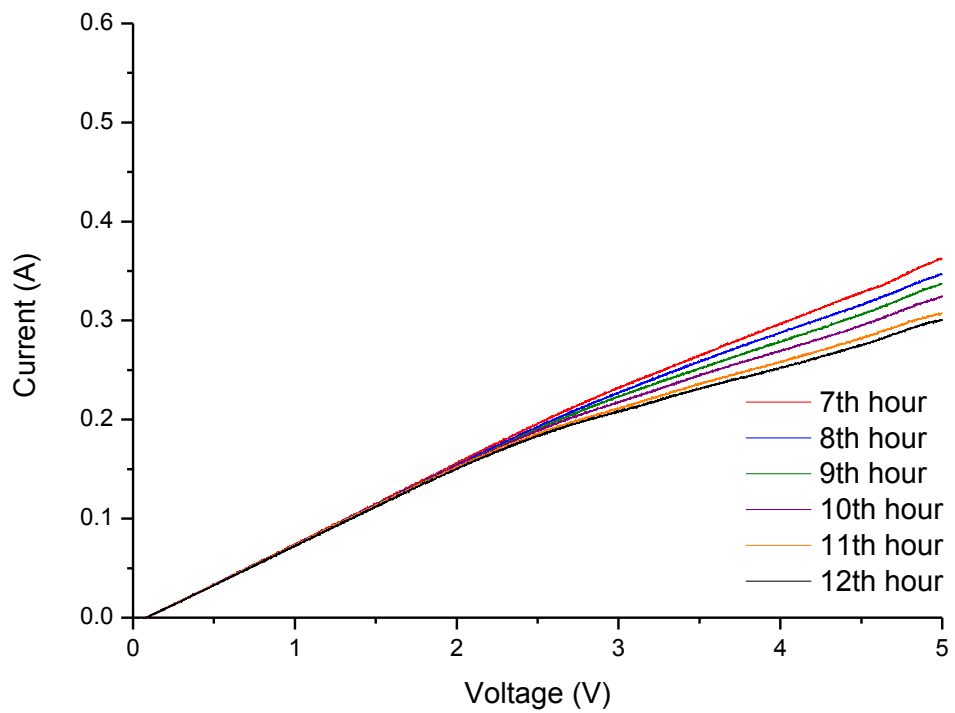


Figure 4.49: I-V sweeps for the 7th hour to the 12th hour with 5 V maximum voltage

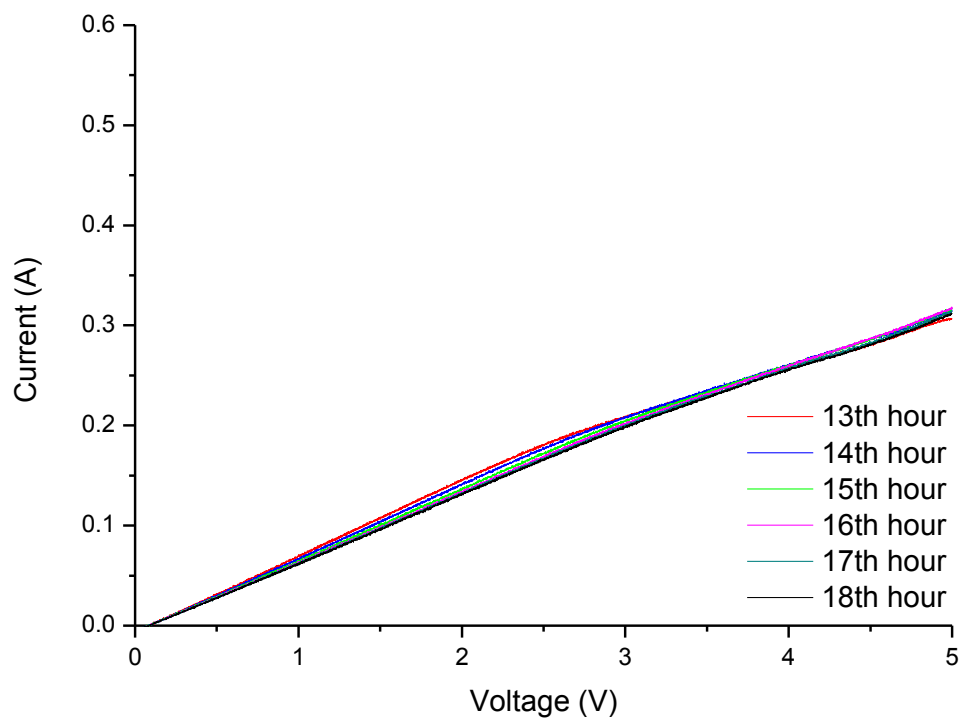


Figure 4.50: I-V sweeps for the 13th hour to the 18th hour with 5 V maximum voltage

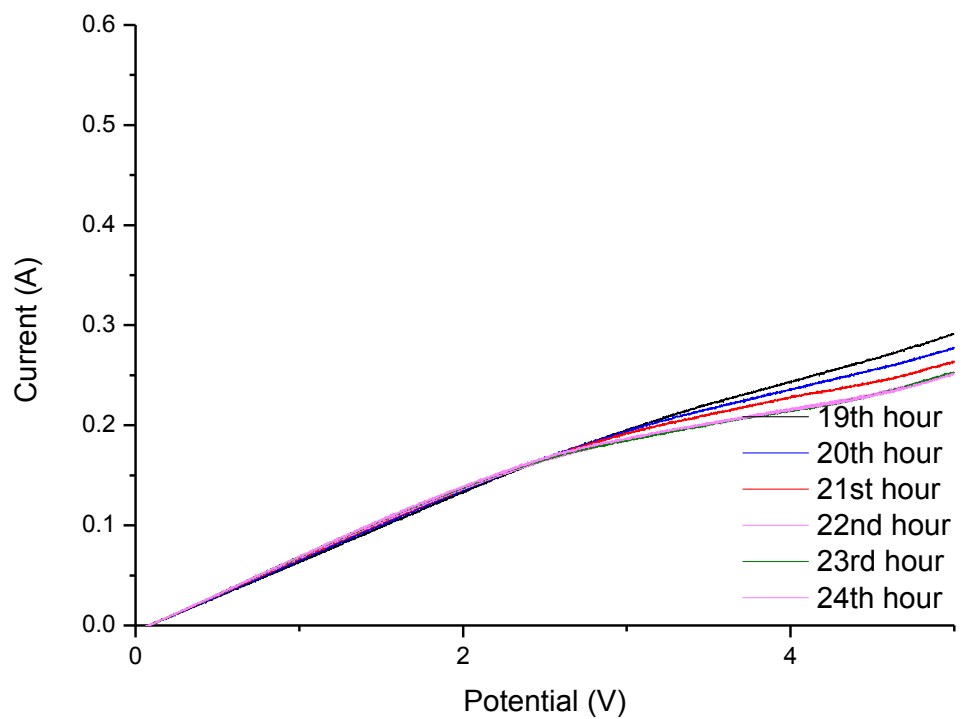


Figure 4.51: I-V sweeps for the 19th hour to the 24th hour with 5 V maximum voltage

Results with maximum 5 V immediately showed noticeable changes in the I-V trend from the first hour. Initial resistance of the device is 2.1 Ω and the resistance increased gradually with each I-V sweep up to the 8th hour. After that, the resistance increased changed gradually up to the last run at the 24th hour.

Another device was then run for 24 hours with maximum potential of 9 V. Device initial resistance was 1.2 Ω and after the 144th run the device resistance increased up to 11.2 Ω . Results are presented in Fig. 4.52 to Fig 4.55.

The polymer film is reacting to a joule heating effect due to higher potential level across the device repeatedly. Most previous studies have shown that protonated polyaniline displays a slow decrease in electrical conductivity at temperature below 200°C. At temperatures exceeding that level, the electrical conductivity decreases and the material will gradually turn into an insulator. At higher level of voltage it is expected that the device will reach the temperature where the polymer film can be damaged.

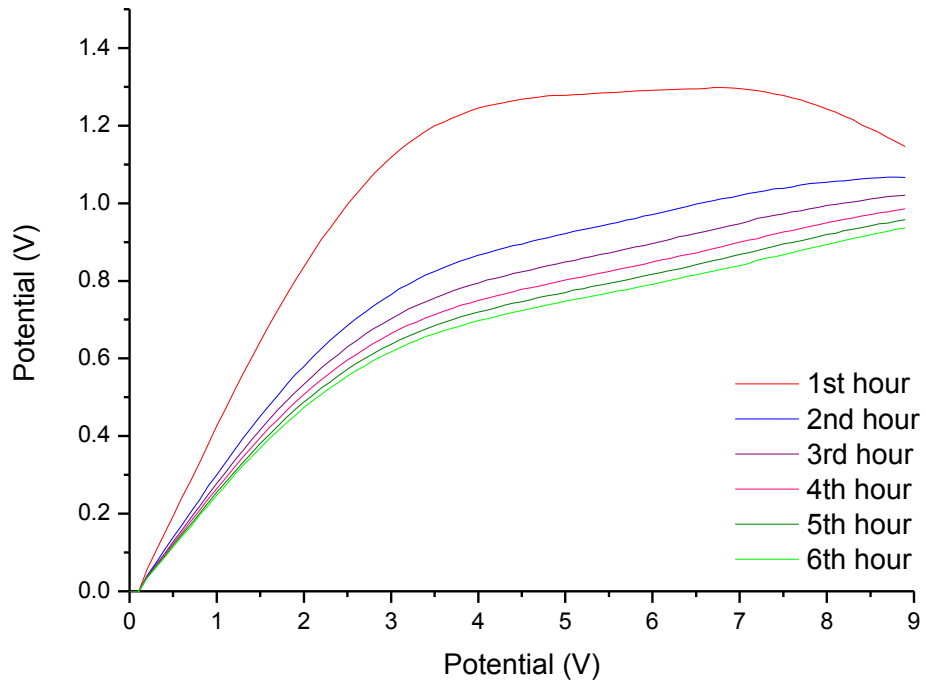


Figure 4.52: I-V sweeps for the 1st hour to the 6th hour with 9 V maximum voltage

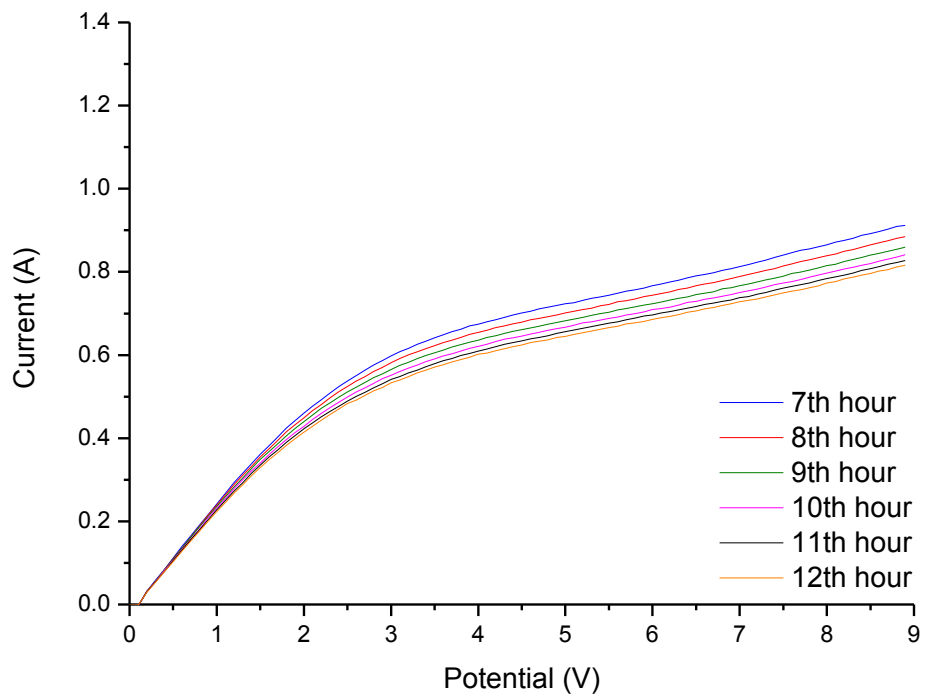


Figure 4.53: I-V sweeps for the 7th hour to the 12th hour with 9 V maximum voltage

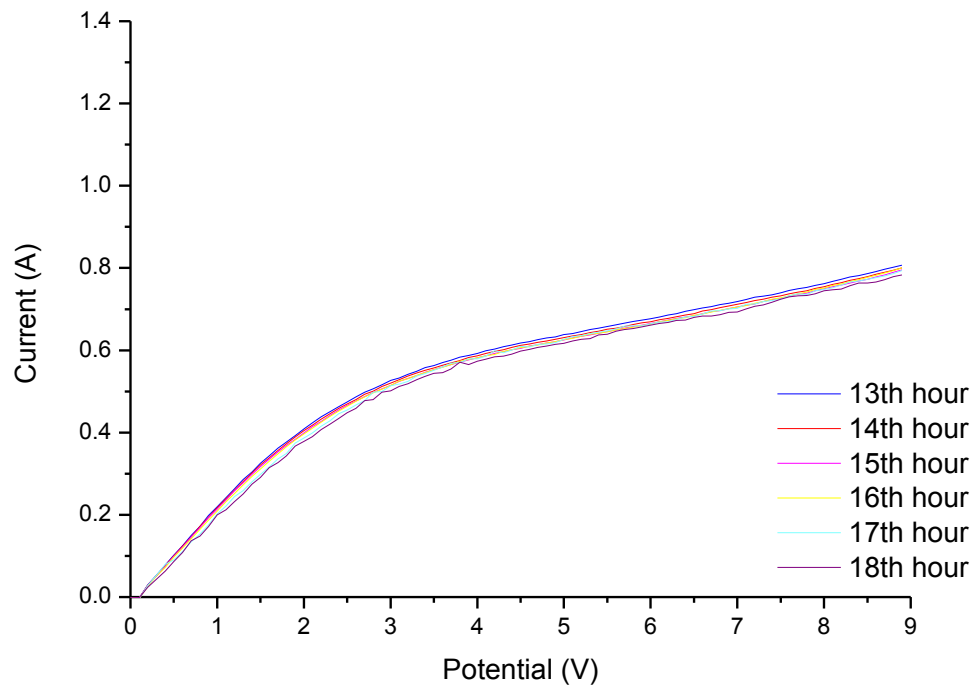


Figure 4.54: I-V sweeps for the 13th hour to the 18th hour with 9 V maximum voltage

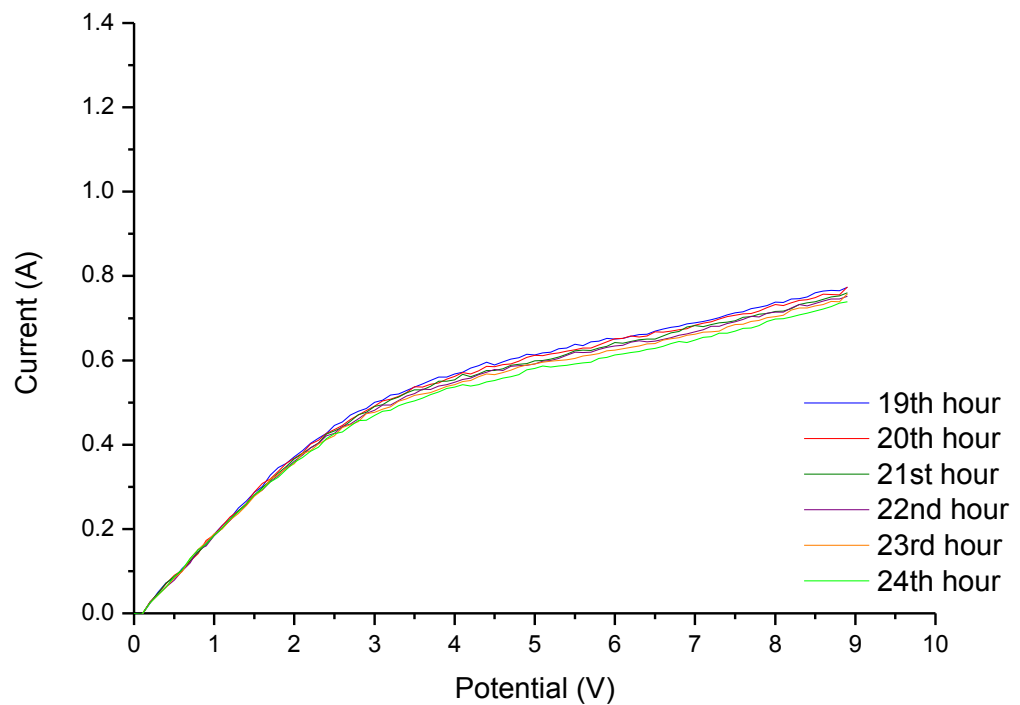


Figure 4.55: I-V sweeps for the 19th hour to the 24th hour with 9 V maximum voltage.

All results for the resistance change for all maximum applied potential are compared in Fig. 4.56. It can be seen that significant changes in resistance happened on the device with 5 V of maximum voltage. The device changes showed some fluctuations in the I-V trend since at this level the polymer was losing the moisture contents in the film but not heated through giving the polymer chance to recover the moisture contents from environment before being heated up again after a few runs.

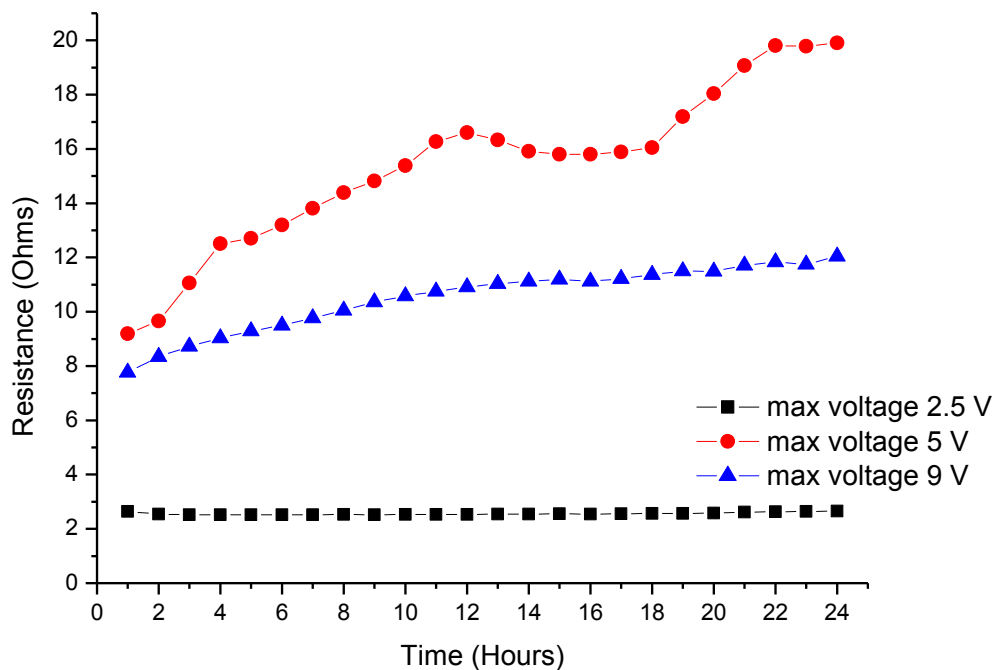


Figure 4.56: Comparison of stability of the device with different maximum voltage level by means of slope resistance change from the first sweep to the final measurement of the 24 hours duration.

Device with maximum voltage of 9 V indicated about 60% of the resistance change from the 1st the 24th hour and showed steady resistance increment. At 9 V the polymer film have lost the water contents attached at the polymer backbone and this can be seen for the first two hours of the repeatable I-V run. After that there was not much increment in resistance but the polymer film is still stable and limiting current. Devices with SAM have been tested and exhibited the same stability where the polymer conductivity dropped in the initial few runs, and once stabilized it still showed current limiting properties. The results are presented in Appendix 2.

Dopant effect on moisture contents

In order to understand the effect of dopant on the electrical behaviour of the current limiting device samples of polyaniline were prepared with different protonic acid dopants which covers the organic, inorganic and aromatic variety. The samples were also studied to understand the stability and degradation effects of the different dopants used. Thermogravimetric analyses (TGA) were performed to further investigate the moisture contents and the polymer decomposition level. A new set of samples were also produced with the same dopants variety to understand any phase change in the polyaniline with effect to different dopants as well as acting as confirmation for the TGA results in moisture contents. These samples were investigated by using Differential Scanning Calorimetry (DSC) analysis. Measurements for the TGA with different dopants have been performed using Perkin Elmer Instruments at a heating rate of 10°C/min, under nitrogen, from 25°C to 600°C. DSC measurement was performed using a Mettler Toledo instrument from 25°C to 500°C for at 10°C/min under nitrogen gas purging.

The TGA for the samples with MSA as dopant is first taken into account in air and in nitrogen results are and presented in Fig 4.57 (a). The first weight loss (about 13%) occurring in the range 50 °C-145 °C is attributed to the expulsion of the free and bonded water [120-122]. The weight loss at this stage is similar to the samples run under nitrogen gas. The second weight loss (about 30%) occurs in the range 220 °C-350 °C for sample tested in nitrogen and higher weight loss (around 34%) occurred at second stage when sample tested in air due to oxidation. At this temperature range removal dopants takes place [123]. Loss of dopants has been reported for polyaniline and its derivatives in this temperature range for different type of dopant ions [124]. The

PANI-MSA sample is then annealed for 30 minutes at 100 °C prior to measurement to see if the first step of the weight loss has is actually due to moisture contents. Results shown in Fig 4.57 (b) showed a flat line at temperature from 100 °C to 200 ° which indicates that the water or moisture contents in the sample had been removed during the annealing process.

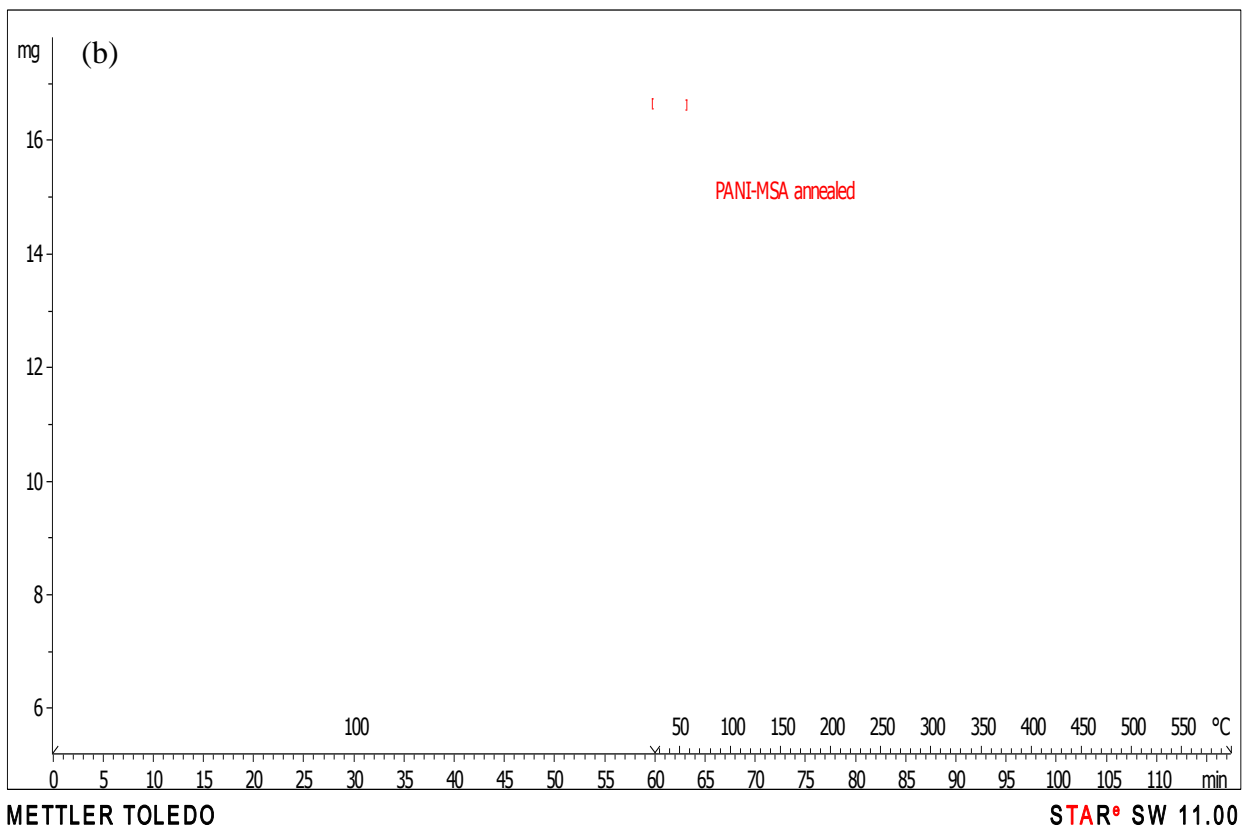
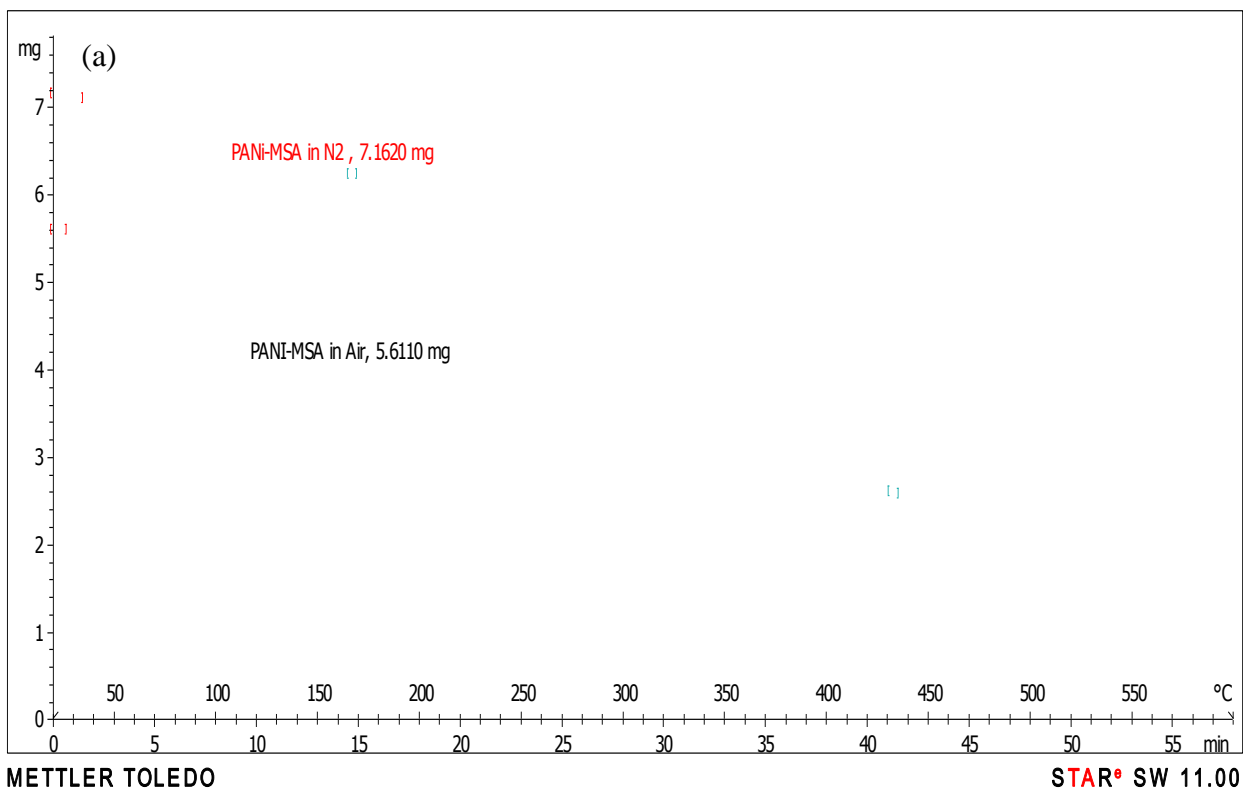
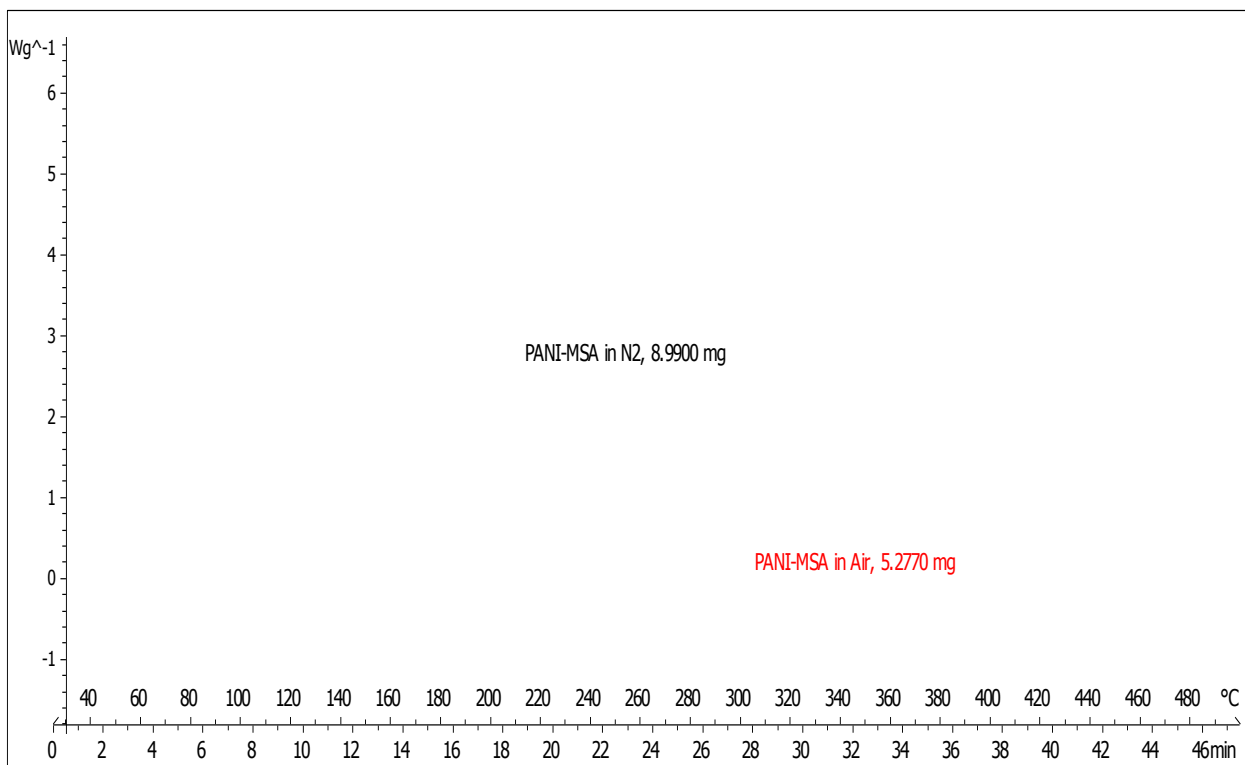


Figure 4.57: Thermograms of PANI-MSA recorded from 100 to 600 °C (a) showed the TGA in air and N₂, (b) showed TGA after annealed at 100°C for 30 minutes



METTLER TOLEDO

STAR® SW 11.00

Figure 4.58: DSC thermogram of PANI-MSA in air and N₂.

Fig.4.58 shows the DSC measurement results of the polyaniline doped with methanesulfonic acid (MSA), under air and nitrogen atmosphere. An endothermic peak at 60 °C to 120 °C and an exothermic peak at 230 °C to 270 °C were observed. Based on the studies previously reported polyaniline has discernible amount of moisture content [122, 125]. Consequently, the first endothermic peak is most likely associated to the removal of water, which was consistent with the TGA results. This endothermic peak in air only showed a very slight shift compared to the result in nitrogen environment. The chemical process attributed with the exothermic peak may be related to a cross-linking [126-129] but not decomposition since there was no weight loss within this temperature range as determined by TGA. However there was a slight weight change on the exothermic peak for the sample measured in air are strongly

related to oxidation especially when samples reached a high temperature as this stimulated the burning process to happen slightly faster and can be seen in the temperature around 360°C.

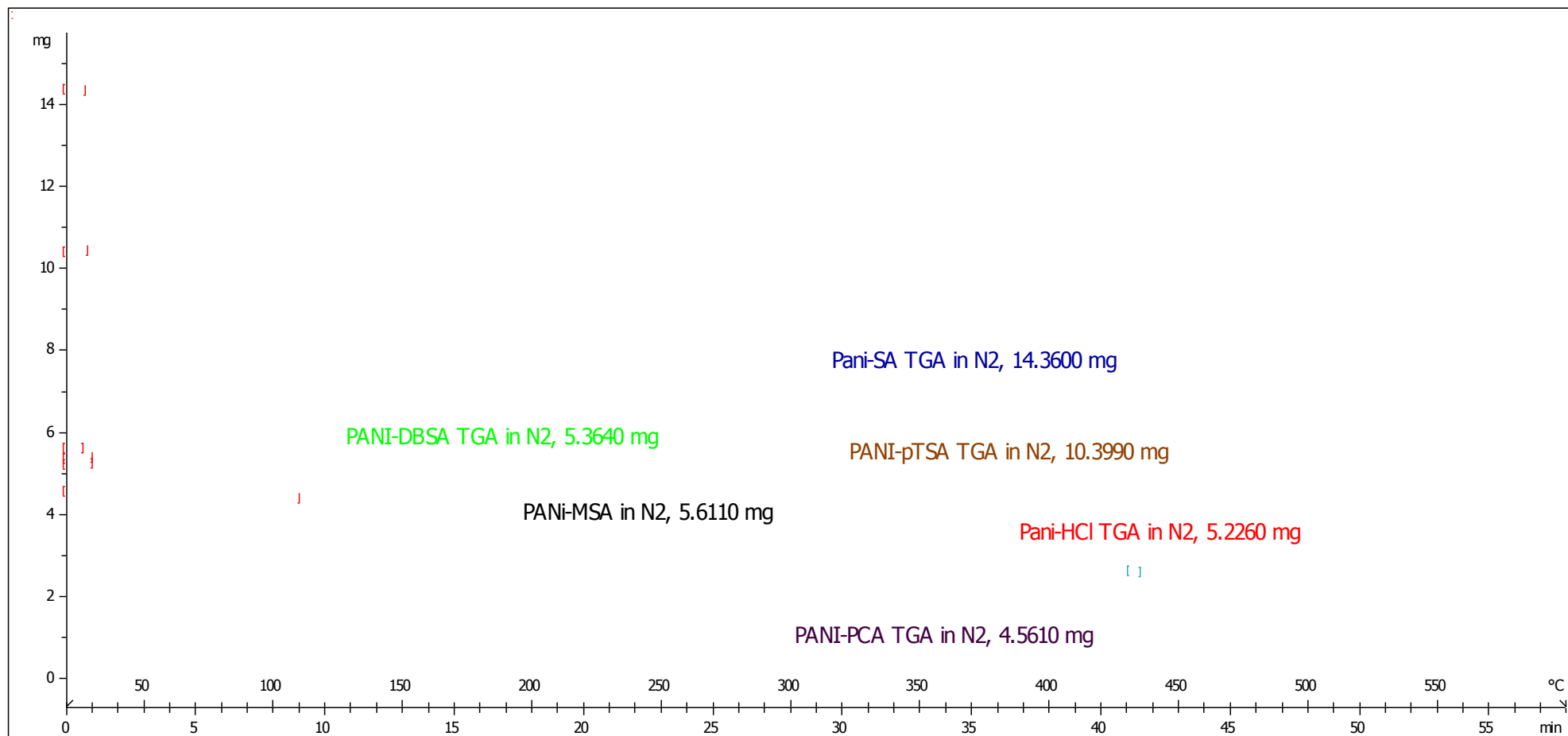


Figure 4.59: Thermogravimetric analysis for different dopant of polyaniline showing weight loss when polymer sample is heated.

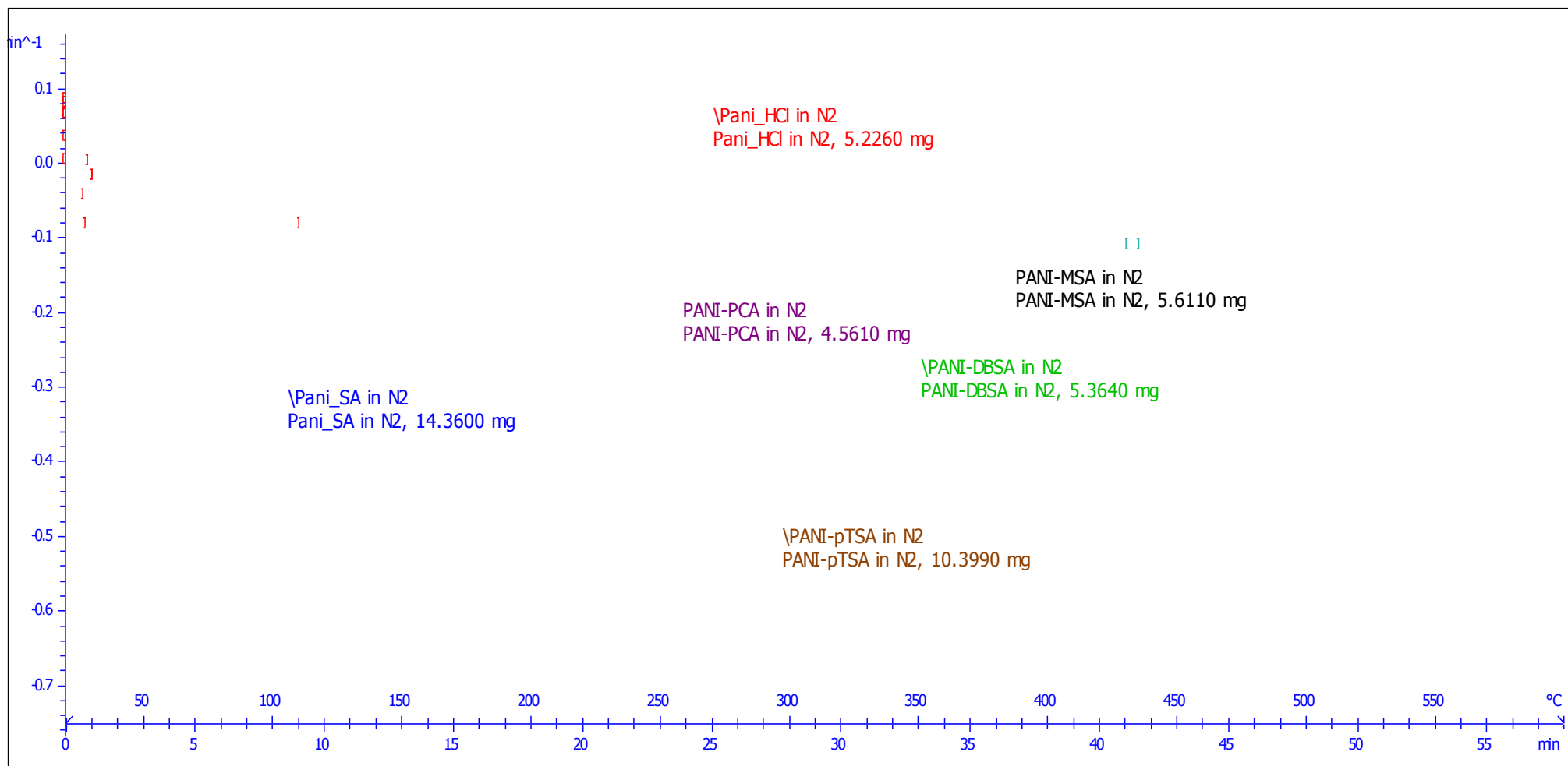


Figure 4.60: Derivatives for the thermogravimetric analysis for different dopant of polyaniline showing the percentage of weight loss at each step.

To understand the effect of dopant on water content or moisture loss, the thermal properties of the polyaniline doped with various acids were studied by TGA under nitrogen atmosphere. Thus the polyaniline base form was doped with acids including HCL, H₂SO₄, CH₃SO₃H, C₁₂H₂₅C₆H₄SO₃H, HClO₄, and *p*-CH₃C₆H₄SO₃H. The thermograms of all the samples demonstrate similar characteristics as the MSA-doped polyaniline. There are three major weight losses of different extent at around 100°C, 200°C and 500°C as showed in Fig. 4.59. The weight loss around 100°C could be attributed to the removal of water or moisture and the loss at around 500°C could be associated to the polymer decomposition. The weight loss around 500°C attributed to the structural decomposition is not of much interest as the current limiting device mainly showed reversible effect below 300°C, therefore it will not be discussed in detail, and the thermal processes at lower temperatures could be associated with the elimination of volatiles and other reactions.

TGA results show that the bound water is much less in PANI-*p*TSA, PANI-DBSA and PANI-HCL compared to other dopants crosslinking chemical decomposition followed by carbonisation generally observed to occur beyond 400°C to 500°C [97, 130, 131]. As the heating is not continued beyond 500°C due to the fact that some samples were sensitive to excessive heating that will create small explosion and distort the results. Thus these changes are very apparent in the given plots.

The acid doped form of polyaniline showed a three step decomposition process as proposed by previous studies [132, 133]. It is suggested that the initial stages of weight loss are due to volatilization of water molecules and oligomers, as well as unreacted monomer elimination which are the most interest to understand more about the effect of dopants on the current limiting device [134, 135]. At temperatures around 100°C, the loss can be deduced from the thermograms as presented in Fig.4.60. The weight loss at

around 100°C are mainly assigned to the loss of water molecules similar to the observation by La Croix and Diaz [126, 136]. Based on the literature on thermograms for the base form of polyaniline, there is no water released [126]. It is therefore suspected that the water molecules of the doped polyaniline could be weakly bonded to the polymer and probably are located at places which otherwise could be occupied by the acids as suggested by Wessling and Volk [137]. The weight loss at temperatures around 200°C to 300°C in various acid-doped polyaniline can be observed due to loss of primary dopant. The TGA results showed that the most significant weight loss in the second stage is happening from the PANI-*p*TSA, DBSA and SA, implying possible reversible de-doping. These results showed that PANI-MSA is stable and showed minimal of thermal doping. Results in Table 4.3 showed the extracted moisture contents from the TGA derivatives plots of different polyaniline forms in percentile. PANI-SA and PANI-MSA hold the most water in the sample. PANI-PCA hold reasonable amount of water but the nature of this dopant is very sensitive to heat, thus rule out the possibility on becoming a good current limiting device. PANI- MSA is one of the most stable dopants in temperature range around 200 °C compared to other dopants according to study conducted by Bhadra and Khastgir [138]. This could explain the good reversible current limiting behaviour presented in previous sections.

Table 4-3: The moisture contents for different protonated polyaniline extracted from the TGA plot at around 100°C.

Type of Dopant	Moisture Contents (%)
PANI-MSA (Methane-sulfonic acid)	12.5438
PANI-SA (Sulphuric acid)	17.7857
PANI-HCL (Hydrochloric acid)	4.518
PANI-PCA (Perchloric acid)	8.1008
PANI-DBSA (Dodecylbenzenesulfonic acid)	3.2229
PANI-pTSA (p-Toluenesulfonic acid)	5.4566

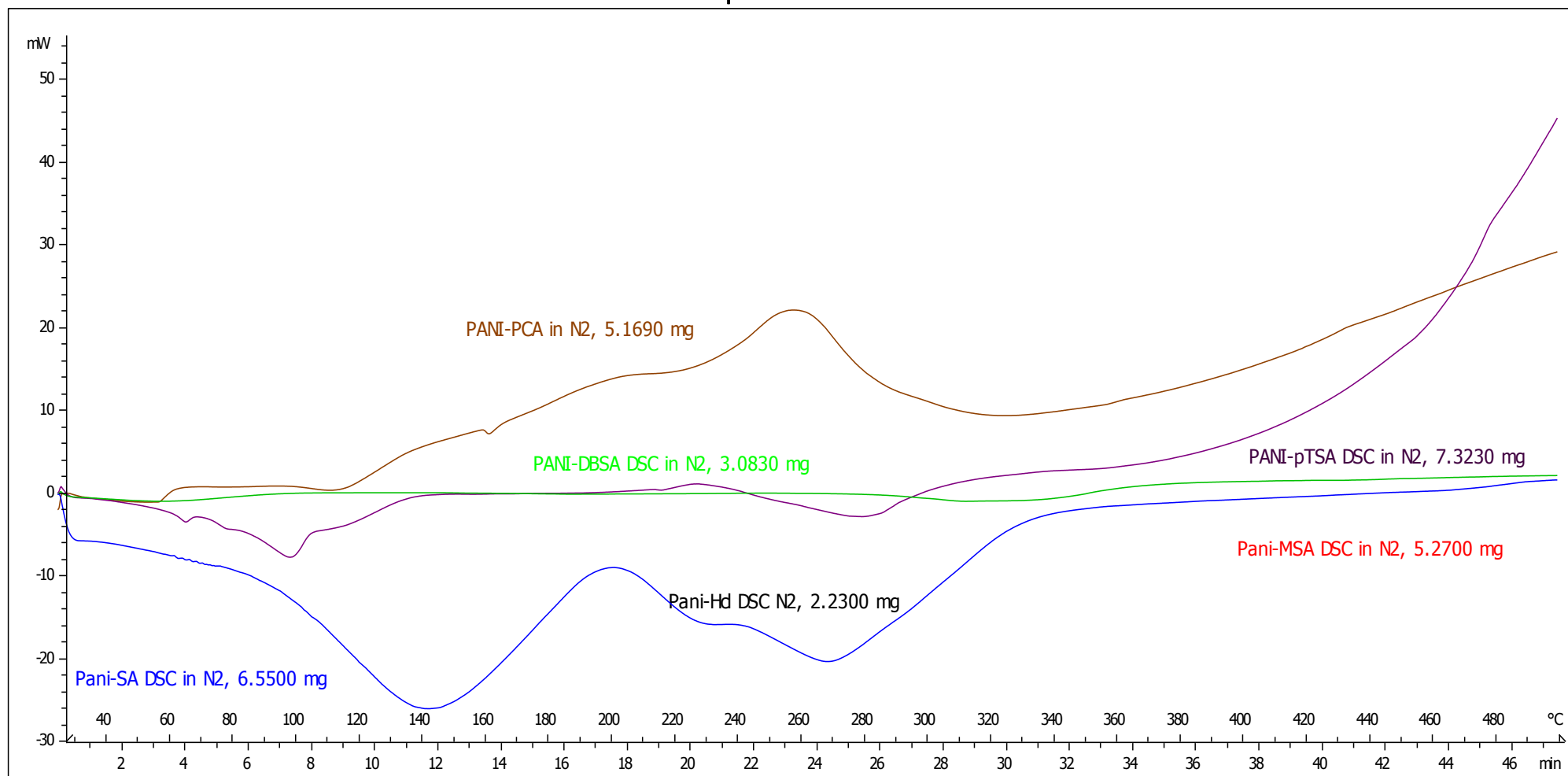


Figure 4.61: Differential scanning calorimetry for different protonated polyaniline showing thermal transition of the polymer samples.

Fig. 4.61 presents the DSC plots of doped polyaniline samples. All samples showed two endothermic peaks at around 100°C to 150°C and another one around 200°C to 350°C. The first endothermic peak may be due to the loss of loosely associated moisture and the second for the loss of relatively strongly bonded water molecules often termed as bound water, which act as secondary dopant [139-141], which is in agreement with the TGA results. The second peak is stronger for PANI-SA and PANI-MSA.

Results obtained with different water contents for the polyaniline with different dopants could be due to different morphology of the polymerised polymer film. SEM images have been taken and presented in Fig 4.62 to look at the polyaniline structure with all the different dopants. All samples SEM were taken at same magnification which is x10000 times. Results shown some differences in fibre diameter for SA with smaller fibres and shorter fibres compared to MSA which have bigger diameter with longer spaghetti type fibres. DBSA dopants sample showed the most significant morphology different, where there is no fibrillar morphology but showed agglomeration and bigger size particles clustered together. This could be the explanation of the low moisture content due to its bulky structure. HCL produced the finest and closely packed fibre morphology. Polyaniline with PTSA and PCA as the dopant exhibited similar fibrillar morphology but a much finer and smaller polymer structure which also can be seen as closely packed polymer fibres with smaller porosity almost identical to HCL which contain medium moisture contents.

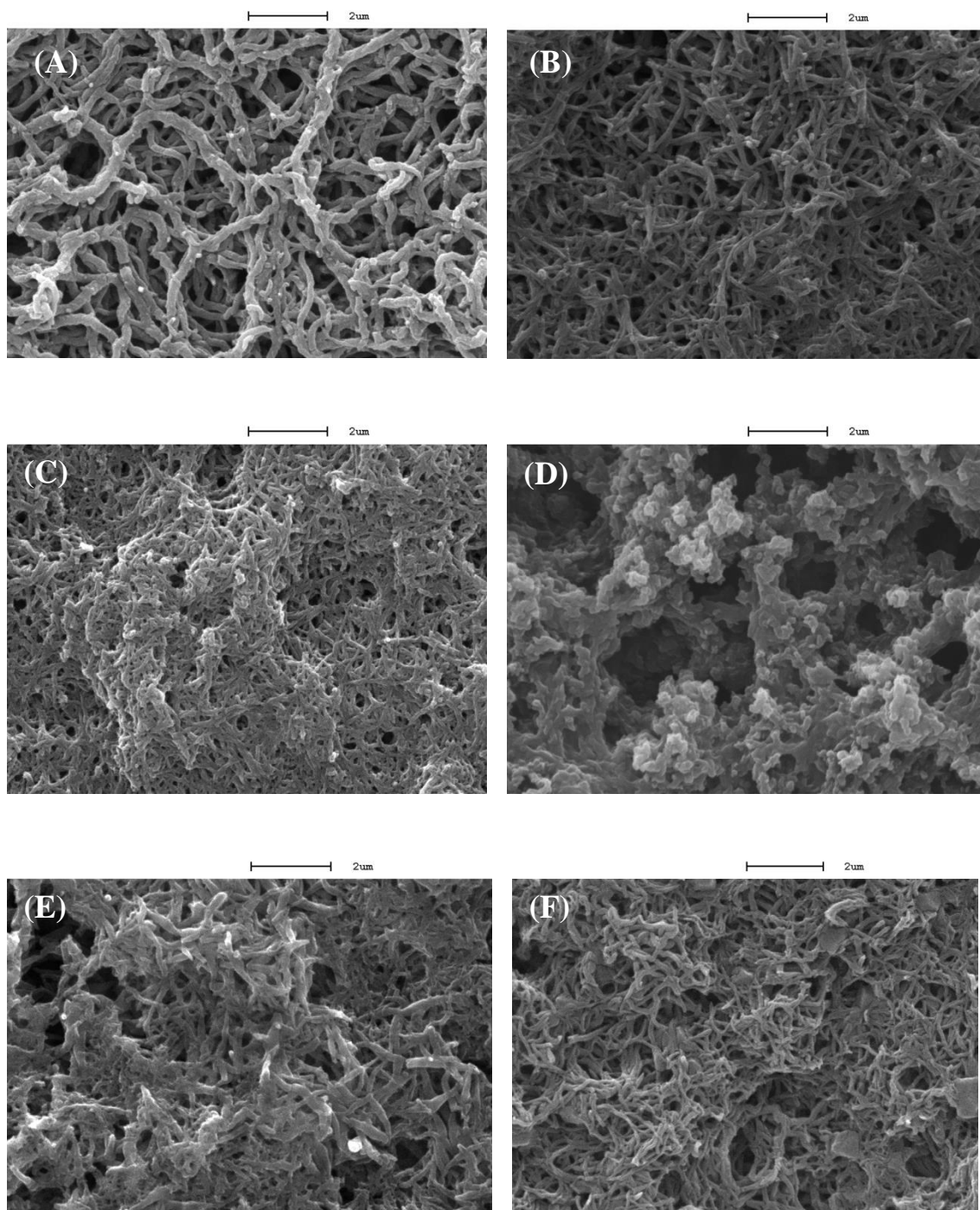


Figure 4.62: SEM images for the polyaniline doped with different dopants (A) methanesulfonic acid (B) Sulphuric acid (C) Hydrochloric acid (D) Dodecylbenzenesulfonic acid (E) Perchloric acid and (F) *p*-tolouenesulfonic acid

TGA and DSC results for different dopants have shown significant moisture contents in samples doped with methane-sulfonic acid and sulphuric acid. This could be the device with sulphur contents in the dopants such as MSA and H₂SO₄ help to contain more water in the polyaniline. The current limiting device with polyaniline doped with sulphuric acid has been produced and I-V measurements have been performed. This is due to the moisture content hence slightly higher as displayed by the TGA results. Results have been presented in Fig 4.63.

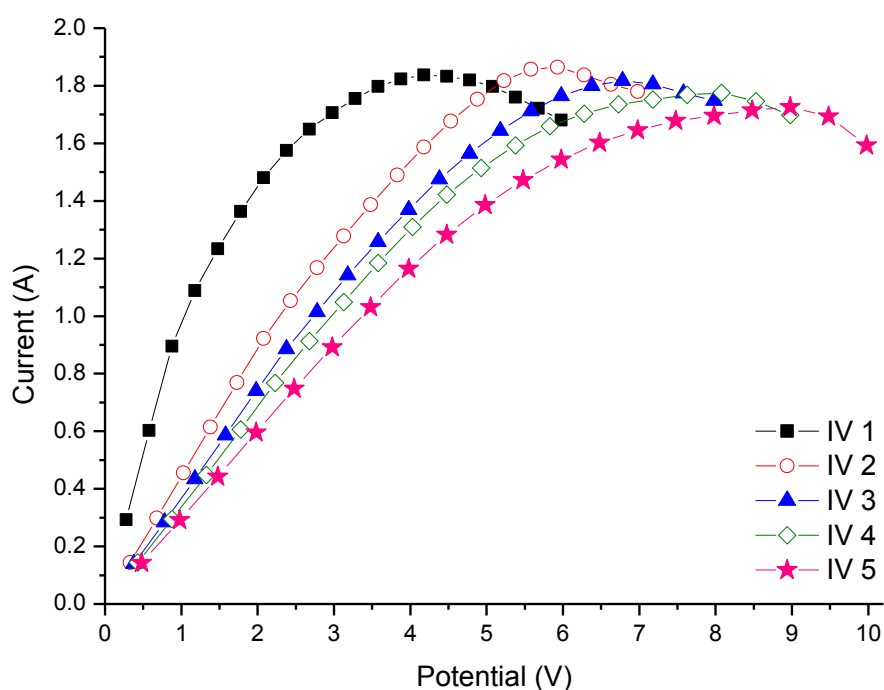


Figure 4.63: I-V sweep for PANI-SA without SAM

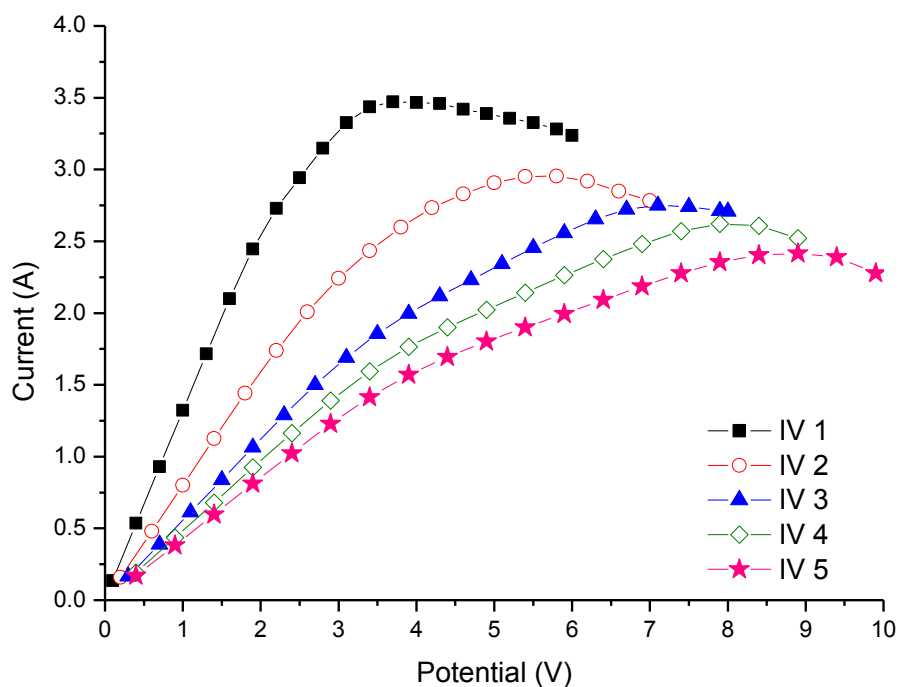


Figure 4.64: I-V sweeps for PANI-SA with SAM.

The I-V sweeps for polyaniline doped with sulphuric acid do not show much difference from polyaniline doped with methane-sulfonic acid. Another device is then produced with SAM modified electrode and then polymerised with polyaniline doped with sulfonic acid to see if there is some significant difference compared to the previous results and presented in Fig.4.63. From the results it is shown that the results is very similar to the electrical measurement for CLD with results with PANI-MSA on self-assembled monolayer in the section earlier.

Chapter 5 CONCLUSIONS

The aim of this thesis was to explore the potential of intrinsic conducting polymers for current limiting devices (CLDs). Using both established and novel methods of devices fabrication, as well as electrical and material characterization, much evidence has been gathered to elucidate the mechanism of current switching in these materials. Armed with this knowledge, a number of improvements have been made in the fabrication of devices to enhance their electrical switching properties.

The current limiting devices were investigated using current-voltage measurements in different environmental conditions. The expected current limiting response (*i.e.*, peak dissipating current response with increasing voltage) has been shown to be dependent on the device temperature and presence of moisture in the polymer film. It was found that the occurrence of an overcurrent in the polymer film lead to increased joule heating in the polymer material. This drives out water molecules from within the polymer film, causing a partial de-doping effect, which leads to conductivity loss. When the current surge has dissipated, the device cools down and moisture from the environment is drawn back into the polymer film, causing re-doping and a return of conductivity to its initial value. This hypothesis was supported by a series of measurements in vacuum and in air with different humidity levels. Current-voltage sweeps in environments of different humidity also showed that the optimal conditions for maximum current limitation lie in the range of 70% - 100% relative humidity.

Temperature dependent conductivity measurements were performed on the device since it is known that some polyaniline films exhibit a cross-over to metallic behaviour at near room temperature, which could be a possible cause of the current limiting

behaviour. Results obtained fitted well with Mott's 3D variable range hopping model and there was no indication of a crossover to metallic behaviour in this polymer.

Morphology studies using SEM were conducted and results showed that the polymer film has a very porous structure with fibrous polymer strands that are less than a micrometre in diameter. The high porosity of the polyaniline fibers is a likely reason for the rapid diffusion of water loss during overcurrent and recovery of moisture in the polymer film upon cooling.

To explore whether the switching occurs in the bulk or only at the metal-polymer interface, a new type of device with modified electrodes was developed. The gold electrode surface was altered via the deposition of a self-assembled monolayer prior to the polymerization of polyaniline. Different concentrations, from 1mM to 10mM of dodecanethiol (DDT), and varying times of immersion, 12 to 72hrs, were investigated. Overall the CLD with the longest immersion time and highest concentration produced the best current limiting behaviour. This is believed to be due to better formation and coverage of the self-assembled monolayer.

It was further suggested that devices with the SAM modified electrodes might have a different polymer growth structure than those using unmodified electrodes. Scanning electron microscopy was used to compare the morphology of both types of devices. The SAM devices were found to have a rougher surface and only minimal fibrillar morphology, which is a possible explanation for the different performance of the CLDs. SEM micrographs and thickness monitoring results showed that the monolayer hindered the initial growth of the polymer thus changing the final structure of the film. Different growth times were also important in this respect since longer times formed thicker films which showed a similar spaghetti-like morphology to that found in non-SAM devices, whilst shorter growth time devices had thinner films but having a more compact morphology.

The stability and reproducibility of the polymer device was also investigated. Samples were measured using TGA and DSC analysis. Results obtained suggested that the PANI-MSA CLD have a large thermal transient at 200°C which is a similar temperature that devices were found to reach from infrared imaging spectroscopy taken during typical current surges. TGA and DSC measurements also showed that at higher temperatures the polymer begins to break-down, which fitted well with irreversible effects seen in the electrical resistance at higher currents than those normally used for testing. Thus it is likely that at a very high temperature the polymer degrades causing irreversible change in the resistance of the device which in turn affects the resetability.

The type of dopant used in the polyaniline films was also shown to play an important role. Six different acids, belonging to the organic, inorganic and aromatic acid groups were examined. Samples with aromatic rings showed the least moisture content, most likely because of the bulky size of the benzene rings which prevents the bond formation of water molecule with the backbone nitrogen present on the polymer, as found in studies performed by Badhra *et al.* and studies by Wei and Hsueh. PANI-SA showed the highest amount of moisture contents. However, devices prepared with the same method as PANI-MSA showed no significant differences.

In summary, current limiting devices made from intrinsic conducting polymer show significant surge protection behaviour. The combination of electrode modification by means of self-assembled monolayer and a high moisture environment produced current limiters with the best performance. The results demonstrate that commercial current limiting devices based on these materials could be viable for certain applications but further investigations are needed to make the devices more robust and reliable upon repeated overcurrents.

Chapter 6 FUTURE WORK

Results presented indicated that PANI-MSA does indeed show current limiting properties. Results have also showed evidences that moisture content in the film with higher humidity level produced device with a better current limiting behaviour. However there are many areas that still require further investigation and will be proposed for consideration of future research subject.

The polyaniline doped sulphuric acid dopant has shown the highest moisture level. This device would show a good current limiting device based on the preliminary results obtained. Further studies could involve the device produced in moisture rich environment by adding one additional layer of hydrogel on the polymer film and encapsulation. This is to ensure that the current limiting device always has moisture to replenish the polymer film once the moisture has been driven out by the overcurrent activity. The devices would also have improved stability and reproducibility level by the hydrogel mixture with the conducting polymer.

The material used in the current limiting device would be able to show good performance and efficiency if other ICPs such as polythiophene are used to produce the device due to this material being among one of the bestconducting polymer with good conductivity level in protonated form and can easily be synthesized electrochemically in room temperature. It also would be useful to compare the best dopants that work with the new material. This might promote better conductivity as polythiophene has different mechanical properties and might exhibit better stability of electrical properties with regards to temperature changes.

The results shown that modified electrodes by means of self-assembled monolayer have significantly improved the current limiting behaviour. Variation of the alkanethiol allows for the study of the polymer growth and the effect on the device. Some type of monolayers can help to increase the adhesion of the polymer, improve uniformity, and change the density and morphology. A study of this would allow for the selective performance of conductive polymers based on differences in monolayer and surface properties. This will also help to provide further understanding of the effect of monolayers on the deposition of conjugated polymers and to optimize the device performance.

The polyaniline with organic acid protonation showed promising performance due to the moisture content and the stability to certain levels of applied voltages and warrants further investigation. Therefore current limiting devices produced using polymer blends such as Poly(ethylene glycol) (PEG) with aniline or poly(3,4-ethylenedioxythiophene) (PEDOT) with aniline will increase the amount of water content in the polymer film. It turned out that in a number of applications, PEDOT surpasses polypyrrole and polythiophene with its electrochemical stability. The combination of different polymer blends and SAM can be aimed at producing better device with good switching properties, excellent thermal stability and reproducibility.

Chapter 7 Appendices

Appendix 1

The contact angle measurement showed advancing and receding lines on each device and the drop shape analysis image that helps to characterise the surface of each sample prior to electrochemical polymerization of the polyaniline. Further explanations for the samples are covered in section 3.2.1

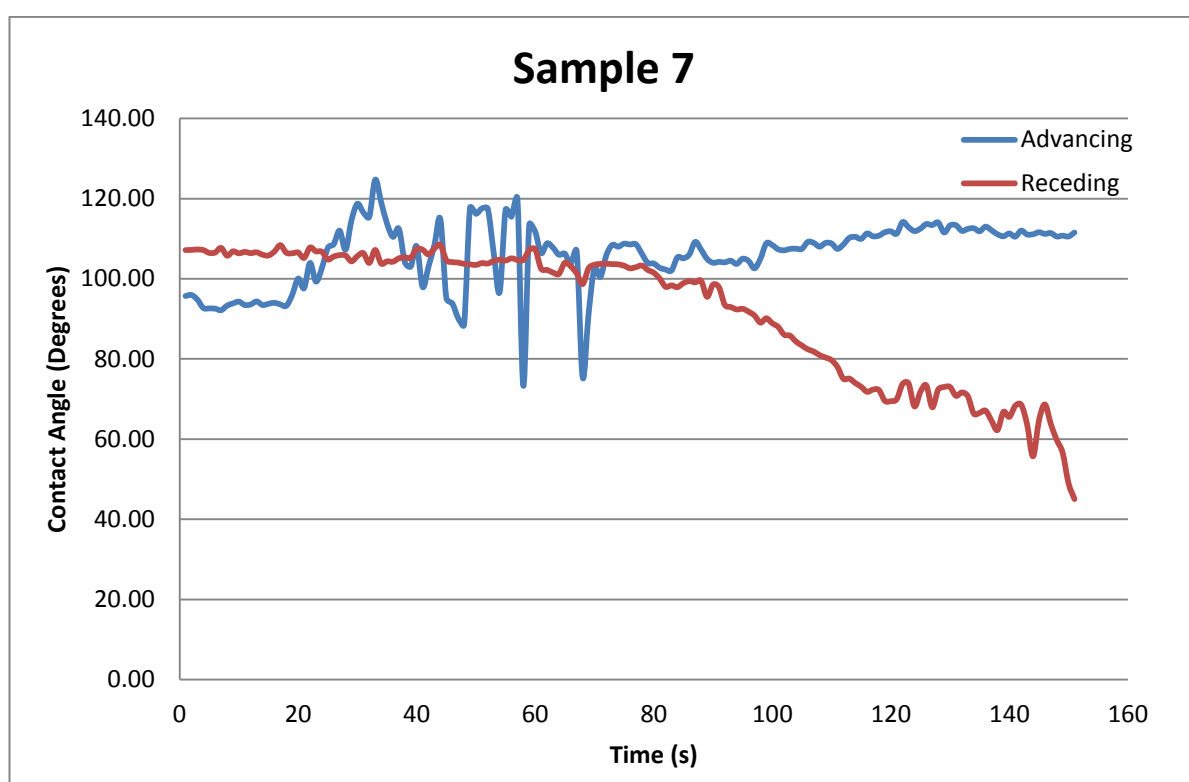
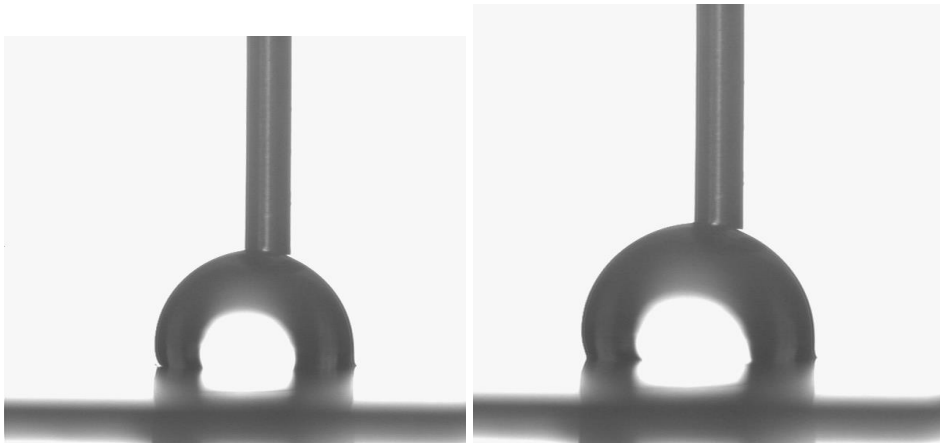


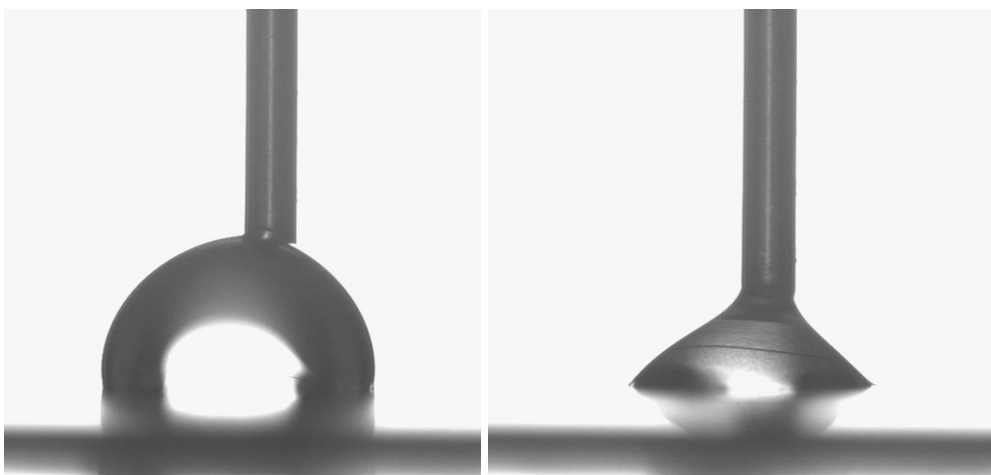
Figure 7.1: Advancing and receding angles for Sample 7



$97.9^\circ \pm 18.15$

$100.5^\circ \pm 3.56$

Figure 7.2: Sample 7 Drop images during advancing



$103.9^\circ \pm 3.61$

$49.0^\circ \pm 9.85$

Figure 7.3: Sample 7 drop images during receding

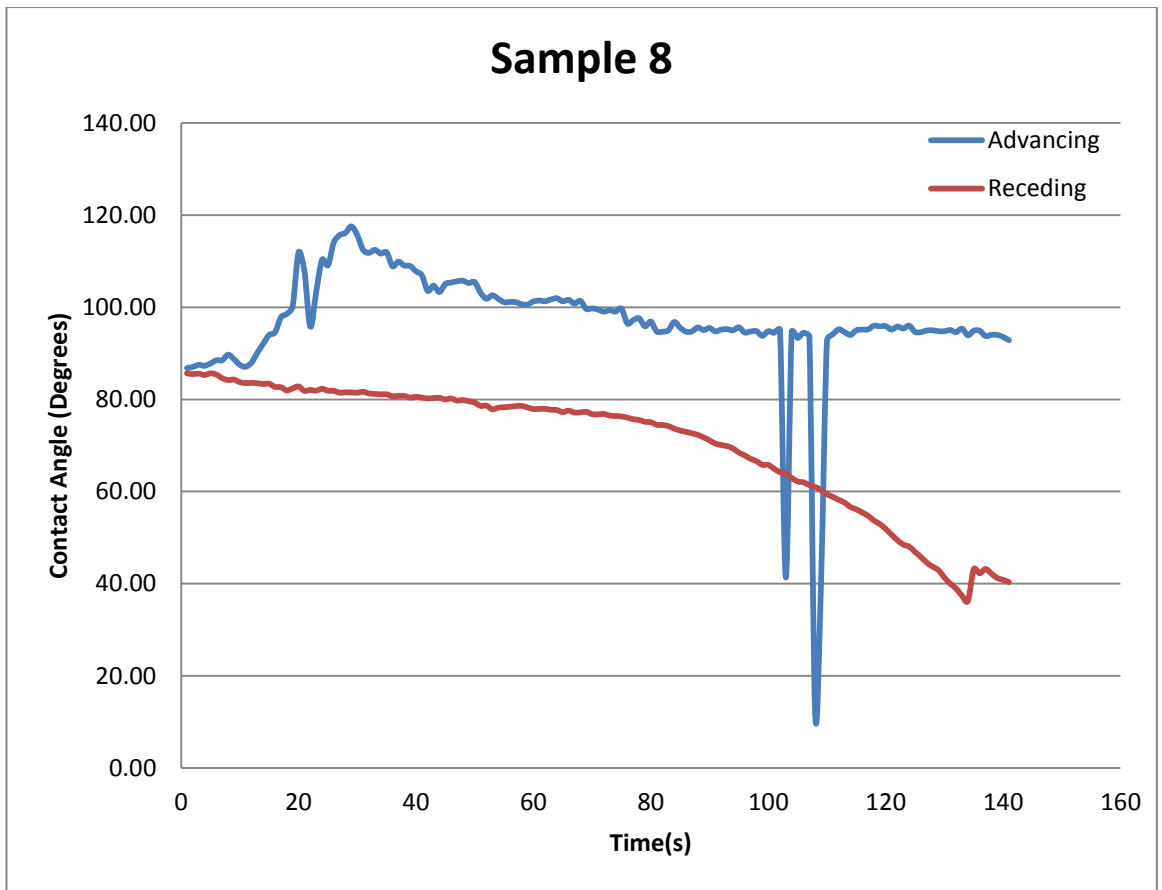
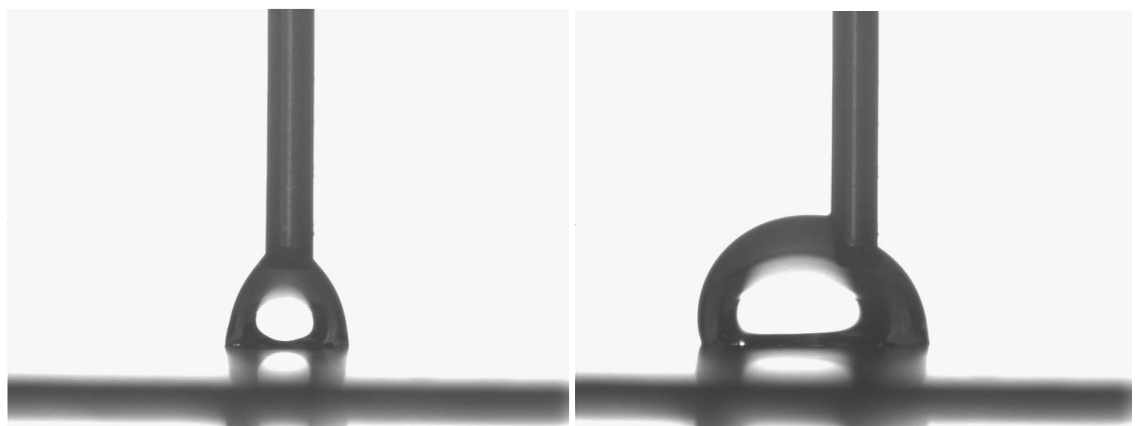


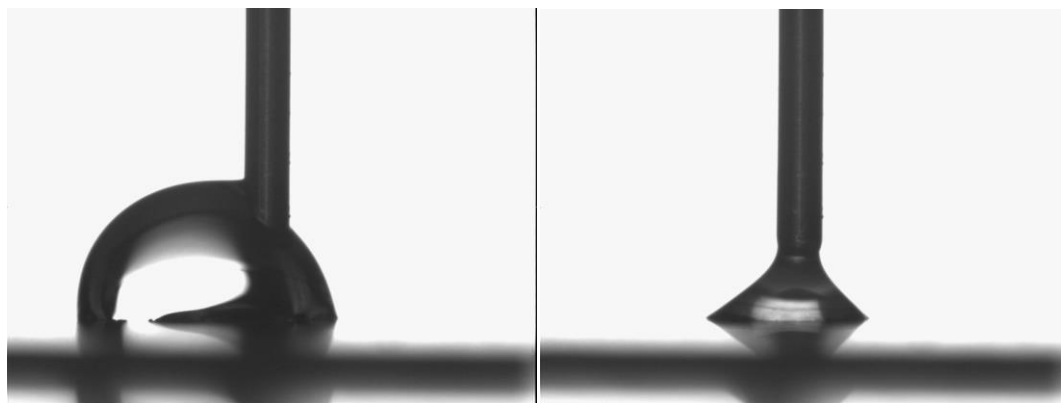
Figure 7.4: Advancing and receding angles for Sample 8



88.5° ± 2.63

96.8° ± 14.21

Figure 7.5: Sample 8- Drop images during advancing



83.6° ± 10.06

38.3° ± 6.01

Figure 7.6: Sample 8 drop images during receding

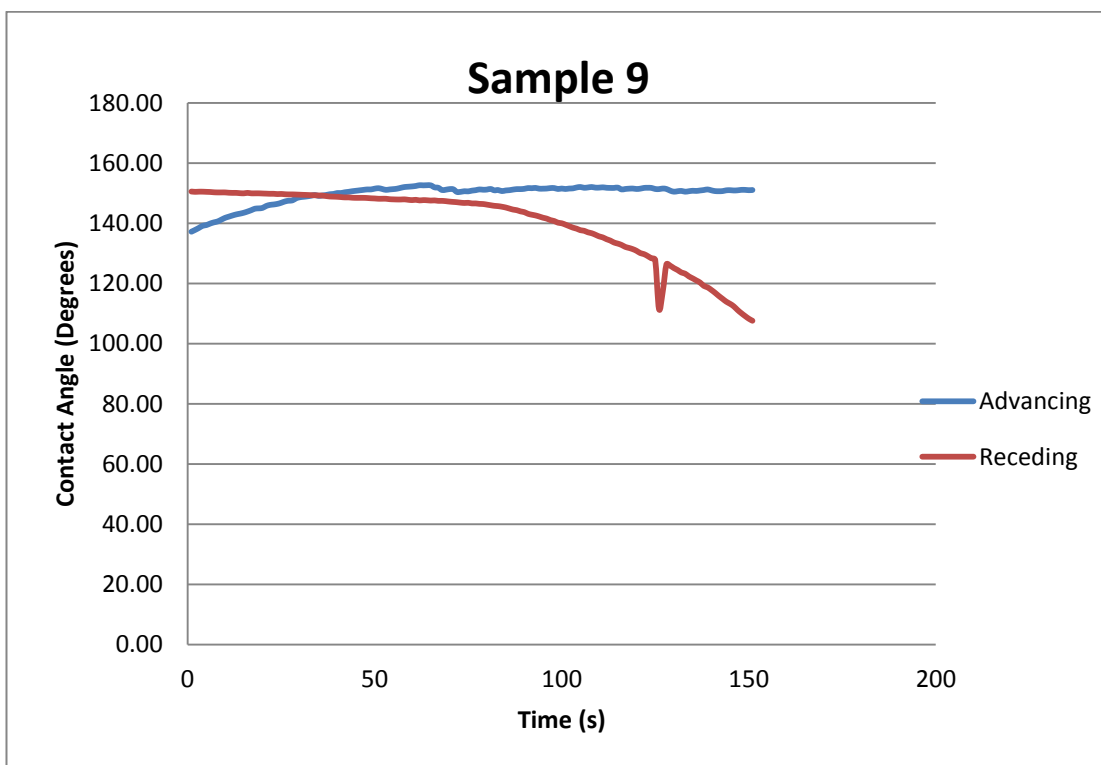
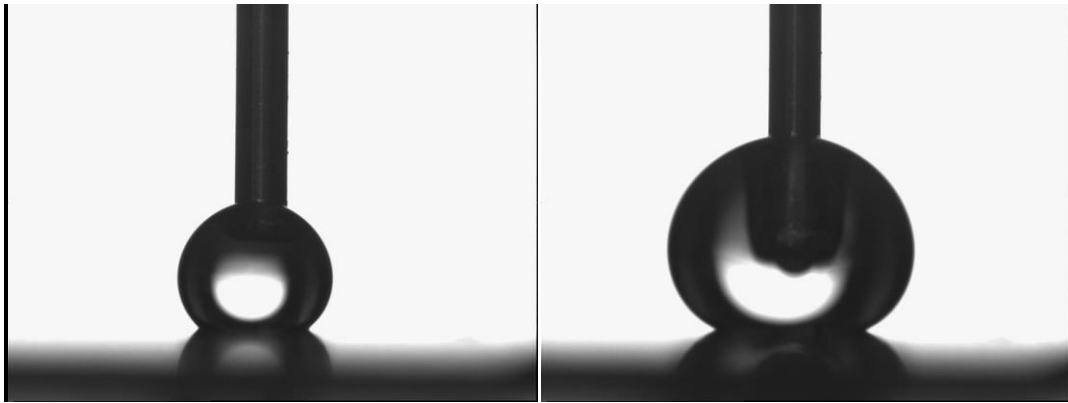


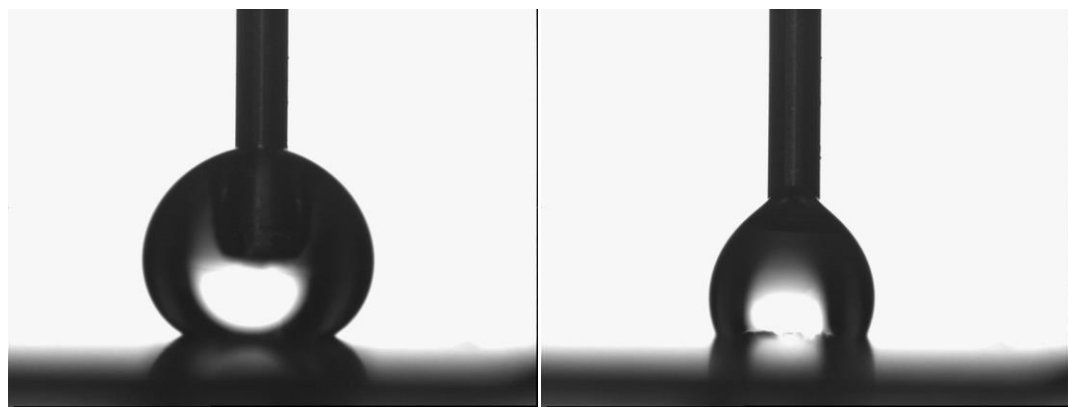
Figure 7.7: Advancing and receding angles for Sample 9



$138.5^{\circ} \pm 2.35$

$150.9^{\circ} \pm 0.06$

Figure 7.8: Sample 9- Drop images during advancing



$145.5^{\circ} \pm 0.72$

$114.9^{\circ} \pm 0.31$

Figure 7.9: Sample 9- Drop images during receding

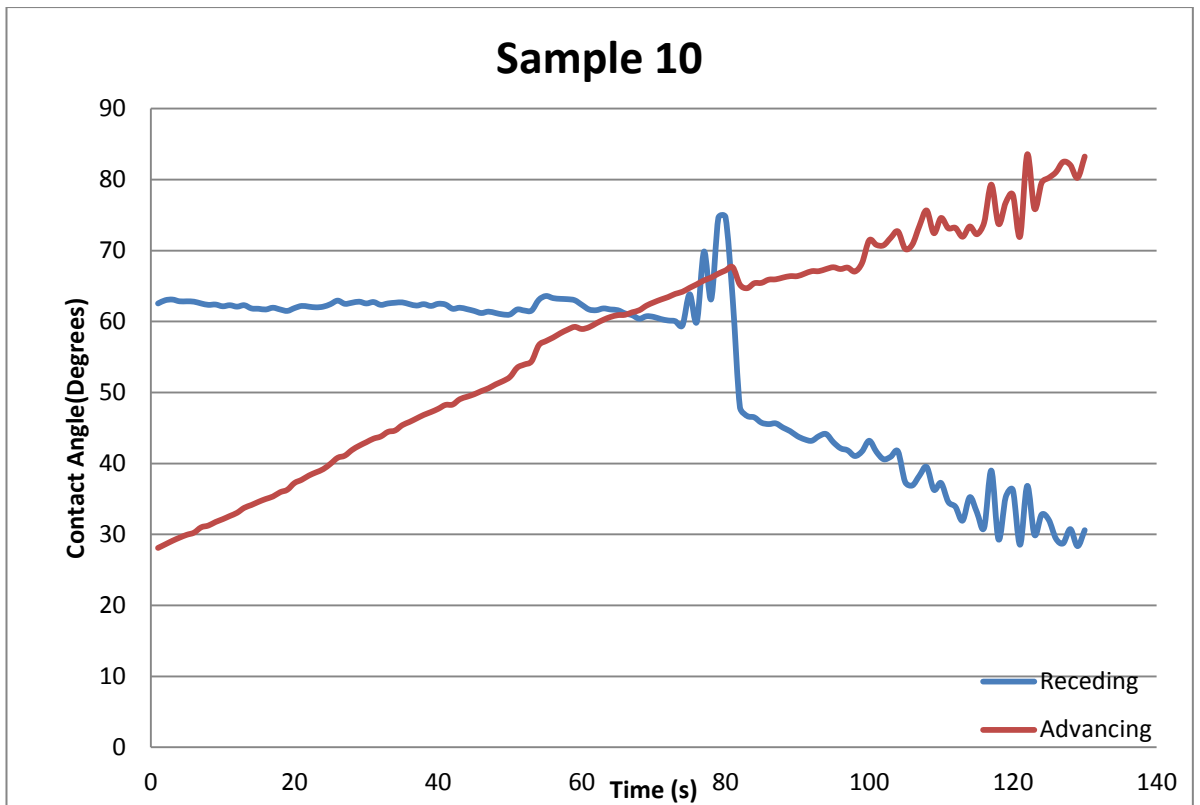
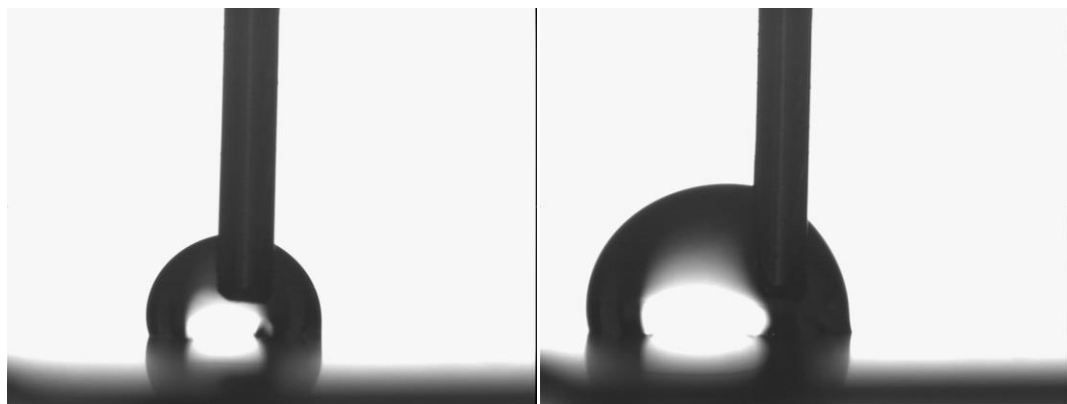


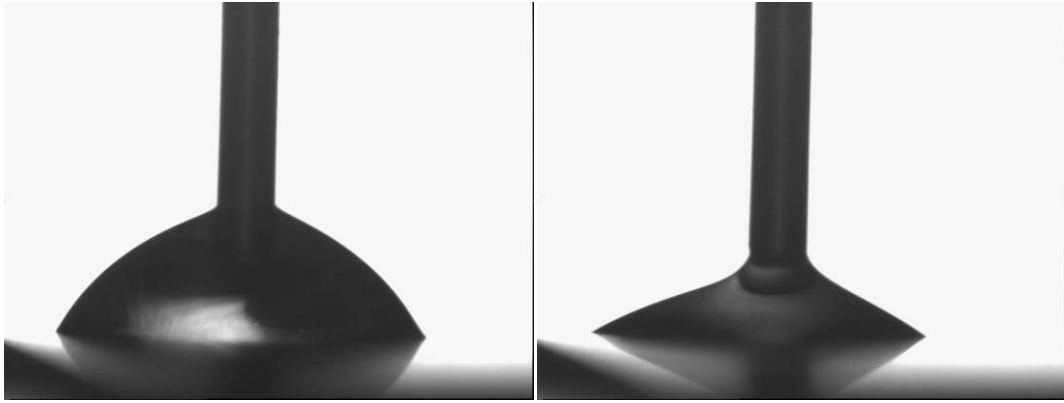
Figure 7.10: Advancing and receding angles for Sample 10



101.3° ± 9.08

84.5° ± 10.59

Figure 7.11: Sample 10- Drop images during advancing



61.7° ± 7.81

34.6° ± 0.74

Figure 7.12: Sample 10- Drop images during receding

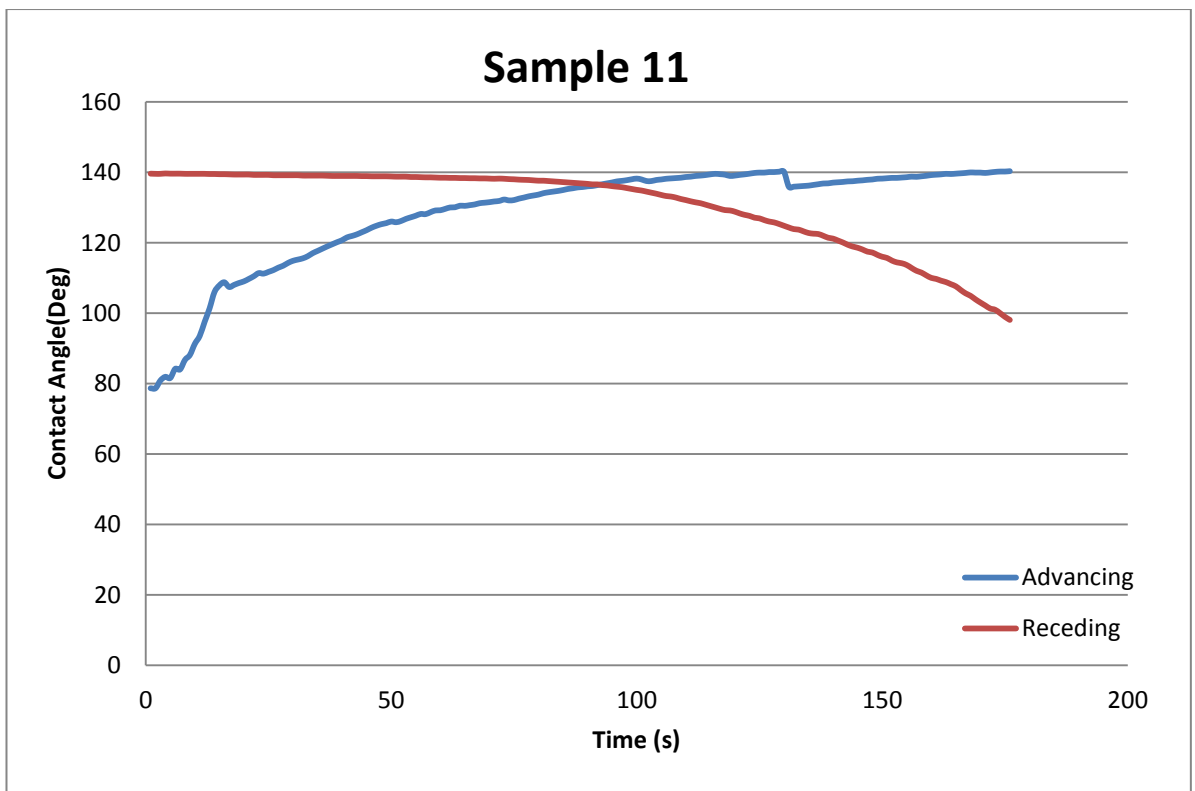
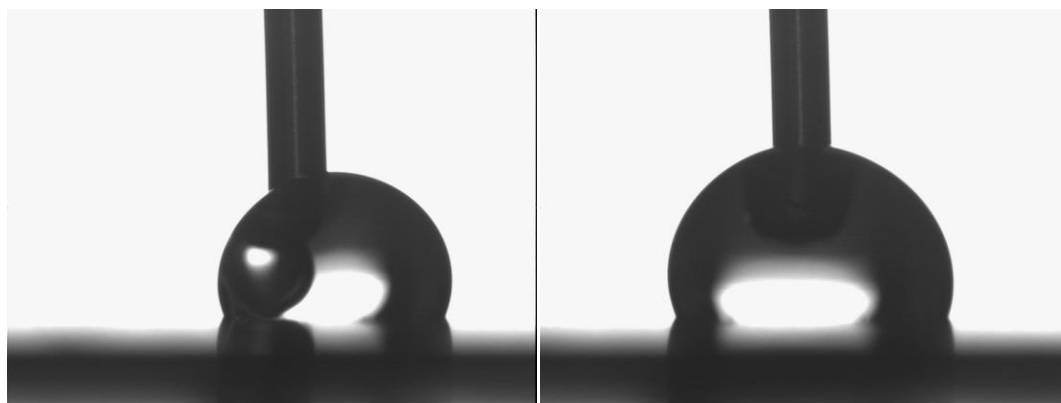


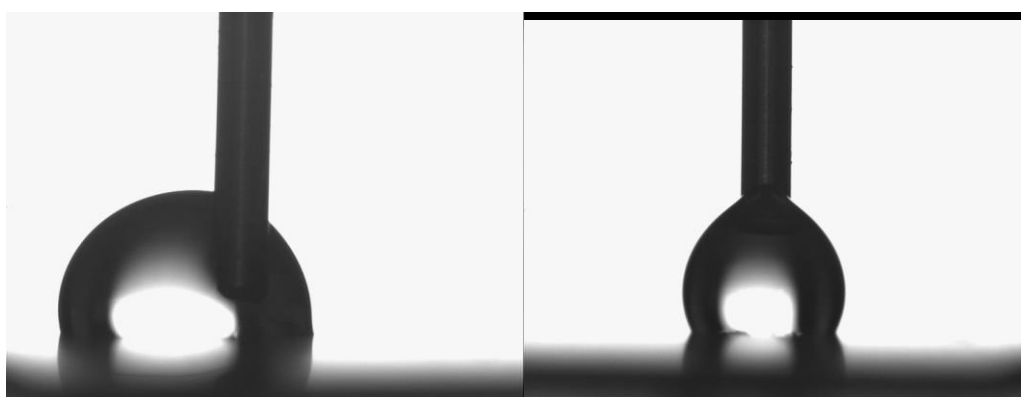
Figure 7.13: Advancing and receding angles for Sample 10



$80.9^\circ \pm 0.92$

$140.1^\circ \pm 0.11$

Figure 7.14: Sample 11- Drop images during advancing



$137.6^\circ \pm 0.05$

$99.0^\circ \pm 2.87$

Figure 7.15: Sample 11- Drop images during receding

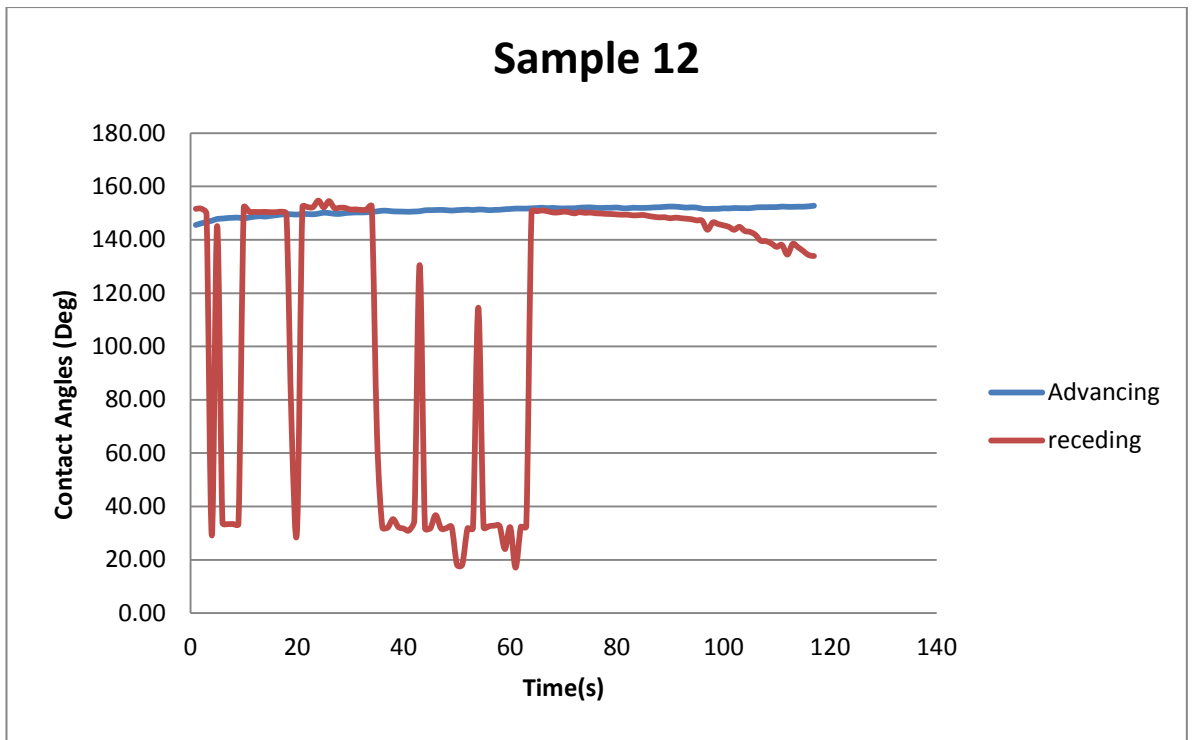
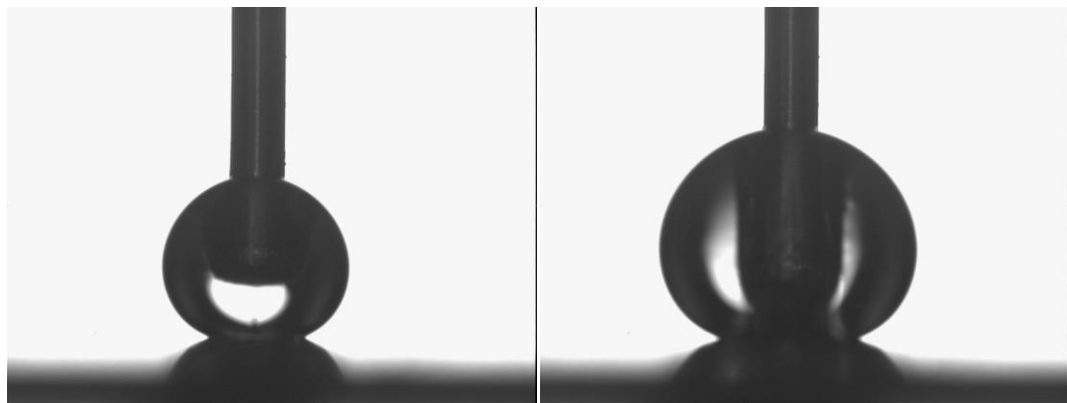


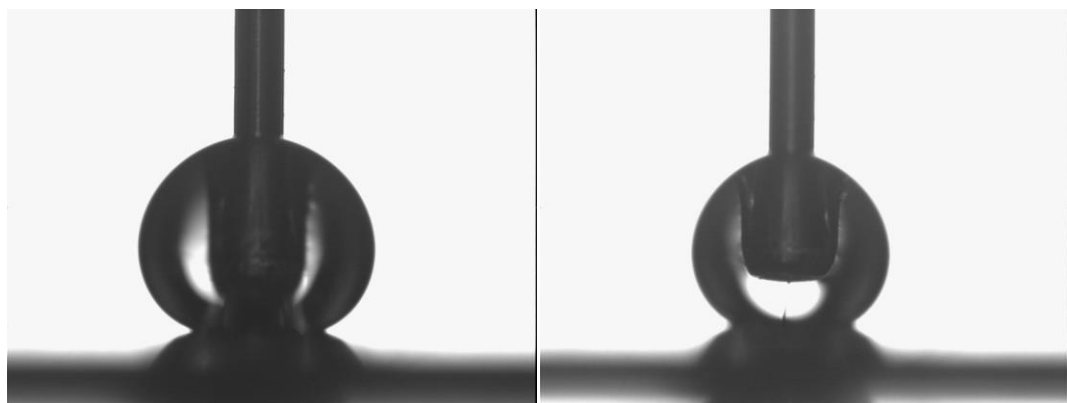
Figure 7.16: Advancing and receding angles for Sample 12



$150.5^\circ \pm 0.31$

$152.3^\circ \pm 0.21$

Figure 7.17; Sample 12- Drop images during advancing



150.5° ± 0.11

138.5° ± 1.93

Figure 7.18: Sample 12- Drop images during receding

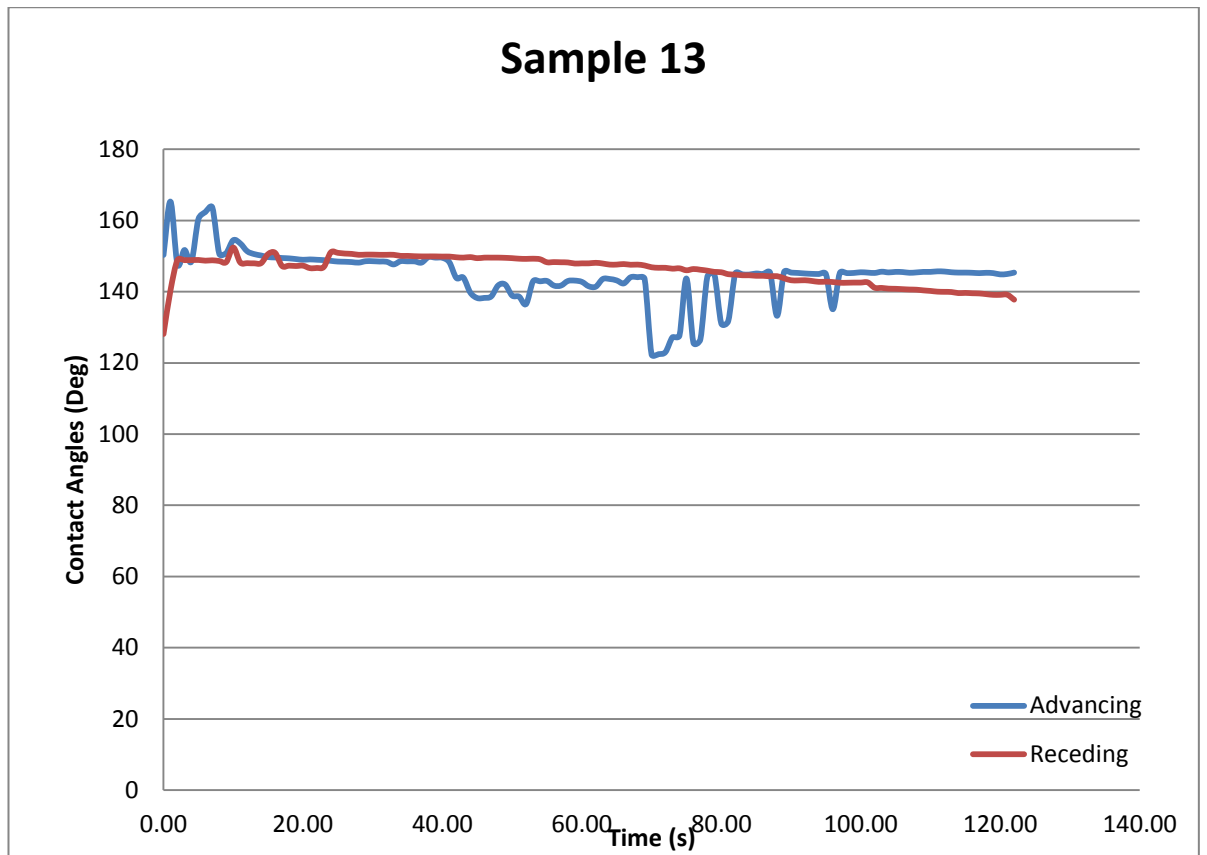
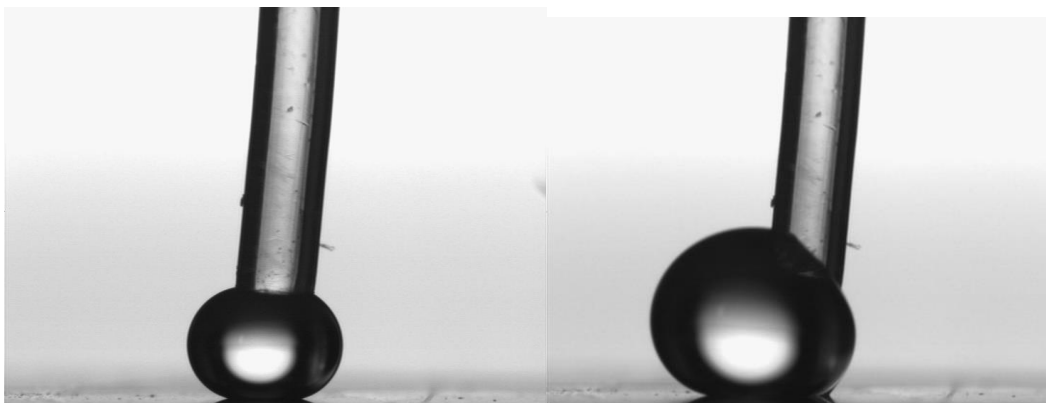


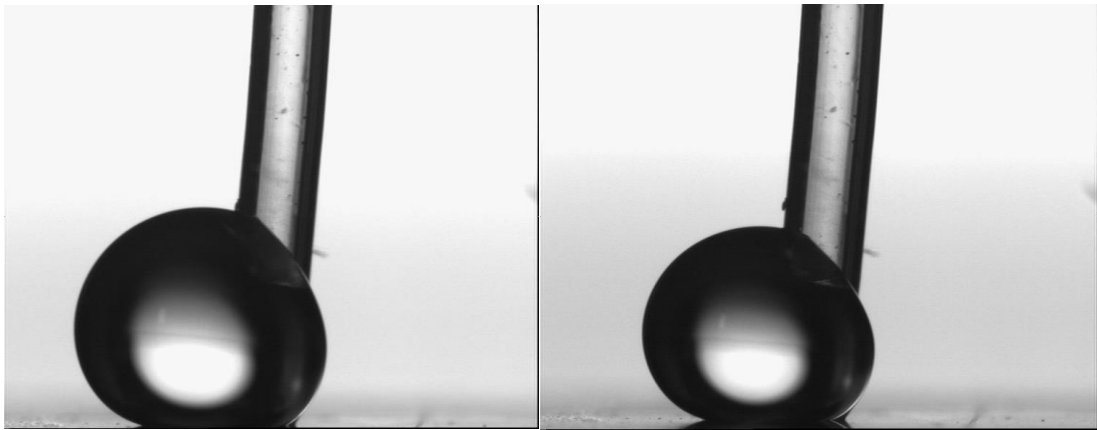
Figure 7.19: Advancing and receding angles for Sample 13



149.4°

145°

Figure 7.20: Sample 13- Drop images during advancing



$148.8 \pm 0.41^\circ$

$137.8 \pm 0.52^\circ$

Figure 7.21: Sample 13- Drop images during receding

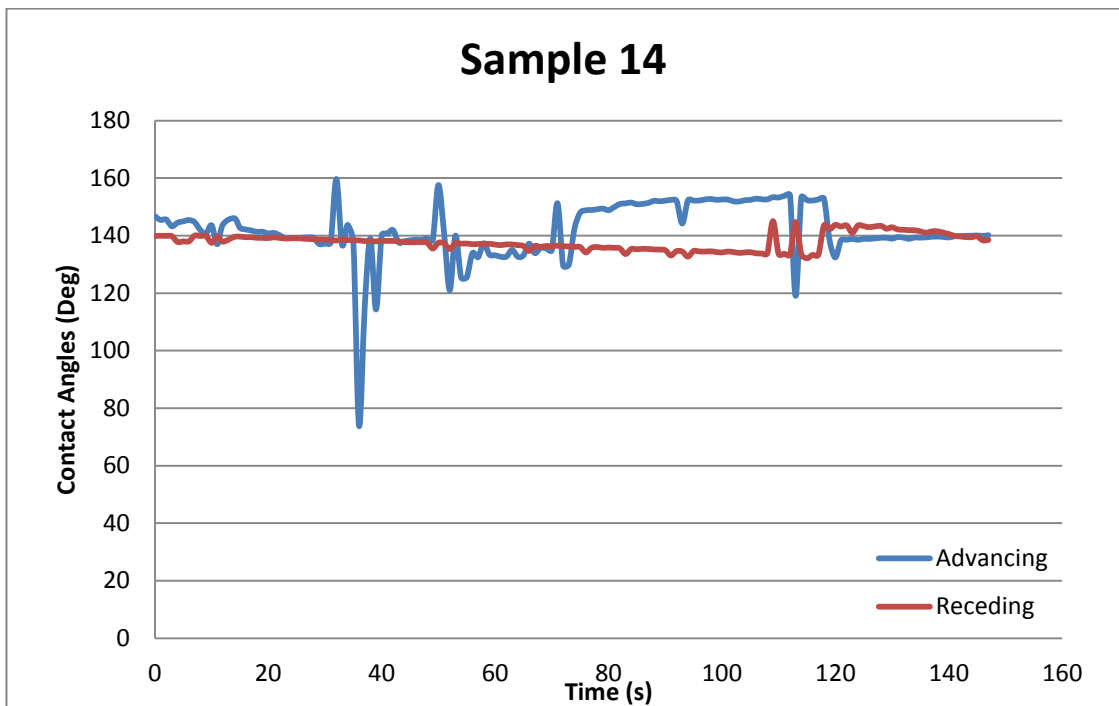
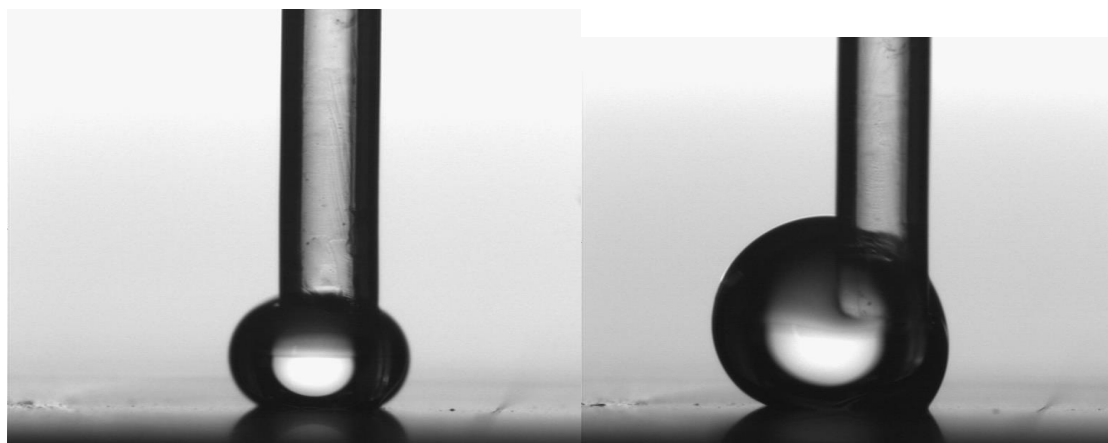


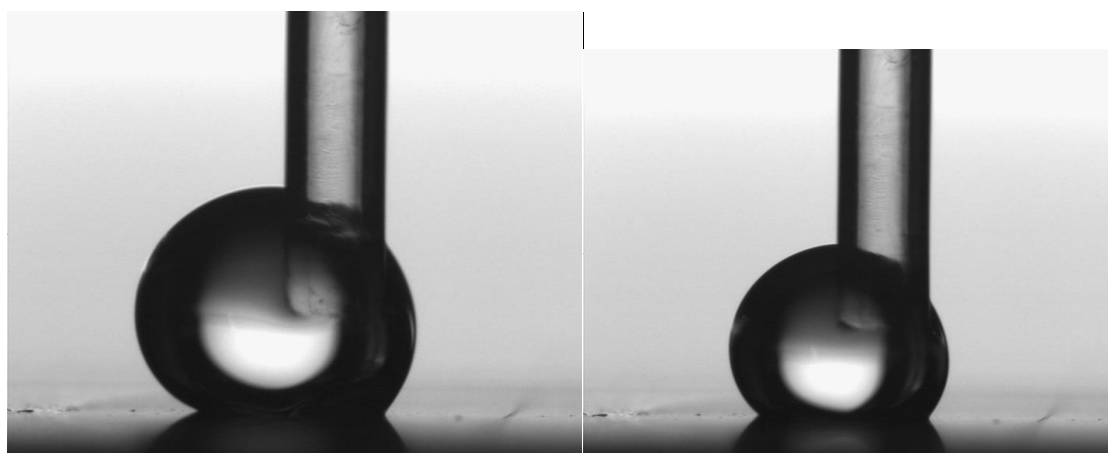
Figure 7.22: Advancing and receding angles for Sample 14



$137.0 \pm 3.23^\circ$

$154.1 \pm 0.41^\circ$

Figure 7.23 Sample 13- Drop images during advancing



$140.0 \pm 1.89^\circ$

$132.1 \pm 1.80^\circ$

Figure 7.24: Sample 14 - Drop images during receding

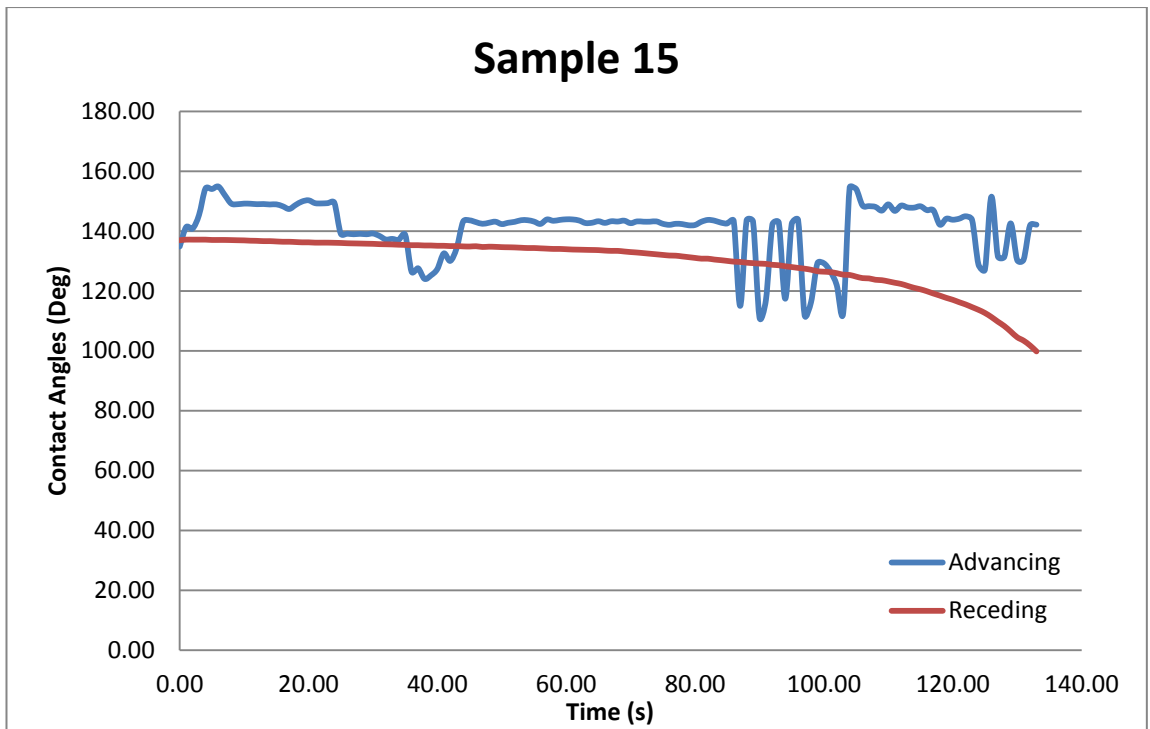
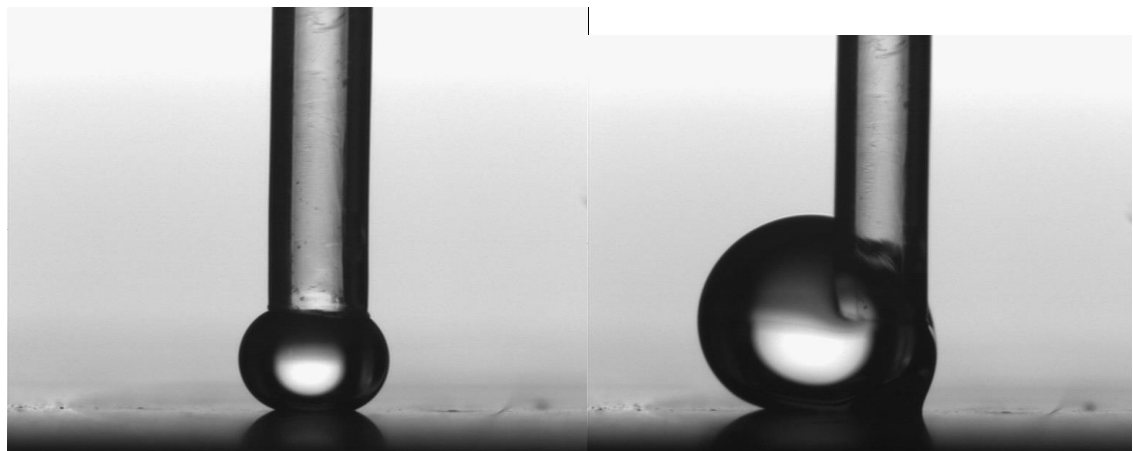


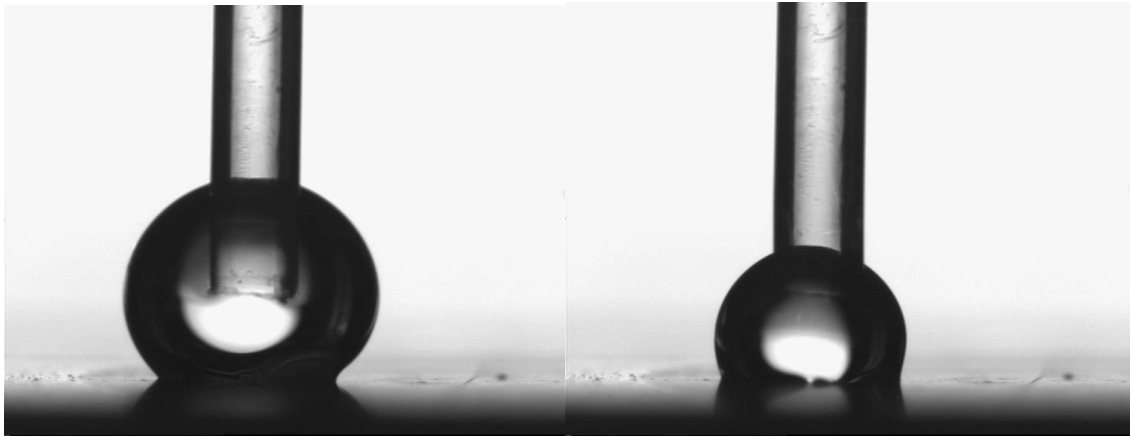
Figure 7.25: Advancing and receding angles for Sample 15



$134.8 \pm 0.52^\circ$

154.1 ± 0.11

Figure 7.26: Sample 15- Drop images during advancing



$137.1 \pm 0.45^\circ$

$112.6 \pm 0.16^\circ$

Figure 7.27: Sample 14 - Drop images during receding

Appendix 2

Histories of the SAM in different concentrations of thiols and immersion time that have been made are studied to understand reproducibility and stability of the samples. I-V sweeps have been performed with a ten minute interval and a of total 10 runs. The results offer more understanding towards the effect on the changes in resistivity produced by joule heating as potential is applied to the device. All the measurement voltages used are 10 V. Results were presented in graphical forms in Chapter 4 in Figures 4.47, 4.48 and 4.49. Measurement after the 5th run showed significantly reduced current values in all samples which is due to the sample being heated and leads to loss of moisture in the polyaniline.

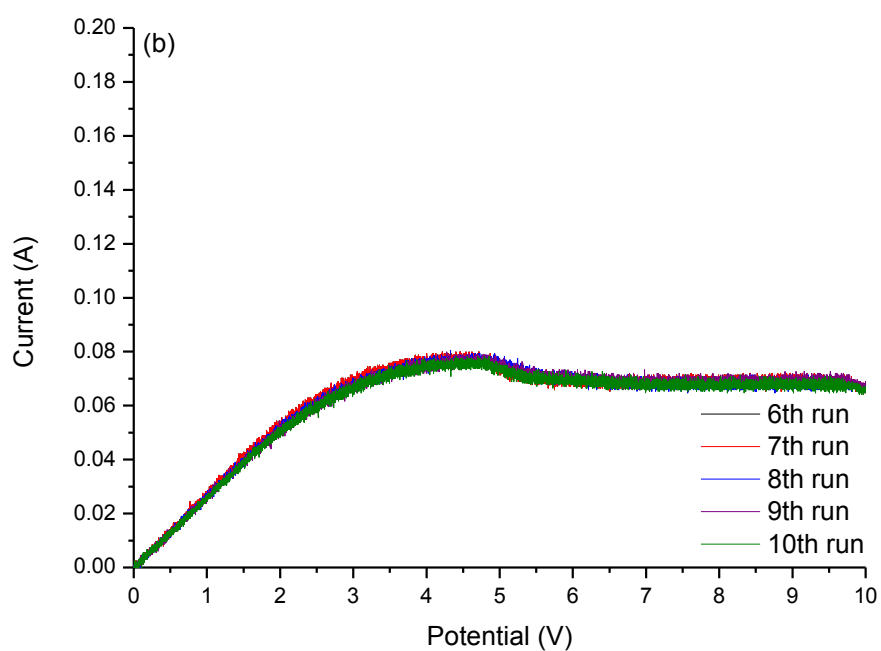
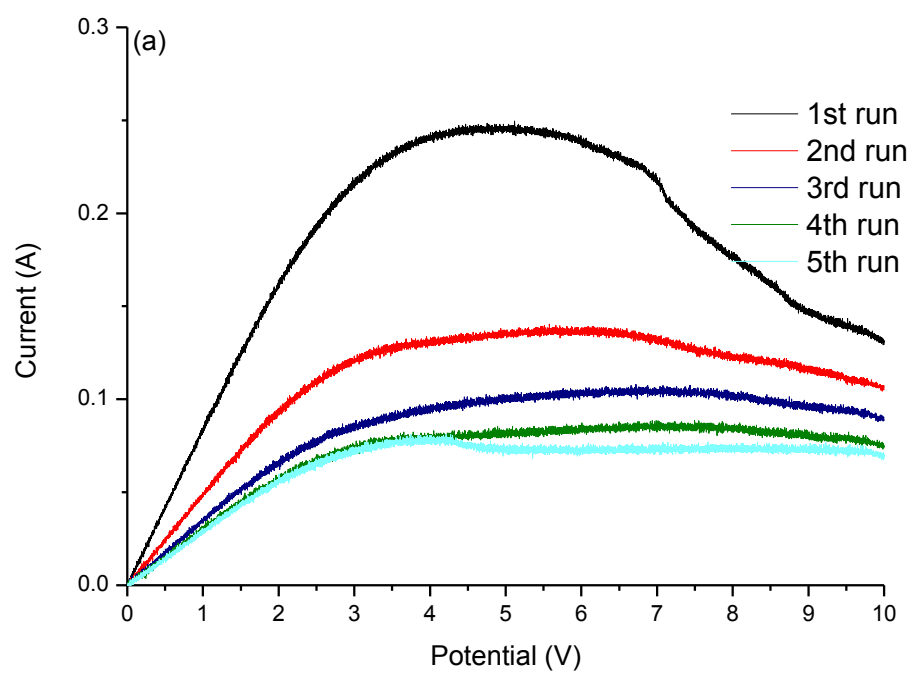


Figure 7.28: The I-V sweep with 10 V of potential applied for sample with 24H SAM of 1mM DDT with total 10 consecutive runs with 10 minute interval between each run.

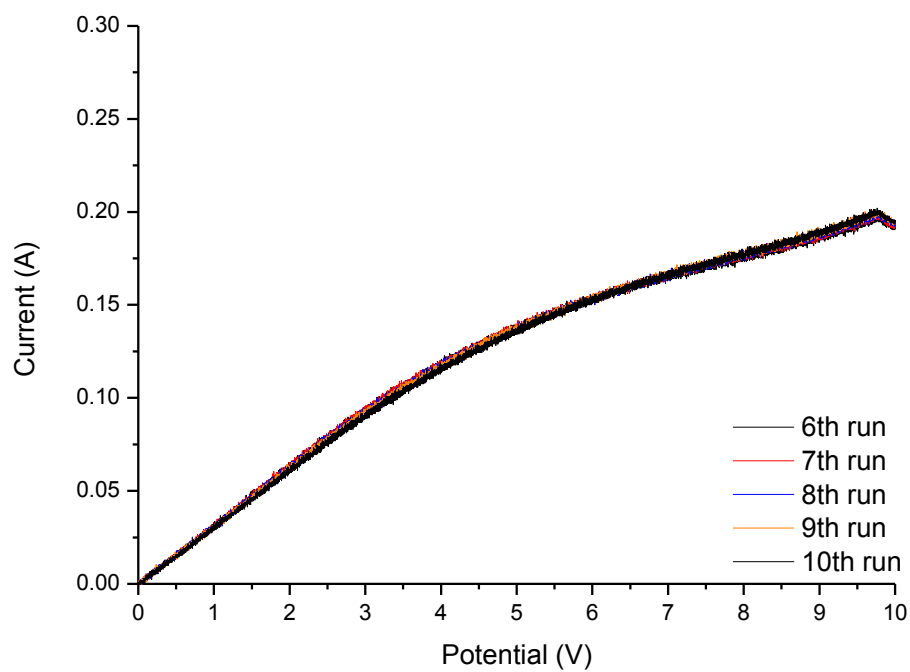
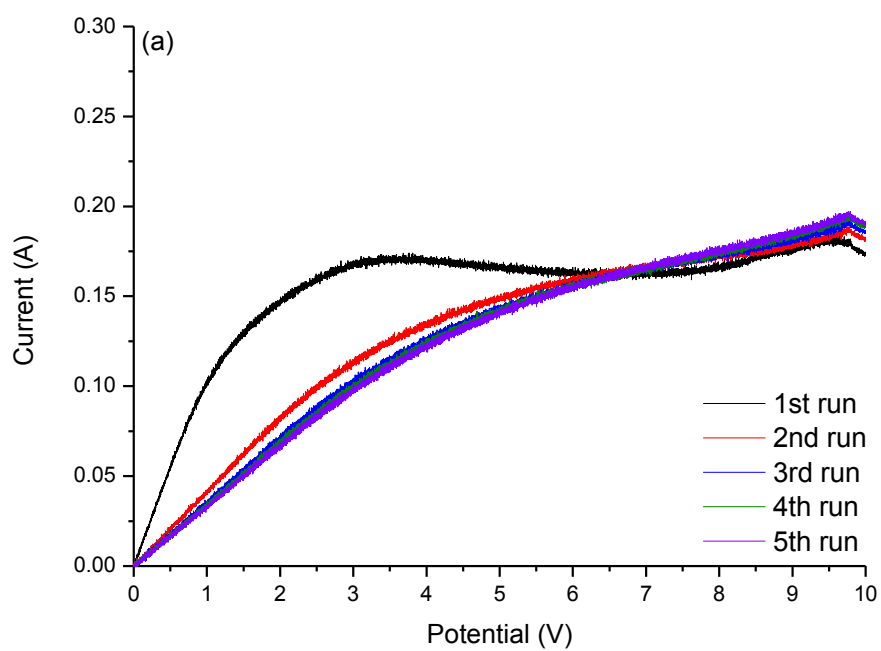


Figure 7.29: The I-V sweep with 10 V of potential applied for sample with 24H SAM of 5mM DDT with total 10 consecutive runs with 10 minute interval between each run.

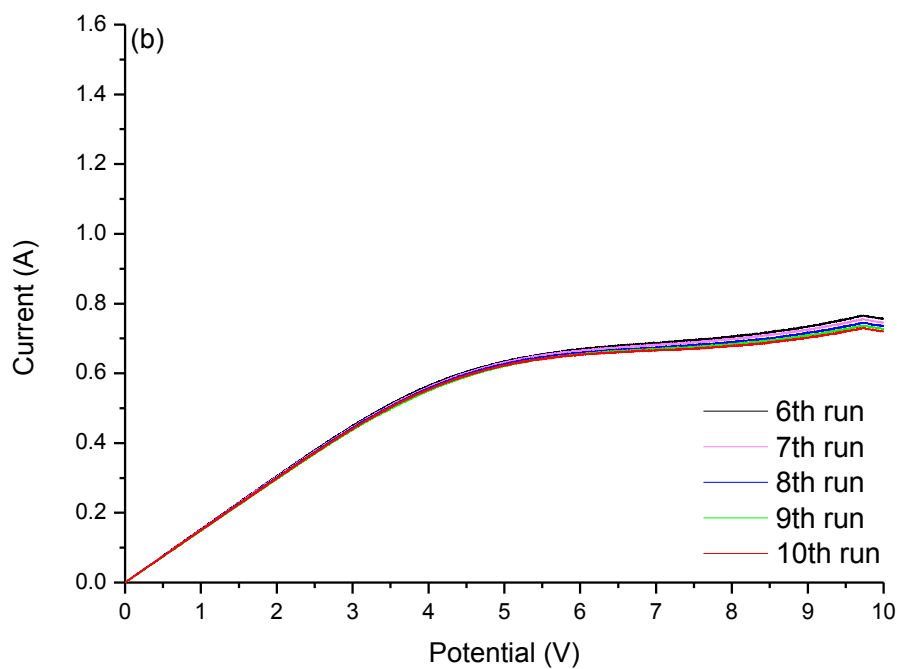
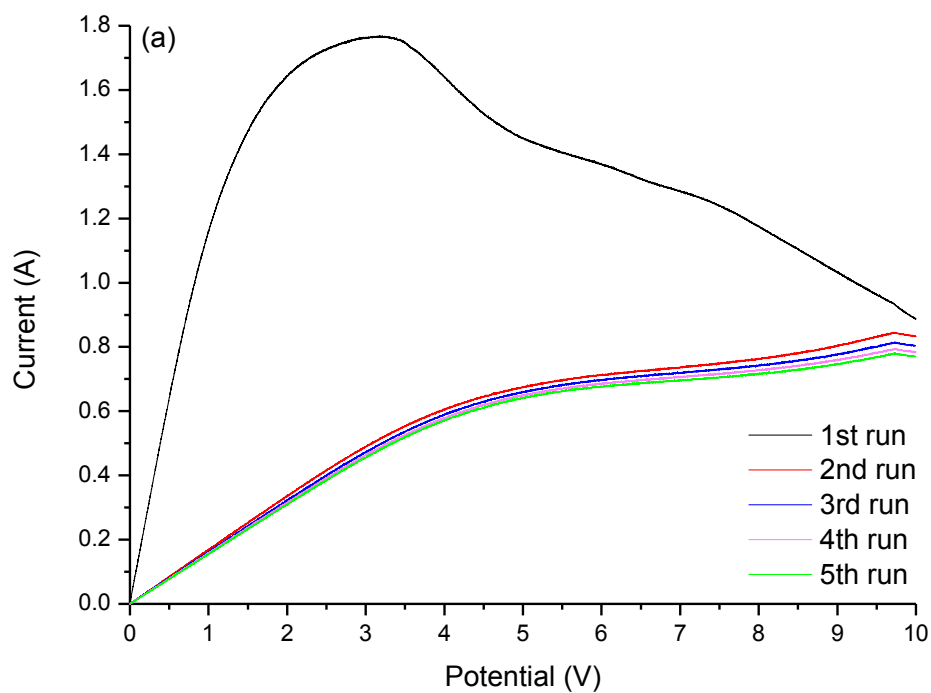


Figure 7.30: The I-V sweep with 10 V of potential applied for sample with 24H SAM of 10mM DDT with total 10 consecutive runs with 10 minute interval between each run.

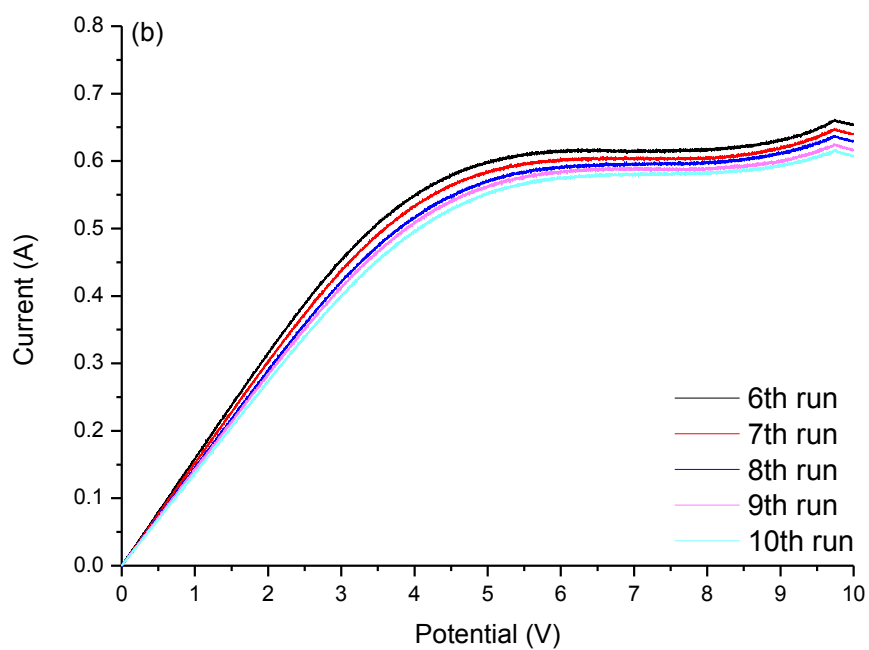
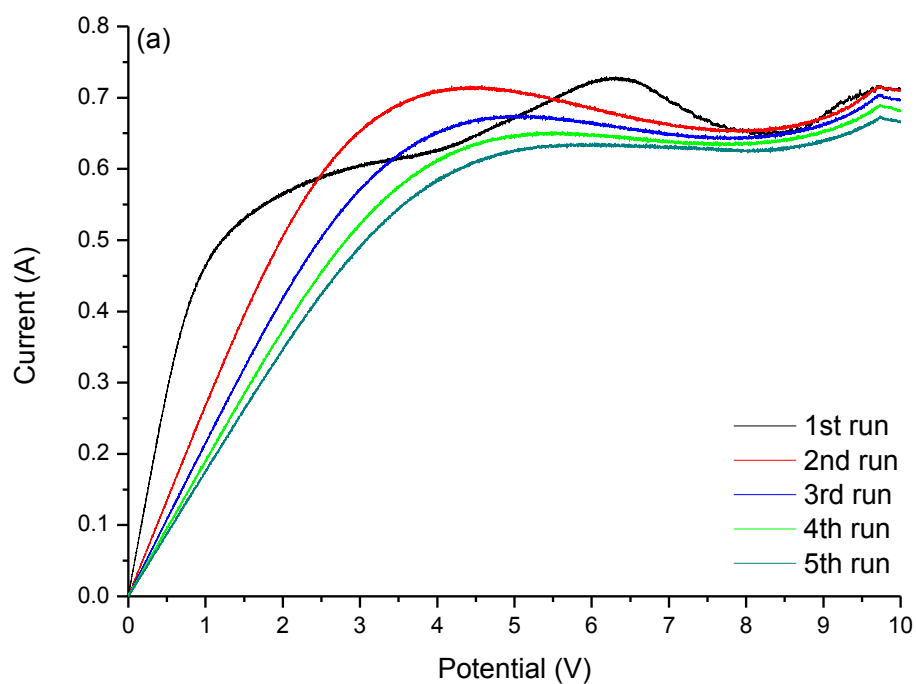


Figure 7.31: The I-V sweep with 10 V of potential applied for sample with 48H SAM of 1mM DDT with total 10 consecutive runs with 10 minute interval between each run.

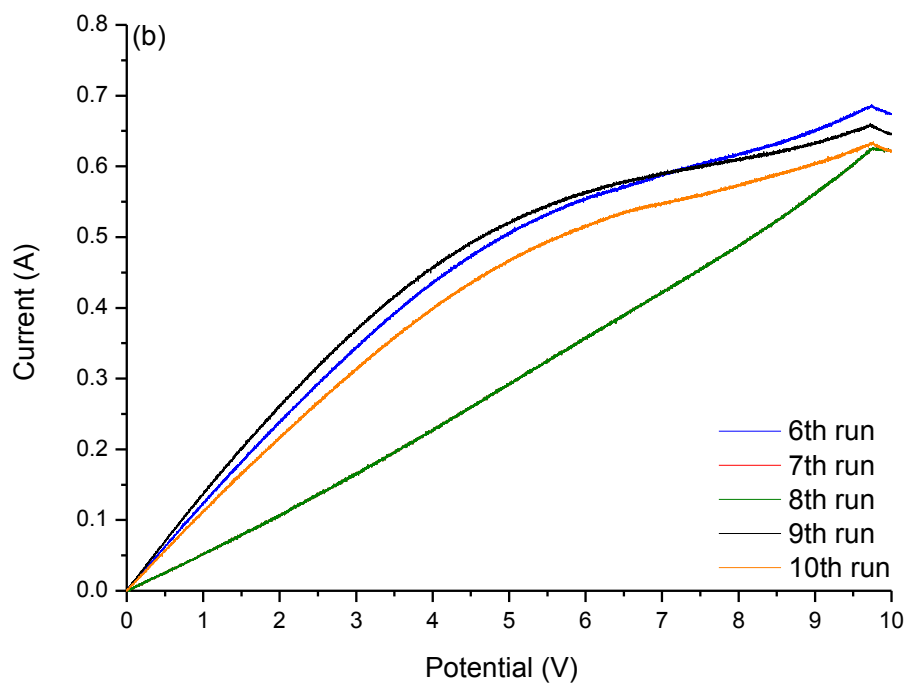
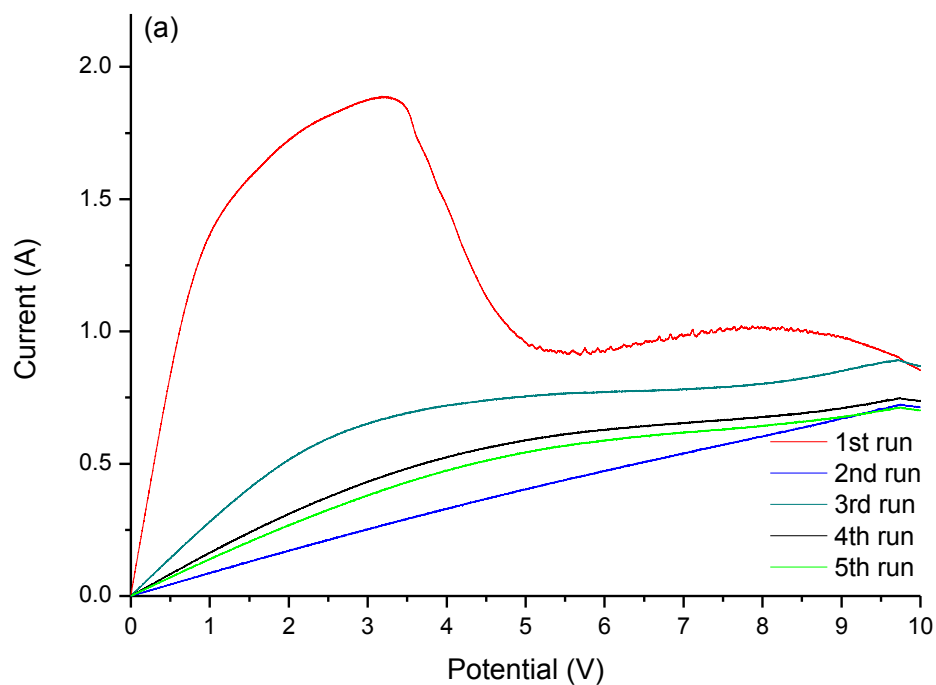


Figure 7.32: The I-V sweep with 10 V of potential applied for sample with 48H SAM of 5mM DDT with total 10 consecutive runs with 10 minute interval between each run.

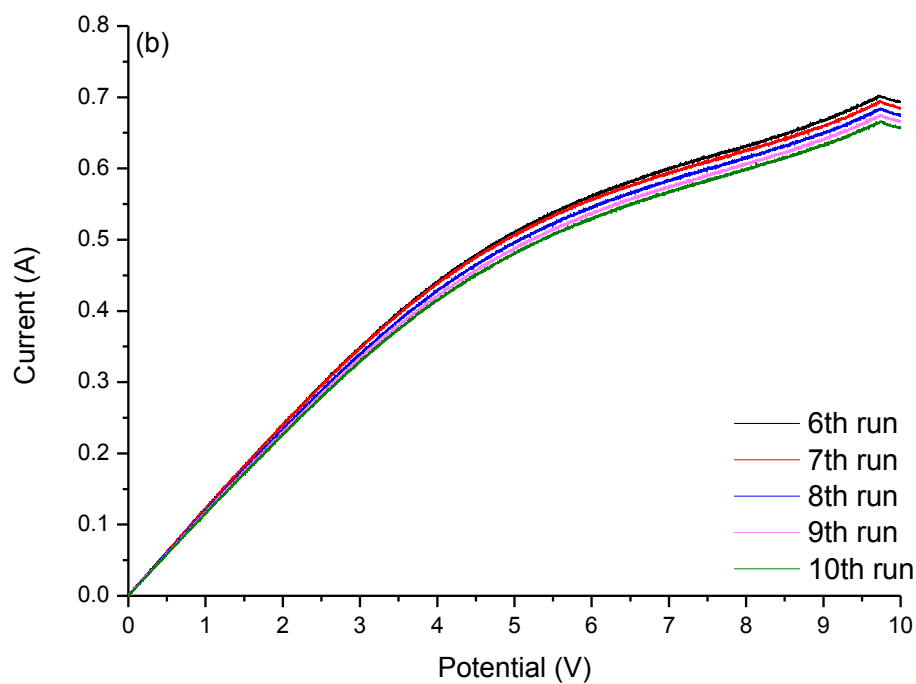
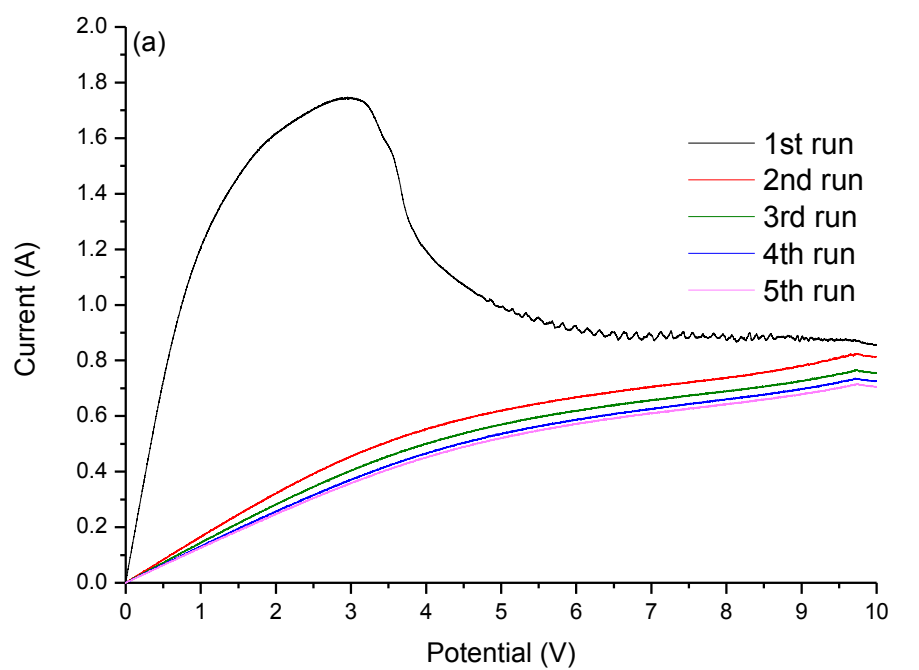


Figure 7.33: The I-V sweep with 10 V of potential applied for sample with 48H SAM of 10mM DDT with total 10 consecutive runs with 10 minute interval between each run.

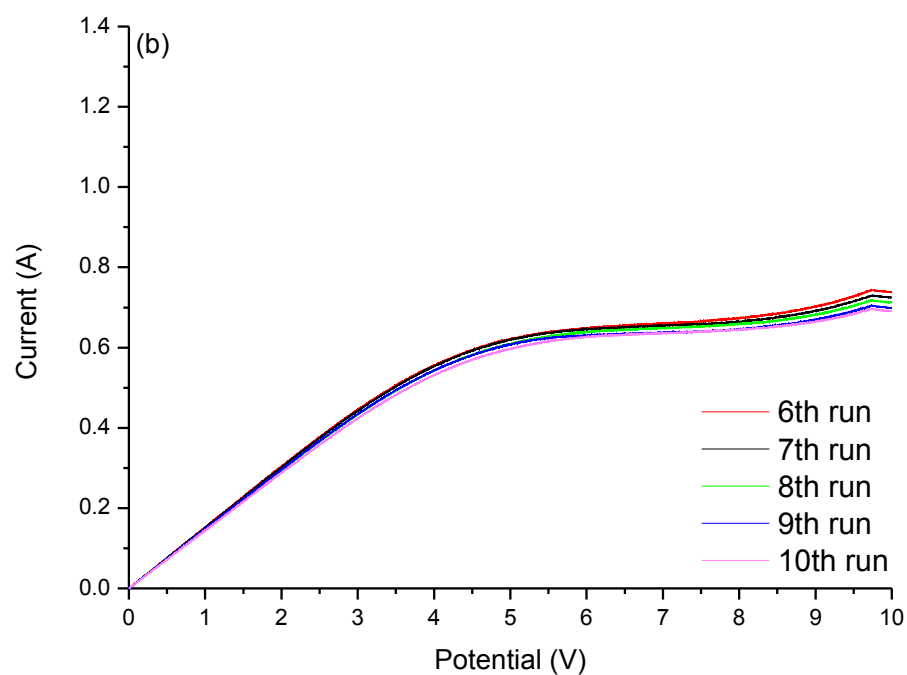
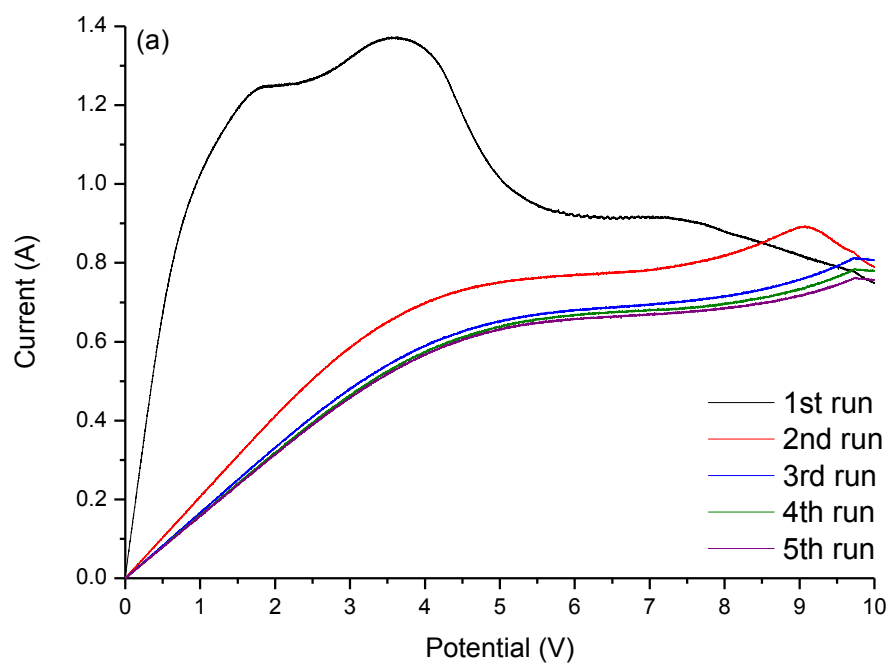


Figure 7.34: The I-V sweep with 10 V of potential applied for sample with 72H SAM of 1mM DDT with total 10 consecutive runs with 10 minute interval between each run.

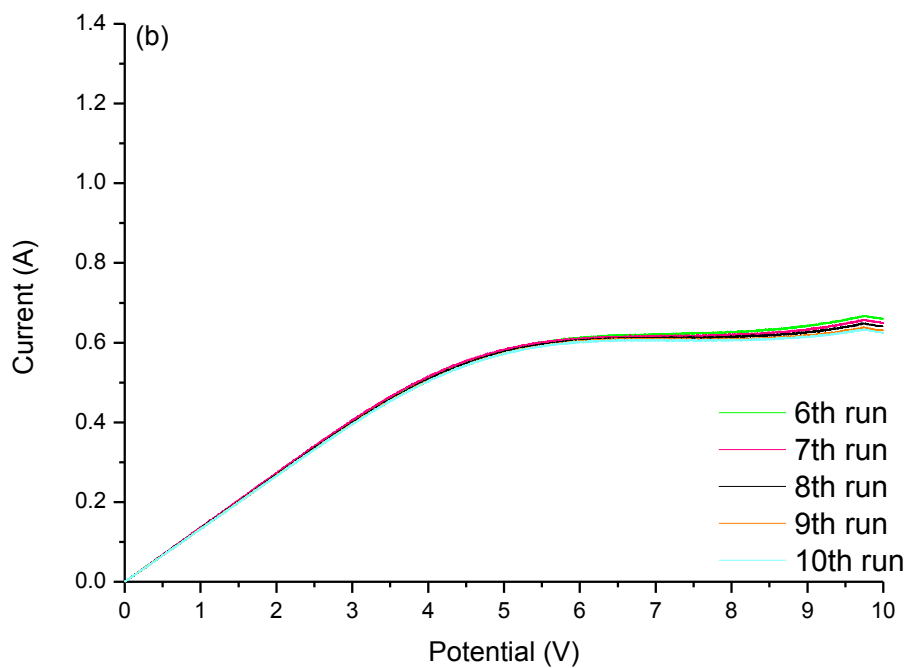
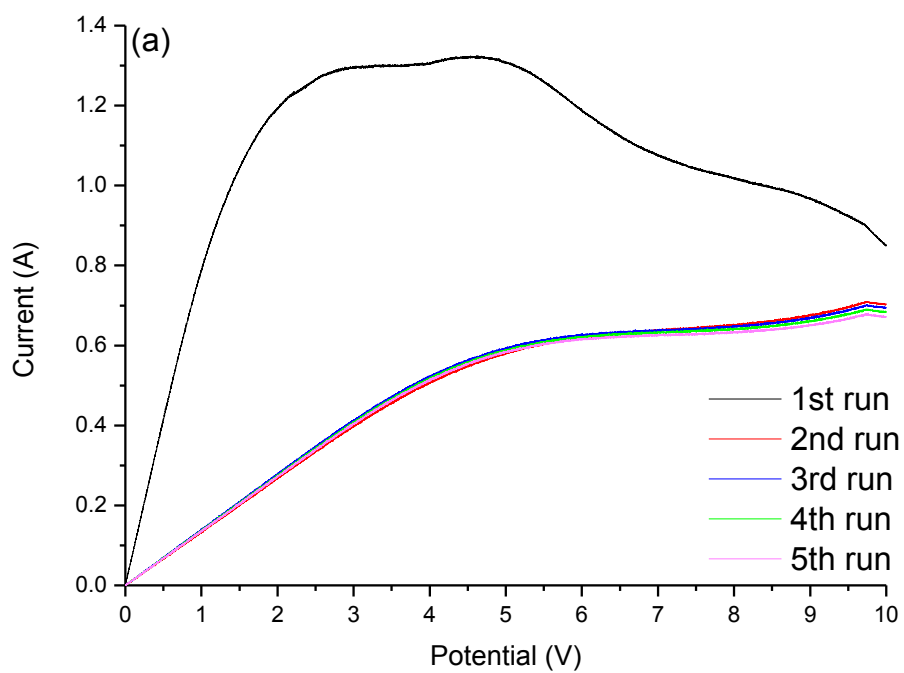


Figure 7.35: The I-V sweep with 10 V of potential applied for sample with 72H SAM of 5mM DDT with total 10 consecutive runs with 10 minute interval between each run.

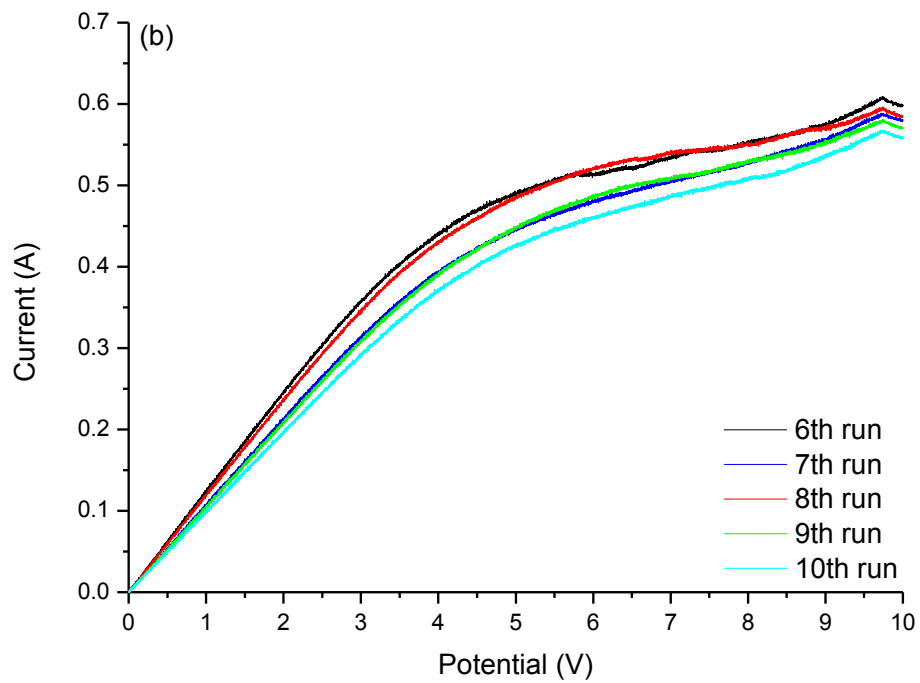
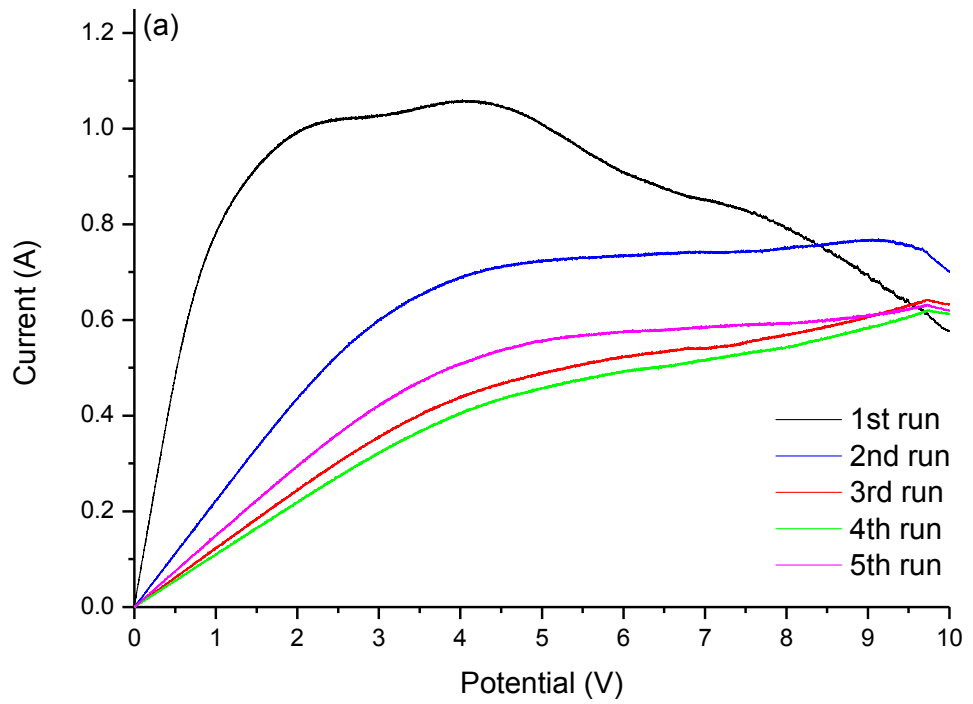


Figure 7.36: The I-V sweep with 10 V of potential applied for sample with 72H SAM of 10mM DDT with total 10 consecutive runs with 10 minute interval between each run.

Chapter 8 REFERENCES

- [1] R. Strumpler, G. Maidorn, and J. Rhyner, "Fast current limitation by conducting polymer composites," *Journal of Applied Physics*, vol. 81, pp. 6786-6794, 1997.
- [2] L. Navarro, "Tyco Electronics Introduction: ICPs for Current Limiting Devices." California: T.E Connectivity Internal Report 2011.
- [3] R. Friend, "Materials science: Polymers show they're metal," *Nature*, vol. 441, pp. 37-37, 2006.
- [4] A. Heeger, A. G. MacDiarmid, and H. Shirakawa, "The Nobel Prize in Chemistry, 2000:Conductive polymers," vol. 2011. Stockholm: Press Officer, the Royal Swedish Academy of Sciences, 2000.
- [5] H. Letheby, "XXIX.-On the production of a blue substance by the electrolysis of sulphate of aniline," *Journal of the Chemical Society*, vol. 15, pp. 161-163, 1862.
- [6] A. J. Heeger, "Nobel Lecture: Semiconducting and metallic polymers: The fourth generation of polymeric materials," *Reviews of Modern Physics*, vol. 73, pp. 681-700, 2001.
- [7] M. Angelopoulos, "Conducting polymers in microelectronics," *IBM Journal of Research and Development*, vol. 45, pp. 57-75, 2001.
- [8] N. Gospodinova and L. Terlemezyan, "Conducting polymers prepared by oxidative polymerization: polyaniline," *Progress in Polymer Science*, vol. 23, pp. 1443-1484, 1998.
- [9] K. F. Schoch, "Update on electrically conductive polymers and their applications," *Electrical Insulation Magazine, IEEE*, vol. 10, pp. 29-32, 1994.

- [10] J. Unsworth, B. A. Lunn, P. C. Innis, Z. Jin, A. Kaynak, and N. G. Booth, "Technical Review : Conducting Polymer Electronics," *Journal of Intelligent Material Systems and Structures*, vol. 3, pp. 380-395, 1992.
- [11] E. M. Geniès, A. Boyle, M. Lapkowski, and C. Tsintavis, "Polyaniline: A historical survey," *Synthetic Metals*, vol. 36, pp. 139-182, 1990.
- [12] J. Roncali, P. Marque, R. Garreau, F. Garnier, and M. Lemaire, "Structural control of conjugation in functionalized polythiophenes," *Macromolecules*, vol. 23, pp. 1347-1352, 1990.
- [13] R. J. Waltman and J. Bargon, "Electrically conducting polymers: a review of the electropolymerization reaction, of the effects of chemical structure on polymer film properties, and of applications towards technology," *Canadian journal of chemistry*, vol. 64, pp. 76-95, 1986.
- [14] G. Inzelt, "Conducting Polymers: A New Era in Electrochemistry." Berlin Springer, 2012.
- [15] G. Inzelt, "Rise and rise of conducting polymers," *Journal of Solid State Electrochemistry*, vol. 15, pp. 1711-1718, 2011.
- [16] J. H. Perlstein, "'Organic Metals"—The Intermolecular Migration of Aromaticity," *Angewandte Chemie International Edition in English*, vol. 16, pp. 519-534, 1977.
- [17] A. F. Garito and A. J. Heeger, "Design and synthesis of organic metals," *Accounts of Chemical Research*, vol. 7, pp. 232-240, 1974.
- [18] M. Aldissi, M. Hou, and J. Farrell, "Physical characteristics of diblock polyacetylene copolymers: Processability-conductivity correlation," *Synthetic Metals*, vol. 17, pp. 229-234, 1987.

- [19] G. Inzelt, "Classification of Electrochemically Active Polymers," in *Conducting Polymers, Monographs in Electrochemistry*: Springer Berlin Heidelberg, 2008, pp. 7-65-65.
- [20] V. N. Prigodin and A. J. Epstein, "Nature of insulator–metal transition and novel mechanism of charge transport in the metallic state of highly doped electronic polymers," *Synthetic Metals*, vol. 125, pp. 43-53, 2001.
- [21] D. D. F. Shriver and P. P. W. Atkins, *Inorganic Chemistry*: Oxford University Press, Incorporated, 1999.
- [22] T. R. Marrero, D. L. Cowan, D. C. Bradford, H. W. White, J. L. Wragg, and F. F. Oldfield, "Metallic polyaniline: Charge transport, moisture effects and magnetism," *Chemical Engineering Communications*, vol. 183, pp. 61-70, 2000.
- [23] J. M. Ginder, A. F. Richter, A. G. MacDiarmid, and A. J. Epstein, "Insulator-to-metal transition in polyaniline," *Solid State Communications*, vol. 63, pp. 97-101, 1987.
- [24] S. Stafström, J. L. Brédas, A. J. Epstein, H. S. Woo, D. B. Tanner, W. S. Huang, and A. G. MacDiarmid, "Polaron lattice in highly conducting polyaniline: Theoretical and optical studies," *Physical Review Letters*, vol. 59, pp. 1464-1467, 1987.
- [25] N. Mott, "On metal-insulator transitions," *Journal of Solid State Chemistry France*, vol. 88, pp. 5-7, 1990.
- [26] K. Lee, S. Cho, S. Heum Park, A. J. Heeger, C.-W. Lee, and S.-H. Lee, "Metallic transport in polyaniline," *Nature*, vol. 441, pp. 65-68, 2006.
- [27] P. Sheng, "Fluctuation-induced tunneling conduction in disordered materials," *Physical Review B*, vol. 21, pp. 2180-2195, 1980.
- [28] T. A. Skotheim, R. L. Elsenbaumer, and J. R. Reynolds, *Handbook of Conducting Polymers*. New York: Marcel Dekker Incorporation, 1998.

- [29] C. O. Yoon, R. M. D. Moses, and A. J. Heeger, "Transport near the metal-insulator transition: Polypyrrole doped with PF₆" *Physical Review B*, vol. 49, pp. 10851-10863, 1994.
- [30] N. F. Mott, "The effect of electron interaction on variable-range hopping," *Philosophical Magazine*, vol. 34, pp. 643-645, 1976.
- [31] A. A. Syed and M. K. Dinesan, "Review: Polyaniline--A novel polymeric material," *Talanta*, vol. 38, pp. 815-837, 1991.
- [32] J. C. Michaelson, "Aniline in history and technology," *Endeavour*, vol. 17, pp. 121-126, 1993.
- [33] O. Meth-Cohn and M. Smith, "What did W. H. Perkin actually make when he oxidised aniline to obtain mauveine?," *Journal of the Chemical Society, Perkin Transactions 1*, pp. 5-7, 1994.
- [34] A. S. Travis, "Anilines: Historical Background," in *PATAI'S Chemistry of Functional Groups*. Sussex, England: John Wiley & Sons, Ltd, 2007.
- [35] H. S. Nalwa, *Handbook of Organic Conductive Molecules and Polymers: Conductive polymers : transport, photophysics, and applications*. University of Michigan: Wiley Blackwell, 1997.
- [36] A. G. Green and A. E. Woodhead, "CCXLIII.-Aniline-black and allied compounds. Part I," *Journal of the Chemical Society, Transactions*, vol. 97, pp. 2388-2403, 1910.
- [37] A. G. MacDiarmid and A. J. Epstein, "Polyanilines: a novel class of conducting polymers," *Faraday Discussions of the Chemical Society*, vol. 88, pp. 317-332, 1989.

- [38] M. Zic, "The influence of the PANI structure on the conductive mechanism and on the electrical equivalent circuit analysis," *Journal of Electroanalytical Chemistry*, vol. 635, pp. 29-38, 2009.
- [39] R. V. Gregory, W. C. Kimbrell, and H. H. Kuhn, "Conductive textiles," *Synthetic Metals*, vol. 28, pp. 823-835, 1989.
- [40] A. J. Epstein, J. M. Ginder, F. Zuo, R. W. Bigelow, H. S. Woo, D. B. Tanner, A. F. Richter, W. S. Huang, and A. G. MacDiarmid, "Insulator-to-metal transition in polyaniline," *Synthetic Metals*, vol. 18, pp. 303-309, 1987.
- [41] A. G. MacDiarmid, "Polyaniline and polypyrrole: Where are we headed?," *Synthetic Metals*, vol. 84, pp. 27-34, 1997.
- [42] F. Lux, "Properties of electronically conductive polyaniline: a comparison between well-known literature data and some recent experimental findings," *Polymer*, vol. 35, pp. 2915-2936, 1994.
- [43] F. G. Sun and A. R. Duggal, *The voltage dependence of switching in a polymer current limiter device*, vol. 84: AIP, 1998.
- [44] X. J. He, J. H. Du, Z. Ying, and H. M. Cheng, *Positive temperature coefficient effect in multiwalled carbon nanotube/high-density polyethylene composites*, vol. 86: AIP, 2005.
- [45] A. R. Duggal and L. M. Levinson, "High power switching behavior in electrically conductive polymer composite materials," *Applied Physics Letters*, vol. 71, pp. 1939-1941, 1997.
- [46] R. G. Nuzzo and D. L. Allara, "Adsorption of bifunctional organic disulfides on gold surfaces," *Journal of the American Chemical Society*, vol. 105, pp. 4481-4483, 1983.

- [47] L. Strong and G. M. Whitesides, "Structures of self-assembled monolayer films of organosulfur compounds adsorbed on gold single crystals: electron diffraction studies," *Langmuir*, vol. 4, pp. 546-558, 1988.
- [48] J. C. Love, L. A. Estroff, J. K. Kriebel, R. G. Nuzzo, and G. M. Whitesides, "Self-Assembled Monolayers of Thiolates on Metals as a Form of Nanotechnology," *Chemical Reviews*, vol. 105, pp. 1103-1170, 2005.
- [49] A. Ulman, "Formation and Structure of Self-Assembled Monolayers," *Chemical Reviews*, vol. 96, pp. 1533-1554, 1996.
- [50] Xue-Mei Li, Jurriaan Huskens, and D. N. Reinhoudt, "Towards in-plane metathesis polymerization at self-assembled monolayers of norbornene adsorbates on gold surfaces " *Nanotechnology*, vol. 14, pp. 1064-1070, 2003.
- [51] R. Yamada, H. Sakai, and K. Uosaki, "Solvent Effect on the Structure of the Self-Assembled Monolayer of Alkanethiol," *Chemistry Letters*, vol. 28, pp. 667-668, 1999.
- [52] C. D. Bain, E. B. Troughton, Y. T. Tao, J. Evall, G. M. Whitesides, and R. G. Nuzzo, "Formation of monolayer films by the spontaneous assembly of organic thiols from solution onto gold," *Journal of the American Chemical Society*, vol. 111, pp. 321-335, 1989.
- [53] P. E. Laibinis, R. G. Nuzzo, and G. M. Whitesides, "Structure of monolayers formed by coadsorption of two n-alkanethiols of different chain lengths on gold and its relation to wetting," *The Journal of Physical Chemistry*, vol. 96, pp. 5097-5105, 1992.
- [54] F. Bensebaa, R. Voicu, L. Huron, T. H. Ellis, and E. Kruus, "Kinetics of Formation of Long-Chain n-Alkanethiolate Monolayers on Polycrystalline Gold," *Langmuir*, vol. 13, pp. 5335-5340, 1997.

- [55] M. Kawasaki, T. Sato, T. Tanaka, and K. Takao, "Rapid Self-Assembly of Alkanethiol Monolayers on Sputter-Grown Au(111)," *Langmuir*, vol. 16, pp. 1719-1728, 1999.
- [56] K. Tamada, M. Hara, H. Sasabe, and W. Knoll, "Surface Phase Behavior of n-Alkanethiol Self-Assembled Monolayers Adsorbed on Au(111): An Atomic Force Microscope Study," *Langmuir*, vol. 13, pp. 1558-1566, 1997.
- [57] R. S. Nicholson, "Theory and Application of Cyclic Voltammetry for Measurement of Electrode Reaction Kinetics," *Analytical Chemistry*, vol. 37, pp. 1351-1355, 1965.
- [58] S. Pruneanu, E. Veress, I. Marian, and L. Oniciu, "Characterization of polyaniline by cyclic voltammetry and UV-Vis absorption spectroscopy," *Journal of Materials Science*, vol. 34, pp. 2733-2739, 1999.
- [59] P. T. Kissinger and W. R. Heineman, "Cyclic voltammetry," *Journal of Chemical Education*, vol. 60, pp. 702-706, 1983.
- [60] F. Rourke and J. A. Crayston, "Cyclic voltammetry and morphology of polyaniline-coated electrodes containing $[\text{Fe}(\text{CN})_6]^{3-/4-}$ ions," *Journal of the Chemical Society, Faraday Transactions*, vol. 89, pp. 295-302, 1993.
- [61] K. Mizoguchi and K. Kume, "Metallic temperature dependence in the conducting polymer, polyaniline: Spin dynamics study by ESR," *Solid State Communications*, vol. 89, pp. 971-975, 1994.
- [62] J. Heinze, B. A. Frontana-Urbe, and S. Ludwigs, "Electrochemistry of Conducting Polymers—Persistent Models and New Concepts," *Chemical Reviews*, vol. 110, pp. 4724-4771, 2010.
- [63] C. Q. Cui, X. H. Su, and J. Y. Lee, "Measurement and evaluation of polyaniline degradation," *Polymer Degradation and Stability*, vol. 41, pp. 69-76, 1993.

- [64] H. H. Zhou, J. B. Wen, X. H. Ning, C. P. Fu, J. H. Chen, and Y. F. Kuang, "Comparison of the growth process and electrochemical properties of polyaniline films prepared by pulse potentiostatic and potentiostatic method on titanium electrode," *Journal of Applied Polymer Science*, vol. 104, pp. 458-463, 2007.
- [65] G. Mengoli, M. T. Munari, P. Bianco, and M. M. Musiani, "Anodic Synthesis of Polyaniline Coatingd Onto Fe Sheets," *Journal of Applied Polymer Science*, vol. 26, pp. 4247-4257, 1981.
- [66] D. M. Mohilner, R. N. Adams, and W. J. Argersinger Jr, "Investigation of the kinetics and mechanism of the anodic oxidation of aniline in aqueous sulfuric acid solution at a platinum electrode," *Journal of the American Chemical Society*, vol. 84, pp. 3618-3622, 1962.
- [67] A. Hickling, "A simple potentiostat for general laboratory use," *Electrochimica Acta*, vol. 5, pp. 161-168, 1961.
- [68] F. A. Settle, *Handbook of instrumental techniques for analytical chemistry*. National Science Foundation, Arlington, Virginia Prentice Hall PTR, 1997.
- [69] A. J. Bard and L. R. Faulkner, *Electrochemical Methods: Fundamentals and Applications*: Wiley, 2000.
- [70] A. Adamson, *Physical chemistry of surfaces*. University of Michigan: Wiley-Interscience Publication, 1990.
- [71] W. A. Zisman, "Relation of the Equilibrium Contact Angle to Liquid and Solid Constitution," *Contact Angle, Wettability, and Adhesion*, vol. 43, pp. 1-51, 1964.
- [72] D. Li and A. W. Neumann, "Contact angles on hydrophobic solid surfaces and their interpretation," *Journal of Colloid and Interface Science*, vol. 148, pp. 190-200, 1992.

- [73] A. B. Kaiser, "Electronic transport properties of conducting polymers and carbon nanotubes," *Reports on Progress in Physics*, vol. 64, pp. 1-49, 2001.
- [74] V. Percec, C. H. Ahn, W. D. Cho, A. M. Jamieson, J. Kim, T. Leman, M. Schmidt, M. Gerle, M. Möller, S. A. Prokhorova, S. S. Sheiko, S. Z. D. Cheng, A. Zhang, G. Ungar, and D. J. P. Yeardley, "Visualizable Cylindrical Macromolecules with Controlled Stiffness from Backbones Containing Libraries of Self-Assembling Dendritic Side Groups," *Journal of the American Chemical Society*, vol. 120, pp. 8619-8631, 1998.
- [75] A. B. Kaiser, "Systematic Conductivity Behavior in Conducting Polymers: Effects of Heterogeneous Disorder," *Advanced Materials*, vol. 13, pp. 927-941, 2001.
- [76] Z. H. Wang, E. M. Scherr, A. G. MacDiarmid, and A. J. Epstein, "Transport and EPR studies of polyaniline: A quasi-one-dimensional conductor with three-dimensional "metallic" states," *Physical Review B*, vol. 45, pp. 4190-4202, 1992.
- [77] W. Lee, G. Du, S. M. Long, A. J. Epstein, S. Shimizu, T. Saitoh, and M. Uzawa, "Charge transport properties of fully-sulfonated polyaniline," *Synthetic Metals*, vol. 84, pp. 807-808, 1997.
- [78] S. Roth, H. Bleier, and W. Pukacki, "Charge transport in conducting polymers," *Faraday Discussions of the Chemical Society*, vol. 88, pp. 223-233, 1989.
- [79] M. Campos and B. Braz, Jr., "Mechanism of conduction in doped polyaniline," *Journal of Physics D: Applied Physics*, vol. 30, pp. 1531-1535, 1997.
- [80] V. M. Mzenda, S. A. Goodman, F. D. Auret, and L. C. Prinsloo, "Characterization of electrical charge transfer in conducting polyaniline over the temperature range $300 < T(K) < 450$," *Synthetic Metals*, vol. 127, pp. 279-283, 2002.

- [81] Q. Li, L. Cruz, and P. Phillips, "Granular-rod model for electronic conduction in polyaniline," *Physical Review B*, vol. 47, pp. 1840-1845, 1993.
- [82] J. Li, K. Fang, H. Qiu, S. Li, and W. Mao, "Micromorphology and electrical property of the HCl-doped and DBSA-doped polyanilines," *Synthetic Metals*, vol. 142, pp. 107-111, 2004.
- [83] P. Sheng and B. Abeles, "Voltage-Induced Tunneling Conduction in Granular Metals at Low Temperatures," *Physical Review Letters*, vol. 28, pp. 34-37, 1972.
- [84] W. Shockley, "Research and investigations of epitaxial UHF power transistors," Air Force Atomic Laboratory Technical Report, Wright-Patterson Base, Ohio A1-TOR-207, 1964.
- [85] H. H. Berger, "Contact Resistance and Contact Resistivity," *Journal of The Electrochemical Society*, vol. 119, pp. 507-514, 1972.
- [86] S. B. Schuldt, "An exact derivation of contact resistance to planar devices," *Solid-State Electronics*, vol. 21, pp. 715-719, 1978.
- [87] Y. Kong and J. N. Hay, "The measurement of the crystallinity of polymers by DSC," *Polymer*, vol. 43, pp. 3873-3878, 2002.
- [88] R. W. Seymour and S. L. Cooper, "Thermal Analysis of Polyurethane Block Polymers," *Macromolecules*, vol. 6, pp. 48-53, 1973.
- [89] A. W. Coats and J. P. Redfern, "Thermogravimetric analysis. A review," *Analyst*, vol. 88, pp. 906-924, 1963.
- [90] R. Egerton, "The Scanning Electron Microscope," in *Physical Principles of Electron Microscopy*: Springer US, 2005, pp. 125-153.
- [91] P. K. Kahol, A. J. Dyakonov, and B. J. McCormick, "An electron-spin-resonance study of polymer interactions with moisture in polyaniline and its derivatives," *Synthetic Metals*, vol. 89, pp. 17-28, 1997.

- [92] N. J. Pinto, P. D. Shah, P. K. Kahol, and B. J. McCormick, "Conducting state of polyaniline films: Dependence on moisture," *Physical Review B*, vol. 53, pp. 10690-10694, 1996.
- [93] M. Nechtschein, C. Santier, J. P. Travers, J. Chroboczek, A. Alix, and M. Ripert, "Water effects in polyaniline: NMR and transport properties," *Synthetic Metals*, vol. 18, pp. 311-316, 1987.
- [94] J. P. Travers and M. Nechtschein, "Water effects in polyaniline: A new conduction process," *Synthetic Metals*, vol. 21, pp. 135-141.
- [95] H. H. S. Javadi, M. Angelopoulos, A. G. MacDiarmid, and A. J. Epstein, "Conduction mechanism of polyaniline: Effect of moisture," *Synthetic Metals*, vol. 26, pp. 1-8, 1988.
- [96] N. J. Pinto, P. D. Shah, B. J. McCormick, and P. K. Kahol, "Dependence of the conducting state of polyaniline films on moisture," *Solid State Communications*, vol. 97, pp. 931-934, 1996.
- [97] S. Bhadra, N. K. Singha, S. Chattopadhyay, and D. Khastgir, "Effect of different reaction parameters on the conductivity and dielectric properties of polyaniline synthesized electrochemically and modeling of conductivity against reaction parameters through regression analysis," *Journal of Polymer Science Part B: Polymer Physics*, vol. 45, pp. 2046-2059, 2007.
- [98] I. Šeděnková, J. Prokeš, M. Trchová, and J. Stejskal, "Conformational transition in polyaniline films – Spectroscopic and conductivity studies of ageing," *Polymer Degradation and Stability*, vol. 93, pp. 428-435, 2008.
- [99] V. I. Krinichnyi, S. D. Chemerisov, and Y. S. Lebedev, "EPR and charge-transport studies of polyaniline," *Physical Review B*, vol. 55, pp. 16233-16244, 1997.

- [100] B. Sanjai, A. Raghunathan, T. S. Natarajan, G. Rangarajan, S. Thomas, P. V. Prabhakaran, and S. Venkatachalam, "Charge transport and magnetic properties in polyaniline doped with methane sulphonic acid and polyaniline-polyurethane blend," *Physical Review B*, vol. 55, pp. 10734-10744, 1997.
- [101] Y. Long, Z. Chen, N. Wang, J. Li, and M. Wan, "Electronic transport in PANI-CSA/PANI-DBSA polyblends," *Physica B: Condensed Matter*, vol. 344, pp. 82-87, 2004.
- [102] M. Gosh, A. Barman, A. K. Meikap, S. K. De, and S. Chatterjee, "Hopping transport in HCl doped conducting polyaniline," *Physics Letters A*, vol. 260, pp. 138-148, 1999.
- [103] V. Luthra, R. Singh, S. K. Gupta, and A. Mansingh, "Mechanism of dc conduction in polyaniline doped with sulfuric acid," *Current Applied Physics*, vol. 3, pp. 219-222, 2003.
- [104] C. O. Yoon, M. Reghu, D. Moses, A. J. Heeger, Y. Cao, T. A. Chen, X. Wu, and R. D. Rieke, "Hopping transport in doped conducting polymers in the insulating regime near the metal-insulator boundary: polypyrrole, polyaniline and polyalkylthiophenes," *Synthetic Metals*, vol. 75, pp. 229-239, 1995.
- [105] S. Bhadra, S. Chattopadhyay, N. K. Singha, and D. Khastgir, "Improvement of conductivity of electrochemically synthesized polyaniline," *Journal of Applied Polymer Science*, vol. 108, pp. 57-64, 2008.
- [106] C. N. Sayre and D. M. Collard, "Electrooxidative Deposition of Polypyrrole and Polyaniline on Self-Assembled Monolayer Modified Electrodes," *Langmuir*, vol. 13, pp. 714-722, 1997.
- [107] L. W. Shacklette, "Dipole and hydrogen-bonding interactions in polyaniline: a mechanism for conductivity enhancement," *Synthetic Metals*, vol. 65, pp. 123-130, 1994.

- [108] P. K. Kahol, H. Guan, and B. J. McCormick, "Moisture effects on the magnetic state in polyaniline," *Physical Review B*, vol. 44, pp. 10393-10395, 1991.
- [109] N. J. Pinto, C. M. Torres, P. K. Kahol, and B. J. McCormick, "Conducting properties of polyaniline blends," *Journal of Applied Physics*, vol. 79, pp. 8512-8515, 1996.
- [110] A. G. MacDiarmid, "Polyaniline and polypyrrole: Where are we headed?," *Synthetic Metals*, vol. 84, pp. 27-34, 1997.
- [111] P. C. Wang, Z. Huang, and A. G. MacDiarmid, "Critical dependency of the conductivity of polypyrrole and polyaniline films on the hydrophobicity/hydrophilicity of the substrate surface," *Synthetic Metals*, vol. 101, pp. 852-853, 1999.
- [112] P.-C. Wang, R. E. Lakis, and A. G. MacDiarmid, "Morphology-correlated electrical conduction in micro-contact-printed polypyrrole thin films grown by in situ deposition," *Thin Solid Films*, vol. 516, pp. 2341-2345, 2008.
- [113] J. K. Avlyanov, J. Y. Josefowicz, and A. G. MacDiarmid, "Atomic force microscopy surface morphology studies of 'in situ' deposited polyaniline thin films," *Synthetic Metals*, vol. 73, pp. 205-208, 1995.
- [114] J. Stejskal, I. Sapurina, and M. Trchová, "Polyaniline nanostructures and the role of aniline oligomers in their formation," *Progress in Polymer Science*, vol. 35, pp. 1420-1481, 2010.
- [115] H. H. S. Javadi, F. Zuo, M. Angelopoulos, A. G. Macdiarmid, and A. J. Epstein, "Frequency Dependent Conductivity of Emeraldine: Absence of Protonic Conductivity," *Molecular Crystals and Liquid Crystals Incorporating Nonlinear Optics*, vol. 160, pp. 225-233, 1988.

- [116] L. F. Rozsnyai and M. S. Wrighton, "Controlling the Adhesion of Conducting Polymer Films with Patterned Self-Assembled Monolayers," *Chemistry of Materials*, vol. 8, pp. 309-311, 1996.
- [117] L. F. Rozsnyai and M. S. Wrighton, "Selective Electrochemical Deposition of Polyaniline via Photopatterning of a Monolayer-Modified Substrate," *Journal of the American Chemical Society*, vol. 116, pp. 5993-5994, 1994.
- [118] B. Wang, J. Tang, and F. Wang, "Electrochemical polymerization of aniline," *Synthetic Metals*, vol. 18, pp. 323-328, 1987.
- [119] S.-J. Choi and S.-M. Park, "Electrochemistry of Conductive Polymers. XXVI. Effects of Electrolytes and Growth Methods on Polyaniline Morphology," *Journal of The Electrochemical Society*, vol. 149, pp. E26-E34, 2002.
- [120] T. Hagiwara, M. Yamaura, and K. Iwata, "Thermal stability of polyaniline," *Synthetic Metals*, vol. 25, pp. 243-252, 1988.
- [121] H. S. O. Chan, M. Y. B. Teo, E. Khor, and C. N. Lim, "Thermal analysis of conducting polymers part I," *Journal of thermal analysis*, vol. 35, pp. 765-774, 1989.
- [122] J. A. Conklin, S.-C. Huang, S.-M. Huang, T. Wen, and R. B. Kaner, "Thermal Properties of Polyaniline and Poly(aniline-co-o-ethylaniline)," *Macromolecules*, vol. 28, pp. 6522-6527, 1995.
- [123] H. De Santana, J. D. R. Matos, and M. L. A. Temperini, "Characterization of polydiphenylamine electrochemically synthesized by spectroscopic and thermal techniques," *Polymer Journal*, vol. 30, pp. 315-321, 1998.
- [124] S. W. Byun and S. S. Im, "Physical properties and doping characteristics of polyaniline-nylon 6 composite films," *Polymer*, vol. 39, pp. 485-489, 1998.

- [125] L. Ding, X. Wang, and R. V. Gregory, "Thermal properties of chemically synthesized polyaniline (EB) powder," *Synthetic Metals*, vol. 104, pp. 73-78, 1999.
- [126] Y. Wei and K. F. Hsueh, "Thermal analysis of chemically synthesized polyaniline and effects of thermal aging on conductivity," *Journal of Polymer Science Part A: Polymer Chemistry*, vol. 27, pp. 4351-4363, 1989.
- [127] S.-A. Chen and L.-C. Lin, "Polyaniline Doped by the New Class of Dopant, Ionic Salt: Structure and Properties," *Macromolecules*, vol. 28, pp. 1239-1245, 1995.
- [128] S. A. Chen and H. T. Lee, "Polyaniline plasticized with 1-methyl-2-pyrrolidone: structure and doping behavior," *Macromolecules*, vol. 26, pp. 3254-3261, 1993.
- [129] Y. Wei, G.-W. Jang, K. F. Hsueh, E. M. Scherr, A. G. MacDiarmid, and A. J. Epstein, "Thermal transitions and mechanical properties of films of chemically prepared polyaniline," *Polymer*, vol. 33, pp. 314-322, 1992.
- [130] S. Bhadra, N. K. Singha, and D. Khastgir, "Electrochemical synthesis of polyaniline and its comparison with chemically synthesized polyaniline," *Journal of Applied Polymer Science*, vol. 104, pp. 1900-1904, 2007.
- [131] S. Bhadra, N. K. Singha, and D. Khastgir, "Dual functionality of PTSA as electrolyte and dopant in the electrochemical synthesis of polyaniline, and its effect on electrical properties," *Polymer International*, vol. 56, pp. 919-927, 2007.
- [132] R. Ansari, W. E. Price, and G. G. Wallace, "Effect of thermal treatment on the electroactivity of polyaniline," *Polymer*, vol. 37, pp. 917-923, 1996.
- [133] M. J. R. Cardoso, M. F. S. Lima, and D. M. Lenz, "Polyaniline synthesized with functionalized sulfonic acids for blends manufacture," *Materials Research*, vol. 10, pp. 425-429, 2007.

- [134] K. Amano, H. Ishikawa, A. Kobayashi, M. Satoh, and E. Hasegawa, "Thermal stability of chemically synthesized polyaniline," *Synthetic Metals*, vol. 62, pp. 229-232, 1994.
- [135] S. Palaniappan and B. H. Narayana, "Temperature effect on conducting polyaniline salts: Thermal and spectral studies," *Journal of Polymer Science Part A: Polymer Chemistry*, vol. 32, pp. 2431-2436, 1994.
- [136] J. C. LaCroix and A. F. Diaz, "Electrolyte Effects on the Switching Reaction of Polyaniline," *Journal of The Electrochemical Society*, vol. 135, pp. 1457-1463, 1988.
- [137] B. Wessling and H. Volk, "Post-polymerization processing of conductive polymers: A way of converting conductive polymers to conductive materials?," *Synthetic Metals*, vol. 15, pp. 183-193, 1986.
- [138] S. Bhadra and D. Khastgir, "Extrinsic and intrinsic structural change during heat treatment of polyaniline," *Polymer Degradation and Stability*, vol. 93, pp. 1094-1099, 2008.
- [139] S. Bhadra, N. K. Singha, and D. Khastgir, "Effect of aromatic substitution in aniline on the properties of polyaniline," *European Polymer Journal*, vol. 44, pp. 1763-1770, 2008.
- [140] S. Bhadra and D. Khastgir, "Degradation and stability of polyaniline on exposure to electron beam irradiation (structure–property relationship)," *Polymer Degradation and Stability*, vol. 92, pp. 1824-1832, 2007.
- [141] A. A. Athawale, M. V. Kulkarni, and V. V. Chabukswar, "Studies on chemically synthesized soluble acrylic acid doped polyaniline," *Materials Chemistry and Physics*, vol. 73, pp. 106-110, 2002.

